CELL AND DEVELOPMENTAL BIOLOGY

MOLECULAR ANALYSIS OF *unc-4* PATHWAY GENES THAT REGULATE SYNAPTIC CHOICE

RACHEL L. SKELTON

Dissertation under the direction of Professor David M. Miller

Neural function depends on the creation of synapses between specific neurons. Across species, transcription factor codes regulate the precise connectivity between neurons. In the *C. elegans* motor circuit, these critical features are controlled by the UNC-4 homeodomain protein. *unc-4* mutants are unable to execute backward locomotion due to the miswiring of VA motor neurons with inputs normally reserved for VB sisters. Thus, we have proposed that UNC-4 preserves VA inputs and backward movement by repressing genes that promote VB-type wiring. Here we show that UNC-4 opposes the function of multiple downstream components, discovered in a genetic screen for UNC-4 pathway interactors. Specifically, we show that UNC-4 disables a signaling cascade involving the Frizzled proteins MOM-5 and MIG-1 to prevent VAs from responding to an EGL-20/Wnt cue that drives the creation of VB-type inputs. EGL-20/Wnt acts through a canonical Wnt signaling pathway to promote

expression of the VB protein and transcription factor CEH-12/HB9 which in turn leads to the miswiring of *unc-4* mutant VAs. This effect is regionally limited to VA motor neurons in the posterior nerve cord nearest the source of EGL-20/Wnt. The work also revealed *unc-4* interactions with G-protein signaling pathways that regulate VA input specificity. UNC-4 antagonizes the Gαo homolog, GOA-1/Gαo. GOA-1 has been previously shown to inhibit acetylcholine (Ach) release in opposition to the Gαq homolog, EGL-30 and the Gαs homolog, GSA-1. Intriguingly, *egl-30* and *gsa-1* also antagonize *goa-1* in the *unc-4* pathway. However, the roles for these G-proteins in synaptic choice are independent of their function in regulating Ach secretion and thus are likely to involve other downstream components of the Gαo, Gαq and Gαs signaling pathways. Our results show that GOA-1 signaling functions in parallel to the *egl-20*/Wnt pathway to regulate VA inputs. Together, these findings demonstrate the critical role of precise transcriptional control in the regulation of responses to signaling pathways that specify connectivity in the nervous system.

Approved: _____ Date_____

MOLECULAR ANALYSIS OF UNC-4 PATHWAY GENES THAT REGULATE SYNAPTIC CHOICE

By

Rachel Leah Skelton

Dissertation

Submitted to the Faculty of the

Graduate School of Vanderbilt University

in partial fulfillment of the requirements

for the degree of

DOCTOR OF PHILOSOPHY

in

Cell and Developmental Biology

August, 2012

Nashville, Tennessee

Approved:

David M. Miller III

Christopher V.E. Wright

Ethan Lee

Joshua Gamse

Chin Chiang

To my husband, Lou,

and to my family

ACKNOWLEDGEMENTS

I first need to thank my family. I absolutely could not have done this without my husband, Lou. We have gone through many tumultuous events during the 6 years that I have been in school, starting with moving our whole lives to Nashville from Hawaii so that I could come to Vanderbilt. Next came Lou's deployment to Iraq, our wedding, buying, gutting and renovating our house, Lou living in Nevada, then Washington DC, then Fort Chaffe, AR, having 13 bulldog puppies, Lou living in Amarillo, TX, then Oak Ridge, TN, losing 4 grandparents, and on a better note, finally enjoying our house and our houseboat. Lou has worked tirelessly to make sure that he could support us throughout this time and has made so many sacrifices in doing so. Now it is his turn to find something that he really wants and go after it, knowing that I support him.

Both of my parents and their significant others are scientists, so I have been surrounded by this environment my entire life. Having those role models and the unending support from my family has allowed me to dive head-first into things without the worry of whether I would fail or not. Although frustrating at times, since I have sometimes just wanted a parent to coddle me when I complain about how hard I have been working, or how annoying it is that my experiments keep failing, or how difficult it is to write a dissertation, it is also motivational to hear instead of sympathy, something like, "Well, we did it, so you definitely will be able to do it. Go for it." My Mom is the ideal role model for a strong woman in science that I hope I can one day emulate. I appreciate all of the sacrifices she has had to make to ensure that we grew up relatively normal and happy. My Dad is a forever optimist that truly has the "fire in his belly" about science. I admire his tenacity and the fact that he loves what he does. Jon has helped me in so many ways, from dog sitting on a moment's notice, to literally giving us a car, to being such a calm sounding board during moments of chaos. I am so happy that Jon and Lou

get along as well as they do. Nadene is a great role model for a strong woman in science who won't stay stuck in a job she isn't happy with. Thanks to Nadene's confidence in her skills, I realize that if I am not satisfied with the job I am doing, there are others out there and after all of this work, I don't want to just settle on something that I don't like. I want to thank Louis and Patti (another scientist!), who have helped us on countless occasions, from moving to Nashville to putting up with all of our dogs. I need to thank my sister, who has been there for me when I needed someone to vent to and even came and lived with me while Lou was in Iraq. It is so nice to have someone who I can relate to on so many different levels and still laugh with. I want to thank my grandmother, Bubbie. Although we mainly only get a chance to talk on my short walk home from work, her enthusiasm and support is unending. She is the best Bubbie I could ever ask for.

Of course, I have to thank my wonderful mentor, David Miller. Because my mom is a neuroscientist, I decided early on that I did not want to go in to that field. However, the first day that David taught IGP, I was so excited to see someone who cared so much about teaching first year students. After rotating, I was hooked. Finally, I had found a place where someone who was good at algebra and terrible at all other kinds of math, could excel-- with genetics! David has helped me to get an NRSA, develop my skills as an independent thinker and scientist, and at the same time he is so "normal," the one quality I was really searching for in a mentor. David's dedication to his family is one that I share, and I appreciate that he understands that, especially with mine and Lou's odd living situations, you have to have things right at home to be successful at work.

My lab mates, past and present, have made this entire process enjoyable. When I first joined the Miller lab, the group was a tight-knit clan of older students. Steve, Joseph, Kathie, Clay, Sarah and Jud were all incredibly helpful to me. I need to thank Jud Schneider for collaborating with me on the Genetics and Wnt portions of this thesis.

One reason I joined the Miller lab was because everyone took everyone else's science seriously and tried to help however they could. For instance, if someone had to give a public presentation, the whole lab would sit in for a practice talk and give detailed suggestions afterwards. We have strived to maintain this collaborative and supportive environment and I believe that all labs should strive for these attributes.

As the lab transitioned from an older wave of students to the entrance of two new students, Mallory and Cody, our fun definitely increased. From timer "cake" games to beer birthday, we maintained the supportive nature of the lab and had a great time doing it. I will be forever thankful to Mallory for being the best bay mate; she always listened, commiserated, and gave practical, solid advice. Cody has always been great to bounce ideas off of, and I appreciate his insightful comments on my science, as well as his sense of humor and music taste, both similar to mine. Tim and Becky have held the lab together and work so hard to make sure that things run smoothly. I know that Tim will succeed in his new PhD endeavor. Lastly, I would like thank Tyne, who has brought light and a new sense of enthusiasm to the lab. I know she will do great things in the future, hopefully all the while maintaining her positive and kind attitude.

I would like to thank my rotation students (all 10 of them!) for teaching me how to effectively teach, for their hard work in the lab and for taking pieces of this project further than they would have gone if I had needed to conquer them alone.

I would like to thank my thesis committee, Chris Wright (Chair), Chin Chiang, Ethan Lee and Josh Gamse, for giving me feedback and helping me improve as a scientist. I want to extend a special thanks to the Chair of my committee, Chris Wright. Chris consistently has gone out of his way to ensure that I succeed. Chris has written me numerous recommendations for all sorts of endeavors I have tried, including an application for a Dissertation Enhancement Grant, two NRSA submissions, an application for a summer internship as at the National Security Analysis and Intelligence

Summer Seminar, and most importantly, Chris really went out of his way to help me get a job following graduation. Not only did Chris write letters and help me with my CV, he also spent a lot of time talking with me about how to improve my confidence level as a speaker, and even went so far as to take his own time to have a late-night wine session with me to really get to know me and coach me on how to be a successful woman in science. I will be forever grateful to Chris for establishing and maintaining the Program in Developmental Biology (PDB), which funded me for two years and provides an incredible amount of support and opportunities to graduate students.

Kim Kane works tirelessly to provide activities to members of PDB. The Program is notorious for having the best retreat, best journal club, and most engaged members. Kim has been so supportive of me during my career and I really admire how she has incorporated her strengths into her job, it is obvious that it is a labor of love.

Thanks to PDB, I got to be the Student Director in Training and then Student Director of the Introduction to Developmental Biology (Boot Camp) class, taught by David Bader. David is an incredible scientist and mentor. His love of teaching is reflected not only by his dedication to the students in the class, but also the opportunities that he gave us Student Directors to both learn how to create a lesson plan and really get students involved in the class. David has a gift for getting people excited about science, and he has taught me many tricks to get people engaged. In addition, although he is a very accomplished scientist, David is very humble, and meets new ideas with enthusiasm. As a result, Boot Camp is constantly evolving to what sounds like will be the best class ever this year. I am jealous of the students who get to take it this summer.

I would like to thank my funding sources, which have included the Program in Developmental Biology NIH T32 HD007503 and the Ruth L. Kirschstein National Research Service Award F31 NS66597.

TABLE OF CONTENTS

LIST OF TABLES

LIST OF FIGURES

CHAPTER I

MULTIPLE FACTORS REGULATE SYNAPTIC SPECIFICITY

Introduction

The creation of functional circuits depends on the formation of active connections between neurons. Neurons are present in complex arrays and partner recognition is required for targeted specificity. The large number of potential synaptic partners that are available in complex neuronal environments suggests that mechanisms of cell specific recognition are necessary for selective synapse formation. For example, neurons in *C. elegans* synapse with only one out of six contacting cells [1]. Evidence of partner selectivity is even more compelling in the mammalian retina, where a given neuron makes synapses with only four of the 43 other neurons that it touches [2]. Thus, synaptic specificity can be defined as the selection interaction of pre and postsynaptic neurons among a wide array of possible partners.

Many factors contribute to synaptic specificity including the identity of specific neurons and their morphological development. Neuronal progenitors respond to morphogens and express distinct transcription factor codes that specify the identity of each neuron. For example, the developing vertebrate neural tube contains eleven discrete neural progenitor domains, each determined by differential expression of transcription factors [3]. These transcription factor codes and the neuron types that they specify are defined by the graded distribution of the morphogens Sonic Hedgehog, Wnt and BMP [3].

Following cell fate specification, each neuron extends an axonal projection, which must be positioned near its postsynaptic partner. The mechanism, known as axon guidance, is regulated by many conserved molecular cues, including Netrin, Slit, Semaphorin, and Wnt [4-6]. Because axon targeting is tightly coupled with synapse specification in projecting neurons, it is has proven difficult to determine which components are required for axon guidance versus those required for postsynaptic partner recognition. In the *C. elegans* motor circuit, motor neuron processes occupy a tight fascicle in the ventral nerve cord. In this case, synapses are formed *en passant*, indicating that these neurons must utilize a mechanism that recognizes specific partners [1]. Once the neuronal architecture is established via guidance and fasciculation events, the presynaptic axon must then correctly identify its postsynaptic partner, termed synaptic choice [7]. The focus of this dissertation will be on the molecules, pathways, and mechanisms involved in synaptic choice.

Cell surface components regulate synaptic choice

Both positive and negative regulators orchestrate synaptic choice (Fig. 1.1A). Cell surface components, including neurexins, neuroligins, and members of the cadherin and Ig-domain families, have been shown to affect synaptic assembly (Fig. 1.1A) [8-13]. Adhesion molecules may drive mutual attraction of partner neurons. These recognition events can involve either identical (homophilic) or dissimilar (heterophilic) pairs of interacting proteins. For example, N-cadherin is required for the targeting of photoreceptor (R) cells in the *Drosophila* eye [14]. N-cadherin expression in R1-6 axons directs R axons to the appropriate target lamina, which also expresses N-cadherin. It is thought that N-cadherin may play a stabilizing role in the interaction between the R axon and lamina target [14]. In another example of cell surface molecules regulating synaptic

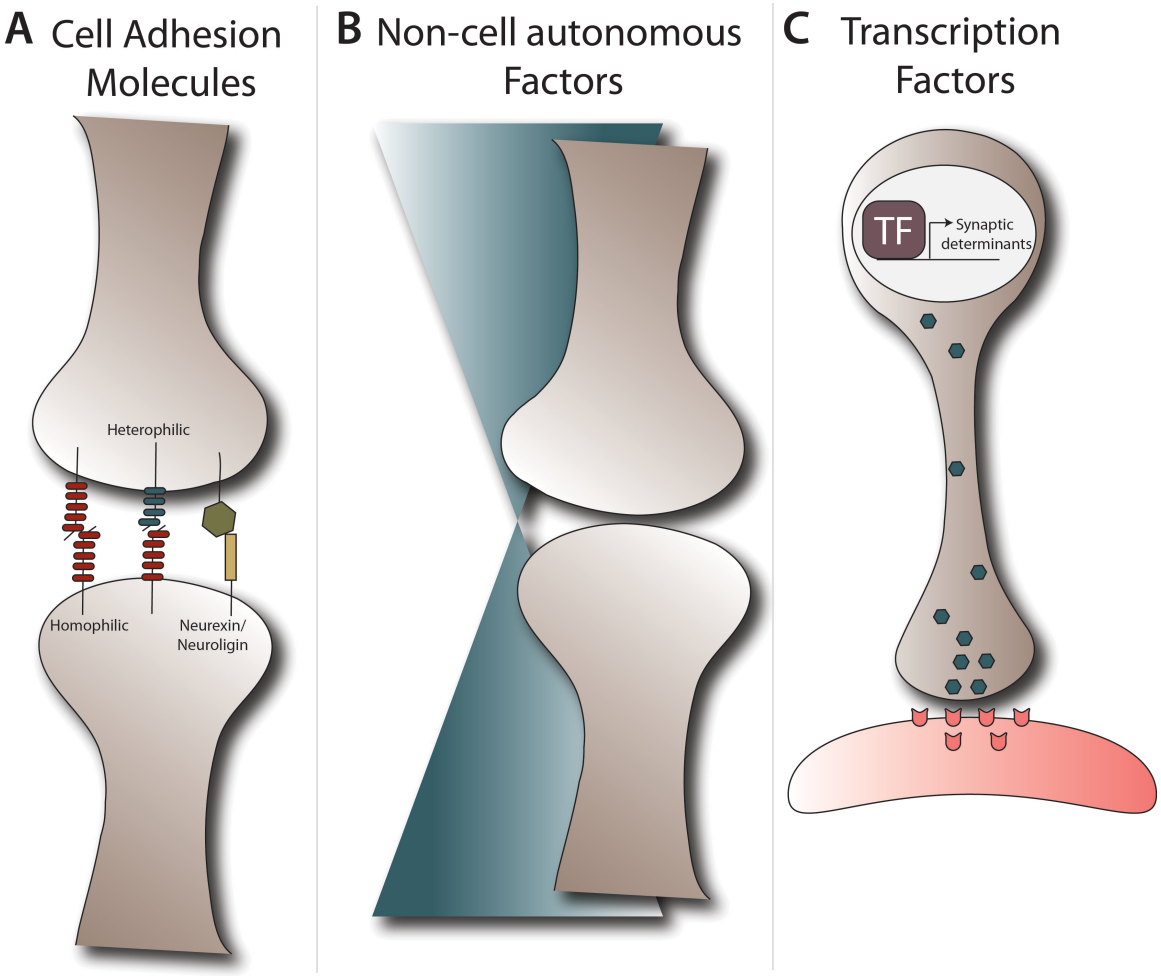

Figure 1.1. Multiple factors can regulate synaptic specificity. **A.** Cell-surface adhesion molecules can interact via heterophilic or homophilic mechanisms. Neurexin (presynaptic) and Neuroligin (postsynaptic) interact to maintain synapses. **B.** Non-cell autonomous factors (blue wedges) regulate synaptic choice. Neighboring cells may express cell surface determinants or secrete morphogens that control synaptogenesis. **C.** Transcription factors regulate expression of synaptic determinants (blue hexagons) that specify connections between pre and postsynaptic targets, marked with neurotransmitter receptors (red blocks).

choice, the IgSF-proteins, SideKick and Dscam, utilize homophilic interactions to direct innervation of specific target lamina in the vertebrate retina [10, 15].

Neurexin and neuroligin are transmembrane proteins that function via heterophilic interaction [16]. Neurexin is expressed presynaptically and neuroligin is located on the postsynaptic membrane. The many splice variants of both neurexin and neuroligin may afford a large number of unique partner combinations. Interestingly, heterologous expression of Neurexin or Neuroligin in non-neuronal cells induced synapse-like contacts with co-cultured neurons. Additionally, the overexpression of either Neurexin and Neuroligin showed an increase in synapse number in these cultured cells [16]. However, it is believed that Neurexin and Neuroligin serve a maintenance role at the synapse, as loss of either protein *in vivo* did not affect total synapse number but instead resulted in less efficient synapses [16]. In addition to interacting with each other, Neurexin and Neuroligin have other binding partners. These include the postsynaptically expressed leucine rich repeat transmembrane neuronal proteins (LRRTMs), which bind to Neurexin and may function redundantly with Neuroligin to promote synaptic differentiation [16]. The presynaptically secreted glycoprotein, Cerebellin1 precursor protein (Cbln1), mediates the binding of presynaptic Neurexin with the postsynaptically expressed glutamate receptor (GluR) δ2 and is required for synapse formation between cerebellar granule cells and Purkinje cells [16]. Thus, multiple protein-types mediate the functions of Neurexins and Neuroligins, thereby providing additional levels of specificity to synapse formation [16].

Negative regulators that prevent the creation of dysfunctional synapses are also critically important to the mechanism of synaptic specificity. Studies of the *Drosophila* neuromuscular junction have shown that Toll, a transmembrane protein with leucine-rich repeats, inhibits synapse formation between multiple motor neuron and muscle partners [17, 18]. Toll is expressed in all ventral muscles with the exception of the M12 muscle,

where the transcription factor, Tey, represses Toll expression, thus permitting selective innervation by the MN12 neuron. Tey expression in M12, and consequent repression of Toll, effectively insures the specificity of motor neuron inputs [17].

Wnt signaling has been shown to function as a negative regulator of synaptic choice. The same group that discovered the Tey/Toll interaction (above), previously discovered a difference in Wnt4 mRNA expression in the M12 *vs.* M13 muscles that contributes to motor neuron specific innervation [19]. Wnt4, along with the receptors Frizzled 2, Derailed-2 and the cytosolic component Dishevelled, are expressed in M13 and inhibit the M12 motor neuron partner from inappropriately connecting with M13 [19]. Thus, the combined action of these local repulsive cues is required for synaptic target specificity.

Non-cell autonomous factors regulate synaptic choice

In addition to the cell autonomous components that regulate synaptic specificity, extracellular cues that affect synaptic choice may be contributed by nearby "guidepost" cells that are not directly involved in synaptic formation (Fig. 1.1B) [20-23]. For example, the atypical cadherin, Flamingo, which has been implicated in planar cell polarity (PCP) signaling [24], also controls the trajectory of the R retinal cell axons in the *Drosophila* ommatidia. Flamingo is expressed in all R cells, but functions non-cell autonomously in an adjacent R cell to direct postsynaptic photoreceptor target selection of the neighboring R cell [20, 25].

Another example of role for a non-cell autonomous cell surface determinant of synaptic specificity is provided by the interaction of the Ig-domain proteins SYG-2 and SYG-1 in *C. elegans*. SYG-2 and SYG-1 function as guidepost and synaptic-location regulators, respectively, for the *C. elegans* HSN neuron [22, 26, 27]. SYG-2 is expressed in vulval epithelial cells adjacent to the HSN neuron in a location that defines the site of

the HSN synapse. SYG-1 is expressed in the HSN neuron and the SYG-1/SYG-2 interaction stabilizes local synapses by blocking the activity of the ubiquitin-and proteasome-dependent system of protein degradation [27]. The axon targeting of the HSN neuron is normal in both *syg-1* and *syg-2* mutants, suggesting that these Ig domain proteins function specifically to regulate synaptic choice. This mechanism of specific synapse formation in the *C. elegans* egg laying circuit also reveals a critical role for adjacent, non-neuronal guidepost cells (e.g. SYG-2 localization).

Recent work in *C. elegans* has implicated the morphogen UNC-6/Netrin as both a regulator of axon guidance and presynaptic assembly molecule [23]. The presynaptic AIY and postsynaptic RIA interneurons both express the UNC-6 receptor, UNC-40/DCC. An adjacent glial cell expresses UNC-6. The UNC-6 cue from the glial cell is necessary for ventral migration of the RIA neuron to a position proximal to AIY. Interestingly, the Netrin cue from the sheath cell is also independently required for presynaptic assembly in AIY and the synapse with RIA [23]. This work provides a striking example of the diverse roles of a morphogen that can provide both long and short-range signals for establishing the exact location of a synapse.

Transcription factors regulate synaptic choice

Transcription factors may directly regulate synaptic components, or may function in transcriptional cascades with indirect roles in synaptic choice (Fig. 1.1C). For example, a transcriptional mechanism regulates the lamina targeting specificity of *Drosophila* R7 *vs.* R8 photoreceptor axons. The R8-specific transcription factor, Senseless, promotes expression of the leucine-rich repeat cell surface protein, Capricious, that specifies R8 photoreceptor targeting in the medulla. Senseless expression is normally blocked in R7 neurons by the NF-Y transcription factor. The crucial role of NF-Y function in R7 targeting is revealed in an NF-Y mutant, in which R7

adopts R8-type connections [28]. Thus, in this case, one transcription factor, Senseless, exercises a direct role in synaptic targeting by controlling expression of the cell surface protein, Capricious, whereas a second transcription factor, NF-Y, functions in R7 cells in an indirect mechanism that prevents expression of Capricious by transcriptional repression of Senseless. Interestingly, the effects of NF-Y are likely specific to synaptic choice, *versus* affecting cell fate, as the R8-type targeting defect observed in NF-Y mutant R7 cells happens later in development and does not perturb expression of other R7-specific genes [29].

Hox genes are essential in determining body plan organization. In addition to this role in early development, Hox genes also regulate motor neuron pool identity and connectivity between motor neurons and muscle [30, 31]. The motor neuron classes of preganglionic column (PGC) motor neurons normally innervate sympathetic ganglia and hypaxial motor column (HMC) neurons normally innervate the intercostal and abdominal wall musculature [31]. However, forced expression of Hoxc6 or Hoxd10 in PGC or HMC neurons converts these neurons to lateral motor column (LMC) neurons and alters their axonal projections to project into the limb, the target area of endogenous LMC neurons [30, 32]. Instead of directly controlling expression of synaptic components, Hox genes control intermediate targets (*i.e.* RALDH2) that regulate downstream signaling cascades required for proper synaptic connectivity [31].

In another example of transcription factor regulation of synaptic choice, the ETS-type transcription factor, Pea3, regulates expression of a Semaphorin protein, Sema3e. Normally, Pea3 and Sema3e are expressed in the cutaneous motor neuron pool, which does not receive direct inputs from proprioceptor neurons. In contrast, triceps motor neurons do not express Pea3 (or Sema3e) and receive direct, monosynaptic inputs from proprioceptor neurons. This difference in connectivity may be attributed in part to the selective expression of the Sema3a receptor Plexin d1 in proprioceptor neurons where it

prevents the creation of inputs to cutaneous motor neurons [33, 34]. Interestingly, a loss of Sema3e is not sufficient to induce the complete disruption of specificity, as ectopic inputs from proprioceptor neurons are limited to the cutaneous motor neuron pool and are not made onto other motor neuron pools. This finding suggests that additional levels of regulation contribute to the overall wiring structure of this sensory-motor circuit.

The UNC-4 transcription factor regulates synaptic choice in *C. elegans* motor neurons

Work in the Miller lab has shown that the UNC-4 transcription factor controls synaptic specificity in the *C. elegans* motor circuit by repressing a VB-motor neuron program in sister VA motor neurons [35]. *unc-4* is selectively expressed in larval VA motor neurons, which arise from a common progenitor with sister VB motor neurons [36, 37]. VA motor axons (1.2, **BLUE**) project anteriorly and inputs are provided by the command interneurons AVA (gap junction & chemical synapse) and AVD, AVE (chemical synapse); together these neurons confer backward locomotion. VB motor neurons (Fig. 1.2, **RED**) extend posteriorly directed axons and receive inputs from interneurons in the forward motor circuit, AVB (gap junction) and PVC (chemical synapse).

unc-4 mutants display a striking behavioral defect, the inability to move backward. Serial electron micrograph (EM) reconstruction of the *unc-4*(*e120*) mutant indicates that the impaired movement phenotype is due to a specific miswiring defect [38]; VA motor neurons lose connections from interneurons in the backward motor circuit

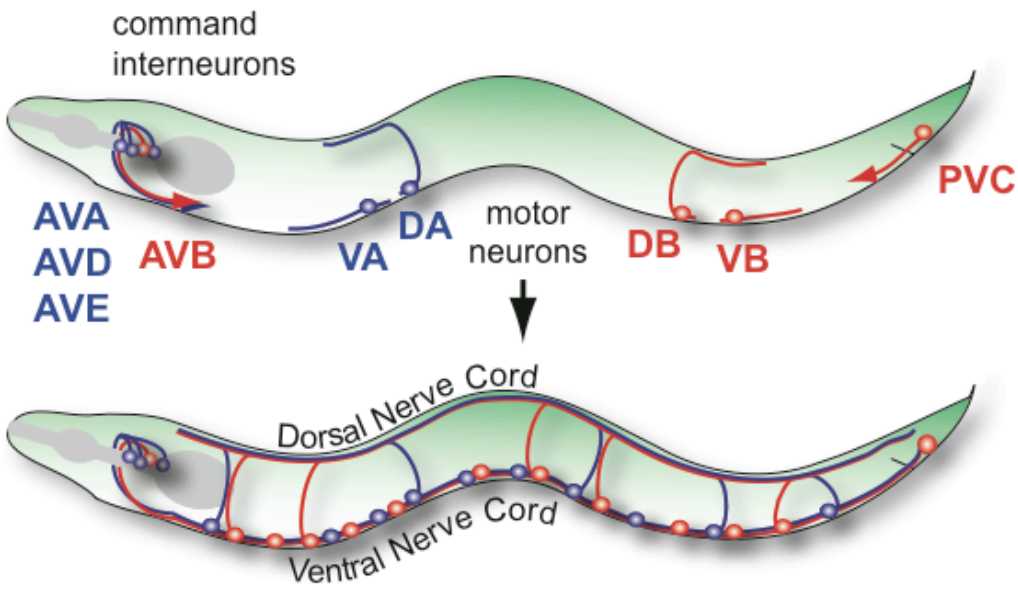

Figure 1.2. *C. elegans* motor circuit. *C. elegans* command interneurons extend axons from either the head or tail regions and synapse with specific motor neuron cell bodies located on the ventral side of the animal. Interneurons (AVA, AVD, AVE) and motor neurons (DA, VA) in the backward locomotory circuit are labeled in blue. Interneurons (AVB, PVC) and motor neurons (DB, VB) of the forward movement circuit are labeled in red.

and adopt synaptic partners normally reserved for VB sisters (Fig. 1.3). However, the anterior polarity of VA motor axons is preserved, indicating that *unc-4* regulates downstream components that specify VA class specific inputs but not other morphological features that distinguish VA and VB sisters [38].

Genetic and biochemical studies in the Miller Lab have shown that UNC-4 function depends on interaction with the transcriptional co-repressor UNC-37/Groucho. Thus, we hypothesize that the UNC-4/UNC-37 complex functions in VA motor neurons to repress VB genes [39-42]. In this model, VB genes are ectopically expressed in VA motor neurons in *unc-4* mutants, leading to the adoption of VB-type synaptic inputs and impaired backward locomotion (Fig. 1.3). Repression by UNC-4 of genes that regulate VB-type inputs in VAs resembles the mechanisms illustrated above in regulation of Toll by the Tey transcription factor [17] and the repression of R8 motor neuron specific inputs onto R7 by NF-Y [28]. Thus, repression of "default" synaptic programs is a conserved mechanism for regulating synaptic specificity.

Cell-specific microarray technology developed by the Miller Lab has revealed potential downstream targets of UNC-4/UNC-37 (Table 1.1) [42-44]. One of these *unc-4* target genes is the HB9 homolog, *ceh-12*. The HB9 transcription factor specifies motor neuron fate in multiple systems [45, 46]. *ceh-12*/HB9 expression is normally limited to VB motor neurons but is ectopically expressed in VAs in an *unc-4* mutant. A role for *ceh-12* in motor circuit development is likely to be evolutionarily ancient, as the *ceh-12* homolog, HB9, directs motor circuit fate in *Drosophila*, birds, and mammals [46-48]. Interestingly, ectopic expression of *ceh-12* in *unc-4* mutant VAs is limited to VA motor neurons in the posterior nerve cord. This effect is required for the formation of ectopic gap junctions between AVB and posterior VAs and thus confirms that *ceh-12*/HB9 regulates synaptic specificity [42].

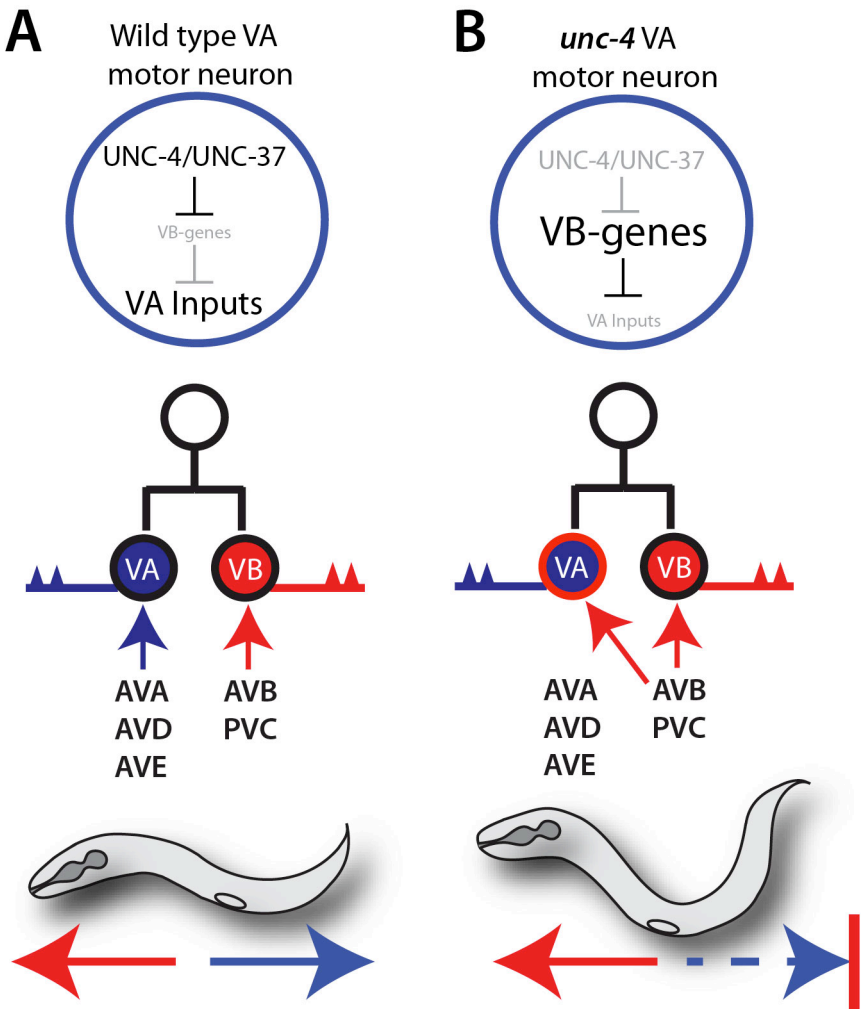

Figure 1.3. *unc*-4 regulates the specificity of synaptic inputs to VA motor neurons. **A.** VA and VB motor neurons arise from a common progenitor cell but adopt opposite trajectories and inputs from separate sets of interneurons. In wild-type VAs, the UNC-4 transcription factor, with the UNC-37/Groucho cofactor represses VB-specific gene expression, to preserve inputs from presynaptic partners (AVA, AVD, AVE) that drive backward locomotion. **B.** In *unc*-4 mutant VA motor neurons, VB-genes are derepressed and in turn block the creation of normal VA inputs and favor synapses from AVB (gap junctions) and PVC (chemical synapse). Thus, VA motor neurons are miswired with inputs from forward motor circuit interneurons that are normally reserved for their VB sister cells.

A *ceh-12* mutant partially suppresses the Unc-4 backward movement defect; in *ceh-12(0);unc-4(0)* double mutants, normal inputs to posterior VAs are restored and backward locomotion is improved [42]. VB-type inputs to anterior VAs are not eliminated in *ceh-12(0); unc-4(0)* mutants, however. This result has led to the proposal that additional parallel pathways are likely to function downstream of *unc-4* to specify inputs to anterior VAs [42].

Chapter II describes results from a reverse genetic screen was designed to identify additional *unc-4* pathway genes. The genetic strategy was based on the observation that *ceh-12(0)* regulates synaptic specificity to a subset of VAs and affords only partial restoration of the Unc-4 backward movement defect. Thus, mutations in other *unc-4* regulated genes with partial roles in synaptic specificity should also show "weak" Unc-4 suppression phenotypes.

The canonical Wnt signaling pathway

The secreted polypeptide, Wnt, is a morphogen with potent roles in a wide range of developmental processes, including cell polarity, tissue patterning, and cell migration [49-51]. Wnts have been shown to act as patterning cues along the anterior/posterior body axis in organisms ranging from planaria to humans [52-57]. Wnt activates a downstream signaling cascade by binding to a seven transmembrane Frizzled receptor and the co-receptor LRP-5/6/Arrow (Fig. 1.4). To date, a homolog for LRP-5/6/Arrow has not been identified in *C. elegans*; however, other Wnt components (*i.e. pry-1*/Axin) were initially thought to not exist in *C. elegans* due to the lack of sequence identity with Axin proteins in other species [58]. Thus, there remains the possibility of future identification of an LRP-5/6/Arrow homolog in *C. elegans*. In the canonical Wnt pathway, the cytoplasmic Dishevelled protein transduces the active Wnt signal to inhibit binding of the

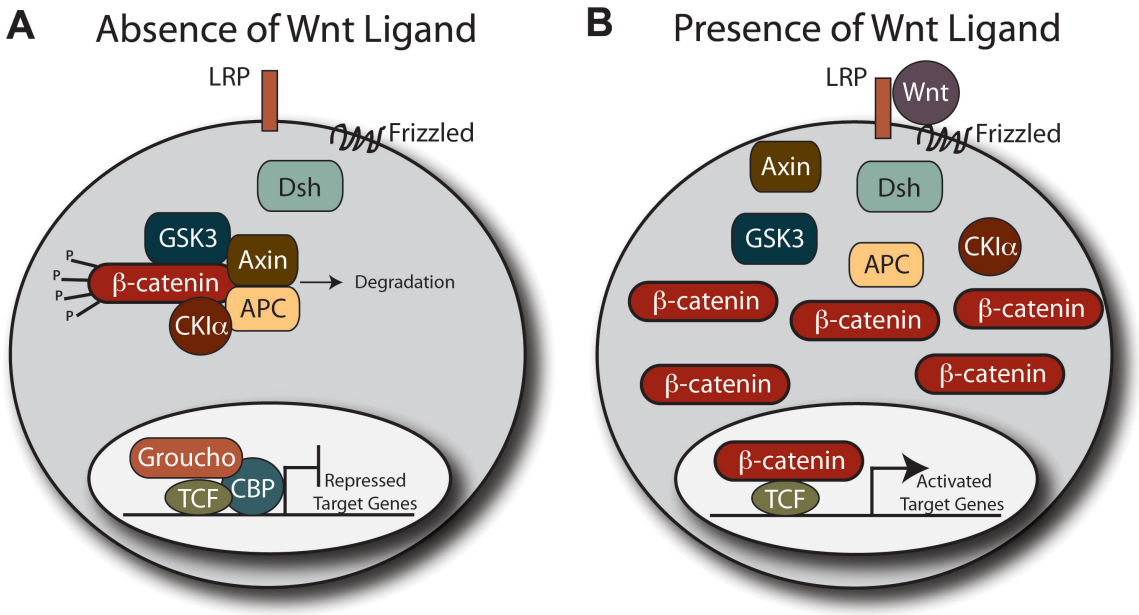

Figure 1.4. Schematic of the canonical Wnt signaling pathway. **A.** In the absence of Wnt ligand, β-catenin is sequestered by the "Destruction Complex," composed of the scaffold proteins Axin and APC and the kinases, GSK3β and CKIα, which phosphorylate β-catenin and target it for degradation by the ubiquitin proteasome pathway. The TCF transcription factor, bound by Groucho and CBP, represses Wnt target genes. **B.** Upon binding of the Wnt ligand to Frizzled receptor and LRP5/6/Arrow co-receptor, components of the Destruction Complex are sequestered at the plasma membrane, thereby preventing degradation of β-catenin. β-catenin translocates to the nucleus and competes with Groucho for binding to TCF and consequent activation of Wnt pathway target genes.

Table 1.1. Wnt pathway components that are enriched (bold text) or not enriched (gray text) in A-class motor neurons. Suppressors of the "Unc-4/Unc-37 Suppressor" indicates that mutation in the Wnt pathway gene suppresses the backward movement defect. "Additional Wnt pathway genes" enhance the Unc-4 backward movement defect or have not been tested.

Component	Unc-4/Unc-37 Suppressor	Additional Wnt Pathway Genes
Wnt	*egl-20*	***cwn-1, cwn-2,*** *lin-44, mom-2*
Frizzled	***mom-5, mig-1***	***lin-17, cfz-2***
Disheveled	***dsh-1***	***dsh-2,*** *mig-5*
Destruction Complex	Not tested	***pry-1*****/Axin, *gsk-3*****/GSK-3β, *apr-1*****/APC**
β-catenin	***bar-1***	*sys-1, wrm-1, hmp-2*
TCF-LEF	*pop-1*	N/A

Destruction Complex to β-catenin (Fig. 1.4B). In the absence of an active Wnt signal, components of the Destruction complex, which include the scaffold protein Axin, the kinase GSK-3β and the Adenomatous Polyposis Coli (APC) protein, phosphorylate β-catenin to mark it for ubiquitin-mediated degradation (Fig. 1.4A). Wnt binding results in the translocation of intact β-catenin to the nucleus where it interacts with the TCF-LEF transcription factor to activate a transcriptional program (Fig. 1.4B). Homologous proteins for most of these Wnt signaling components are expressed in *C. elegans* (Table 1.1) [58-64]. In addition to BAR-1, the specific β-catenin that functions in canonical Wnt signaling, *C. elegans* also has three other β-catenins with distinct functions in non-canonical pathways that regulate polarity (*wrm-1*), asymmetric cell divisions (*sys-1*) or the assembly of cadherin complexes (*hmp-2*) [60, 65, 66]. *C. elegans* has only one TCF-LEF homolog, *pop-1*, which regulates transcription in both canonical and non-canonical Wnt signaling pathways [67, 68].

Noncanonical Wnt signaling

As described above, canonical Wnt signaling involves the regulation of β-catenin and subsequent effects on target gene transcription. However, Wnt pathway components are also involved in many other essential cellular and developmental processes, including polarized cell migration, cytoskeletal organization in epithelial cells and asymmetric cell fate determination [69]. These processes involve some components that are also utilized for canonical Wnt signaling, but do not converge on β-catenin regulation. Thus, these pathways are termed “noncanonical”. Two broadly defined noncanonical Wnt signaling pathways have been identified in *C. elegans*. These are the Wnt/PCP/JNK and Wnt/calcium pathways. The PCP pathway regulates cytoskeletal dynamics and utilizes the Frizzled (receptor), Van Gogh (transmembrane protein),

Flamingo (atypical cadherin), Prickle, Diego and Dishevelled (cytosolic proteins), and the GTPases Rac1 and RhoA, which activate c-Jun-N-terminal kinase (JNK) and Rock, respectively [51, 70]. To date, a Wnt ligand that activates PCP signaling in *Drosophila* has not been identified; however, mammalian Wnt5a and Wnt11 have both been shown to activate noncanonical PCP signaling by binding Frizzled receptors [70]. The Wnt/calcium pathway regulates transcriptional and cytoskeletal events. This pathway involves G proteins that are activated by Wnt-bound Frizzled receptors. The G proteins activate phospholipase C, which increases intracellular calcium levels and activates protein kinase C (PKC) and calcium calmodulin mediated kinase II (CAMKII) [70].

Interestingly, although it was previously believed that different Wnt ligands and Frizzled receptors functioned characteristically through either “canonical” or “noncanonical” pathways, recent evidence shows that receptor-ligand affinity and regional concentrations may dictate the downstream cascade activated by a particular ligand [71]. Thus, the localization, whether spatial or temporal, of Wnt components may be just as important in signaling as the affinity between particular Wnts and Frizzled receptors.

Noncanonical Wnt signaling pathways have been shown to regulate asymmetric division of different *C. elegans* cell types (*i.e.* the embryonic blast cell, Z1/Z4 gonadal precursor cells and T blast cells) [72]. For instance, nuclear levels of the Wnt transcription factor POP-1/TCF, determine asymmetric cell fate in many different cell types in the early embryo [69]. The noncanonical β-catenin, WRM-1, along with LIT-1/Nemo-like kinase, is expressed in posterior daughter cells, facilitating the nuclear export of POP-1. Thus, POP-1 expression is low in posterior daughter cells and high in anterior daughter cells that do not express WRM-1 and LIT-1 [72]. Because PCP homologs are non-essential in *C. elegans*, there is speculation as to whether *C. elegans* utilizes a “true” PCP-type pathway [72]. However, asymmetric division of at least one *C.*

elegans cell type has been shown to utilize PCP components including Dishevelled (*C. elegans,* MIG-5), Van Gogh (*C. elegans,* VANG-1), and Prickle (*C. elegans* PRKL-1) [72]. Recent work has revealed a role for *vang-1* and *prkl-1* in regulating neurite outgrowth in *C. elegans* [73]. In this case, *prkl-1* functions downstream of *vang-1* and *dsh-1* in VC4 and VC5 neurons of the egg-laying circuit to regulate VC polarity. Interestingly, other aspects of VC4 and VC5 morphology are unchanged, suggesting that this PCP-like pathway specifically regulates neurite outgrowth in these neurons [73].

Wnt signaling at the synapse

Wnt signaling is required for many aspects of synaptic formation, including synaptic assembly and axon guidance [19, 74-80]. Bi-directional Wnt signaling coordinates the formation of both presynaptic and postsynaptic domains at the *Drosophila* neuromuscular junction (NMJ). Interestingly, postsynaptic assembly depends on Wnt-regulated gene transcription whereas presynaptic effects are mediated by a local mechanism that controls the stabilization of microtubules [76, 81]. In this case, Shaggy/GSK3 phosphorylates the microtubule-associated protein, Futsch, independent of β-catenin and TCF, which regulate transcription of Wnt target genes [81]. Additionally, a pathway involving the ligand Wnt7a has been implicated in presynaptic function in rat hippocampal neurons as a critical control mechanism of synaptic vesicle clustering, recycling, and transmission [82]. Wnt7a is required in the mouse cortex for proper targeting and presynaptic assembly in mossy fiber neurons [83, 84]. Additional regulation of synapse formation in the hippocampus involves Wnt7a, Wnt7b and Wnt5a. Wnt7a and Wnt7b function through a canonical Wnt pathway to increase synaptic inputs to cultured hippocampal neurons, whereas Wnt5a, functioning through a noncanonical Wnt pathway, may reduce the number of inputs [51, 85]. Opposing Wnt pathways have also been shown to regulate cell polarity in *C. elegans* vulval precursor cells [86]. Thus,

interactions between opposing Wnt pathways to regulate neuronal processes is a conserved mechanism.

Emerging evidence indicates that other Wnt receptors, in addition to Frizzled proteins, regulate synapse formation. For example, the vertebrate Wnt receptor, Ryk/Derailed (*C. elegans*, LIN-18 [87]), mediates a repulsive response to an A/P Wnt gradient to drive caudal outgrowth of corticospinal tract axons [88, 89]. Additionally, the Ror1 and Ror2 tyrosine kinase receptors (*C. elegans,* CAM-1 [90]) are required for the formation of presynaptic components in cultured hippocampal neurons [91].

In *C. elegans,* a Wnt pathway regulates the physical location of a specific motor neuron synapse with body muscle [79]. In this example, the Wnt ligands LIN-44 and EGL-20 interact with the Frizzled protein, LIN-17, in the DA9 motor axon to prevent synapse formation in a posterior axonal compartment. The proximity of the position source of LIN-44 and EGL-20 defines the location of this negative interaction. In this case, the Wnt receptor, LIN-17, blocks the formation of a local synapse. Although the cellular mechanism of this effect is largely unknown, this work provides a striking example of a Wnt signal (LIN-44, EGL-20) effectively inhibiting synaptic assembly in a particular axonal domain [79].

Chapter IV describes our discovery of a second role for these Wnt signals in regulating synaptogenesis in the motor circuit. In this case, EGL-20 and LIN-44 activate opposing pathways that control the specificity of synaptic inputs to VA motor neurons.

G protein signaling

G protein signaling pathways have been implicated in many cellular processes, including regulation of metabolic enzymes, ion channels and transcriptional cascades

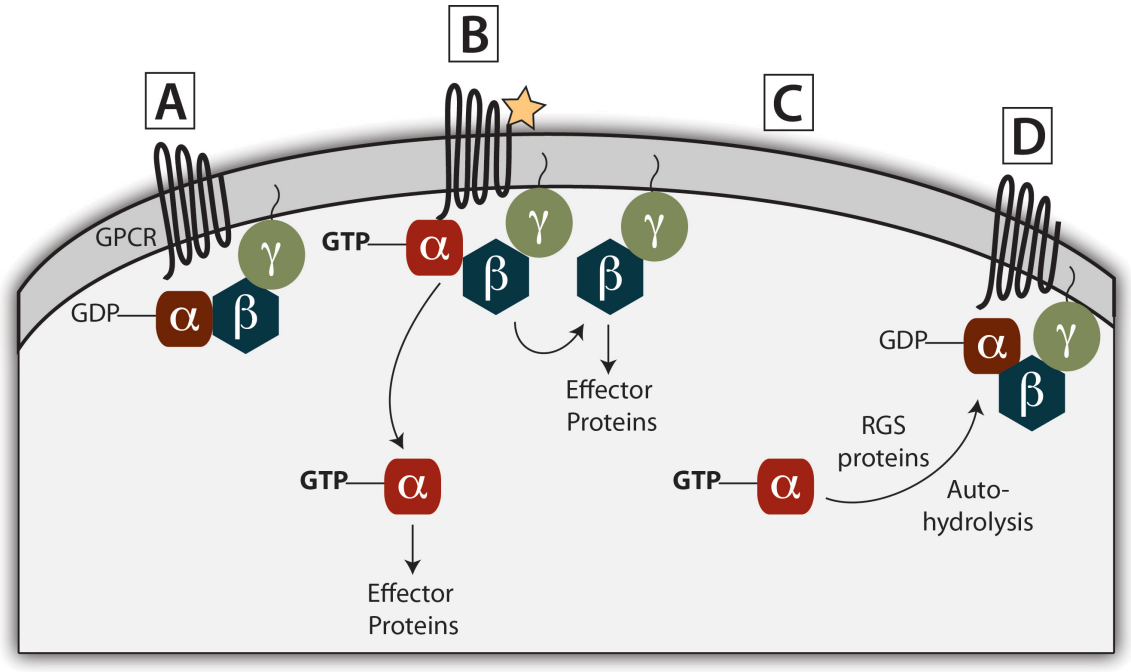

Figure 1.5. Schematic of canonical G-protein signaling. **A.** In the absence of signal, G protein α, β and γ subunits exist in a heterotrimeric complex, with the α subunit bound to GDP. **B.** Ligand (yellow star) binding induces the 7-transmembrane G protein coupled receptor (GPCR) to exchange the GDP for GTP bound to the α subunit. The GTP-α subunit dissociates from the βγ complex and both components can then regulate effector proteins. **C.** Regulator of G protein signaling (RGS) proteins may enhance the auto-catalytic hydrolysis of GTP-α to GDP-α. **D.** The GDP-α subunit reassociates with the βγ complex into an inactive heterotrimer.

[92]. The mechanistic output of G protein signaling is to transduce signals from receptors at the cell surface to intracellular effector proteins at the inner surface of the plasma membrane. The steps of G protein signaling are outlined in Fig. 1.5. G proteins are heterotrimeric complexes comprised of α, β and γ subunits. The α subunit is bound to GDP in the heterotrimeric complex with the β and γ subunits. Ligand binding to the 7-transmembrane G protein coupled receptor (GPCR) results in exchange of GDP for GTP on the Gα subunit. The Gα subunit then dissociates to interact with different downstream effector molecules. β and γ subunits are tightly associated in a complex and thus regulate effector molecules together. Regulator of G protein signaling (RGS) proteins and/or the auto-catalytic mechanisms of the α subunit return the α subunit to the GDP-bound state [93], resulting in subsequent reassociation with the βγ subunits and inactivation of the α protein [94]. There are 21 genes that encode Gα proteins in *C. elegans* with at least one ortholog of each mammalian Gα family [95]. Additionally, there are two genes that encode Gβ and Gγ proteins, *gpb-1, gpb-2* and *gpc-1* and *gpc-2*, respectively [95]. The roles for G proteins in *C. elegans* are varied, including in embryo spindle pole positioning, viability and hatching. Additionally, substantial genetic evidence implicates a coordination of G protein pathways involving GOA-1/Gαo, EGL-30/Gαq and GSA-1/Gαs in egg laying and locomotion through the regulation of acetylcholine release [95]. Chapter V discusses this topic more extensively, focusing on the role for *goa-1*, *egl-30* and *gsa-1* in synaptic choice.

Multiple downstream signaling cascades have been identified for Gαq, Gαs and Gαo pathways (Fig. 1.6) [92]. Upon activation of the Gαq pathway, phospholipase C β (PLCβ) produces inositol tri-phosphate (IP3) and diacylglycerol (DAG). IP3 diffuses through the cytosol and binds to the IP3 receptor on the endoplasmic reticulum, which activates the release of calcium into the cytosol. DAG binds several downstream effectors, including PKC and UNC-13 [92, 95]. Downstream of the Gαs pathway,

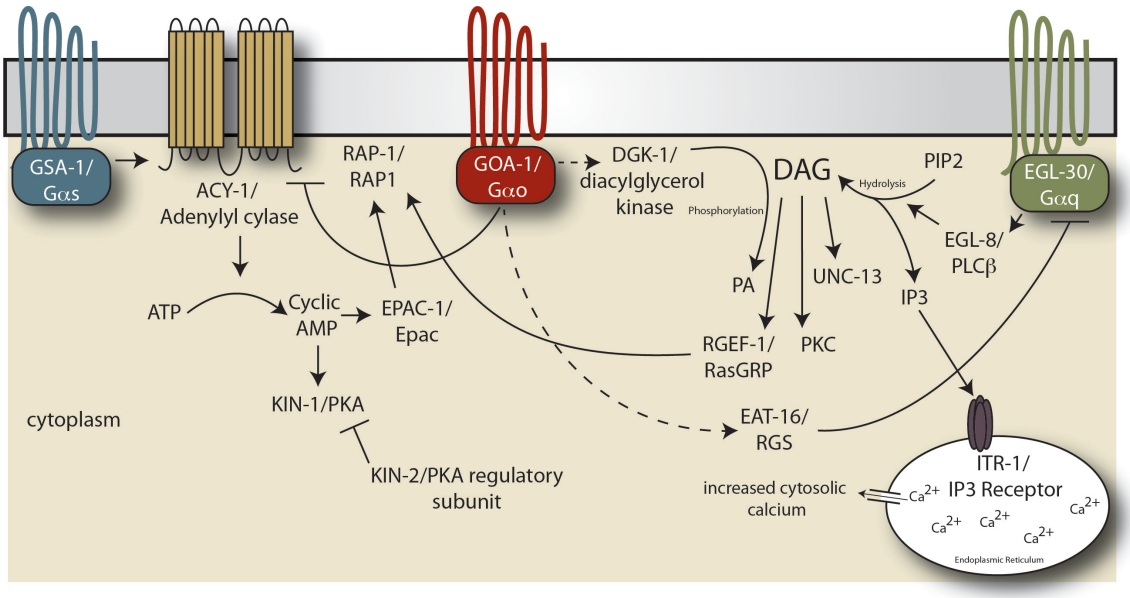

Figure 1.6. G-protein signaling pathways in *C. elegans*. The GSA-1/Gαq pathway activates ACY-1/Adenylyl cylase, which synthesizes cyclic (cAMP) from ATP. cAMP can go on to bind many proteins, including KIN-1/protein kinase A (PKA) and EPAC-1/Effector protein activated by cAMP (EPAC). The GOA-1/Gαo pathway might antagonize the GSA-1 pathway by binding to and inactivating ACY-1. GOA-1 signals through DGK-1/Diacylglycerol kinase and EAT-16/Regulator of G protein signaling (RGS). Dashed arrows indicate genetic interactions. EGL-30/Gαq activates EGL-8/Phospholipase C β (PLCβ), which hydrolyzes phosphatidylinositol 4,5-bisphosphate (PIP2) to form diacylglycerol (DAG) and inositol triphosphate (IP3). DAG binds target proteins including RGEF-1 (RasGRP), protein kinase C (PKC) and UNC-13. RGEF-1 and EPAC-1 can bind to and activate RAP-1, which has been implicated in gap junction assembly. IP3 diffuses to the endoplasmic reticulum (ER) and binds to ITR-1/IP3 receptor, which induces transport of calcium (Ca^{2+}) out of the ER and into the cytoplasm. The GOA-1 effector EAT-16/RGS antagonizes the Gαq pathway by inactivation of EGL-30.

adenylyl cyclase synthesizes cAMP, which activates effector molecules including PKA and Epac (Fig. 1.6) [92].

G protein signaling regulates gap junction function

G proteins regulate both chemical and electrical synapses in the brain. Chemical synapses utilize synaptic vesicles filled with neurotransmitters and electrical synapses consist of gap junction channels. In *C. elegans*, *goa-1*/Gαo, *egl-30/*Gαq and *gsa-1/*Gαsregulate synaptic vesicle release at the neuromuscular junction [95]. *goa-1*/Gαo and *gsa-1/*Gαs have also been shown to function antagonistically to control the formation of gap junctions within developing oocytes in *C. elegans* [96]. Multiple examples of G- protein regulation of gap junctions exist in vertebrate systems. For instance, assembly of connexin 43 (Cx43) channels, a vertebrate gap junction channel protein, is regulated by G-protein signaling [97]. The Gαi/o and Gαs pathways regulate intracellular localization of gap junction components [98] and gap junction assembly [95, 99]. The Gαs second messenger, cAMP, regulates the synthesis and trafficking of Cx43 to the plasma membrane [100]. Additionally, phosphorylation of Cx43 is mediated by cAMP through PKA, which results in the regulation of gap junction gating [100]. Recently, the cAMP binding protein, Epac, has been shown to function cooperatively with PKA to enhance gap junction function; PKA regulates gap junction gating while Epac binds the small GTPase, Rap1. Rap1 may regulate Cx43 trafficking to the plasma membrane [101]. Despite the various roles described for G proteins in synapses, G-protein signaling has not been previously implicated in regulating synaptic specificity.

Chapter V describes a role for GOA-1/Gαo in regulating synaptic choice in the *unc-4* pathway. Both *goa-1* and its downstream effector, EAT-16/RGS are required for

ectopic AVB gap junctions with *unc-4* mutant VA motor neurons. In contrast, EGL-30/Gαq, functioning through EGL-8/PLCβ and GSA-1/Gαs via ACY-1/adenylyl cyclase, opposes AVB gap junctions with VA motor neurons. Based on the roles for G proteins in gap junction formation, we hypothesize that these G-protein pathways converge on gap junction regulation of VA motor neurons.

Chemical synapses

In addition to gap junctions that constitute "electrical synapses," neurons also communicate via chemical synapses that utilize neurotransmitter signals. Visualization techniques have been critical for revealing salient aspects of chemical synapse formation, including the identification of key synaptic proteins, synaptic assembly dynamics, identification of synaptic partners, and the correlation of synaptic structure with function [102]. Electron microscopy (EM) has been used for detailed ultrastructural analysis of synapses, and for localization of specific synaptic components by immunogold labeling [102]. However, EM technology is labor intensive and precludes live cell imaging techniques that can monitor synaptic assembly mechanisms. In contrast, fluorescent imaging allows for the visualization of multiple components during synaptic assembly [102]. The use of fluorophore-labeling techniques has facilitated visualization of synaptic protein trafficking and assembly. In addition, a recently developed imagining strategy, GFP Reconstitution Across Synaptic Partners (GRASP) [103] utilizes intracellular GFP interactions to visualize neuron-specific synapses. In the GRASP method, an incomplete, or "split," GFP molecule is localized to a potential presynaptic domain with the complementary piece of GFP limited to a potential postsynaptic partner. Because of the narrow width of the synaptic cleft (<100 nm across [103]), the two parts of the split GFP molecule are sufficiently close to interaction and reconstitute a GFP fluorescent signal. Recently, GRASP has been implemented in *C.*

elegans [103-105], *Drosophila* [106, 107] and in mouse [108, 109] to identify synaptic partners. Thus, GRASP technology can provide a much more specific assay for synaptic interaction versus other fluorescent methods such as colocalization of two synaptic proteins.

As described in Chapter III, we utilized a presynaptic component (GFP::RAB-3) and GRASP to assay for effects on chemical synapse wiring in *unc-4* mutants. EM reconstruction showed that chemical synaptic inputs from AVA, AVE and AVD interneurons to VA motor neurons are eliminated in *unc-4* mutants [38]. Using RAB-3::GFP and GRASP tools, we have recapitulated the EM findings as well as expanded on our knowledge of the effects of mutation in *unc-4* on chemical synapses.

Summary

Synaptic specificity is a highly coordinated process that emerging evidence suggests that if disrupted, can lead to diseases such as autism and schizophrenia [110]. Thus, understanding the molecular mechanisms required for this process should lead to working models of brain diseases that can be utilized to develop therapeutic treatments. Because a diverse complement of proteins is likely involved in synaptic specificity, including cell surface molecules, morphogens, and transcription factors, studies in model organisms should be highly useful for achieving these goals. In this dissertation, I will discuss my findings in *C. elegans* that have contributed to an understanding of the pathways that regulate synaptic choice. In Chapter II, I describe the isolation of 16 new genes identified by interactions with *unc-4*. Phenotypic analysis has revealed roles for these genes in specific ventral cord regions and defined their effects on the specificity of gap junction and chemical synapse assembly. In Chapter III, I describe our efforts to visualize synapses in the *C. elegans* motor circuit. In Chapters IV and IV.A, I describe our findings that a canonical Wnt signaling pathway functions upstream of *ceh-12* to

promote VB-type inputs in posterior VA motor neurons and that this mechanism is opposed by a noncanonical cascade, involving a different set of Wnt ligands and receptors, that promotes normal VA inputs in these cells. In Chapter V, I show that distinct G protein pathways can either promote or inhibit VB-type inputs with VA motor neurons. We propose that the mechanism for G protein regulation of synaptic choice involves a role in gap junction localization. On the basis of these studies, we have identified conserved developmental pathways define the synaptic specificity in a model nervous system.

CHAPTER II:

A GENETIC SCREEN REVEALS UNC-4 SUPPRESSORS THAT REGULATE SYNAPTIC CHOICE IN THE MOTOR CIRCUIT

INTRODUCTION

Coordinated movement depends on the creation of specific connections in the motor circuit. Interneurons enter the axial nerve cord to synapse with selected motor neuron targets to establish functional circuits. Although guidance cues and receptors that direct interneuron outgrowth to target destinations have been identified, much less is known about how neurons choose synaptic partners.

Multiple types of proteins regulate synaptic specificity, including cell surface components, morphogenic gradients, and transcription factors. For example, the transmembrane proteins Golden Global (Gogo) and Flamingo (Fmi) regulate targeting of the R8 axon to specific layers in the *Drosophila* visual system [111]. Soluble cues are also implicated in synaptic targeting.

The morphogen Wnt regulates synaptic inputs to hippocampal neurons. In this case, Wnt7a and 7b activate canonical Wnt signaling to increase synaptic inputs to cultured hippocampal neurons, whereas Wnt5a, acting through a noncanonical Wnt pathway exercises an opposing function that decreases the number of synapses [51, 82, 85]. Wnt may modulate synaptic choice through transcriptional regulation of Wnt target genes or the increase of cytosolic β-catenin levels. Stabilization of β-catenin in turn stabilizes N-cadherin, which regulates synapse formation via cell adhesion [85].

We have previously shown that the UNC-4 homeodomain transcription factor regulates synaptic choice in the *C. elegans* motor circuit [35, 36, 42]. UNC-4 is

expressed in larval VA motor neurons, but not in sister VB motor neurons [36, 37]. Anteriorly projecting VA motor neuron processes receive input from the command interneurons, AVA (gap junction & chemical synapse) and AVD, AVE (chemical synapse) (Fig. 2.1). Together, these interneuron inputs mediate backward locomotion. VB motor neurons receive inputs from interneurons in the forward motor circuit, AVB (gap junction) and PVC (chemical synapse) (Fig. 2.1A). *unc-4* mutants are unable to crawl backward because the usual inputs to VA motor neurons are replaced with connections from AVB (gap junction) and PVC (chemical synapse) (Fig. 2.1B). The *unc-4* mutation does not alter the normal anterior polarity of VA motor neurons [38]. Thus, we hypothesize that *unc-4* regulates downstream components that specify VA class-specific inputs but not other morphological features that distinguish VA and VB sisters [38].

Genetic and biochemical studies in our lab have led to the hypothesis that UNC-4, which functions with UNC-37/Groucho [40, 41], acts in VA motor neurons to repress VB genes (Fig. 2.2A). Mutation in *unc-4* or *unc-37* results in ectopic expression of VB genes, which inhibit normal VA-type inputs to VA motor neurons (Fig. 2.2B). Thus, mutation in one or more of the VB genes should restore backward locomotion to *unc-4* mutants, termed Suppression. We have previously identified *ceh-12*/HB9 as one of these VB genes. Mutations in *ceh-12* partially rescue the Unc-4 backward movement defect in the *unc-4(e120)* null allele. Interestingly, we have found that *ceh-12*/HB9 is regulated by UNC-4 only in posterior VA motor neurons, thus suggesting that UNC-4 represses parallel pathways to regulate synaptic choice in VA motor neurons [42] (Fig. 2.2C).

In an effort to identify genes that function in parallel to UNC-4, Jud Schneider conducted a sensitized genetic screen to isolate mutations that suppress the Unc-4 backward movement defect. This idea is based on the observation that mutations that

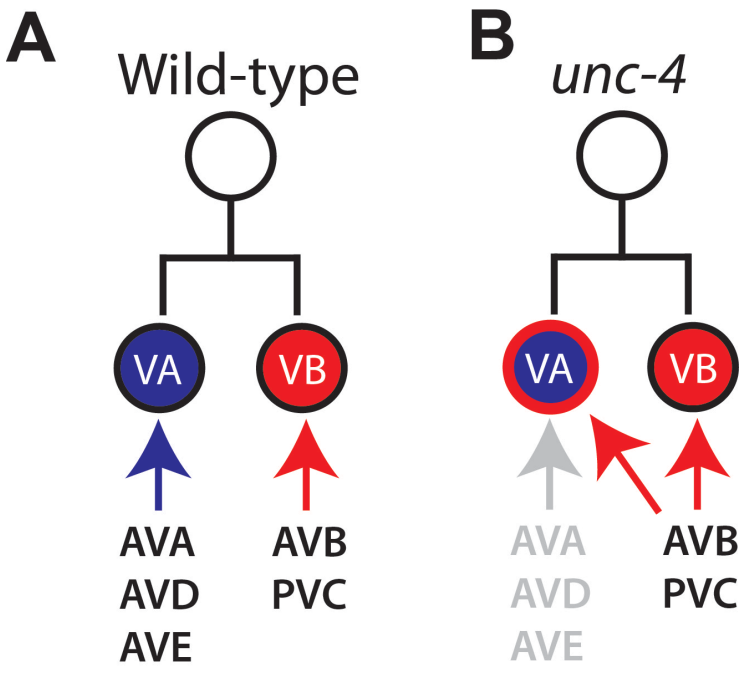

Figure 2.1. Schematic of wiring defect in *unc-4* mutants. **A.** In wild-type animals, sister VA and VB motor neurons receive inputs from different interneurons. VA motor neurons receive inputs from backward circuit command interneurons (AVA, AVE, AVD). VB motor neurons receive inputs from forward circuit command interneurons (AVB, PVC). **B.** In *unc-4* mutants, VA motor neurons lose connections with backward circuit command interneurons and gain ectopic connections from forward circuit command interneurons.

disable *ceh-12* partially restore backward locomotion to an *unc-4* mutant (Fig. 2.2C). Thus, we reasoned that mutations in other *unc-4*-regulated genes that function in parallel to *ceh-12* might also result in weak suppression of the Unc-4 backward movement defect (Fig. 2.2D, E). In collaboration with Jud Schneider (Vanderbilt, Miller Lab) and others (see acknowledgements throughout this section), we have uncovered 16 independent complementation groups with a Blr (Backward Locomotion Restored) phenotype. We have undertaken a detailed characterization of these alleles, designed to assess their roles in defining the specificity of synaptic inputs to VA motor neurons. Whole Genome Sequencing (WGS) of eight alleles from this screen identified candidate Blr mutant genes. Because these *blr* loci regulate distinct aspects of *unc-4* dependent wiring in VA motor neurons, future molecular analysis of these loci should reveal genes with key roles in synaptic choice.

MATERIALS AND METHODS

Nematode Strains and Genetics

Nematodes were cultured using standard methods [112]. Mutants were obtained from the Caenorhabditis Genetics Center (CGC) or by generous donations from other labs. Table 2.5 describes the alleles and sequencing primers (when applicable) used in this study. The N2 strain was used as a wild type reference and all mutant lines were derived from the N2 background.

Genetic Markers

Strains carrying integrated GFP arrays were used in genetic crosses to mark the chromosome *in trans* to selected mutants: *euIs82a (unc-129*::GFP*; dpy-20+)* (I), *okIs59* (*myo-2*::GFP) (I), *juIs76 (unc-25*::GFP*; lin-15+)* (II), *rhIs2 (glr-1*::GFP*)* (III),

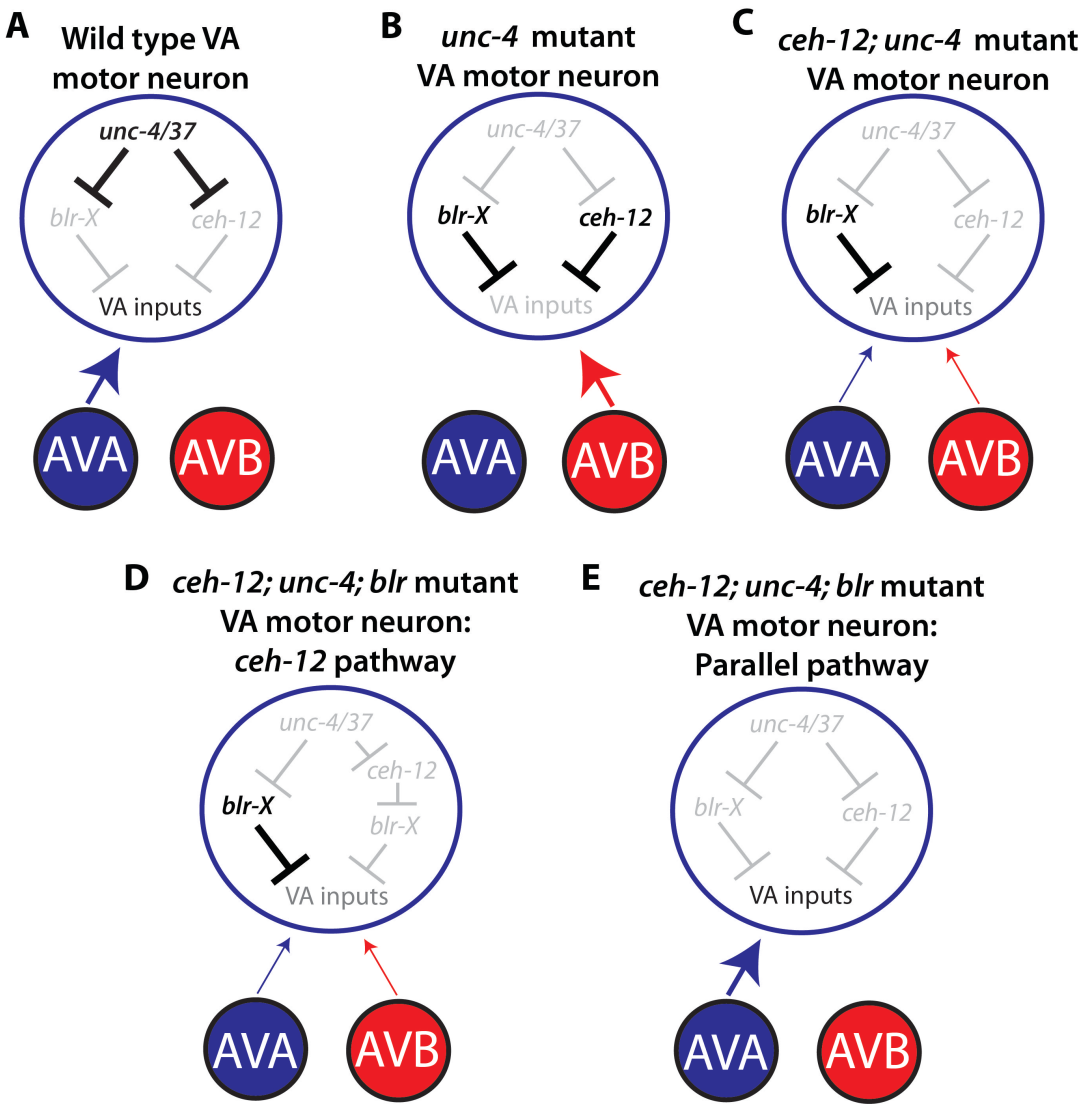

Figure 2.2. Genetic Models for interactions between *blr* alleles and *ceh-12* downstream of *unc-4/unc-37*. **A.** In wild-type VA motor neurons, UNC-4 and UNC-37 repress VB-type genes, including *ceh-12* and *blr* alleles. This allows for expression of VA genes and VA inputs from interneurons AVA, AVD and AVE. AVA and AVB interneurons are shown for simplicity. **B.** In *unc-4* or *unc-37* mutant VAs, VB genes including *ceh-12* and *blr* are derepressed, thus turning off VA genes and resulting in the miswiring of mutant VAs with inputs from AVB and PVC. **C.** In *ceh-12; unc-4* double mutants, connections with AVB are removed and AVA connections are restored to posterior VAs. Full restoration of VA-type inputs to anterior Vs is inhibited because of the ectopic expression of *blr* genes. **D.** If *blr* mutant functions in the same pathway as *ceh-12*, then *ceh-12; unc-4; blr* triple mutants will be phenotypically indistinguishable from *ceh-12; unc-4* mutants. **E.** If a *blr* mutant functions in parallel to *ceh-12*, then *ceh-12; unc-4; blr* triple mutants should show enhanced suppression of the ectopic AVB to VA defect.

aylS2 (egl-15::GFP*)* (IV), *mls11 (myo-2*::GFP*, pes-10*::GFP*, gut*::GFP*)* (IV), *ccls9753 (myo-2::*GFP*)* (V), *oyls44 (odr-1::*RFP*)* (V), *oxls12 (unc-47::*GFP*)* (X).

Construction and injection of *srh-136* genomic DNA rescue plasmid

A genomic rescuing clone containing 1.7 kb 5' to the *srh-136* start codon, 1.6 kb *srh-136* genomic DNA and 2.75 kb 3' to the *srh-136* stop codon was amplified with primers: srh-136-rescue-SphI 5'-gcatgcgaataaggagtacgaaaaatg and srh-136-rescue-ApaI 5'- gggcccatattctgacgtcttgtttgtc. 1.5 ul of the PCR product was injected with 15 ng/ul of *ceh-22*::GFP into *unc-4; srh-136; wdIs54* animals.

Construction and injection of *srh-136* fosmid DNA rescue plasmid

A fosmid containing the *srh-136* coding region (WRM0628aH05) was obtained from the University of British Columbia *C. elegans* Knockout Laboratory. Colonies were streaked onto an LB/chloramphenicol plate from the stab culture provided. A single colony was grown in liquid culture of LB broth + 12.5 ug/ml chloramphenicol and the DNA was miniprepped with Qiagen miniprep reagents according to a previously published BAC miniprep protocol [113], with the replacement of the 70% EtOH pellet wash with instead one pellet wash with Qiagen PB buffer and a second pellet wash with Fermentas wash buffer. The pellet was resuspended in 30ul of water. 20ng/ul of the purified WRM0628aH05 fosmid + 15 ng/ul of *ceh-22*::GFP + 40 ng/ul of pBluescript DNA was injected into *unc-4(e120); srh-136; wdIs54* animals.

Detecting AVB gap junctions (UNC-7S::GFP) with ventral cord motor neurons

The NC1694 *wdIs54* (*Punc-7*::UNC-7S:GFP, *col-19*::GFP) *unc-7*(*e5*) X was integrated by gamma irradiation (4000 Rads) of the EH578 strain [114] and 10X

backcrossed into wild-type. Synchronized L4 larvae were immunostained with anti-GFP to visualize AVB gap junctions with ventral cord motor neurons [42, 104]. Specific motor neurons were identified based on the stereotypic position of their DAPI-stained nuclei [42, 104]. For animals carrying transgenic arrays, the *ceh-22*::GFP co-selectable marker was injected with the plasmid DNA of interest. Transgenic animals were identified based on expression of the *ceh-22*::GFP in the pharynx. The experimenter was blinded to genotype to avoid bias. n ≥10 for each neuron.

Isolation of Unc-4 suppressor mutations

Figure 2.3 depicts a schematic of the genetic screen.

EMS mutagenesis screen to identify Unc-4 suppressor mutations

Two genetic screens were conducted to identify recessive genes that function in the *unc-4* pathway. More extensive details of the screens are discussed in his thesis (Chapter III). In the first instance, a small-scale screen of 5,000 haploid genomes was conducted to detect genes that function in parallel to *ceh-12* (see Results). The second screen of 40,000 haploid genomes utilized a synthetic 'Stuck' phenotype, based on mutations in *unc-24* (unable to crawl forward) and *unc-4* (unable to crawl backward) [39] to detect weak Unc-4 suppressors with improved locomotion. Synchronized populations of worms were exposed to 0.05M ethyl methansulfonate (EMS) during the L4 larval stage (Fig. 2.3). F2 animals emerging from the Stuck Screen were tested for backward locomotion in response to a head touch with a platinum wire. Animals showing the "*B*ackward *l*ocomotion *r*estored," or Blr phenotype in the F3 generation were retained for genetic mapping and phenotypic analysis. Two alleles, *blr-1(wd76)* and *blr-2(wd77)* were identified in the first screen; 50 independent *blr* mutant lines were isolated from the second 'Stuck' screen.

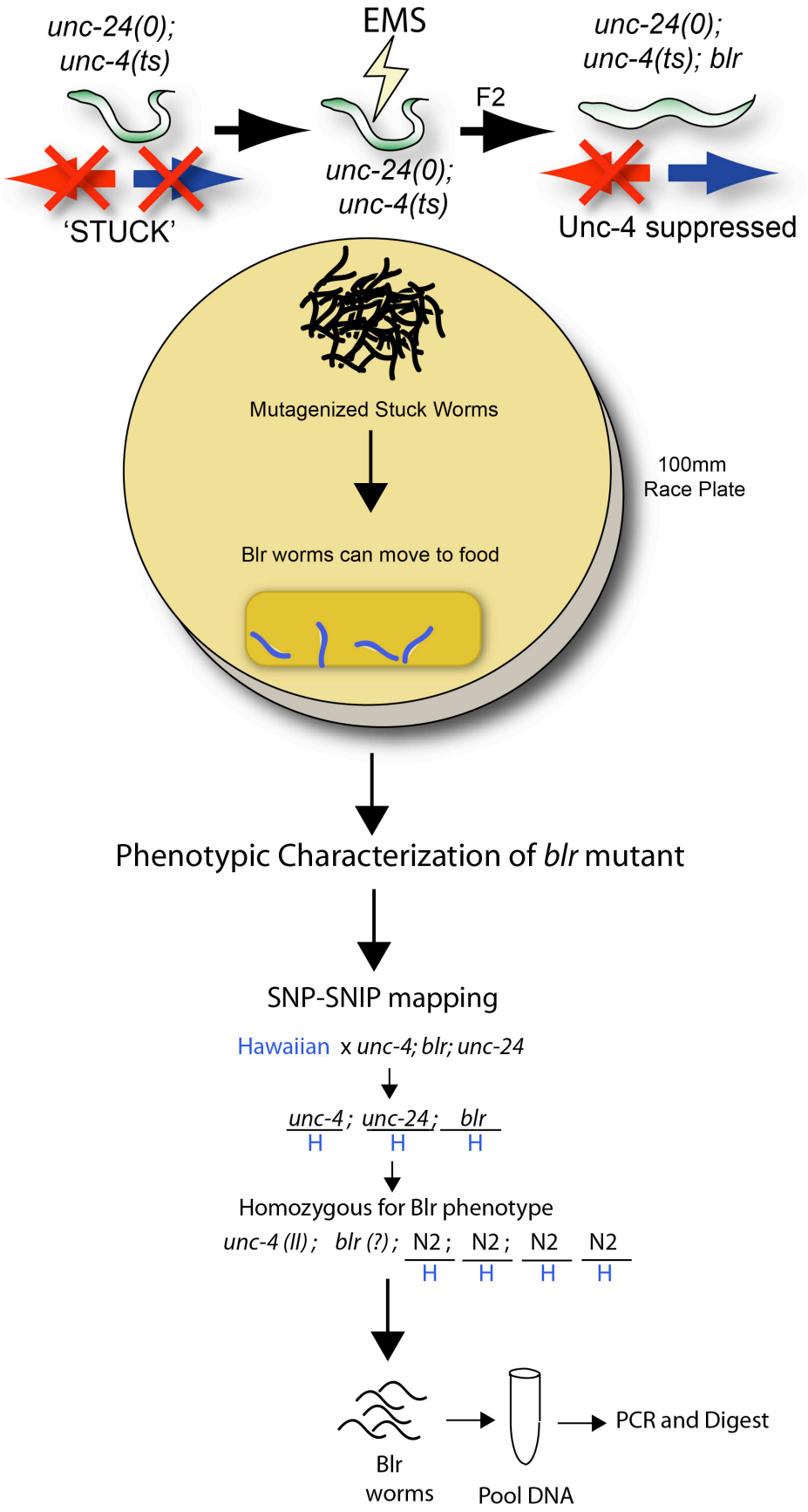
unc-24(0);
unc-4(ts)
EMS
unc-24(0);
unc-4(ts); blr
F2
'STUCK'
unc-24(0);
unc-4(ts)
Unc-4 suppressed
Mutagenized Stuck Worms
Blr worms can move to food
100mm
Race Plate
Phenotypic Characterization of blr mutant
SNP-SNIP mapping
Hawaiian x unc-4; blr; unc-24
unc-4 ; unc-24 ; blr
H H H
Homozygous for Blr phenotype
unc-4 (II) ; blr (?) ; N2 ; N2 ; N2 N2
H H H H
Blr
worms
Pool DNA
PCR and Digest

Figure 2.3. Schematic of Stuck screen protocol. “Stuck” *unc-4(e2322ts); unc-24(0)* animals were mutagenized with EMS. The F2 progeny were placed on a 100mm plate opposite a patch of bacteria on the other side. Animals with restored locomotion crawled to the bacterial patch and were tested for suppression of the Unc-4 backward movement defect. These *blr* mutants were classified based on strength of Unc-4 suppression (see Table 1). *blr* mutants were crossed with the Hawaiian strain, according to the SNIP-SNP mapping protocol [115]. F3 animals were picked with Unc-4 suppression phenotypes. Blr animals were pooled and DNA extracted. SNP-SNIP analysis was performed by PCR amplification and restriction enzyme digestion. The digested fragments were run on an agarose gel and band size was compared to an N2 control to determine approximate map location (see Methods). Figure adapted from Jud Schneider.

Blr phenotype classification

blr mutants were outcrossed with *unc-4(e2322ts)* males grown at the permissive temperature of 16 °C (described in detail in Jud Schneider's thesis, Chapter III). All *blr* mutants were outcrossed multiple times to reduce the number of random mutations caused by the EMS mutagenesis and the Blr phenotype (suppression of Unc-4) was recovered after outcrossing. We established a rubric to classify the *blr* mutants based on the degree of suppression of *unc-4(e2322ts)* at the nonpermissive temperature of 23 °C. As described in Table 2.2: Class I mutations could execute backward locomotion in a near wild-type fashion. Class II mutants showed execute backward movement but generally with less frequency than Class I mutants. Class III mutants would execute at least two complete backward body bends but required repeated stimulation to sustain backward locomotion. Class IV mutants executed only a single body bend following significant prodding.

Mapping and complementation

Jud Schneider, Dan Ruley (visiting Wooster College undergraduate) and I used a SNIP SNP mapping protocol [115] to assign *blr* alleles to specific chromosomes. To sensitize the *unc-4(e2322ts)* phenotype, mapping experiments for the weaker Class III and Class IV mutations were performed at 23 °C. The stronger Class I and II *blr* alleles were mapped at 25 °C.

Additional descriptions of reagent recipes and reaction conditions and a detailed protocol can be found in Jud Schneider's thesis (Chapter III) and in [115]. Briefly, Hawaiian males (CB4856) were mated with each 'Stuck' allele (*e.g.*, *blr-5; unc-4(ts); unc-24*), which was derived from the N2/Bristol strain. Heterozygous F1 animals were

Table 2.1. Mapping data of Blr alleles. Chromosomal boundaries were determined by SNIP-SNP mapping and genetic linkage, as stated.

Suppressor Allele	blr	Chromosome	Left Genetic Boundary	Left Boundary	Right Genetic Boundary	Right Boundary	# of bases	Method	Modified genetic location
wd98	not assigned	3	4	10652476	21	13715622	3063146	Fails to complement wd87	
wd104	not assigned	Unclear	-	-	-	-			
not assigned	not assigned	Unclear	-	-	-	-			
wd83	ceh-12	1	-3.3	APPX- 3467134	3.3	APPX- 8590000		Map against dpy-5= 5433059..5432161	4765755..4767645 - 5196081..5200105
wd88	blr-9	1	-19	169017	-6	2818973	2649956		
wd87	blr-8	3	4	10652476	21	13715622	3063146	Fails to complement wd98	10621442..10626284-10894421..10895633
wd85	blr-6	1	-	-	-	-			
wd84	*blr-5*	1	-12	1905969	14	12,729,812	10823843	SNIP SNP	
wd82	blr-3	5	6	13951850	13	17610508	3658658	SNIP SNP	17376712..17371519
wd103	blr-21	5	-5	4550757	13	17610508	13059751	SNIP SNP	
wd102	blr-20	3	-	-	-	-			
wd86	blr-2	4	0.02	4248463	1.5	4798171	549708	Fails to Complement wd77	
wd77	blr-2	4	0.02	4248463	1.5	4798171	549708	mDF8 and mDF8 between ama-1 and eor-1	
wd101	blr-19	1	-	-	-	-			
wd100	blr-18	1	-19	169017	14	12729812	12560795	SNIP SNP	5840292..5841891
wd99	blr-17	1	End	0	26	14682016	14682016	SNIP SNP	11221967..11216110-1651382..1644590
wd97	blr-16	1	-19	169017	14	12729812	12560795	SNIP SNP	11221967..11216110-1651382..1644590
wd95	blr-15	5	-13	2726662	13	17610508	14883846	SNIP SNP	3316357..3318024
wd96	blr-14	1	-12	1905969	14	12729812	10823843	SNIP SNP	5840292..5841891
wd92	blr-13	1	End	0	-1	4594014	4594014	SNIP SNP	11221967..11216110-1651382..1644590
wd91	blr-12	X	End	0	8	12750713	12750713	SNIP SNP	
wd90	blr-11	5	-13	2726662	13	17610508	14883846	SNIP SNP	
wd89	blr-10	1	-12	1905969	14	12729812	10823843	SNIP SNP	5840292..5841891
wd76	blr-1	5	6	13,951,850	13	17,610,508	3658658	SNIP SNP and dpy-11 recombination	16497575..16495973

Table 2.2. Unc-4 suppressor *blr* mutants were classified based on a qualitative assessment of suppression of the Unc-4 backward movement defect. The majority of these recessive alleles show weak suppression of Unc-4 movement (Class III and IV).

Class	*Description*	*blr Alleles*
Class I	Fully suppressed at 25 ℃	*wd85, (wd90, wd91)*
Class II	Suppressed	*wd76*, wd89, wd98, wd104, (wd101, wd102)*
Class III	Weak Suppressor	*wd77*, wd82, wd83, wd87, wd88, wd93, wd94, wd96*
Class IV	Weaker Suppressor	*wd84, wd92, wd95, wd86, wd97, wd99, wd100, wd103*

allowed to self-fertilize and F2 animals with Unc-4, non-Blr phenotypes, (*unc-4(ts); blr/+; unc-24/+*) were isolated. For each *blr* allele, > 40 F3 Suppressed (*unc-4(ts); blr; unc-24/+*) animals were picked to individual plates and allowed to lay eggs overnight. F3 *blr* adults were then collected in lysis buffer for bulk segregate analysis [115]. Sets of PCR primers were used to amplify the DNA surrounding eight DraI restriction sites that differ between N2 and Hawaiian *C. elegans* strains. Following amplification, samples were digested with DraI and examined by gel electrophoresis with the N2/Bristol control adjacent to the *blr* sample. This arrangement allowed for rapid detection of predominantly N2/Bristol regions in the Suppressor strain, which represented the chromosomal interval of the *blr* mutation. Individual recombinants from the F4 generation were expanded and put through the PCR/DraI digest protocol to narrow the chromosomal region that contained the *blr* allele. In total, we outcrossed and mapped 22 independent *blr* mutations (Fig. 2.4, Table 2.1).

In addition to using the SNIP-SNP mapping protocol to map *blr* mutants, I utilized a genetic recombination technique to determine map locations for *wd85* and *wd83*. Because *wd85* was a dominant Unc-4 suppressor, we tested whether *wd85* was an allele of *unc-37*. Previous genetic screens in the Miller lab uncovered dominant Unc-4 suppressors that mapped to the *unc-37* locus on LGI [39, 40]. Homozygous *wd85; unc-4(e2322ts)* males were crossed with *dpy-5(I)*; *unc-4(e2322ts)* hermaphrodites. Recovery of only six Dpy and Unc-4-Suppressed (Dpy-Sup) recombinant animals from 182 F2 progeny was indicative of linkage to *dpy-5(I)*. *wd83* is a recessive suppressor of *unc-4*. *unc-4(e2322ts)* males were crossed with *dpy-5 wd83* linked hermaphrodites. I assayed the movement of 284 F2 animals as above, and detected 10 Dpy-Sup animals. These results were indicative of linkage (~3 map units) of *wd83* to *dpy-5*.

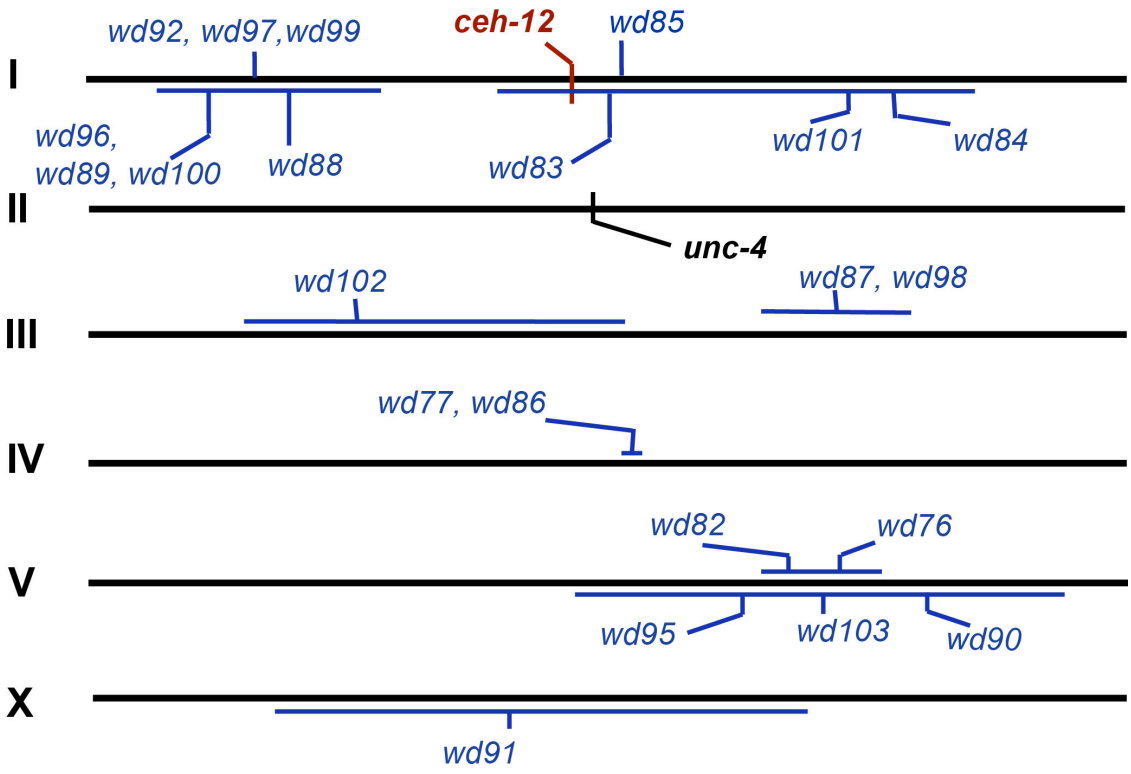

Figure 2.4. Approximate map locations of *blr* mutants, determined by SNP-SNIP mapping. The six *C. elegans* chromosomes are indicated (I-X). Alleles assigned to general chromosomal regions are represented with horizontal lines. Alleles within complementation groups are separated by commas.

Complementation tests

Individual *blr* alleles that mapped to a similar chromosomal region were tested for complementation to detect allelic mutations. *unc-4(e2322ts)* males (grown at 16 °C), were mated with *unc-4(ts); blr-A* hermaphrodites, and F1 progeny matured at 16 °C to generate F1 *unc-4(ts); blr-A/+* males. These *unc-4(ts); blr-A/+* males were mated with a *unc-4(ts); blr-B* strain, generating 50% progeny *unc-4(ts); blr-A/blr-B*, and 50% *unc-4(ts); +/blr-B*. Thus, ~50% of cross progeny should show a Blr phenotype for allelic mutations (Fail to complement) whereas Blr cross progeny should be rare for non-allelic *blr* alleles. Weak Blr alleles (Class III, IV) were tested in duplicate and independently scored for complementation by two observers blinded to genotype. Using this strategy, we assigned 22 independent suppressor mutations to 16 different complementation groups (Fig. 2.4).

Genetic tests

Quantification of the blr phenotype

A movement assay, “tapping assay”, was used to detect effects of specific *blr* mutants on Unc-4-dependent backward locomotion [42]. The experimenter was blinded to genotype to avoid bias. For each genotype, $\geq$ 50 L4-young adult animals (at 23 °C, unless otherwise noted) were tapped a single time on the head with the tip of a platinum wire. Backward movement was scored as either **Unc** (coiled instantly with no net backward movement) or as **Suppressed** (detectable backward movement of posterior region or entire body). Statistical tests of differential effects on backward locomotion were performed using the Fisher's Exact Test.

Whole genome sequencing of *blr* alleles

We used whole genome sequencing (WGS) to search for the mutated gene responsible for each Blr phenotype. We performed two rounds of whole genome sequencing. Table 2.3 describes results from the strains sequenced. In the first round of sequencing, Jud Schneider isolated genomic DNA from triple mutant strains (*i.e. blr-1(wd76); blr-2(wd77); unc-4(e2322ts)*) using a Qiagen genomic DNA isolation kit. The Vanderbilt Genome Technology Core prepared Genomic DNA libraries using standard Illumina Protocols. Each DNA library was run on one flow cell of an Illumina Genome Analyzer IIX. Clay Spencer (Vanderbilt, Miller Lab) analyzed the quality of reads and compiled the relevant sequencing reads with the Fastqc and MaqGene programs, respectively [116] (See Clay Spencer's thesis, Chapter V). For the second round of sequencing, we collected genomic DNA using modified protocols from the Hobert (http://biochemistry.hs.columbia.edu/labs/hobert/protocols.html) and Blakely labs (below).

Genomic DNA Extraction for Sequencing

Worm Preparation

For each strain to be sequenced, ¼ of a recently starved 60 mm plate was chunked onto four 150 mm NGM + OP^{50-} plates and grown to confluency (~4 days) at room temperature. Worms were collected with M9 into 2x 50 ml conical tubes and spun in a Beckman J2-21M centrifuge at 3000 rpm for 5 mins at 4 °C. During washes, worms from each strain were combined into 1x 50 ml conical tube. Tubes were washed 2-3 times with M9 buffer to remove residual bacteria. Next, 25 ml of M9 was added to each pellet and tubes were mixed in a nutator at 20 °C for 2 hours to remove food from the gut. Tubes were spun in a Beckman J2-21M centrifuge at 3000 rpm for 5 mins at 4 °C

and transferred to a 15 ml conical tube. Worms were pelleted at 2500 rpm for 2.5 mins. M9 buffer was aspirated from the worm pellet and tubes were frozen at -80 °C.

Genomic DNA Isolation

The Gentra Puregene Kit (Qiagen #158622) was used in a modified protocol to isolate genomic DNA. Each tube was removed from -80 °C and thawed until the pellet was loose. 15 ul Proteinase K (PK) (20 mg/ml) was added and the PK/worm mixture was split into 3x 1.5 ml tubes and incubated at 55 °C for 3 hours. Tubes were inverted periodically. Lysates were cooled to room temperature for 10 mins and 5 ul of RNase A solution was added to each tube. Tubes were incubated at 37 °C on a nutator for 2 hours. Tubes were cooled on ice for 3 mins and tubes from each strain were pooled into a 15 ml conical tube. 1 ml of Protein Precipitation Solution was added to each 15 ml tube and contents were vortexed vigorously for 20 sec at high speed. Tubes were centrifuged in a Beckman J2-21M centrifuge at 3500 rpm for 10 mins at 4 °C. The supernatant was transferred to a new 15 ml conical tube, 3 ml isopropanol was added, and the tube was mixed gently 50 times. A precipitate was visible after precipitation with isopropanol; however, if no precipitate was visible, 3 ul of glycogen (Sigma) was added to the tube. Tubes were incubated at -20 °C for 15 mins and centrifuged for 3 mins in a Beckman J2-21M centrifuge at 4700 rpm for 3 mins at 4 °C. The supernatant was removed and the pellet was air-dried overnight at room temperature. After drying, 400ul of DNA Hydration Solution was added. The pellet was resuspended with repeated pipetting and transferred to a new tube. The DNA solution was incubated at 65 °C for 2 hours. The DNA solution was purified with phenol choloroform extraction, followed by precipitation of the DNA with 2.5 volumes of 100% ethanol and 1/10 volumes of sodium acetate. The DNA pellet was washed with 70% ethanol and spun at top speed for 10 mins. The DNA pellet was resuspended with 100 ul of EB solution (Qiagen).

Table 2.3. Summary of candidate genes based on whole genome sequencing (WGS) data. Data were filtered to remove SNPs shared among different strains. List is limited to genes in mapped regions with mutations that affect coding sequences. All missense mutations are non-conservative substitutions.

allele	WGS candidate	protein	WGS coding mutation
wd24	*unc-37*	Groucho	G438E
wd85	*unc-37*	Groucho	E580K
wd76	*srh-136* F57G8.7	GPCR unknown	Deletion Prem. Stop
wd77			
wd82	*Y20C6A.1*	F-box	T581I
wd83	*pde-5*	P-diesterase	W34->Stop
wd87	*hpr-9* *fbxb-87*	DNA chckpnt F-box	G276R S316N
wd88			
wd95			
wd97	*mab-20* *rsy-1*	semaphorin RSY-1	A522T G139E

Using the Nanodrop spectrophotometer, the DNA concentration should be about 500 ng/ul with an OD (260/280) between 1.8-2.0. The DNA (~1 ug) was tested on an agarose gel for the presence of a single bright band at 10 kb and no RNA at the bottom of the lane. To submit samples for whole genome sequencing, DNA was diluted to 100 ng/ul in water. The Vanderbilt Genome Technology Core prepared Genomic DNA libraries using standard Illumina Protocols. DNA libraries were multiplexed and four samples each were sequenced on 2 lanes of Paired-End 100 flow cells on the Illumina HiSeq2000 machine.

Analyzing whole genome sequence data

For the second round of sequencing, and in collaboration with Clay Spencer, we utilized the MaqGene program to annotate the WGS data with: chromosomal location, class of mutation (i.e. missense, nongenic), and description of mutation (i.e. amino acid change) [116]. Explicit details about the MaqGene program and additional analysis of the whole genome sequencing data from the *blr* mutants are outlined in Clay Spencer's thesis (Chapter V). To specify candidate mutations, we used approximate mapping data (Table 2.1) to narrow our search for potential *blr* loci. We then manually eliminated mutations that shared by multiple sequenced strains. In addition, we limited our scope to mutations in coding regions, *i.e.* deletions, nonconservative amino acid substitutions or stop codons. Table 2.3 details the candidate mutations from this round of sequencing.

RESULTS

Isolation of recessive Unc-4 suppressor mutants

Identification of genes that function in parallel to ceh-12

Jud Schneider conducted a pilot genetic screen that was designed to detect genes that function downstream of *unc*-4 and in parallel to *ceh-12*. This strategy was motivated by the evidence indicating that more than one pathway regulates inputs to VA motor neurons: *ceh-12(0)* is a weak suppressor null *unc-4* alleles and *ceh-12* function is uniquely required for miswiring of posterior VAs (Fig. 2.2C). Thus, mutation in a gene that functions in parallel to *ceh-12* was expected to result in improved backward locomotion *vs. ceh-12(0); unc-4(0)* (Fig. 2.2E). Additional details of this screen are presented in Jud's thesis. Briefly, Jud mutagenized *ceh-12; unc-4(wd1)* mutants with EMS and used the tapping assay to screen the F2 progeny of ~5,000 F1 animals for improved backward locomotion. Two alleles, *blr-1(wd76)* and *blr-2(wd77)* were identified with this strategy.

Identification of Unc-4 suppressors from a synthetic "Stuck" strain

Although *ceh-12(0)* is a weak suppressor of *unc-4* null alleles, the *ceh-12(0)* affords strong suppression of weak or hypomorphic *unc-4* mutants. For example, 96% of *ceh-12; unc-4(e2322ts)* animals show virtually wild-type backward locomotion at the restrictive temperature of 25 °C (Table 2.4). Thus, mutations in genes that function in parallel to *ceh-12* (*e.g.* specify inputs to anterior VA motor neurons) could show comparably strong suppression of *unc-4(e2322ts)* animals. Jud confirmed this idea by showing that *unc-4(e2322ts); blr-1(wd76)* and *unc-4(e2322ts); blr-2(wd77)* double mutants show improved backward locomotion in comparison to *unc-4(e2322ts)* single mutants at 23 °C (Table 2.4).

In this case, a synthetic uncoordinated phenotype was utilized to enhance the sensitivity and throughput of the screen. A similar screen previously utilized in the Miller lab to isolate dominant, allele specific suppressor mutations in the *unc-37* locus [39]. In

Table 2.4. List of strains and tapping assay results from this work. Modified from Table 3.3, Jud Schneider's thesis. Significance is * p<0.05 student's T test *vs.* parent strain in that grouping. n ≥ 50.

Strain	% Unc	% Suppressed	p < 0.05
WT	0	100	
unc-4(e2320)	98	2	
unc-4(e120)	99	1	
*ceh-12(gk391); unc-4(e120)**	54	46	*
ceh-12(gk391); unc-4(e2320)	58	42	*
ceh-12(gk391); unc-4(wd1)	62	38	*
unc-37(e262)	87	13	
blr-2(wd77)	0	100	
blr-1(wd76)	0	100	
blr-9(wd88)	0	100	
blr-8(wd87)	2	98	
blr-3(wd82)	0	100	
wd95	0	100	
ceh-12(gk391); blr-2(wd77)	0	100	
ceh-12(gk391); blr-1(wd76)	2	98	
ceh-12(gk391); blr-8(wd87)	0	100	
ceh-12(gk391); blr-3(wd82)	0	100	
ceh-12(gk391); blr-15(wd95)	ND	ND	
unc-4(e2323)	63	38	
Ceh-12(gk391); unc-4(e2323)	11	89	*
unc-4(e2323); blr-1(wd76)	50	50	
unc-4(e2323); blr-2(wd77)	23	77	*
blr-9(wd88); unc-4(e2323)	62	38	
unc-4(e2323); blr-8(wd87)	28	72	*
unc-4(e2323); blr-3(wd82)	64	36	
unc-4(e2323); blr-15(wd95)	20	80	*
unc-4(e2320)	98	2	
unc-4(e2320); blr-2(wd77)	99	1	
unc-4(e2320); blr-1(wd76)	100	0	
blr-9(wd88); unc-4(e2320)	100	0	

Table 2.4 Cont.			
unc-4(e2320); blr-3(wd82)	96	4	
unc-4(e2320); blr-15(wd95)	ND	ND	
unc-4(e120)	99	1	
unc-4(e120); blr-2(wd77)	100	0	
blr-9(wd88); unc-4(e120)	94	6	
unc-4(e120); blr-8(wd87)	80	20	*
unc-4(e120); blr-3(wd82)	96	4	
unc-4(e120); blr-15(wd95)	64	36	*
ceh-12(gk391); unc-4(e2320)	58	42	
ceh-12(gk391); unc-4(e2320); blr-2(wd77)	96	4	*
ceh-12(gk391); unc-4(e2320); blr-1(wd76)	46	54	
ceh-12(gk391); unc-4(e2320); blr-8(wd87)	51	49	
ceh-12(gk391); unc-4(e2320); blr-3(wd82)	38	62	*
ceh-12(gk391); unc-4(e2320); wd95	36	64	*
ceh-12(gk391); unc-4(wd1)	62	38	
ceh-12(gk391); unc-4(wd1); blr-2(wd77)	86	14	*
ceh-12(gk391); unc-4(wd1); blr-1(wd76)	24	76	*
*ceh-12(gk391); unc-4(e120)**	54	46	
ceh-12(gk391); unc-4(e120); blr-15(wd95)	16	84	*
ceh-12(gk391); unc-4(e120); blr-1(wd76)	1	99	*
ceh-12(gk391); unc-4(e120); blr-2(wd77)	ND	ND	
ceh-12(gk391); unc-4(e120); blr-3(wd82)	16	84	*
ceh-12(gk391); unc-4(e120); blr-8(wd87)	ND	ND	
unc-37(e262)	87	13	
ceh-12(gk391) unc-37(e262)	49	51	*
unc-37(e262); blr-2(wd77)	94	6	*
unc-37(e262); blr-2(wd76)	80	20	
unc-37(e262); blr-8(wd87)	ND	ND	
unc-37(e262); blr-3(wd82)	ND	ND	
unc-37(e262); blr-15(wd95)	ND	ND	
unc-4(e120); blr-8(wd87)	80	20	
blr-9(wd88); unc-4(e120); blr-8(wd87)	82	18	

Table 2.4 cont.			
*unc-4(e2320); egl-20(n585)**	46	54	
blr-9(wd88); unc-4(e2320); egl-20(n585)	96	4	*
*ceh-12(gk391); unc-4(e120)**	54	46	
ceh-12(gk391); unc-4(e120); blr-1(wd76)	1	99	*

this case, the “Stuck” screen was implemented to isolate homozygous recessive *blr* mutants from the F2 generation. A double mutant of *unc-4(e2322ts)*, which prevents backward locomotion and *unc-24(0)* which blocks forward movement, displays a synthetic “Stuck” phenotype [39] (Fig. 2.3). The *unc-4; unc-24* worms are unable to crawl across a 100 mm agar plate to food (*i.e.* bacteria). In this setting, a mutation that suppresses the Unc-4 movement defect (*e.g. ceh-12(0)*) can be detected as a rare animal that reaches the distant patch of bacteria after an overnight trial.

unc-4(e2322ts); unc-24(0) animals were mutagenized with EMS and F2 progeny were allowed to “race” across a 100mm plate to a small patch of bacteria (Fig. 2.3). Mutations in genes that suppress the Unc-24 defect were also identified, but these can be recognized as animals with restored forward locomotion and were discarded. This simple movement assay allowed us to screen ~10^6 F2 animals and identify > 50 *blr* (*b*ackward *l*ocomotion *r*estored) mutants. A more detailed description of this genetic screen is provided in Jud Schneider’s thesis. Blr alleles from this screen were categorized into four groups based on a qualitative assessment of the strength of Unc-4 suppression (Table 2.2). 22 independent *blr* alleles were assigned to chromosomal intervals by SNP-SNIP mapping [115] (Fig. 2.4, Table 2.1). Mutations that mapped to overlapping chromosomal regions were tested for complementation, resulting in the identification of 16 different complementation groups (see Methods). Experiments characterizing a selected group of Blr alleles are described in detail below.

Testing *blr* mutants for lesions in candidate genes

Mapping results identified *blr* alleles on chromosome I that were located in the vicinity of known Unc-4 suppressor loci. These included the complementation groups of *wd96, wd89, wd100* (*mig-1*) and *wd92, wd97, wd99* (*pop-1*) as well as *wd85* (*unc-37*) and *wd83* (*ceh-12*). *wd83* failed to complement *ceh-12* but DNA sequencing defects

were detected in the third *ceh-12* intron and not in coding regions. Complementation tests revealed that *wd96, wd89, wd100* failed to complement *mig-1* and *wd92, wd97, wd99* failed to complement *pop-1* and *wd83* failed to complement *ceh-12*. Sequencing of exonic regions for *pop-1* in *blr-6(wd97)* and for *mig-1* in *blr-16(wd97)* and *blr-10(wd89)* failed to detect coding sequence mutations. Thus, the results of this analysis are inconclusive.

Phenotypic characterization of *blr* mutants

The following phenotypes were evaluated for selected *blr* alleles: 1) enhancement of *ceh-12* suppression of null alleles of *unc-4*; 2) regulation of *ceh-12*::GFP expression and 3) suppression of ectopic AVB to VA gap junctions. A *blr* mutation in a gene that functions in parallel to *ceh-12* would show enhanced suppression of *ceh-12; unc-4(0)* (Fig. 2.2E) and would have no effect on ectopic *ceh-12*::GFP expression in posterior VA motor neurons. *blr* mutations required for ectopic AVB to VA gap junctions would either function in posterior VAs, if in the *ceh-12* pathway, or would be required in a different region of the ventral nerve cord (*e.g.* in anterior VA motor neurons). These criteria were evaluated for independent *blr* mutations from different complementation groups: *blr-1(wd76), blr-2(wd77), blr-3(wd82), blr-8(wd87), blr-9(wd88), blr-15(wd95)* (Table 2.1). Additional *blr* alleles (*e.g. wd83, wd85)* were analyzed with selected assays described above.

Genetic interactions detect a subset of *blr* alleles that function in parallel to *ceh-12*.

Our results showing that *blr* alleles suppress *unc-4* hypomorphic mutations are consistent with the alternative possibilities that the *blr* mutations disrupt genes that function either in the *ceh-12* pathway or in parallel (Fig. 2.2). To distinguish between

these models, we tested *blr* alleles for enhancement of *ceh-12(0)* suppression of *unc-4(0)* mutants, which would be indicative of function in a parallel pathway. (*wd88* was not tested in this assay because of linkage to *ceh-12* on chromosome I).

Experiments with three different *unc-4* null mutations (*e120, e2320, wd1*) detected four recessive *blr* alleles (*wd76, wd82, wd87, wd95*) that enhance *ceh-12* suppression of Unc-4 (Table 2.4). All three of these *unc-4* alleles are predicted nulls: *e120* creates a frame shift in the translational reading frame in the conserved C-terminal UNC-37/Groucho domain; *wd1* is a large deletion that removes the *unc-4* gene and upstream regions; *e2320* deletes exons encoding the UNC-4 homeodomain and disrupts the reading frame [41]. Although *wd76, wd82, wd87,* and *wd95* enhance suppression of *ceh-12; unc-4(e120)*, they show different interactions with other null alleles of *unc-4*. *wd76* enhances suppression in the *ceh-12(0); unc-4(wd1)* background (Table 2.4) and *wd82* enhances backward locomotion of *ceh-12; unc-4(e2320)*. However, *wd95* and *wd87* only enhance *ceh-12* suppression of *unc-4* in the *e120* background. In addition, *wd76* enhances *ceh-12* suppression of *unc-4(e120)* and *unc-4(wd1)* but has no effect on *ceh-12; unc-4(e2320).* The reasons for the different genetic interactions of these *unc-4* alleles with *ceh-12* and *blr* mutants are unclear. In any case, the observed enhancement of the *ceh-12* Blr phenotype in at least one of these *unc-4(0)* genetic backgrounds is consistent with the proposal that four of these *blr* alleles, *wd76, wd82, wd87,* and *wd95*, function in parallel to *ceh-12*.

Curiously, *wd77* does not enhance *ceh-12*-mediated suppression of *unc-4 e2320* or *e120*, although it was originally isolated in the *ceh-12; unc-4(wd1)* background. Additionally, our tapping assay with the outcrossed strain *ceh-12; unc-4(wd1); blr-2(wd77)* actually showed a stronger backward movement defect than the control *ceh-12; unc-4(wd1)* strain (Table 2.4). These results could arise from a synthetic phenotype in the original isolated strain involving an additional Unc-4 suppressor mutation that was

removed upon outcrossing and reisolation of the *ceh-12; unc-4(wd1); blr-2(wd77)* strain. However, because the *blr-2(wd77)* allele strongly suppresses hypomorphic alleles of *unc-4,* we hypothesize that *wd77* is likely to function in the *ceh-12* pathway.

blr mutants differentially affect *ceh-12*::GFP expression

Genetic data presented above predict that *blr-1(wd76), blr-3(wd82), blr-8(wd87),* and *blr-15(wd95)* function in parallel to *ceh-12*, whereas *blr-2(wd77)* is likely to act in the *ceh-12* pathway. As an independent test of these results, we examined these *blr* alleles for potential effects on *ceh-12*::GFP expression. As previously described [42], the *wdIs85* (*ceh-12*::GFP) transgene is selectively expressed in VB motor neurons in the wild-type and is ectopically expressed in posterior VA motor neurons in an *unc-4* mutant (Fig. 2.5). The Wnt pathway components, *egl-20*/Wnt, *mom-5* and *mig-1*/Frizzled are required for ectopic *ceh-12*::GFP expression in posterior VAs (Chapter IV) [104]. We tested *blr-15(wd95), blr-2(wd77), blr-9(wd88), blr-16(wd97*), *blr-1(wd76)* and *blr-3(wd82)* for effects on *ceh-12*::GFP expression in *unc-4(e120)* mutants (Fig. 2.5). *blr-8(wd87)* was not tested due to its close linkage to *wdIs85* on LGIII. The *blr-15(wd95)* allele showed no visible effect on ectopic expression of *ceh-12*::GFP in posterior VAs. This finding is consistent with genetic results indicating that *blr-15(wd95)* functions in parallel to *ceh-12*. Surprisingly, other *blr* alleles result reduced levels of *ceh-12*::GFP expression in posterior *unc-4* mutant VA motor neurons. These effects, however, are limited to subsets of VA motor neurons in the posterior region (VA8, VA9, VA10). For example, *blr-2(wd77)* and *blr-9(wd88)* block expression of *ceh-12*::GFP in VA9 but not in VA8 or VA10 (Fig. 2.5). Similarly, ectopic *ceh-12*::GFP is significantly reduced in VA8 and VA9 but not in VA10 in *blr-16(wd97)* and *blr-1(wd76)* (Fig. 2.5). Finally, *blr-3(wd82)* results in lower levels of *ceh-12*::GFP in VA8 and VA10 but not in VA9. These results can be interpreted to mean that these *blr* alleles affect genes with distinct functions in different

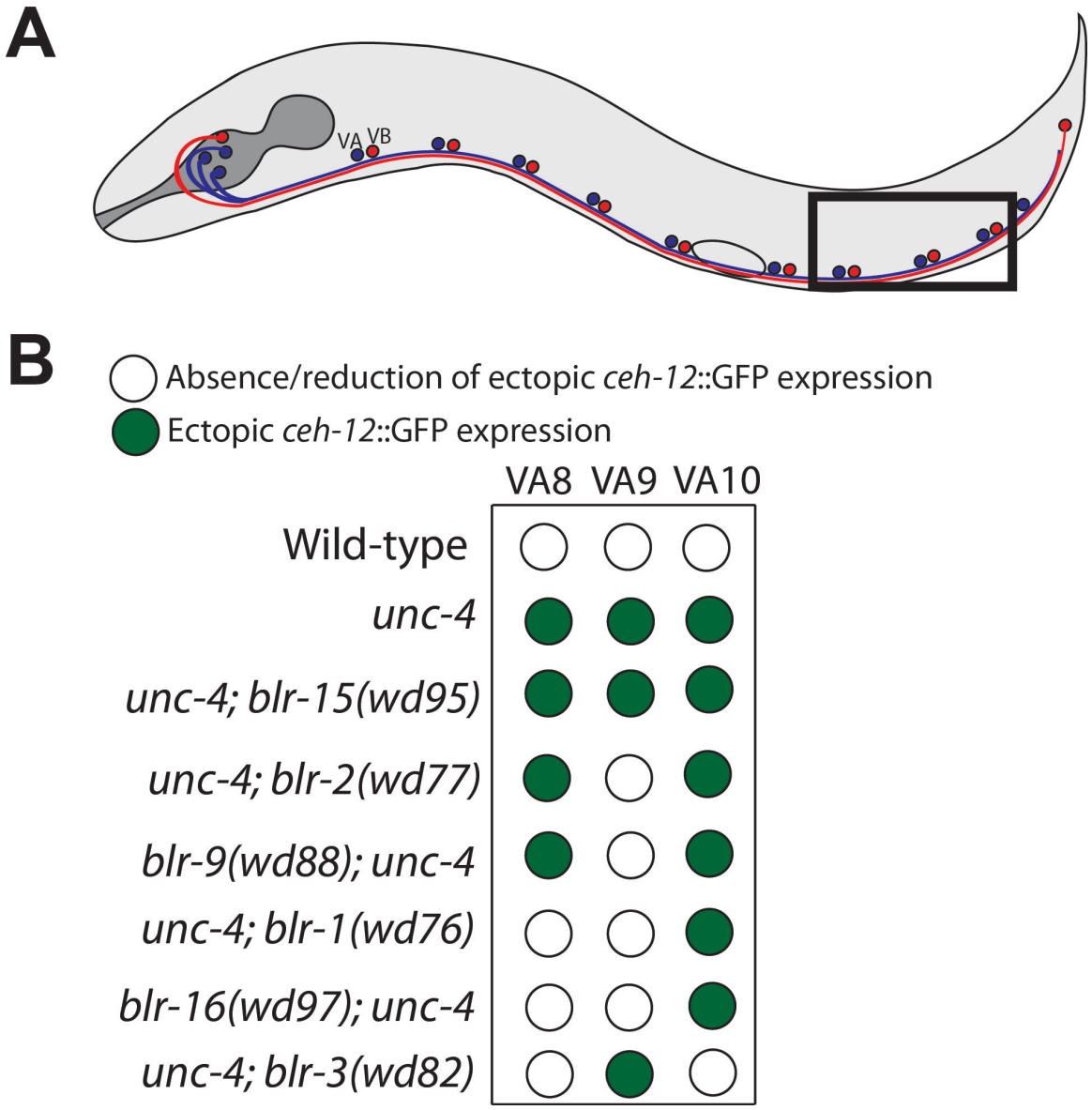

Figure 2.5. *ceh-12*::GFP is differentially regulated in *blr* mutants. **A.** VA and VB motor neurons are located side-by-side along the length of the ventral nerve cord. Location of posterior neurons VA8, VA9, VA10 is denoted by inset. **B.** *ceh-12*::GFP is exclusively expressed in VB motor neurons in wild-type. *unc-4(e120)* mutants show ectopic *ceh-12*::GFP expression in VA8-VA10. *wd95* does not affect ectopic *ceh-12*::GFP expression in *unc-4* animals. *wd77* and *wd88* are required for ectopic *ceh-12*::GFP expression in VA9. *wd97* and *wd76* are required for ectopic *ceh-12*::GFP expression in VA8 and VA9. *wd82* is required for ectopic *ceh-12*::GFP expression in VA8 and VA10. n ≥10 for each neuron. All *blr* alleles are compared to *unc-4*; green circles indicate significance ($p \leq 0.05$), Fisher's Exact test.

VA motor neurons where they either regulate *ceh-12* expression (*e.g. blr-9* in VA9) or function in a parallel pathway (*e.g. blr-9* in VA8 and VA10) (Fig. 2.5).

blr mutations suppress the Unc-4 miswiring defect of specific VA motor neurons

We utilized an *in vivo* gap junction assay to directly investigate the roles of the *blr* mutants in the creation of VB-type inputs to specific VA motor neurons. In wild-type animals, gap junctions with the forward circuit interneuron, AVB, are normally reserved for B-class motor neurons (DB and VB). Gap junctions between AVB and ventral cord motor neurons can be visualized with the GFP-tagged innexin protein, UNC-7S::GFP [38, 114]. AVB gap junctions are recognized as GFP puncta adjacent to the cell soma of motor neuron partners (see Methods). In *unc-4(e120)* mutants, VA motor neurons (VA2-VA10) are miswired with gap junctions from AVB (Fig. 2.6) [38, 42]. We have previously shown that *ceh-12* and genes in the EGL-20-mediated Wnt pathway that function upstream of *ceh-12* are required in posterior VA motor neurons for gap junctions with AVB [42]. Thus, *blr* mutants that function exclusively in the *ceh-12* pathway should be required in only posterior VAs. Conversely, mutations in *blr* genes that function in parallel to *ceh-12* are predicted to eliminate AVB gap junctions with anterior VAs.

We confirmed the previous finding that *ceh-12* is required for ectopic AVB gap junctions with posterior VAs [42] (Fig. 2.6). The finding that *blr-4(wd83)* has no effect on AVB gap junctions with *unc-4* mutant VAs is not consistent with the results of genetic complementation tests suggesting that *wd83* is an allele of *ceh-12*, which clearly is required for AVB to VA gap junctions [42]. Thus disparity and the results of whole genome sequencing (WGS) which failed to detect a *ceh-12* coding sequence defect argue that *wd83* is likely to affect a novel gene that does not have a role in gap junction specificity. A potential role for the *wd83* locus in the choice of chemical synaptic inputs to VAs remains a possibility (see Discussion). Consistent with the finding that the

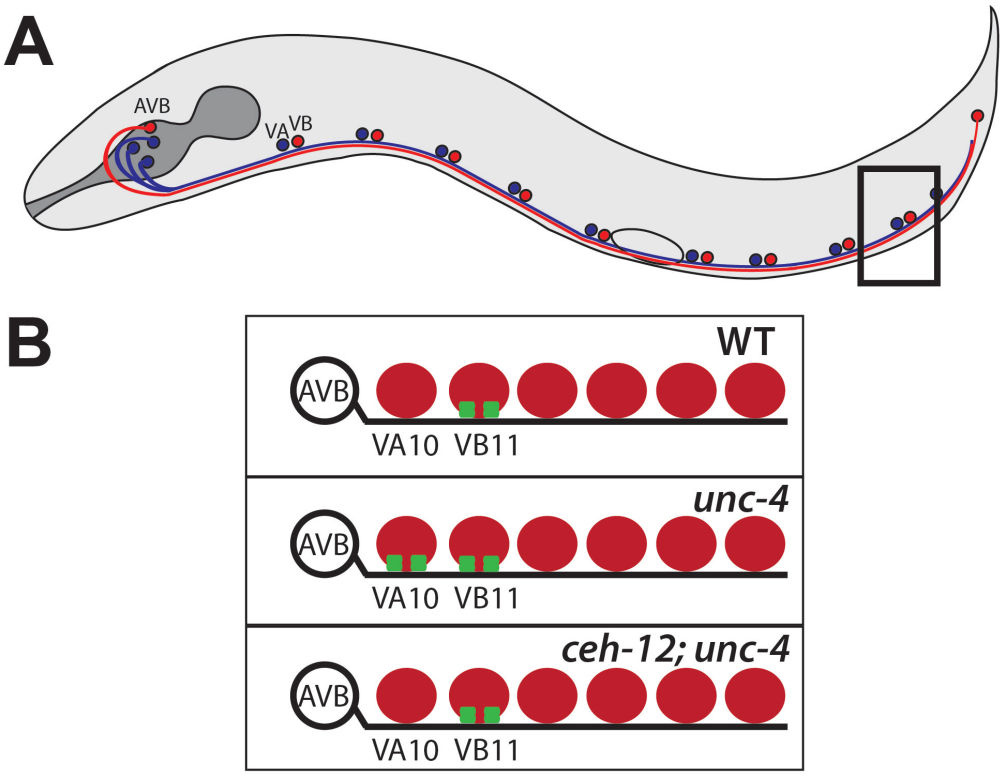
A
AVB
VA
VB
B
WT
AVB
VA10 VB11
unc-4
AVB
VA10 VB11
ceh-12; unc-4
AVB
VA10 VB11
C
VA2 VA3 VA4 VA5 VA6 VA7 VA8 VA9 VA10
Wild-type
unc-4
ceh-12; unc-4
blr-4(wd83); unc-4
unc-4; blr-2(wd77)
unc-4; blr-3(wd82)
unc-4; blr-1(wd76)
blr-9(wd88); unc-4
unc-4; blr-15(wd95)
unc-4; blr-8(wd87)
unc-4; blr-16(wd97)
Absence/reduction of ectopic UNC-7S::GFP expression
Ectopic UNC-7S::GFP expression

Figure 2.6. *blr* mutants are required for AVB gap junctions in specific VA motor neurons. **A.** Diagram of *C. elegans* motor circuit. Black box denotes VA10/VB11 interval represented in panel (B). **B.** Schematic of gap junction phenotype in *unc-4* mutants. The AVB command interneuron makes gap junctions with VB motor neurons in wild type animals and with VA motor neurons in *unc-4*. Mutations in *ceh-12* suppresses ectopic gap junctions with posterior VAs. **C.** Wild-type animals have no significant AVB to VA gap junctions. *unc-4* mutants have ectopic AVB to VA gap junctions along the length of the nerve cord. Mutation in *ceh-12* suppresses ectopic AVB to VA gap junctions in VA2, 8, 9. *wd83* is not required for ectopic AVB to VA gap junctions. *wd77* and *wd82* are required in VA10 and VA9, respectively, suggestive of a role in the posterior *ceh-12* pathway. *wd76, wd88, wd95, wd87* and *wd97* are all required for ectopic AVB gap junctions with anterior VAs, suggesting that these genes function in parallel to *ceh-12*. Green circles indicate significance $p \leq 0.05$, Fisher's Exact test. $n \geq 10$ for each neuron.

blr-2(wd77) allele does not enhance *ceh-12* suppression *unc-4(e120)*, *blr-2(wd77)* also does not suppress the AVB to VA gap junction phenotype of anterior VAs. The role for *blr-2(wd77)* in gap junction inputs to posterior VAs appears complex with *blr-2(wd77)* suppressing the AVB to VA gap junctions in VA10 but regulating *ceh-12*::GFP exclusively in VA9. This suggests that *blr-2(wd77)* functions downstream of *ceh-12* in VA10.

blr-1(wd76), blr-9(wd88), blr-15(wd95), *blr-8(wd87)* and *blr-16(wd97)* are all required for ectopic AVB gap junctions with anterior VA motor neurons (Fig. 2.6). This finding indicates that these genes function in parallel to *ceh-12*. Genetic results showing that *blr-1(wd76), blr-15(wd95)* and *blr-8(wd87)* enhance *ceh-12(0)* suppression of *unc-4* are consistent with this conclusion. However, because *blr-1(wd76), blr-9(wd88)* and *blr-16(wd97)* are also required for ectopic *ceh-12*::GFP in specific posterior VAs (Fig. 2.5), these genes likely exercise the additional role of functioning in the *ceh-12* pathway in selected VA motor neurons (see Discussion). In contrast, *blr-15(wd95)*, which does not regulate ectopic *ceh-12*::GFP expression (Fig. 2.5) and is required for AVB to VA gap junctions only in anterior VA motor neurons (Fig. 2.6) appears to function exclusively in a separate pathway.

Compound mutant analysis reveals complex genetic interactions between *blr* mutants

Testing compound genetic mutants for additive effects on suppression of *ceh-12; unc-4(e120)* and on AVB to VA gap junctions further elucidated the complex roles for *blr* mutants in individual VAs. Jud Schneider completed some of these experiments, detailed in his thesis, Chapter III. For example, Jud found that *blr-8(wd87)* and *blr-9(wd88)* do not enhance each other's suppression of *ceh-12; unc-4(e120)* and therefore may function in a common pathway. Our results are also consistent with the

observations that *blr-8(wd87)* and *blr-1(wd76)* function in parallel to *ceh-12*, as both mutations enhance suppression of the backward locomotion defect in *unc-4* mutant animals. As explained above, *blr-1(wd76)* is the only allele in this group that enhances *ceh-12* suppression of anterior gap AVB junction connections and regulates posterior *ceh-12*::GFP. Therefore, we predict that *blr-1(wd76)* may play a role in both the *ceh-12* pathway and in additional anterior pathways. This model predicts that the *ceh-12; blr-1(wd76)* double mutant would suppress the AVB gap junction defect in both posterior (*ceh-12* pathway) and anterior (*blr-1(wd76)*) pathways.

Whole genome sequencing reveals candidate loci for *blr* mutations

We used whole genome sequencing to identify candidate genes for eleven *blr* alleles (Table 2.3). Jud Schneider initially sequenced five *blr* mutants: *blr-8(wd87), blr-9(wd88), blr-15(wd95), blr-1(wd76)* and *blr-2(wd77)*. To minimize the cost of this effort, Jud and Ian Boothby (Hume Fogg High School, Nashville, TN) constructed triple mutant strains, *e.g. blr-8(wd87); unc-4; blr-9(wd88)*, such that two *blr* alleles could be sequenced in one sequencing reaction. The strains sequenced in this first round were:

blr-8(wd87); unc-4(e120); blr-9(wd88)

ceh-12(gk391); unc-4(e120); blr-1(wd76); blr-2(wd77)

ceh-12(gk391); unc-4(e120); blr-8(wd87); blr-15(wd95)

With Clay Spencer's extensive bioinformatics knowledge, we were able to compile a short list of interesting candidates (Table 2.3) from this first round of sequencing. For example, the *blr-1(wd76)* allele had mutations in two potential genes, F57G8.7 and *srh-136*. F57G8.7 is an uncharacterized, nematode-specific gene (Wormbase). Whole genome sequencing identified a premature stop codon in the first exon of F57G8.7. *srh*-136 encodes a putative 7-transmembrane G protein coupled receptor (GPCR). Whole genome sequencing identified a 299bp deletion that spans the

first two exons of *srh-136* (Fig. 2.7). I chose to focus on testing if *blr-1(wd76)* was an allele of *srh-136* with the hypothesis that it might function as a GPCR for GOA-1/Gαo to promote VB-type inputs in VA motor neurons (see Chapter V).

blr-1(wd76)* is not an allele of *srh-136

With the help of an international summer student, Zhouran Jerry Li (Boston University), I confirmed by Sanger sequencing that the *blr-1(wd76)* strain has a 299bp deletion in *srh-136* (Fig. 2.7). We constructed a strain for analyzing potential effects on AVB to VA gap junctions, *unc-4(e120); blr-1(wd76); wdIs54* (Fig. 2.8 "New") and confirmed homozygosity for the 299bp deletion in *srh-136.* We confirmed that this "NEW" line showed statistically equivalent suppression of ectopic gap junctions to VAs compared with the original (Fig. 2.6, Fig. 2.8 "OLD").

If the 299 bp deletion in *srh-136* is responsible for the suppression of AVB to VA gap junctions in *unc-4; blr-1(wd76)* animals, then we would expect to restore an Unc-4-like gap junction phenotype when wild-type *srh-136* is introduced into this background. To test this, we injected either a genomic *srh-136* DNA clone or a fosmid that spans the *srh-136* chromosomal region (Fig. 2.9A). However, introduction of either the genomic clone (*srh-136 Gen*) or of the fosmid (*srh-136 Fos*) showed similar suppression of ectopic AVB to VA gap junctions compared to *unc-4; blr-1(wd76)* (Fig. 2.9B) and *unc-4* (Fig. 2.9C). These data suggest that *srh-136* is not involved in the *unc-4* pathway and does not encode the *blr-1(wd76)* allele. These data also suggest that *wd76* may be a mutation in the uncharacterized F57G8.7 gene.

Figure 2.7. *srh-136* is an uncharacterized nematode-specific G protein coupled receptor. The *wd76* allele includes a 299bp deletion that spans the first two exons of *srh-136*.

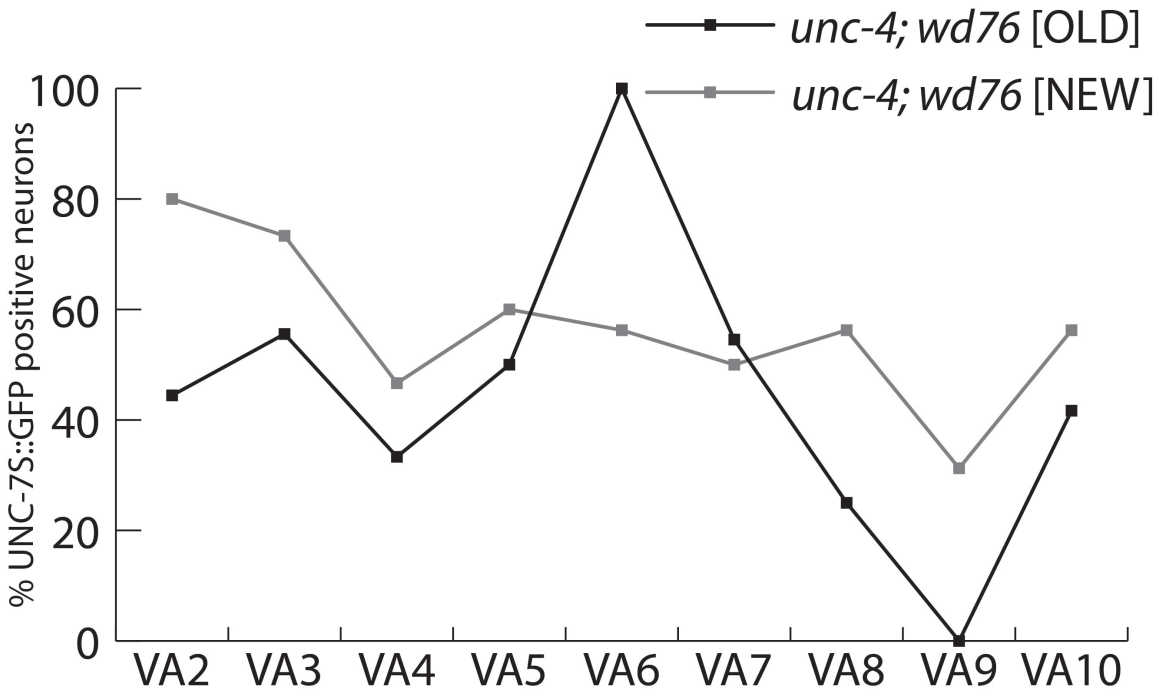

Figure 2.8. Two separately constructed *unc-4; wd76; wdIs54* lines have statistically similar degrees of suppression of ectopic AVB to VA gap junctions. “OLD” refers to the strain that was constructed and characterized at the beginning of the study (data also shown in Fig. 2.6). The “OLD” strain was confirmed to have the 299bp deletion in *srh-136*. “NEW” refers to the strain constructed at a later date that was genotyped to confirm the presence of the *srh-136* deletion. p = 0.0525 for VA9, Fisher’s Exact Test.

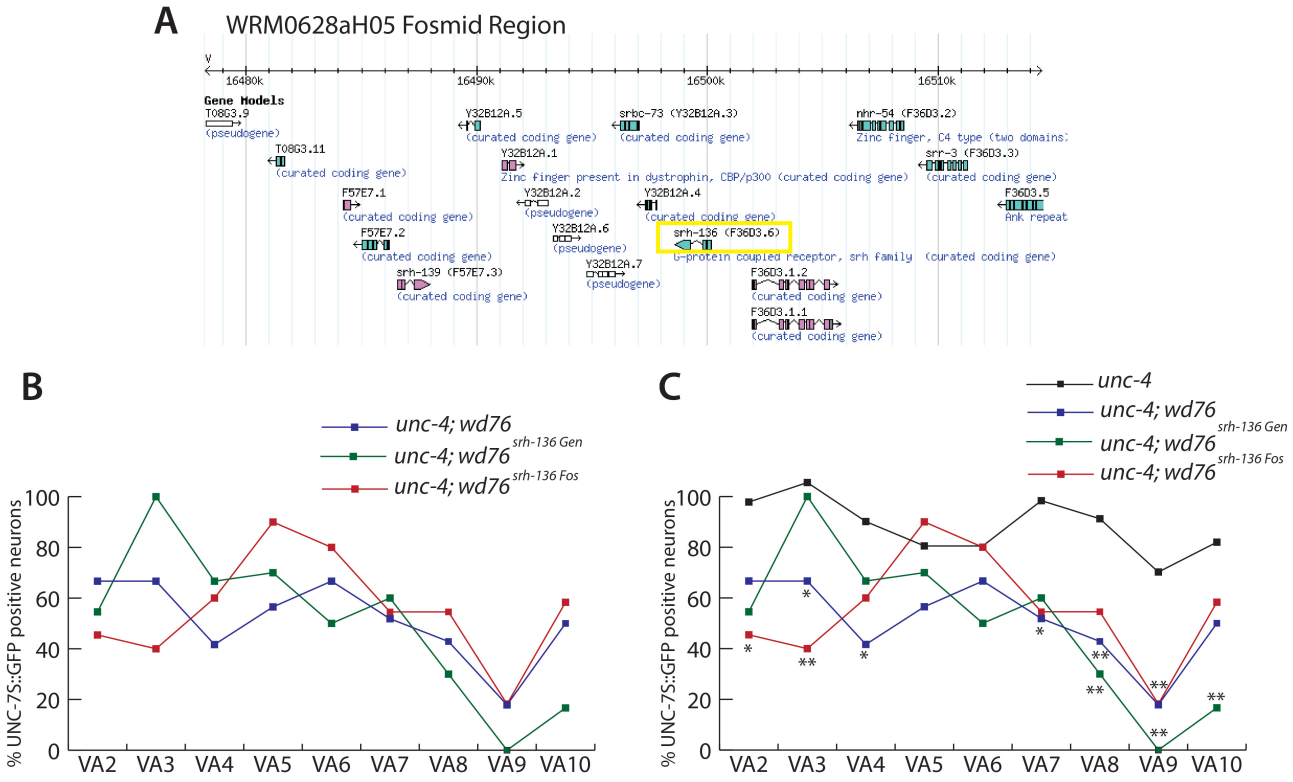

Figure 2.9. *srh-136*/GPCR is not required for suppression of AVB to VA gap junctions in *unc-4; wd76* mutants. **A.** Region of coverage of the WRM0628aH05 fosmid. Yellow box marks location of *srh-136*. **B.** Introduction of wild-type genomic DNA of *srh-136* (*srh-136 Gen*) or of a fosmid containing the full length chromosomal region surrounding *srh-136* (*srh-136 Fos*) does not significantly affect suppression of AVB to VA inputs in the *unc-4; wd76* strain (statistics *vs. unc-4; wd76*). Data were pooled from Fig. 2.8 for the *unc-4; wd76* values. **C.** Transgenic rescue with *srh-136* genomic or fosmid DNA in *unc-4; wd76* animals still shows suppression *vs. unc-4* in most VAs. ** $p \leq 0.01$, * $p \leq 0.05$, Fisher's Exact test *vs unc-4*. $n \geq 10$ for each neuron.

Whole genome sequencing identifies potential *blr* loci

The second round of sequencing focused on the alleles *wd24* (isolated by L. McGrew in an *unc-4(e2322ts)* suppressor screen, 1994) and *wd85* (both presumed *unc-37* alleles)*, blr-3(wd82), blr-4(wd83)* (fails to complement (FTC) *ceh-12*, see above)*, blr-16(wd97)* (FTC *pop-1*), *blr-10(wd89)* (FTC *mig-1*)*, wd98* (FTC *blr-8(wd87)*), and *wd86* (FTC *blr-2(wd77)*). Genomic DNA extraction methods used are described in Methods.

Using the approximate chromosomal map locations from the SNIP-SNP mapping results (Table 2.1) [115], we selected candidate mutations within these intervals with coding sequence variants that were deletions, stop codons, or nonconservative substitutions [116, 117]. In addition, we manually eliminated mutations that were present in multiple strains, as these were unlikely to be the molecular lesion associated with the *blr* phenotype (see methods). Initially, we identified mutations in the *unc-37* coding sequence for the dominant alleles, *wd24* and *wd85*. *wd85* corresponds to an E580K mutation that was previously identified as a dominant *unc-37* mutation in the Miller lab [40]. E-580 is located in the predicted sixth propeller-like domain of the WD repeat protein-interacting region [40]. The E580K mutation is predicted to affect the UNC-4-interacting domain but not overall UNC-37 function, as expression of UNC-37(E580K) mutant protein in *unc-37(0)* mutants failed to rescue all Unc-37 mutant phenotypes [40]. The *wd24* mutation corresponds to a G438E change and represents a new *unc-37* allele. The affected glycine is located in a β-sheet within the third propeller-like structure of the WD repeat region (Fig. 2.10). Unc-4 suppression by *unc-37(wd24)* is weaker than that of *unc-37(wd85)* which likely explains why *wd24* was not detected in the original screen for strong, dominant Unc-4 suppressors [39].

As mentioned previously, we did not detect any mutations in the coding regions of candidate genes in *wd96, wd89, wd100* (*mig-1*), *wd92, wd97, wd99* (*pop-1*) or *wd83*

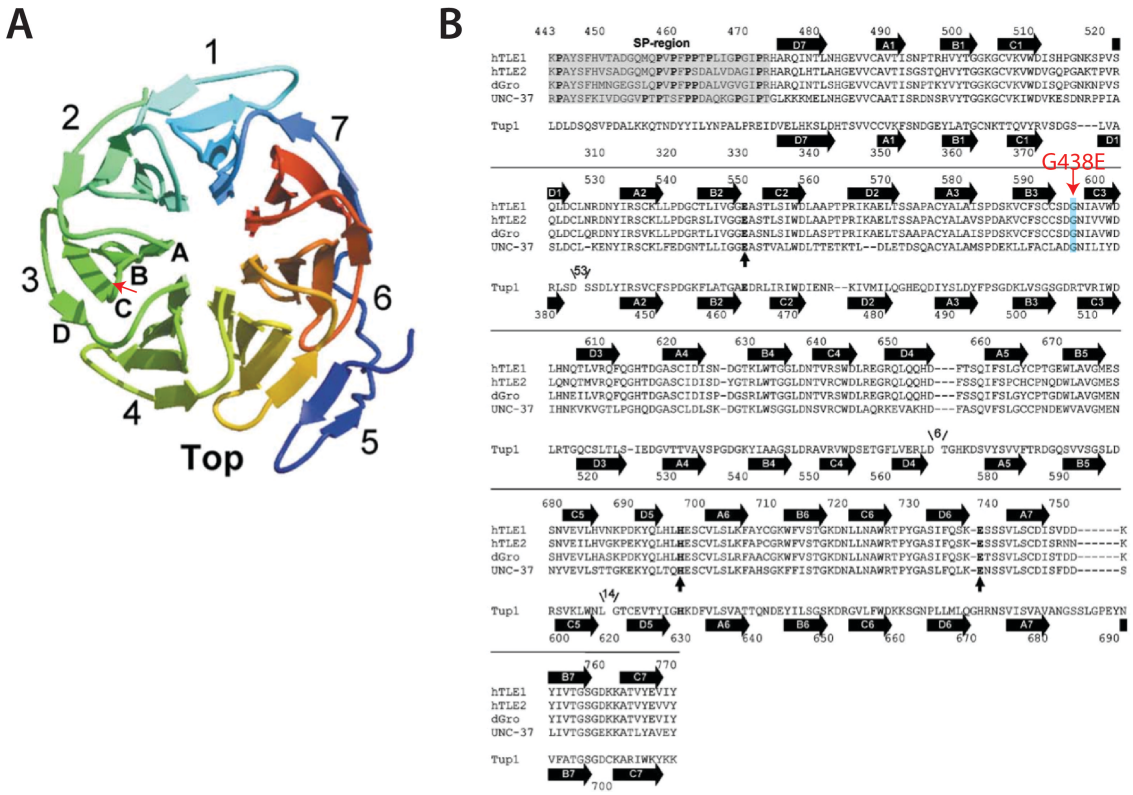

Figure 2.10. *wd24* is a G438E point mutation in a conserved glycine in *unc-37*/Groucho. **A.** Ribbon diagram of *unc-37*. Red arrow represents location of *wd24* mutation in a β-pleated sheet of the third propeller-like structure. Figure adapted from [118]. **B.** The G438E mutation in *wd24* is in a Glycine that is conserved between the two human TLE/Groucho homologs (hTLE1 and hTLE2) and *Drosophila* Groucho (dGro).

(*ceh-12*) with Sanger sequencing. Consistent with these results, whole genome sequencing did not detect mutations in the coding regions of these genes for *wd97 (pop-1), wd89 (mig-1)* or *wd83 (ceh-12)*. Based on the chromosomal map locations of the *blr* mutants (Table 2.1), we then searched for other potential candidate genes for selected *blr* mutants (Table 2.3). For example, *wd83* shows a premature stop in the phosphodiesterase gene, *pde-5*, which likely corresponds to a null allele. *pde-5* is homologous to the human PDE10, which has been shown to cleave both cGMP and cAMP [119]. We have shown that a gain-of-function mutation in *gsa-1*/Gαs inhibits ectopic AVB to VA gap junctions (Chapter V). Because cAMP is a second messenger of *gsa-1*/Gαs and cGMP and cAMP have both been implicated in gap junction biogenesis and function [120], we proposed that mutation in *pde-5* would increase cAMP levels and inhibit VB-type inputs in VA motor neurons. In this scenario, mutations in *pde-5* might suppress the Unc-4 backward movement defect of *unc-4(e2322ts)* mutants.

With the help of Gwynne Davis, a rotation student in the lab, we tested the predicted null allele, *pde-5(ok3102)*, which is a 410 bp deletion that spans exons 9-11 (Wormbase). However, these experiments showed that the *pde-5(ok3102)* mutation has no effect on *unc-4(e2322ts)* movement at 23 °C (Fig. 2.11A) and thereby ruled out the possibility that *wd83* is an allele of *pde-5*. Additional genes with mutations in the *blr-4(wd83)* background include a missense mutation in *xpo-2*, a Cellular Apoptosis Susceptibility (CAS) homolog, two conservative missense mutations in the unnamed, Kelch-like protein, R12E2.1, and a mutation that causes a premature stop in M04F3.2, which is likely an RNA binding protein. Although none of these genes have obvious roles in synaptic choice, it is possible additional analysis that may uncover a novel role for one of these proteins in the nervous system.

The *blr-16(wd97)* mutant failed to complement *pop-1*/TCF. Although whole genome and Sanger sequencing failed to identify mutations in the *pop-1* coding region,

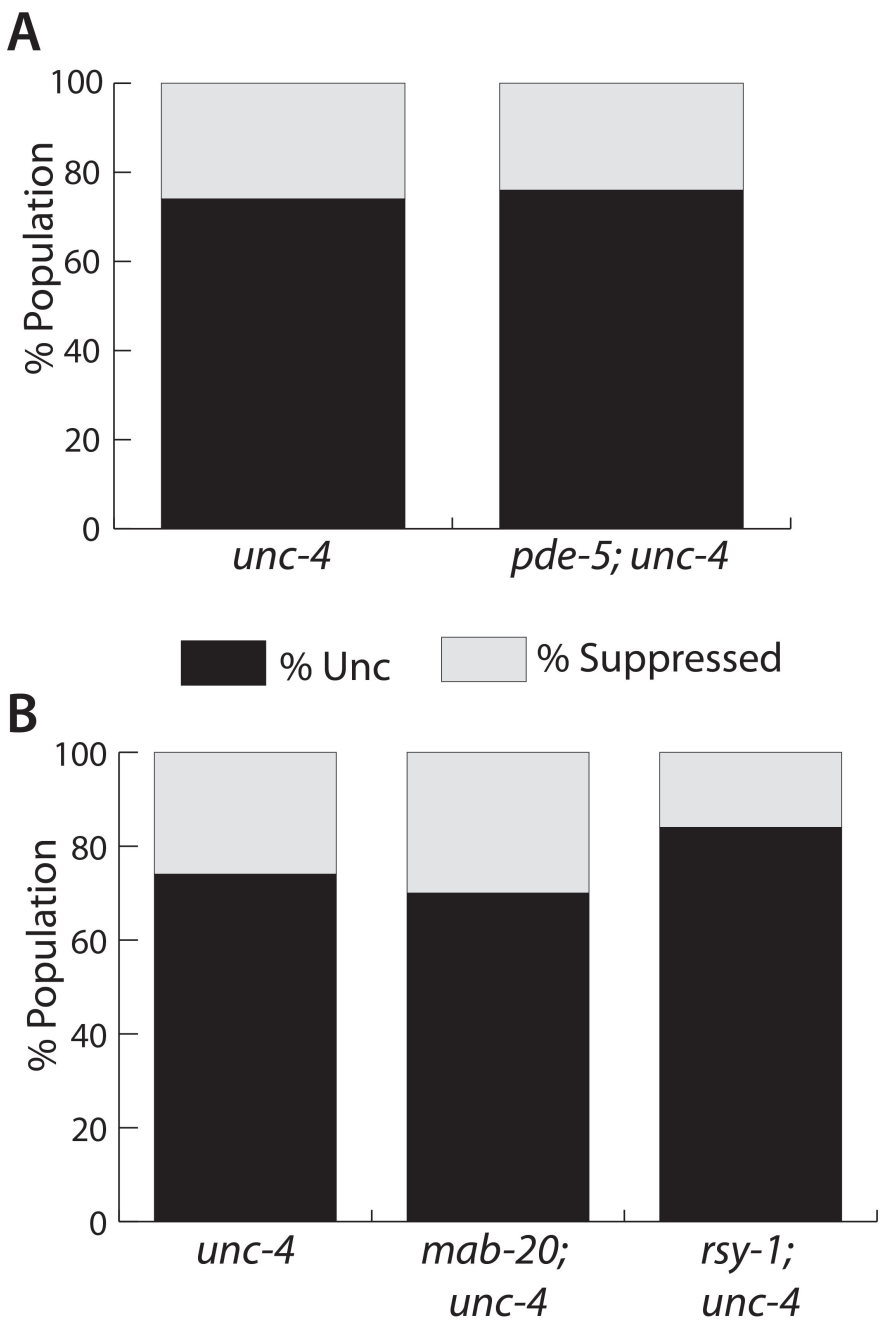

Figure 2.11. Tapping assays of potential *blr* genes. **A.** The *pde-5(ok3102)* mutation does not affect movement of *unc-4(e2322ts)* at 23 °C. **B.** The *mab-20(bx24)* and *rsy-1(wy94)* alleles do not affect *unc-4(e2322ts)* movement at 23 °C.

we did identify one unique nucleotide change in the third intron of *pop-1*. The potential effect of this mutation on POP-1 function is unclear. Missense mutations were identified in two genes, *mab-20*/Semaphorin and *rsy-1*/Regulator of Synaptogenesis for *blr-16(wd97)*. Both *mab-20*/Semaphorin and *rsy-1*/Regulator of Synaptogenesis have been shown to function in the nervous system. Semaphorins function as either repulsive or attractive axon guidance cues [121] and have recently been shown to control input specificity to motor neurons in the vertebrate spinal cord [122]. RSY-1 functions as negative regulator of presynaptic assembly [123]. Thus a mutation in *rsy-1* mutation might be expected to suppress Unc-4 by partially restoring normal VA inputs.

To test whether *blr-16(wd97)* was a mutation in *mab-20* or *rsy-1*, we looked at Unc-4 backward movement in combination with established alleles of each gene. Mutations in either *mab-20(bx24)* or *rsy-1(wy94)* had no effect on *unc-4(e2322ts)* movement at 23 °C (Fig. 2.11B). Thus, *blr-16(wd97)* is likely not an allele of *mab-20* or *rsy-1*. Additional missense mutations detected in the *blr-16(wd97)* strain include a mutation in *unc-87*, which through alternative splicing, produces two proteins that are required to maintain the structure of myofilaments in body wall muscle cells (Wormbase), two predicted secreted proteins, C46H11.7 and M04C9.4, which may have novel signaling roles in the nervous system, and an innexin, *inx-21*. *inx-21* is expressed at low levels in the early embryo and young adult whole animals (Wormviz) and RNAi of *inx-21* yields no visible phenotypes (Wormbase). However, because innexins are components of invertebrate gap junction channels [124], *inx-21* may have a previously unidentified role in synaptic choice.

For *blr-10(wd89)*, which failed to complement *mig-1*/Frizzled, whole genome sequencing identified mutations in both *mig-1* and *ceh-12* intronic regions. Although these mutations are not immediately indicative of an effect on one of these genes, they

may disrupt a potential regulatory site and thus impair the function of one of these known *unc-4* pathway interactors.

We identified candidate mutations in F-box proteins for *blr* alleles *blr-3(wd82)* and *blr-8(wd87)/wd98* (Table 2.3). F-box proteins function as substrate recognition components for E3 ubiquitin ligases [125]. It has been previously shown that F-box proteins are required for selective synapse elimination in *C. elegans* [27], thus, these F-box proteins may normally promote removal of VA synapses in *unc-4* mutants.

Lastly, although *wd86* and *wd77* were predicted to be alleles of the same gene, sequencing of *wd86* revealed no shared mutations in any coding regions within the designated chromosomal interval compared with *blr-2(wd77)*. Intergenic mutations were identified in the uncharacterized genes, F28E10.1 and in F55F10.1, which is homologous to Midasin, a predicted nuclear chaperone protein (Wormbase) that is expressed at low levels in many cell types (Wormviz).

DISCUSSION

Available evidence indicates that neuron-specific gene expression regulates the choice of synaptic partners. In the nematode, *C. elegans*, the UNC-4 transcription factor is selectively expressed in VA motor neurons to repress genes that specify an alternative pattern of presynaptic inputs that is characteristic of VB class motor neurons. One of these VB genes, *ceh-12*/HB9, is ectopically expressed in posterior VA motor neurons in *unc-4* mutants [42]. CEH-12 expression in posterior VAs is required for the formation of ectopic gap junctions with the AVB interneuron of the forward motor circuit. However, ectopic AVB inputs to anterior VA motor neurons are not regulated by *ceh-12*, which suggests that other ectopically expressed *unc-4* target genes function in these cells. With the goal of identifying these additional *unc-4* regulated synaptic specificity genes,

we designed a genetic screen to identify new mutations that restore backward locomotion to *unc-4* mutants. Suppression of the Unc-4 movement phenotype would be expected for mutations that disable genes required for the creation of ectopic VB-type inputs with VA motor neurons. This screen yielded 22 independent Unc-4 suppressor or *blr* (backward locomotion restored) alleles mapping to 16 complementation groups. In this work, we describe detailed phenotypic characterization of a selection of these Unc-4 suppressors mutations, including at least four *blr* loci that function in parallel to *ceh-12*. Additional tests using whole genome sequencing data of the *blr* mutants should reveal the identities and functions of these genes in the *unc-4* pathway.

blr mutants function in individual VA motor neurons to regulate synaptic choice

The neuron-specific resolution of the gap junction assay used in this work allows for the identification of AVB gap junctions with individual VA motor neurons. Using this approach, we determined that specific VA motor neurons require different *blr* genes for these ectopic connections. In addition, the *blr* mutants have VA-specific effects on *ceh-12*::GFP expression. Our results identified *blr* genes that function in one of three different types of interactions between the *blr* alleles and the *ceh-12* pathway: 1) *blr* mutants may function exclusively in the *ceh-12* pathway (*e.g. blr-2(wd77)*); 2) *blr* mutants may function in the *ceh-12* pathway in select VAs and in parallel to *ceh-12* in other VAs (*e.g. blr-1(wd76)*); 3) *blr* mutants may always function in parallel to *ceh-12* (*i.e. blr-15(wd95)*). Fig. 2.12 summarizes the roles of each *blr* mutation in regulating *ceh-12*::GFP expression and AVB to VA gap junctions.

Mutation in *ceh-12* suppresses ectopic AVB gap junctions in posterior *unc-4* mutant VA motor neurons (VA8, VA9, VA10). We identified *blr-2(wd77), blr-3(wd82)* and *blr-1(wd76)* as potential interactors with the *ceh-12* pathway in specific posterior

A

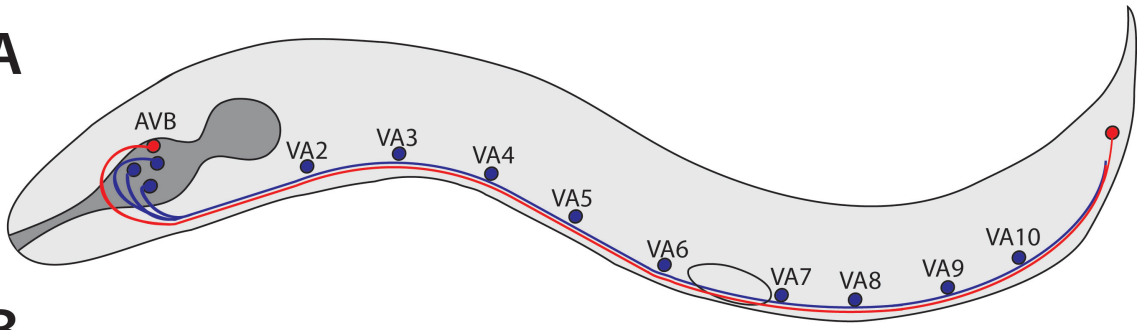

B

	Enhances *ceh-12* suppression of *unc-4(0)*	Required for ectopic AVB to VA gap junctions					Required for ectopic *ceh-12*::GFP expression in VA motor neurons		
		VA2	Anterior VAs	VA8	VA9	VA10	VA8	VA9	VA10
wd76									
wd77									
wd82									
wd83	ND						ND	ND	ND
wd85							ND	ND	ND
wd87							ND	ND	ND
wd88	ND								
wd95									
wd97	ND								

Figure 2.12. Specific *blr* genes are required for synaptic choice in particular VA motor neurons. **A.** Schematic of VA motor neurons and the AVB interneuron. **B.** Summary of data presented in this work. Green boxes denote significant suppression; gray boxes denote no significant difference *vs. unc-4*, Fisher's Exact Test. ND= not done.

neurons. *blr-2(wd77)* does not enhance *ceh-12* suppression of the null *unc-4(e120)* allele (Table 2.4). In addition, *blr-2(wd77)* is required for ectopic *ceh-12*::GFP expression in VA9 and it regulates ectopic AVB to VA gap junctions in VA10. *blr-3(wd82)* results in suppression of ectopic *ceh-12*::GFP expression in VA8 and VA10*)* but is exclusively required for AVB to VA gap junctions in VA9. *blr-1(wd76)* mutants may function upstream to regulate *ceh-12* expression and thereby control regulate AVB to VA inputs in VA8 and VA9 (Figs. 2.5, 2.6, 2.12). However, *blr-1(wd76)* mutants enhance *ceh-12* suppression of the null *unc-4(e120)* allele, suggesting that *blr-1(wd76)* also functions in parallel to *ceh-12* (Table 2.4). We propose that this enhanced suppression phenotype is due to the roles for *blr-1(wd76)* in anterior VA2, VA3, VA4, and VA7, in addition to its role upstream of *ceh-12* in posterior VAs. Based on these data, we hypothesize that *blr-2(wd77)*, *blr-3(wd82)* and *blr-1(wd76)* function in distinct posterior *unc-4* mutant VA motor neurons to control *ceh-12*::GFP expression and ectopic AVB gap junctions.

We identified five *blr* alleles (*blr-1(wd76), blr-8(wd87), blr-9(wd88), blr-15(wd95), blr-16(wd97)*) that are required for ectopic AVB gap junctions with anterior VAs. Three *blr* alleles *(blr-1(wd76), blr-8(wd87), blr-9(wd88))* suppress AVB to VA gap junction within the same group of anterior motor neurons (VA2, VA3, and VA8) (Fig. 2.6), suggesting that these genes function in a common pathway. Through the construction of compound genetic mutants, Jud Schneider showed that *blr-8(wd87)* and *blr-9(wd88)* function in a common pathway and may have additional interactions with *blr-1(wd76)*. Whether *blr-1(wd76)* functions in the *blr-8(wd87)/blr-9(wd88)* pathway can be determined by examining double mutants for enhanced Unc-4 suppression.

blr-15(wd95) is required for ectopic AVB gap junctions in anterior VA3 and in VA6 and VA7 in the midbody (Fig. 2.6). In addition, *blr-15(wd95)* enhances *ceh-12* suppression of the Unc-4 backward movement defect and does not regulate *ceh-12::GFP* expression. These data are consistent with the model in which the *blr-15(wd95)*

mutation affects a gene that functions in parallel to *ceh-12*. Through double mutant analysis, Jud Schneider showed that *blr-15(wd95)* and *blr-8(wd87)* function in parallel to each other and *ceh-12* in posterior VA motor neurons to regulate AVB to VA gap junctions. Our gap junction data also predicts that because *blr-15(wd95)* and *blr-1(wd76)* seem to suppress wiring defects in different neurons, it is possible that these two mutations may genetically enhance suppression of *unc-4(0)*. This hypothesis can be tested by the creation of double and triple mutant strains (e.g. *unc-4(e120); blr-1(wd76) blr-15(wd95)*) with these *blr* mutations.

Surprisingly, the *wd83* allele, which suppresses Unc-4 and failed to complement *ceh-12*, did not suppress ectopic AVB to VA gap junctions. This may be indicative of a role for *blr-4(wd83)* in other aspects of wiring, such as chemical synapses. We have utilized GFP Across Synaptic Partners (GRASP) to assay AVA to VA10 chemical synapse connections (Chapters III and IV).

Complementation tests reveal complex genetic interactions

Complementation tests suggested that specific *blr* mutants were alleles of the known *unc-4* pathway interacting genes *pop-1, mig-1* and *ceh-12*. For example, the *blr-10(wd89)* mutant failed to complement *mig-1*/Frizzled, one of the Wnt receptors we have shown to be required for ectopic *ceh-12* expression in posterior VA motor neurons (Chapter IV) [104]. Whole genome sequencing failed to identify mutations in the coding region of *mig-1* in the *blr-10(wd89)* strain. Similar negative results were obtained for *pop-1(wd97)* and *ceh-12(wd83)*. One explanation of the lack of identification of mutations in the predicted loci is non-allelic non-complementation, which occurs when two different loci behave as though they are mutations in the same gene. This genetic event implies that the two proteins physically interact; mutating both proteins may act as “poison” to a protein complex, or both mutations reduce the dosage, or threshold level of the proteins,

resulting in a similar phenotype [126]. Although initially considered to be a rare event, more recent evidence suggests that non-allelic non-complementation occurs frequently within other organisms [127], and can be especially prevalent in genetic screens [128]. Additional *blr* alleles that failed to complement *pop-1 (wd92, wd99)* or *mig-1 (wd96, wd100)* could be sequenced to address this question.

Whole genome sequencing of *blr* alleles

We utilized whole genome sequencing of *blr* alleles to search for the molecular lesions responsible for Unc-4 suppression. Candidate genes were selected based on genetic intervals established by SNIP-SNP mapping [115] (Table 2.1) and reference alleles of each gene assayed for Unc-4 suppression. Surprisingly, none of the genes tested (*srh-136, pde-5, mab-20, rsy-1*) showed Unc-4 suppressor activity. These results are disappointing but mutations in other candidate genes in these regions could now be tested. For example, we show that *blr-1(wd76)* is not an allele of *srh-136*, as we are unable to rescue the suppression of ectopic AVB to VA gap junctions by introduction of either genomic DNA or fosmid DNA clones of wild type *srh-136* (Fig. 2.8). However, Clay Spencer noted that the *blr-1(wd76)* strain also contains a premature stop in the first exon of F57G8.7. Because this protein is a nematode-specific protein, the functional implications of a mutation in F57G8.7 are unknown. However, it is possible that F57G8.7 exercises an important role in the nervous system to regulate synaptic choice.

It is also possible that the SNIP-SNP mapping technique that we used to assign each *blr* mutation to specific chromosomal regions was misleading. The SNIP-SNP protocol involves crossing the *blr* mutation into the Hawaiian strain of *C. elegans* (Fig. 2.3). Each *blr* allele is recovered by selecting for Unc-4 suppressors from offspring. The Blr phenotyping of at least some of these outcrossed lines could correspond to modifier mutations from the Hawaiian strain. Because the original *blr* mutants were used for

WGS, the map locations of the presumptive Hawaiian-derived *blr* alleles would be misleading. Additionally, it has been reported that there is a high rate of Bristol SNPs on LGI (Bass and Hardaway, personal communication), thus possibly inaccurately linking genes to this region. Advances in techniques used to map mutations from genetic screens have potentially eliminated the need for the SNIP-SNP mapping protocol. For example, a recently published a protocol involves back-crossing the mutagenized line into the un-mutagenized parental (Bristol) strain; a comparison of WGS data from both lines should distinguish between variants showed by both lines *vs.* novel variants that are unique to the mutagenized strain [129]. This approach eliminates the possibility of the spurious introduction of a Blr modifier from the Hawaiian background.

Mutations in *blr* genes have no effect on VB wiring

Our results show that *ceh-12* and other *blr* genes identified in this work promote the creation of VB type inputs (AVB gap junctions) with VA motor neurons. However, we did not detect a role for any of the *blr* genes, including *ceh-12*, in the formation of AVB gap junctions with VB motor neurons (data not shown). Similar negative results were obtained for mutations in Wnt and G-protein pathway genes that selectively affect VA input specificity but are not necessary for AVB gap junctions with VB motor neurons (Chapters IV, V). These results indicate that Blr mutations affect genes that are sufficient to induce VB-type inputs in VAs, but are not necessary in VB motor neurons. The simplest explanation for the phenomenon is that Blr genes encode components with highly redundant functions in VB motor neurons. We could test this model by examining the effects of double mutants of *blr* alleles with Wnt and G protein signaling pathway genes on AVB gap junctions with VB motor neurons.

Table 2.5. List of genes and alleles used in this work. *C. elegans* knockout Consortium is abbreviated CGC.

Gene	Allele	Description	Reference
ceh-12	*gk391*	HB9 transcription factor	[42]
unc-4	*wd1*	Homeodomain transcription factor	[35]
unc-4	*e2322ts*	Homeodomain transcription factor	[112]
unc-4	*e2323*	Homeodomain transcription factor	[112]
unc-4	*e120*	Homeodomain transcription factor	[112]
unc-37	*e262*	Groucho	[112]
unc-37	*wd85*	Groucho	This work
unc-37	*wd24*	Groucho	This work
unc-24	*e138*	Stomatin-like	[112]
mig-1	*e1787*	Frizzled Receptor	[112]
blr-1	*wd76*		This work
blr-2	*wd77*		This work
blr-2	*wd86*		This work
blr-3	*wd82*		This work
blr-4	*wd83*		This work
blr-16	*wd92*		This work
blr-16	*wd97*		This work
blr-16	*wd99*		This work
blr-10	*wd96*		This work
blr-10	*wd89*		This work
blr-10	*wd100*		This work
blr-5	*wd84*		This work
blr-8	*wd87*		This work
blr-8	*wd98*		This work
blr-9	*wd88*		This work
blr-11	*wd90*		This work
blr-12	*wd91*		This work
blr-15	*wd95*		This work
blr-19	*wd101*		This work
blr-20	*wd102*		This work
blr-21	*wd103*		This work
pde-5	*ok3102*	Phosphodiesterase	CGC
rsy-1	*wy94*	Interacts with mammalian pinin	[123]
mab-20	*bx24*	Semaphorin	[130]

Future Directions and Conclusions

The results from this genetic screen have revealed a surprisingly large number of genes that regulate synaptic choice. In combination with our work revealing that Wnt and G-protein signaling also regulate VB-type inputs to *unc-4* mutant VAs (Chapter IV, V), these findings are indicative of roles for multiple developmental pathways in this complex decision. Future experiments will focus on identifying the molecular lesions in these *blr* mutants by first confirming their genetic map locations. For example, *blr-15(wd95)* clearly functions in parallel to *ceh-12. blr-15(wd95)* affects gap junctions outside of the area of *ceh-12* function, in mid-body VAs, and it does not regulate *ceh-12*::GFP expression (Fig. 2.5, 2.6). Thus, identification of the gene that contains the *wd95* mutation might show a role for an additional pathway involved in synaptic choice.

Two other groups of *blr* alleles that would be interesting to pursue on are *blr-2(wd77)*, *blr-8(wd87/wd88)* and *blr-1(wd76*.) Although genetic evidence indicates that *blr-2(wd77)* functions in the *ceh-12* pathway, it does not regulate *ceh-12*::GFP expression (Fig. 2.5) in VA10 and therefore could exercise a downstream role. Because CEH-12 likely functions as a transcription factor, molecular identification of *blr-2(wd77)* could reveal a cell surface or cytoplasmic component with a direct role in synaptic choice. Genetic data indicate that *wd87* and *wd88* are mutations in the same gene (Fig. 2.12). Genetic tests described in Jud Schneider's dissertation indicate that *wd87/wd88* might function with *blr-1(wd76)*.Thus, the identification of proteins encoded by the *blr-1* and *blr-8* loci could identify a signaling pathway and suggest a biochemical mechanism for direct experimental tests.

Lastly, we can test for interactions between *blr* mutants and Wnt or G-protein pathway components, which we have shown to function in both anterior and posterior VA motor neurons (Chapter IV, V). This work has provided a solid genetic characterization of mutations that suppress both the Unc-4 backward movement defect

and the specific wiring defect seen in *unc-4* mutants. Additionally, preliminary genetic interactions have allowed us to create models for how these genes might interact in pathways. These results are expected to provide a foundation for a detailed cell biological analysis of the mechanism of synaptic choice in this motor circuit.

CHAPTER III:

UNC-4 REGULATES CHEMICAL SYNAPSES BETWEEN INTERNEURONS AND VA MOTOR NEURONS

INTRODUCTION

Organization of the motor circuit is crucial for coordinated movement. This organization includes the tight regulation of connections between partner neurons, a requirement for the establishment of a functional circuit. Chemical synapses use transmission of neurotransmitters between two neurons, while gap junctions, which are comprised of channels between apposing cells, allow for electrical signals and small molecules to be transmitted between neurons. Previously established visualization techniques provided many details of the critical aspects of synapse specificity, including the correlation of synaptic structure with function, identification of synaptogenic proteins, trafficking dynamics of synaptic components, and synaptic partner identification. While electron microscopy (EM) reconstruction provides detailed ultrastructural analysis of synapses, the process is arduous and it does not allow for identification of multiple synaptic components [102]. Additionally, EM provides only a static image, whereas more modern techniques, such as time-lapse, allow for dynamic imaging. Utilizing fluorescent molecules to label synaptic proteins has allowed for real-time imaging and analysis, thus providing details about the localization of synaptic proteins and trafficking dynamics that was beyond the resolution of EM technology [102]. Additionally, recent advances in detection technology have allowed for the visualization of single fluorescent molecules, further advancing the ability to resolve protein dynamics [131].

In this Chapter, I describe two techniques that we have utilized to examine the regulation of chemical synapse formation in the *C. elegans* motor circuit. Backward locomotion requires the postembryonic VA motor neurons, which are born and then integrate into the ventral nerve cord during the late L1 stage [1]. VA motor neurons receive chemical inputs from the command interneurons, AVE (Fig. 3.1) and AVD and chemical synapses and gap junctions from AVA [132]. Inputs from these interneurons activate VA motor neurons to synapse onto muscle and drive backward locomotion. The precise connectivity between AVA, AVE and AVD with VA motor neurons is required for coordinated backward movement [133]. To determine how these intricate circuits are organized, we have utilized a genetic mutant that affects backward locomotion. The *unc-4* gene encodes a homeodomain transcription factor that is expressed in VA motor neurons and represses the expression of genes that would otherwise direct VB-type inputs to VA motor neurons [42]. In *unc-4* mutant animals, connections normally made with VA motor neurons are lost, and replaced by ectopic VB-type connections from AVB and PVC [38]. This results in the inability to crawl backward. Using genetic techniques, including forward genetic screening (Chapter II), we have identified many molecular components that regulate synaptic choice.

Preliminarily, we assayed effects on wiring based on movement phenotypes. As mentioned above, *unc-4* mutants are unable to move backward. Mutations in VB-type genes that are ectopically expressed in *unc-4* mutant VAs suppress the Unc-4 backward movement defect. However, to understand the biological roles of these VB-type genes in the *unc-4* pathway, it was necessary to establish an assay to detect wiring connectivity. Previously, the wiring defect in *unc-4* mutants was described by using electron microscopy (EM) reconstruction [38]. While this methodology allowed for ultrastructural analysis of the synapses, it was a difficult and slow undertaking, evident by the fact that

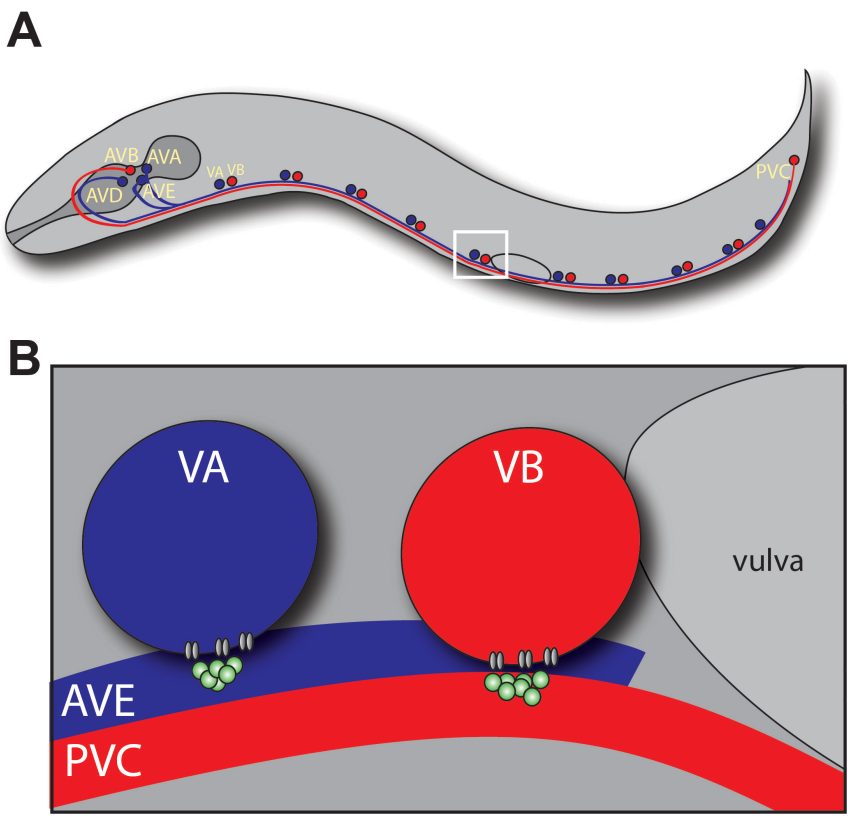

Figure 3.1. Schematic of the *C. elegans* motor circuit. **A.** The cell soma of command interneurons located in the head or tail. Interneuron processes extend in a tight fascicle along the length of the ventral nerve cord and synapse with motor neurons. Interneurons AVA, AVD and AVE synapse with VA motor neurons and control backward locomotion. AVB and PVC synapse with VB motor neurons and control forward locomotion. White box denotes region enlarged in (B). **B.** The process of the AVE interneuron terminates just anterior to the vulva and makes chemical synapses with VA motor neurons to control backward locomotion. The PVC interneuron process extends anteriorly into the ventral nerve cord. PVC makes chemical synapses with VB motor neurons to control forward locomotion. Green circles depict synaptic vesicles filled with neurotransmitter. Gray blocks represent neurotransmitter receptors.

only three partial *unc-4(e120)* worms were reconstructed for this work [38]. Thus, the use of fluorescently labeled synaptic components was required to resolve the synapticwiring defects in *unc-4* mutants. The Miller lab has previously utilized a fluorescently tagged gap junction protein, UNC-7S::GFP, to show that *unc-4* function inhibits AVB to VA gap junctions, and that the VB-gene, *ceh-12* is required for these connections [42]. Here, I describe two other fluorescent markers used to examine how *unc-4* regulates chemical synapse formation.

MATERIALS AND METHODS

C. elegans strains and culturing

Nematodes were cultured under standard conditions [112]. Stains with the transgene *wyIs58* (*opt-3*::GFP::RAB-3, *unc-122*::RFP) were generously provided by the K. Shen lab. Strains carrying the GRASP *wyEx1845* transgene were generously provided by the Shen and M. Van Hoven labs [103].

Microscopy

wyIs58 and GRASP animals were anesthetized with 0.1% tricaine/tetramisole and mounted on a 2% agarose pad. *wyIs58* animals were imaged in a Zeiss Axiovert microscope with a 63x objective, using MetaMorph software. Developmental stage of *wyIs58* animals was determined by gonad structure. GRASP animals were aged-matched to L4 stage. Only animals with a vulval morphology that resembled a fully formed “Christmas tree” were imaged in a Leica TCS SP5 confocal with identical microscope settings (see protocol below).

Quantification of number of GFP::RAB-3 puncta

The number of GFP::RAB-3 puncta was manually counted from live images of *wyIs58* animals. The experimenter was blinded to genotype to avoid bias. n ≥ 20 animals for each genotype. The number of puncta within each genotype was averaged and is reported with standard deviation bars. Statistical significance was determined by Student's T test. n= 20.

Quantification of intensity of GFP::RAB-3 puncta

The intensity of GFP::RAB-3 puncta was quantified for L2 and L4 animals using the linescan tool in the MetaMorph software, which reported the average intensity along the length of the linescan. A threshold was set to standardize between animals. The GFP intensity per animal was pooled and averaged to get an average intensity for each group. The average intensity of each genotype is reported with standard deviation bars. Significance was determined by Student's T Test. n= 20.

GRASP Plasmid Construction and transgenic line construction

All plasmids were created using traditional cloning methods. pRLS2 (*Punc-4*::GFP11::NLG-1) was constructed by digesting out the *unc-4* promoter from *unc-4*::mcherry with SphI and AscI sites and putting into SphI/AscI digested pCJS44 (*Pflp-18*::GFP11::NLG-1). pRLS3 (*Pdel-1*::GFP1-10::NLG1) was constructed by amplifying 1.8kb of the *del-1* promoter from the pJR6gfp construct and adding SphI and AscI sites to the promoter fragment with the primers: pdel-1_SphI 5' GGGGGGGCATGCTCAAGTCCCACCTCAACCCCC and pdel-1_AscI 5' CCCCCCCGGCGCGCCCCTTGCCATTATTTTTTC. This *Pdel-1* PCR fragment was digested with SphI/AscI and put into pWCS61 (*Pdes-2*::GFP1-10::NLG-1) in place of *Pdes-2*. pRLS4 (*Ppag-3*::GFP1-10::NLG-1) was constructed by amplifying 2.4 kb of the

pag-3 promoter from the pJR8 construct and adding SphI and AscI sites to the promoter fragment with the primers: ppag-3_SphI 5' GGGGGGCATGCCTGCAGGTCGACTCTAGAATC and ppag-3_AscI 5' CCCCCCGGCGCGCCCTTCGTCTCAACACACAAA. This *Ppag-3* PCR fragment was digested with SphI/AscI and put into pWCS61 (*Pdes-2*::GFP1-10::NLG-1) in place of *Pdes-2*. Transgenic lines were generated via microparticle bombardment [134] or injection into N2 animals.

Quantification of GRASP signal from *wdIs65* (AVA to VA/DA) transgenic lines

The NC1921 strain with the transgene, *wyEx1845* (20 ng/ul MVC46/unc-4::nlg-1::GFP1-10. 30 ng/ul MVC12/flp-18::nlg-1::GFP11, 5 ng/ul unc-4::mCherry, and odr-1::RFP) [103] was integrated by gamma irradiation (4000 Rads). This line labels AVA to A-class motor neuron synapses. Analysis was focused on the VA10 to DA7 interval [103]. Z-stacks were collected with identical microscope settings. Line scans were collected in the GFP channel. To obtain an average background signal, an equivalent length scan was collected from the posterior dorsal nerve cord (that should be devoid of GFP puncta). For each sample, the intensity score was calculated from the percentage of measurements from the VA10 to DA7 interval that exceeded the background signal. n ≥ 10 for each neuron.

Quantification of GRASP signal from *wdEx828* (AVA to VA/VB) transgenic lines

To quantify the number of GRASP puncta between strains carrying the *wdEx828* transgene, age-matched worms were imaged with the following microscope settings: 1024x1024 resolution. Bidirectional X option active. Argon laser set at 29%; HeNe laser on. Sequential scan setting on, select the "spGFPRachel-1" setting. The GFP laser= 68%; Red laser= 25%; smart gain= 766.3 for GFP channel. DIC gain ≈100. Pinhole was

set to 67.26. Zoom≈ 1.68. Step size 0.5 with the 40x objective. The protocol for imaging each worm and image processing is below:

IMAGING WORM:

1. Find worm with continuous *unc*-4::mcherry expression in the ventral nerve cord
2. Take posterior (P) pic- include ½ of vulva, label *i.e.* e120-1P
3. Take anterior (A) pic- include other ½ of vulva and label i.e. e120-1A
4. Save Lif files
5. In Leica software: Visualize- 3D projection- Apply
6. Save all as Tifs, non-overlapping channels, include micron scale

IMAGE PROCESSING:

1. Open TIFFs in Fiji- open GFP and DIC pics (ch00 and ch03)
2. Click on GFP image
3. IMAGE—8 bit, image will turn B&W
4. Click on GFP image
5. PLUGIN—STRAIGHTEN, opens new window
6. Width/Pixels=10
7. Draw line on VNC Anterior to Posterior * Draw line from pharynx to vulva for Ant pic; draw line from vulva to tail for Post pic
8. Double click line to finish
9. STRAIGHTEN, opens new window of straightened line of puncta
10. IMAGE—TRANSFORM – Rotate 90 degrees to the right (so anterior is up)
11. Save rotated straightened image in “straightened image folder” as i.e. e120-1P
12. ANALYZE—3D OBJECTS COUNTER
13. Threshold= 20—OK

14. Copy and paste data into new worksheet in 3D objects counter excel sheet, rename worm name on top and on worksheet. Input data from anterior to posterior and list the anterior data first (most anterior =0 position and most posterior= last position)

NORMALIZE IMAGE SIZE TO 850 PIXELS

1. Open straightened TIF image in Photoshop
2. IMAGE—IMAGE SIZE—make sure that “constrained proportions” is NOT checked
3. Change height pixels to 850. Width pixels should be 11
4. Save new, normalized image in the “Straightened and sized to 850 pixels” folder
5. Click OK on pop-up box
6. Save normalized images in separate folder
7. Open normalized straightened image in Fiji
8. Open excel file “Normalized intensity values”
9. On the Fiji toolbar, right click on the line tool and select “Segmented Line”
10. Double click on the Segmented Line tool and a box will pop up. Change the line width to 10
11. From top to bottom (Anterior to Posterior), draw a straight line. Double click at the end
12. ANALYZE—PLOT PROFILE—LIST
13. On the list that pops up, check that the values ONLY go from 0-847
14. Copy and paste data from list into “Normalized intensity values” into excel spreadsheet.

RESULTS

unc-4 is partially required for AVE to VA synapses

Previous work from the Miller lab established that the UNC-4 protein is required for proper wiring of VA motor neurons from the late L1 to early L3 larval stages [35]. Thus, we wanted to determine whether UNC-4 was required for the maintenance of these connections. To test this, we used a fluorescently tagged RAB-3 expressed in the AVE interneuron with the *opt-3* promoter. RAB-3 is a member of the RasGTPase family, which has been shown to associate with synaptic vesicles [135]. In *C. elegans,* RAB-3 functions with UNC-10/Rim to target synaptic vesicles to the presynaptic density [136, 137]. The AVE cell body is located in the anterior nerve ring and extends a process into the ventral nerve cord that terminates slightly anterior to the vulva (Fig. 3.1B). AVE primarily makes connections onto A-class motor neurons in the ventral nerve cord (Table 3.1). L2 and L4 larval animals were analyzed for the number of GFP::RAB-3 puncta and GFP intensity along the AVE process in the anterior nerve cord (Fig. 3.2A, B). In wild-type animals, both the number and intensity of GFP::RAB-3 puncta increased from L2 to L4 stages. Two *unc-4* null mutants (*e120)* and *(e2320)* showed significantly fewer GFP::RAB-3 puncta in L2 and L4 stages *vs.* age-matched wild-type animals. Because GFP::RAB-3 localizes to presynaptic domains, these data indicate that *unc-4* is required for the maintenance of AVE to VA chemical synapses during development. Interestingly, although the number of AVE to VA connections was not significantly different between the *unc-4(e120)* and *unc-4(e2320)* mutants at the L2 stage, *unc-4(e2320)* mutant worms had an increased number of puncta in L4 *vs.* L2 animals, while *unc-4(e120)* mutants showed no change in puncta number (Fig. 3.2B). The *e2320* mutation is a deletion early in the coding region of *unc-4*. *e120* is a point mutation that results in a splice donor site

Table 3.1. AVE connections, adapted from wormatlas.org. AVE makes a total of 112 synapses with postsynaptic partners (not all partners shown in table below). 30% of AVE synapses are with DA and VA motor neurons. 12.5% of AVE synapses are with VA motor neurons (Boxed). Synapse Type: S= Neuron 1 is presynaptic to Neuron 2; Sp= polyadic synapse, Neuron 1 is presynaptic to Neuron 2 and other postsynaptic partners. Number= number of synapses between the neuron pairs (wormatlas.org).

Neuron 1	Neuron 2	Synapse Type	Number
AVEL	AS01	Sp	1
AVER	AS01	S	1
AVER	AS01	Sp	2
AVER	AS02	Sp	2
AVER	AS03	S	1
AVEL	AVAL	S	2
AVEL	AVAL	Sp	10
AVER	AVAL	S	2
AVER	AVAL	Sp	5
AVEL	AVAR	Rp	2
AVEL	AVAR	S	4
AVEL	AVAR	Sp	3
AVER	AVAR	Rp	2
AVER	AVAR	Sp	16
AVEL	AVBL	R	1
AVER	AVBL	Rp	2
AVER	AVDR	Sp	1
AVER	AVEL	EJ	1
AVEL	AVER	EJ	1
AVEL	DA01	Sp	5
AVER	DA01	Sp	5
AVEL	DA02	Sp	1
AVER	DA02	S	1
AVER	DA02	Sp	2
AVEL	DA03	S	1
AVEL	DA03	Sp	2
AVER	DA03	S	1
AVEL	DA04	Sp	1
AVER	DB03	Sp	1
AVEL	SABD	Sp	6
AVER	SABD	Sp	2
AVEL	SABVL	Sp	7
AVER	SABVL	Sp	3
AVEL	SABVR	Sp	3
AVER	SABVR	Sp	3
AVEL	VA01	Sp	5
AVER	VA01	Sp	1
AVER	VA02	Sp	1
AVEL	VA03	S	1
AVEL	VA03	Sp	2
AVER	VA03	S	2
AVER	VA04	Sp	1
AVER	VA05	S	1

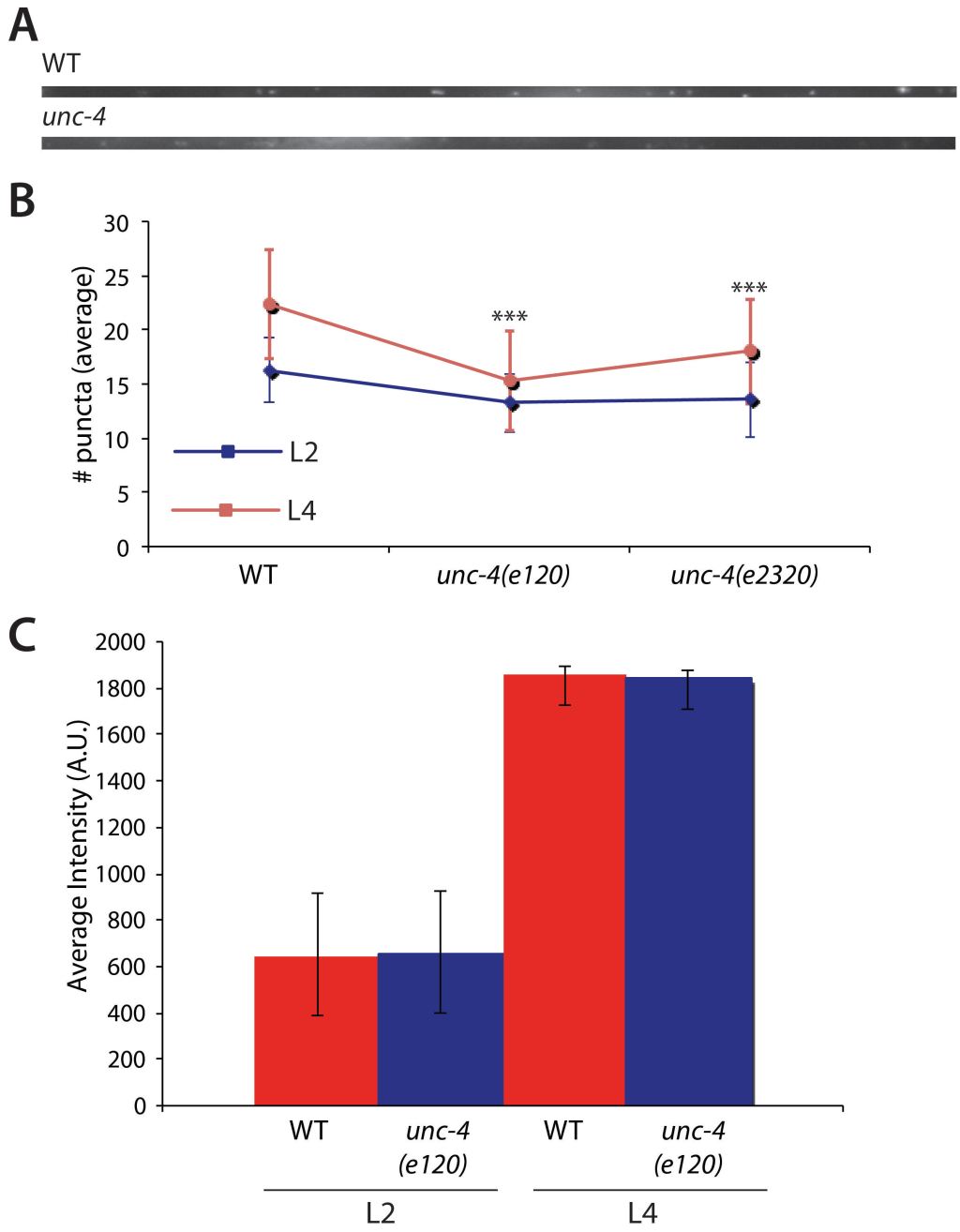

Figure 3.2. AVE to VA synapses change developmentally and are regulated by *unc-4*. **A.** Straightened images of L4 wild type and *unc-4(e120) Popt-3*::RAB-3::GFP. Anterior to the left. **B.** Wild-type animals display an increase in GFP::RAB-3 expression from the L2 to L4 larval stages. The *unc-4* null alleles *e120* and *e2320* have significantly fewer GFP::RAB-3 puncta *vs.* WT in both L2 and L4 stages. *unc-4(e2320)* animals have an increase in GFP::RAB-3 expression in the L4 *vs.* L2 stage; *unc-4(e120)* animals have no change in expression. *** p ≤0.001, Student's T test *vs.* WT. n= 20 animals for each larval stage. **C.** *unc-4* has no effect on intensity of *Popt*-3::RAB-3::GFP puncta. Average intensity is represented in Arbitrary Units (A.U.), see Methods. No significant difference between *unc-4* and WT values for L2 or L4 larval stages, Student's T Test n=20.

exchange [41]. Because these alleles are both predicted to be null *unc-4* alleles, the reason for the difference in results is unclear.

Analysis of the intensity of GFP::RAB-3 puncta showed no difference in average intensity in *unc-4(e120)* animals *vs.* wild type (Fig. 3.2C). Because the overall number of GFP::RAB-3 puncta was decreased in *unc-4(e120) vs.* wild type (Fig. 3.2B), these data suggest that the overall strength of the AVE synapses remain the same. Thus, there might be a compensatory mechanism that regulates AVE to VA synapses in the absence of *unc-4*.

unc-4 is required for AVA to VA synapses

We utilized a split GFP technology, GFP Reconstitution Across Synaptic Partners (GRASP) [103] to confirm if AVA to VA motor neuron chemical synapses were disrupted in *unc-4* mutants, as previously shown by electron microscopy [38]. GRASP utilizes a presynaptic-specific promoter to express a piece of the GFP β-barrel attached to the synaptically localized neuroligin (NLG-1) protein. The complementary piece is expressed in the postsynaptic cell, also fused to NLG-1 (Fig. 3.3). The GFP is reconstituted across the synaptic cleft and is visualized as GFP puncta along the motor neuron processes (Fig. 3.3).

We generated an integrated GRASP transgene, *wdIs65* that marks chemical synapses between the AVA interneuron (*flp-18* promoter) and VA and DA class motor neurons (*unc-4* promoter) (Table 3.2). VA and DA motor neuron processes are arranged in a tight overlapping fascicle in the ventral nerve cord; discrete AVA to VA connections are only visible in a region proximal to the VA10 cell body (Fig. 3.4A). We found that *unc-4* mutants showed a decrease in intensity of GRASP puncta *vs.* wild type (Fig.

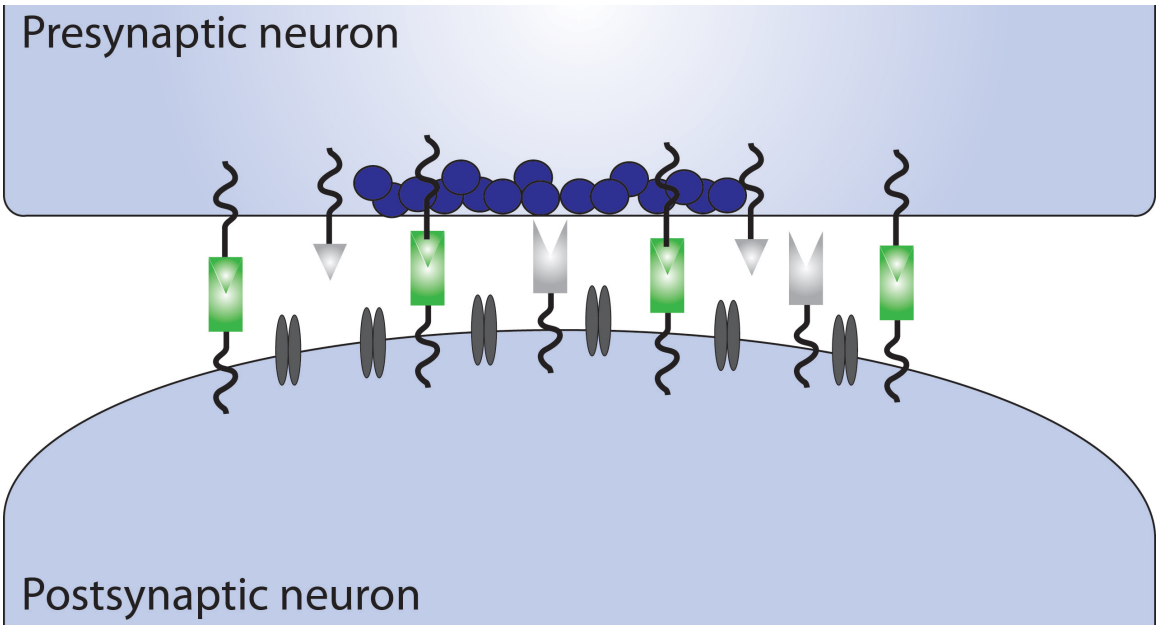

Figure 3.3. Schematic of GFP Reconstitution Across Synaptic Partners (GRASP) technology. One piece of the GFP β-barrel (GFP 1-10) is expressed in the presynaptic neuron with a specific promoter. The complementary piece of GFP (GFP11) is expressed in the postsynaptic partner. Reconstitution of the GFP molecule is visible when the two neurons are in close enough proximity across the synaptic cleft to produce a fluorescent signal. Black squiggle line depicts neuroligin/NLG-1. Green shapes represent reconstituted GFP; light gray shapes are inactive pieces of the GFP molecule. Blue circles represent synaptic vesicles. Dark gray shapes represent neurotransmitter receptors.

Table 3.2. GRASP strains created. "Additional markers" denote the coinjectable markers used to identify transgenic animals. Notes describe observations and results from each experiment.

Transgenic Strain Name	Presynaptic Marker	Postsynaptic Marker	Additional Markers	Transgenic Strain Method	Results/Notes
wdIs65	pCJS44 (*Pflp-18*::GFP11::NLG-1)	pRLS2 (*Punc-4*::GFP11::NLG-1)		Plasmid injection [103]; chromosomal integration via gamma irradiation	Integrated GRASP strain. Decrease in *unc-4* mutant; Suppression seen in *blr, ceh-12* and Wnt mutants (Chapters II, IV)
wdIs76	pCJS44	pRLS4 (*Ppag-3*::GFP1-10::NLG-1)		Microparticle bombardment	Ectopic puncta in dorsal nerve cord; No effect in *unc-4* mutant.
	pCJS44	pRLS4	*Ppag-3*::mcherry, *Pglr-1*::dsRed	Microparticle bombardment	Ectopic mcherry expression in muscle (from *Ppag-3::mcherry*); No GFP puncta.
	pCJS44		*Pglr-1*::dsRed	Microparticle bombardment	Visible for *Pglr-1::dsRed* marker; not tested for puncta because strain with *wdEx772* was too dim to track genetics
wdEx772		pRLS4	*Ppag-3*::mcherry	Microparticle bombardment	*Ppag-3::mcherry* marker was very dim.
	pCJS44	pRLS3 (*Pdel-1*::GFP1-10::NLG1)		Microparticle bombardment	No GFP puncta.
wdEx683	pWCS61 (*Pdes-2*::GFP1-10::NLG-1)	pRLS2	*odr-1*::RFP (25ng/ul)	Plasmid injection	Puncta in VNC and into nerve ring- AVF neuron?
wdEx828	pCJS44	pRLS4	*Pceh-22*::GFP (15ng/ul), *unc-4*::mcherry (5ng/ul)	Plasmid injection	Puncta in VNC; ectopic dorsal puncta; see decrease in *unc-4* mutants vs. WT but no suppression in *ceh-12; unc-4* or *goa-1; unc-4*.

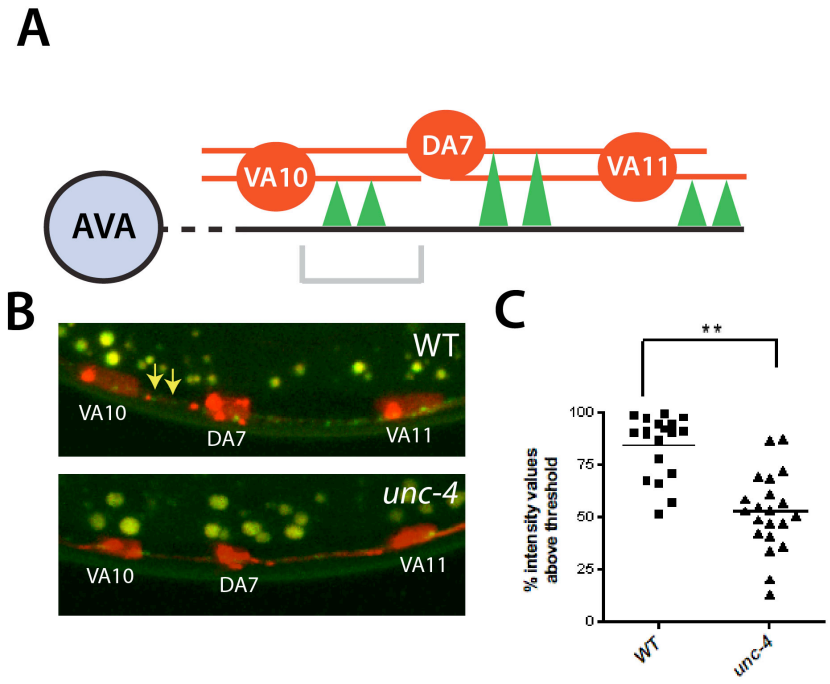

Figure 3.4. The *wdIs65* transgene shows *unc-4* regulation of chemical synapses between AVA and VA10. **A.** Schematic of AVA connections with processes of ventral cord motor neurons. Processes of DA and VA motor neurons overlap with the exception of the VA10 interval (gray bracket). Green triangles denote chemical synapses. **B.** Images of WT and *unc-4* lines with the *wdIs65* transgene. Red= DAPI, Green puncta= GRASP signal. **C.** *unc-4(e120)* mutants have reduced GRASP intensity versus WT. Graph adapted from Jud Schneider.

3.4B,C). These results indicate that *unc-4* is required for normal AVA to VA10 synapses. We have also shown that mutation in *ceh-12* and *egl-20*, which normally promote VB-type inputs to VA motor neurons, are partially required for the loss of AVA to VA synapses in *unc-4* mutants (Chapter IV).

As mentioned above, DA and VA motor neuron processes are in a tightly packed fascicle in the ventral nerve cord. Because the *wdIs65* transgene marks synapses between AVA and both DAs and VAs, this only allows for visualization of AVA to VA10 puncta, eliminating the ability to assay effects on anterior VA motor neurons (Fig. 3.4). Thus, we chose to use the alternative *pag-3* promoter to drives expression of the GRASP piece in VA and VB motor neurons. AVA does not make chemical synapses with VB motor neurons (wormatlas.org), thus driving GRASP fragments with the *flp-18* (AVA) and *pag-3* (VA, VB) promoters should allow for visualization of only AVA to VA synapses. We constructed lines by both microparticle bombardment and plasmid injection that expressed the GRASP components under the *flp-18* and *pag-3* promoters (Table 3.2). The first line constructed by microparticle bombardment (*wdIs76*) contained ectopic GRASP puncta in the dorsal nerve cord, and did not show any difference in GRASP puncta intensity between wild-type and *unc-4* mutants (Table 3.2). The second line constructed expressed the GRASP fragments under the *flp-18* and *pag-3* promoters with the co-selectable markers *Ppag-3*::mcherry and *pglr-1*::dsRed. This line had ectopic mcherry expression in muscle, most likely from the *pag-3* promoter. Additionally, this line showed no visible GRASP GFP signal (Table 3.2).

Because plasmid injection usually results in a higher copy number than microparticle bombardment, we injected animals with the *wdEx828* transgene. This transgenic array contained the *flp-18* and *pag-3* promoters driving the GRASP fragments. Although we again saw ectopic GRASP puncta in the dorsal nerve cord, we saw bright GRASP GFP puncta in the ventral nerve cord (Fig. 3.5A). The intensity of

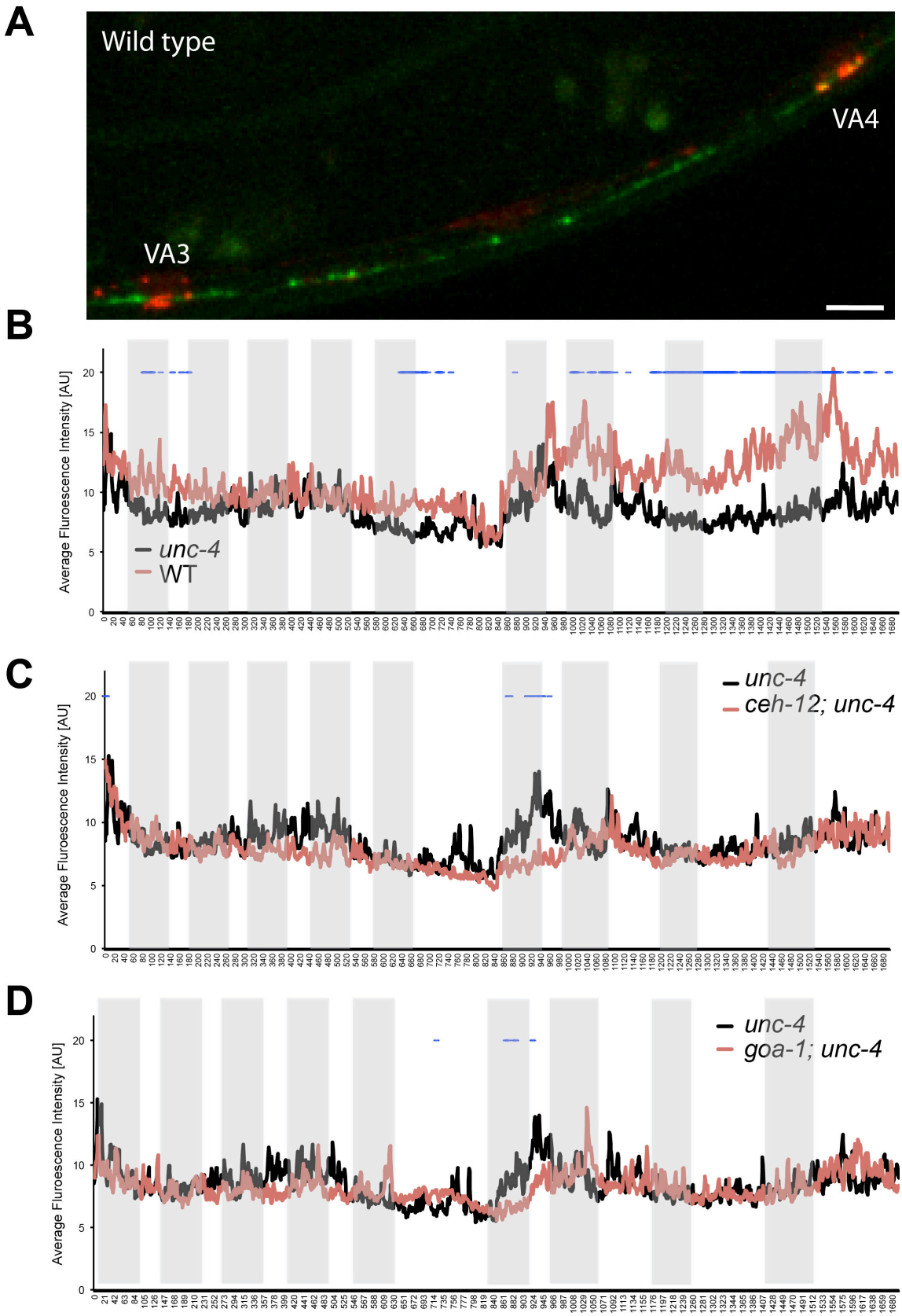
A
Wild type
VA4
VA3
B
Average Fluroescence Intensity [AU]
unc-4
WT
C
Average Fluroescence Intensity [AU]
unc-4
ceh-12; unc-4
D
Average Fluroescence Intensity [AU]
unc-4
goa-1; unc-4

Figure 3.5. *unc-4* but not *ceh-12* or *goa-1* regulates chemical synapses between AVA and VAs. **A.** Image of the *wdEx828* transgenic line in a wild-type background. **B-D.** Average fluorescence intensity in animals with the *wdEx828* transgene was measured in Image J (see Methods). x-axis represents point along body axis (anterior to left, posterior to right). Light gray vertical bars represent approximate location of each VA motor neuron cell body from VA2 (far left) to VA10 (far right). Blue dots indicate points with significantly different ($p < 0.05$, Student's T Test) average fluorescence intensity *vs.* WT (B) or *unc-4* (C-D). **B.** Mutation in *unc-4* results in lower GRASP fluorescence intensity *vs.* WT. **C-D.** Mutation in *ceh-12* or *goa-1* has no effect on chemical synapses between AVA and *unc*-4 mutant VA motor neurons. n=10 animals per genotype.

GRASP puncta was decreased in *unc-4* mutants *vs.* wild type in regions along the length of the nerve cord, although most notably in the posterior (Fig. 3.5B). However, mutation in known Unc-4 suppressors, *ceh-12* [42] and *goa-1* (Chapter V), had no effect on the GRASP signal (Fig. 3.5C,D). These data are contradictory to our finding that mutation in *ceh-12* suppresses a loss of AVA to VA10 synapses using the *wdIs65* GRASP line (Chapter IV). Because of this conflicting data, we decided against further pursuit of a GRASP strain that used the *flp-18* and *pag-3* promoters.

We have previously shown that *unc-4* mutants have ectopic AVB to VA gap junctions [42]. Electron microscopy (EM) reconstruction indicates that *unc-4* mutant VAs also have ectopic chemical synapses from the VB-type command interneuron, PVC. To confirm the EM findings, we used the GRASP assay to test for connections between the PVC interneuron (*des-2* promoter) and A-class motor neurons (*unc-4* promoter). Both GRASP fragments were injected simultaneously in the *wdEx683* transgenic array into N2 worms. Surprisingly, we saw expression throughout the nerve ring and into the ventral nerve cord. Based on the continuous expression and location of the GRASP puncta, we predict that the *wdEx683* transgene most likely marks synapses between the AVA interneuron and the UNC-4-expressing AVF neuron (Fig. 3.6). It has recently been found that in some cases, co-injection or microparticle bombardment of a pair of GRASP plasmids results in a high level of recombination, most likely between the homologous NLG-1 sequences (Garriga lab, personal communication). Instead, separate integrated transgenic lines each expressing one GRASP fragment must be mated together to obtain specific detection of the GRASP signal. We created integrated transgenic lines that expressed individual complementary GRASP fragments in addition to co-selectable fluorescent markers to track expression of the transgene (Table 3.2). Unfortunately, although the co-selectable marker (*Pglr-1*::dsRed) in the transgenic strain that expressed the presynaptic GRASP piece (*Pflp-18*::GFP11::NLG-1) was easily visible,

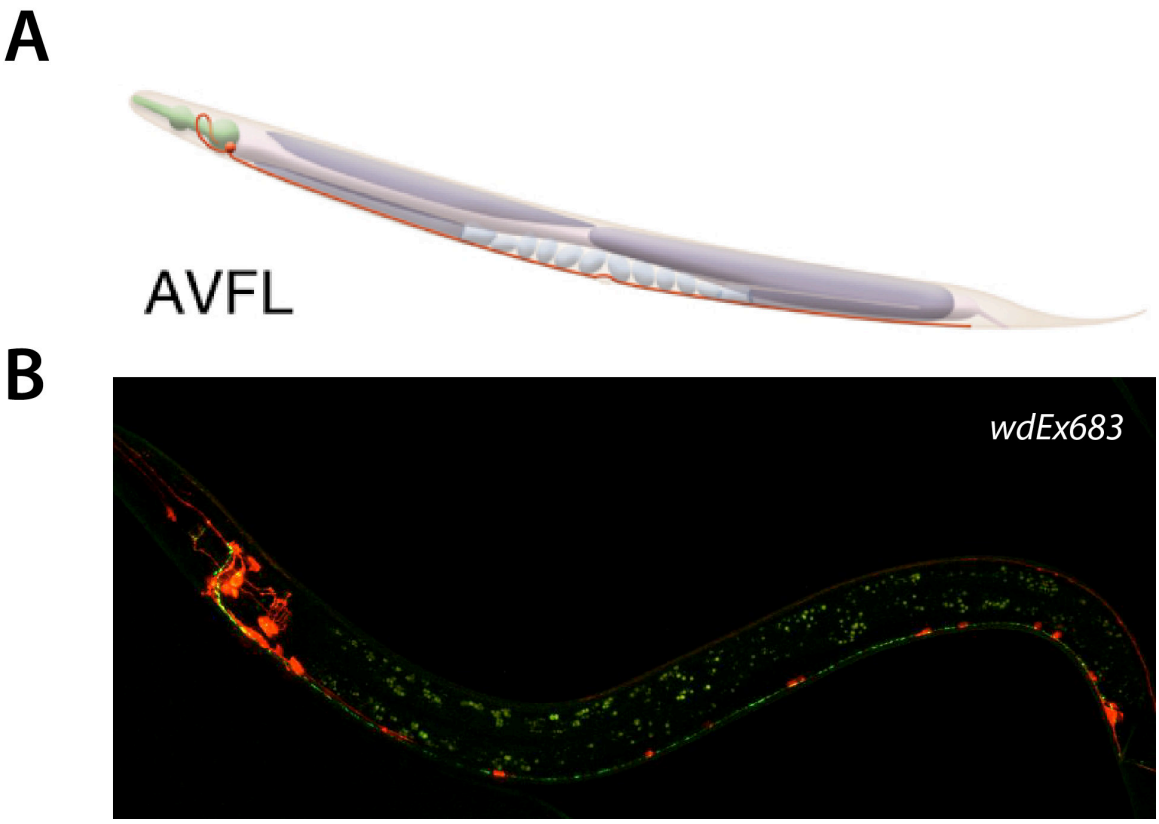

Figure 3.6. Expression of the *wdEx683* transgene (see Table 3.2). **A.** Schematic of AVFL neuron. AVFL cell body is in the nerve ring. The AVF process loops around the posterior pharynx and extends into the ventral nerve cord (wormatlas.org). **B.** Image of L3 animal expressing the *wdEx683* transgene. GRASP signal appears to be in the AVF neuron, as puncta can be seen surrounding the nerve ring and into the ventral nerve cord.

expression levels of the marker (*Ppag-3*::mcherry) injected with the postsynaptic GRASP piece (*Ppag-3*::GFP1-10::NLG-1) were below detectable limits. Thus, additional experiments are needed to identify the proper combination of promoters to accurately assay chemical synapses with VA motor neurons throughout the length of the ventral nerve cord.

DISCUSSION

The use of fluorescent markers in combination with the transparent cuticle of *C. elegans* allows for the *in vivo* visualization of synaptic components in real time. However, as illustrated in the experiments presented in this Chapter, the robustness of the fluorescent assay is dependent upon the proper construction of the visualization tools. Using the presynaptic GFP::RAB-3 (Fig. 3.2) marker and the GRASP assay (Fig. 3.4), we have shown that *unc-4* regulates chemical synapses to specific VA motor neurons. With further refinement of the GRASP assay, we hope to be able to visualize loss of AVA to VA synapses along the length of the ventral nerve cord in addition to the gain of ectopic PVC to VA synapses in *unc-4* mutants.

Using the *Popt-3*::GFP::RAB-3 marker, we showed that *unc-4* is required for the developmental increase in the number of AVE to VA synapses between L2 and L4 larval stages (Fig. 3.2B). However, the intensity of the GFP signal did not change between *unc-4 (e120)* and wild type, suggesting that although the number of presynaptic inputs to VAs is altered in *unc-4* mutants, the strength of the synapses might be higher in the mutant background, leading to the equivalence in GFP intensity (Fig. 3.2C). Because we have shown that components of the EGL-20/Wnt pathway function upstream of *ceh-12* to control both chemical synapses and gap junctions to posterior VAs (Chapter IV), we utilized this AVE marker with the eventual goal of identifying genes that function in anterior VAs. It is clear that select *blr* mutants identified in our genetic screen for Unc-4

suppressors (Chapter II) affect gap junction wiring in anterior VA motor neurons (*i.e. blr-1, blr-8, blr-9, blr-15, blr-16*). Thus, these genes might regulate chemical synapses in this region. Further experiments using the *Popt-3*::GFP-RAB-3 marker would need to repeat the puncta intensity calculations with higher-powered confocal microscopy before proceeding with testing other *unc-4* pathway interacting genes for role in anterior VAs.

Although recent techniques, such as Brainbow [138], array tomography [139], and trans-synaptic tracing [140] have been developed to identify potential synaptic partners, the GRASP technology seems to be the most direct way to determine if two neurons synapse with one another. GRASP has now been successfully used in *C. elegans* [103, 105], *Drosophila* [106] and mouse [108, 109] to detect chemical synapses between specific neuron pairs. However, the specific pairing of plasmids that drive expression of the GRASP fragments is crucial for the ability to utilize the assay [108]. Thus, future experiments should focus on the identification of a more robust pair of promoters for each fragment. Although the *unc-4* promoter resulted in strong expression of the postsynaptic GRASP fragment, *unc-4* is expressed in many cells, including AVF and DA motor neurons, which are intercalated in the ventral nerve cord with VAs. The *pag-3* promoter is expressed in VAs and VBs, thus eliminating the “background” signal from DA motor neurons, but this is a much weaker promoter and may drive ectopic expression in dorsal muscle, seen both with the *pag-3*::mcherry coselectable marker and the observation of GRASP puncta on the dorsal nerve cord. Thus, the ideal postsynaptic promoter would drive expression of the GRASP fragment specifically in VA motor neurons along the length of the nerve cord. Using gene expression data collected from genome initiatives such as ModENCODE, it is possible that a strong VA-specific promoter will be identified in the near future.

Development of a robust GRASP marker could distinguish between genes that regulate chemical synapse or gap junction formation with VA motor neurons. Recent

evidence in other systems suggests that gap junctions and chemical synapses are interdependent; however, the mechanism is still not understood. For example, in leech neurons, transient RNAi knockdown of the gap junction channel protein Innexin 1 (Inx-1), results in impaired formation of chemical synapses. Interestingly, electrical synapses must be present when the chemical synapse is forming; restoration of gap junction function later in development does not rescue the chemical synapse defect. These data led to the hypothesis that gap junctions might be providing signals, electrical or chemical, to the partner neurons. Alternatively, gap junctions might be functioning in an adhesive manner to maintain partner neurons in close proximity during synapse formation and maturation [141].

Additionally, it has been shown that chemical synapses regulate the degree of electrical coupling between cells [142, 143]. For example, in the goldfish, auditory afferents terminate on the M-cell lateral dendrite and signal with both chemical and electrical synapses. This group found that the electrical transmission at the individual synaptic regions was modulated by the local activity of the chemical synapses within the same contact. Chemical synapses might regulate calcium signaling at individual terminals, which in turn modulate the degree of electrical coupling between neurons [142].

This chapter has highlighted the use of tools to visualize the chemical synapse formation in the *C. elegans* motor circuit. As described above, evidence suggests that genes that directly affect chemical synapse formation with VAs might indirectly affect the formation of gap junctions. Thus, with the proper tools, we could have the ability to address the mechanistic interactions between chemical synapses and gap junctions to learn more about the process of circuit assembly.

CHAPTER IV:

UNC-4 ANTAGONIZES WNT SIGNALING TO REGULATE SYNAPTIC CHOICE IN THE *C. elegans* MOTOR CIRCUIT

INTRODUCTION

Nervous system function is defined by connections between specific neurons. These links include chemical synapses that utilize neurotransmitters to evoke postsynaptic responses and electrical synapses comprised of gap junctions that regulate ion flow between coupled neurons. Although some progress has been made toward understanding the molecular basis of chemical synaptic specificity [144, 145], little is known about how neurons choose partners for gap junction assembly [146, 147]. Both types of synapses are active in motor circuits that regulate body movements [148-151]. The key role of transcription factor codes in motor circuit neuron fate suggests that genetic programs define the specificity of these connections [152, 153]. Downstream targets with roles in synaptic specificity are largely unknown but probably include a combination of diffusible cues and cell-surface proteins that regulate synaptogenic responses [34].

Wnt signaling functions as a key regulator of synaptic assembly in the brain and at the neuromuscular junction [154]. For example, in cerebellar neurons, Wnt7a activates a cytoplasmic pathway that promotes local assembly of presynaptic components whereas Wnt-dependent synaptic assembly at the Drosophila neuromuscular junction can also depend on transcriptional regulation [76, 81, 83, 155]. Wnts might also function as antagonistic cues to limit synapse formation [19, 79], and, in

at least one case, adopt opposing roles that either promote or inhibit synaptogenesis [85]. Although multiple members of the Wnt family are expressed in the developing spinal cord and have been shown to regulate axon trajectory and neuron fate, explicit roles in synaptogenesis have not been uncovered [54, 80, 88]. Here, we describe our finding that opposing Wnt signaling pathways regulate the specificity of synaptic inputs in a nematode motor circuit.

In *C. elegans*, backward movement depends on connections between AVA interneurons and VA class motor neurons whereas forward locomotion requires AVB input to VB motor neurons (Fig. 4.1) [133, 156, 157]. The specificity of these connections is controlled by the UNC-4 homeodomain transcription factor, which functions in VA motor neurons [35]. In *unc-4* mutants, AVA inputs to VAs are replaced with gap junctions from AVB and backward locomotion is disrupted. The characteristic anterior polarity of VA motor neurons is not perturbed, however, which suggests that UNC-4 regulates the specificity of synaptic inputs but not other traits that distinguish VAs from sister VB motor neurons [36, 38]. UNC-4 functions as a transcriptional repressor with the conserved Groucho-like protein, UNC-37, to block expression of VB-specific genes [40, 41] (Fig. 4.6). We have shown that one of these VB proteins, the HB9 homolog, CEH-12 (MNX1), is sufficient to rewire VA motor neurons with VB-type inputs [42]. Thus, these findings revealed a regulatory switch in which differential expression of the transcription factors, UNC-4 versus CEH-12/HB9, in VAs results in alternate sets of presynaptic inputs. This mechanism, however, shows regional specificity along the length of the ventral nerve cord. Ectopic expression of *ceh-12*/HB9 in *unc-4* mutants is limited to posterior VA motor neurons and VA input specificity in this location depends on *ceh-12*/HB9. These findings suggest that UNC-4 may regulate multiple targets that function in parallel to specify inputs to selected VA motor neurons in different ventral cord domains [42]. Here we report the discovery that *ceh-12*/HB9 expression in posterior VA

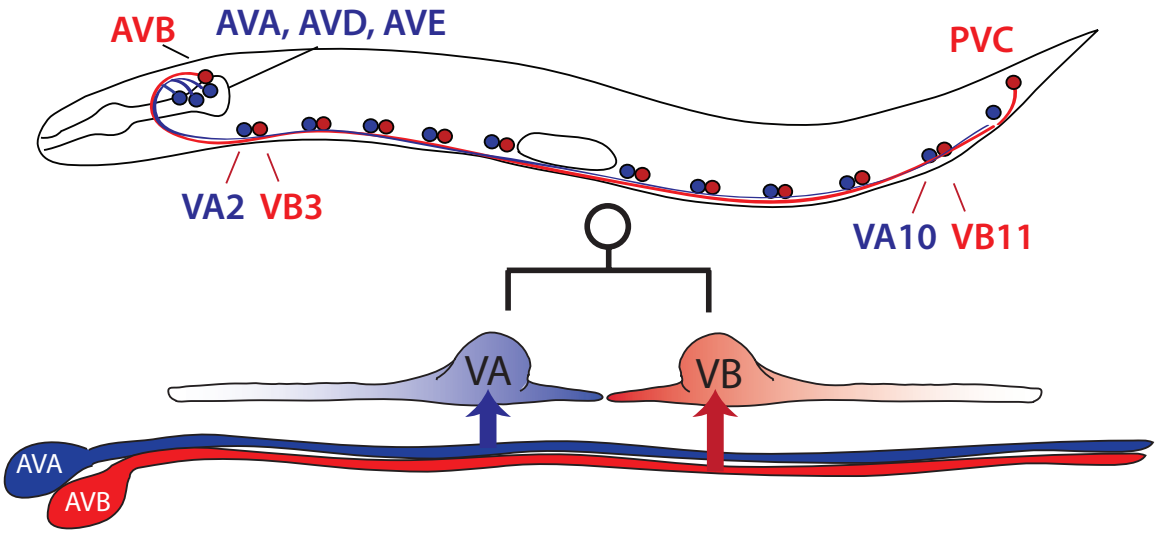

Figure 4.1. Diagram of the *C. elegans* motor neuron circuit. Interneurons from the head and tail extend axons into the ventral nerve cord to synapse with specific motor neurons. The forward circuit (Red) includes AVB and PVC interneurons and DB (not shown) and VB motor neurons. The backward circuit (Blue) includes AVA, AVD and AVE interneurons and DA (not shown) and VA motor neurons. VAs and VBs arise from a common progenitor but are connected to separate sets of interneurons (AVA and AVB shown for simplicity).

motor neurons is activated by a specific Wnt protein, EGL-20, that is secreted from adjacent cells in this region. We propose that UNC-4 normally prevents VAs from responding to EGL-20/Wnt by antagonizing a canonical Wnt signaling pathway utilizing the Frizzled (Frz) receptors MOM-5 and MIG-1. We have also identified a separate Wnt pathway, involving the Frz receptor, LIN-17, and the Wnt ligands LIN-44 and CWN-1,that preserves VA inputs by blocking CEH-12 expression in anterior VAs. Our results have uncovered a key role for the UNC-4 transcription factor in modulating the relative strengths of Wnt signaling pathways with opposing roles in synaptic choice. The widespread occurrence of regional Wnt signaling cues in the developing spinal cord could be indicative of similar functions for transcription factors in regulating synaptic specificity in the vertebrate motor circuit.

MATERIALS AND METHODS

Nematode Strains and Genetics

Nematodes were cultured as described [112]. Mutants were obtained from the *Caenorhabditis* Genetics Center (CGC) or by generous donations from other labs (Tables 4.1 and 4.2). Transgenic strains and primer sequences used for building constructs are listed in Table 4.3.

Molecular Biology

Punc-4::ΔNT-BAR-1 was generated by overlap PCR from plasmid pHCK19 (Table 4.3) [158], microinjected [159] with pMH86 (*dpy-20(+)*) to produce NC1847 *wdEx636 (Punc-4*::ΔNT-BAR-1*, dpy-20(+))* and crossed into *wdIs85* (see below).

Table 4.1. List of alleles used in this study.

	Gene	Allele	Source	Homology
LGI	*lin-44*	*n1792*	CGC	Wnt
	mig-1	*e1787*	CGC	Frizzled
	lin-17	*n671*	CGC	Frizzled
	mom-5	*mom-5(or57) dpy-5(e61)/HT2*	CGC	Frizzled
	pry-1	*mu38*	CGC	Axin
	ceh-12	*gk391*	CGC	HB9
	pop-1	*hu9*	CGC	TCF/LEF
	unc-37	*e262*	CGC	Groucho
LGII	*unc-4*	*e2322ts*		Homeodomain transcription factor
		e2323		
		e120		
	dsh-1	*ok1445*	CGC	Disheveled
	cwn-1	*ok546*		Wnt
LGIV	*egl-20*	*n585*	CGC	Wnt
	egl-20	*mu39*	CGC	
	egl-20	*hu120*	CGC	
	cwn-2	*ok895*	CGC	Wnt
LGV	*cfz-2*	*ok1201*	CGC	Frizzled
LGX	*lin-18*	*lin-18(e620) dpy-7(e1324)*	H.R. Horvitz [87]	Ryk
	bar-1	*ga80*	CGC	β-catenin
		mu63	CGC	

Table 4.2. Primer sequences for verification of mutations in genetic crosses.

Gene(Allele)	Forward Primer Sequence	Reverse Primer sequence	Reference
mig-1(e1787)	CCTAGGCCACCAACTTCAAA	CGCAGACTTCTCAACTCTCA	[56]
lin-17(n671)	GCGAGCATGTGCAGAGAGAG	CCGTAAATCGACACAAGCAC	[160]
lin-44(n1792)	GAGAGCCTTGGTTTGTGAG	GTTCATAATTTTAGCACCCAAT	[59]
pry-1(mu38)	CATGCCTAGGTTCCGTCAAG	AAGTTTTCGCGGTAAGACCC	[62] [161]
pop-1(hu9)	CTTCCGCGGACCTAGTCCC	GAAAGGCAATTGAGGTGGTCC	[161]
dsh-1(ok1445)	GAGAGGAACACTGTCACCAG	GCCAGCAGCAACCAAGTACG	wormbase.org
cwn-1(ok546)	CGAGAATAGAAAAGACCAAGCC	CAGTACAACCGGATGTCGAATA	[162]
egl-20(n585) *egl-20(hu120)*	ATACAGTACGCAACAAGTTC	CACATAAGACAACACCTGATC	[62]
cwn-2(ok895)	GATGATTCCACGGAGAAGTTG	CATTCTTAGGCTTAGAGAAATG	[162]
cfz-2(ok1201)	GCCGGGAACTTGAGATCAATG	CATAACTATAGTCCAGATGGCCC	[162]
bar-1(ga80)	ACCTGGATCCGAACCTAGTTA	GAGCATTGTTGCATGTTGGAA	[163]

Table 4.3. List of transgenes used in this study. Transgenes generated for this work are accompanied by primer sequences used to synthesize the plasmids.

Name	Array	Reference	Primer Sequences
wdIs85, wdEx310	*Pceh-12*::*GFP*, *unc-119(+)*	[164]	
gmEx365	*Plim-4::egl-20::GFP*	[56]	
wdIs4	*Punc-4::GFP*	[165]	
wdIs54	*Punc-7::UNC-7S:GFP, col-19::GFP*	[114], This work	
wdEx639	*Punc-4::MIG-1::YFP; dpy-20(+)*		Punc-4_F2 (CCCGGAACTGGGATATAATTTC); Punc-4_REV (ACCGTATCATTTTCACTTTTTG); pPD95.75 3'UTR and Punc-4_MIG-1GFP_OVER (CAAAAAGTGAAAATGATCGGTATGGGACCATTTCGTGGTTA)
wdEx636	*Punc-4::ΔNT-BAR-1; dpy-20(+)*		Punc-4_F2 (CCCGGAACTGGGATATAA TTTC); Punc-4_REV (ACCGTATCATTTTCACTTTTTG); 3'BAR-1_NT (GCATGTAGGGATGTTGAAGA); ΔNT-BAR-1_OVER (CAAAAAGTGAAAATGATCGGTATGGCCGACTATGAGCCGAT)
wdIs65, wyEx1845	*MVC46/Punc-4::NLG-1::GFP1-10, MVC12/Pflp-18::NLG-1::GFP11, Punc-4::mCHERRY, odr-1::RFP*	[103], This work	

Punc-4::MIG-1::YFP was generated by overlap PCR (Table 4.3) and microinjected to produce NC1870 *wdEx639 (Punc-4*::MIG-1::YFP*, dpy-20(+)).*

***ceh-12::GFP* expression**

A spontaneous integrant, *wdIs85* (LGIII), of *wdEx310* was used to assay *ceh-12*::GFP expression. L2 larval VAs and VBs were scored for either the presence or absence of *ceh-12*::GFP expression (n ≥10 for each neuron). Animals were anesthetized with either 0.25% tricaine/0.025% tetramisole or with 10mM levamisole. VA motor neurons were pooled into Anterior (VA2-6) or Posterior (VA7-10). Table 4.4 shows results used in pie charts.

Detecting AVB gap junctions with ventral cord motor neurons.

The AVB gap junction marker strain, NC1694 [*wdIs54* (*Punc-7*::UNC-7S:GFP, *col-19*::GFP*) unc-7*(*e5*) [114] was integrated by gamma irradiation (4000 Rads) of EH578 [114] and 10X backcrossed into wild type. AVB gap junctions in the ventral cord were detected by anti-GFP immunostaining in L4 larvae and specific motor neurons identified as described [42]. n ≥ 10 for each neuron. Table 4.5 shows values used in pie charts (Figure 4.15).

Single molecule mRNA FISH

in situ hybridization assays were performed [166, 167] in wild type, *unc-4(e120)* and *unc-37(e262)* with *unc-4*::GFP to mark DA and VA neurons. Synchronized worms were fixed in 4% formaldehyde, 70% ethanol. Oligonucleotide probes (www.singlemoleculefish.com) were coupled to Alexa594 (*mig-1*) or Cy5 (*mom-5*). Nuclei were stained with DAPI. z-stacks (0.5 μm per slice) were collected in a Leica DM6000 microscope with 100X objective and Tx2(Alexa594) or Y5 (Cy5) filter cube.

Table 4.4. Compilation of data of *ceh-12*::GFP expression in VA motor neurons. Percentages of VA motor neurons with *ceh-12*::GFP expression *vs.* VAs with no *ceh-12*::GFP expression are listed. n ≥ 10 for each VA scored; sum of pooled VA motor neurons scored is listed.

Anterior VAs	% *ceh-12*::GFP positive neurons	% No *ceh-12*::GFP expression	Σ VA neurons scored
unc-4	0.6	51.3	160
lin-44; unc-4	11.0	45.1	355
cwn-1 unc-4	6.7	48.9	180
lin-17; unc-4	3.6	50.0	196
lin-44 lin-17; unc-4	3.9	51.7	180
lin-44; cwn-1 unc-4	4.2	48.7	189
unc-4; egl-20	0.0	53.9	167
lin-44;unc-4; egl-20	6.3	43.7	190
unc-4; mig-1	0.6	50.6	164
mig-1 lin-44; unc-4	0.0	55.6	180
pop-1; unc-4	0.0	55.1	89
mig-1; unc-4; lin-18	7.2	48.3	180
dsh-1 unc-4	0.6	53.7	175
lin-44; dsh-1 unc-4	0.0	53.7	190
unc-4; lin-18	0.0	54.9	182
Posterior VAs	% *ceh-12*::GFP positive neurons	% No *ceh-12*::GFP expression	Σ VA neurons scored
unc-4	24.38	23.75	160
lin-44; unc-4	23.66	20.28	355
cwn-1 unc-4	20.00	24.44	180
lin-17; unc-4	26.02	20.41	196
lin-44 lin-17; unc-4	21.11	23.33	180
lin-44; cwn-1 unc-4	19.05	28.04	189
unc-4; egl-20	2.40	43.71	167
lin-44;unc-4; egl-20	13.16	36.84	190
unc-4; mig-1	17.68292683	31.09756098	164
mig-1 lin-44; unc-4	11.66666667	32.77777778	180
pop-1; unc-4	20.2247191	24.71910112	89
mig-1; unc-4; lin-18	17.77777778	26.66666667	180
dsh-1 unc-4	20.57142857	25.14285714	175
lin-44; dsh-1 unc-4	7.894736842	38.42105263	190
unc-4; lin-18	12.08791209	32.96703297	182
	% *ceh-12*::GFP positive neurons	% No *ceh-12*::GFP expression	Σ VA neurons scored
WT	0	100	180
wdEx636	9.09	90.91	198

Table 4.5. Percent of VA motor neurons with ectopic AVB to VA UNC-7S::GFP positive gap junctions *vs.* % of cells with no UNC-7S::GFP. n ≥ 10 for each VA scored; sum of pooled VA motor neurons scored is listed. These values were used to construct pie charts in Fig. 4.18.

Anterior VAs	% UNC-7S::GFP positive neurons	% No UNC-7S::GFP puncta	Σ VA neurons scored
WT	9.2	90.8	109
lin-17	24.4	75.6	86
cwn-1	19.7	80.3	71
Posterior VAs	% UNC-7S::GFP positive neurons	% No UNC-7S::GFP puncta	Σ VA neurons scored
WT	11.5	88.5	104
lin-17	22.2	77.8	54
cwn-1	12.1	87.9	58

1024x1024 images were subjected to 2x2 binning. Each VA neuron was identified by position in the ventral nerve cord and its cell soma delineated by the outside edge of *unc-4*::GFP staining (Leica AF Lite). Individual fluorescent puncta (mRNA) from this region were counted by direct inspection of the Z-stack. n ≥ 5 for each neuron.

GRASP assay of AVA to VA10 synapses

The GFP reconstitution across synaptic partners (GRASP) marker *wdIs65* was integrated by gamma irradiation (4000 Rads) of *wyEx1845* [103] and used to label AVA to A-class motor neuron synapses. Z-stacks were collected with identical microscope settings. Line scans in the GFP channel were collected in the VA10 to DA7 interval [103]. An equivalent length scan was obtained from the posterior dorsal nerve cord (devoid of GFP puncta) to obtain an average background signal in the GFP channel for each animal. The intensity score for each experimental sample was calculated from the percentage of measurements from the VA10 to DA7 interval that exceeded this background signal. n ≥ 10 for each neuron.

Microscopy

wdIs85 (Pceh-12::GFP*)* and *wdIs54 (Punc-7*::UNC-7S::GFP) were scored with a 100x objective in a Zeiss Axioplan microscope with a Hammamatsu Orca camera. Images of *wdIs85* were obtained using a Leica TCS SP5 confocal microscope. Images of *wdIs54* were obtained using an Olympus FV-1000 confocal microscope with a 60x/1.45 Plan-Apochromat lens. Pseudocolors and image overlays were generated using Olympus software and Adobe Photoshop.

Movement Assay

A movement assay ("tapping assay") detected effects of specific mutants on backward locomotion [42]. For each genotype, n ≥ 50 L4-young adults were tapped on the head with a platinum wire. Backward movement was scored as either **Unc** (coiled instantly, no net backward movement) or **Suppressed** (detectable backward movement of posterior region or entire body in locomotory sinusoidal waves).

Pyrvinium Assay

Embryos were placed on nematode growth media (NGM) plates streaked with OP50 bacteria, covered with pyrvinium palmoate dissolved in soybean oil, and allowed to hatch. Tapping assays were performed on young adults (n=50).

Lithium chloride treatment

Lithium chloride was added to NGM media before pouring plates to yield a final concentration of 10mM LiCl. Synchronized L1 larvae were grown on LiCl plates for 3 days at 20 °C and tapping assays performed on young adults. (n ≥ 150).

Statistical Analysis

UNC-7S::GFP puncta, movement assays, and *ceh-12*::GFP expression were quantified using a binary rubric (*e.g.,* GFP was scored as 'present' or 'absent' in a given cell). In all cases, the experimenter was blinded to genotype to avoid bias. Fisher's Exact Test was used to calculate a p-value for statistical significance [168]. All graphical representations reflect a percentage of total animals scored. Statistical significance was evaluated using a one-way ANOVA ($p < 0.05$) for GRASP results.

RESULTS

EGL-20/Wnt signaling promotes *ceh-12* expression in posterior VA motor neurons.

We have previously determined that *ceh-12/HB9* contributes to the Unc-4 phenotype in posterior VA motor neurons [42]. *ceh-12* is ectopically expressed in posterior VAs in *unc-4* mutants and is specifically required for the miswiring of VAs in this region [42]. We hypothesized that the biased posterior expression of *ceh-12* could result from an inductive signal provided by nearby cells. The diffusible ligand, EGL-20/Wnt is expressed in this posterior region [167, 169] and is therefore a candidate for a local cue that could promote ectopic *ceh-12* expression.

This idea is substantiated by our finding that *ceh-12*::GFP expression in posterior VAs is significantly reduced in *egl-20; unc-4* double mutants (Fig. 4.2A-D). We tested the additional Wnt ligands *cwn-2, cwn-1, and lin-44* and saw no effect on posterior *ceh-12*::GFP expression in double mutants with *unc-4* (Fig. 4.3, 4.4). *mom-2* mutation is lethal [61] and was not examined. These results are consistent with a model in which EGL-20/Wnt is exclusively required for ectopic *ceh-12* expression in posterior VA motor neurons. *ceh-12::*GFP expression in VB motor neurons is not perturbed in the *egl-20* mutant and is therefore likely to be activated by additional pathways in these cells.

Multiple Wnt receptors are required for EGL-20/Wnt-dependent expression of *ceh-12*.

To test if the Frizzled receptors MIG-1 and MOM-5 mediate EGL-20/Wnt-dependent expression of *ceh-12*/HB9, we scored *ceh-12*::GFP expression in *mom-5; unc-4(e120)* and *mig-1; unc-4(e120)* mutants; ectopic *ceh-12*::GFP expression in posterior VAs was reduced in both of these double mutants (Fig. 4.2A). We note that *mom-5* and *mig-1* suppression of ectopic *ceh-12*::GFP in *unc-4* is weaker than that of the *egl-20* mutant, and attribute this difference to likely roles for multiple Wnt receptors

functioning in parallel (Fig. 4.2A). Indeed, mutations in the Frizzled homolog *cfz-2* and the Ryk family member *lin-18* also reduce ectopic *ceh-12*::GFP expression in a subset of posterior VAs (Fig. 4.3), suggesting that *cfz-2*/Frz *and lin-18*/Ryk might be partially required for ectopic *ceh-12* expression.

EGL-20/Wnt is sufficient to induce *ceh-12*::GFP expression.

To determine if EGL-20/Wnt is sufficient to promote *ceh-12*::GFP expression in VAs, we used a transgenic line, *plim-4*::EGL-20, that ectopically expresses EGL-20/Wnt in anterior cells [56]. This treatment enlarged the region of the ectopic *ceh-12*::GFP signal (Fig. 4.2E-G) to include anterior VA motor neurons in addition to the posterior VAs that express *ceh-12*::GFP in an *unc-4* mutant. *ceh-12*::GFP in anterior VAs was not observed in a wild-type background (Fig. 4.5) nor in an *unc-4* mutant in the absence of anterior *egl-20*/Wnt (Fig. 4.2E). Mutation of *mig-1*/Frz attenuated ectopic *ceh-12*::GFP expression in anterior as well as posterior VAs, indicating that *mig-1/Frz* is necessary for EGL-20-dependent *ceh-12::*GFP expression throughout the ventral nerve cord (Fig. 4.2E). We attribute residual *ceh-12*::GFP expression in these anterior cells to the partially redundant functions of *mom-5*, *lin-18,* and *cfz-2* in this pathway (Fig. 4.2A, 4.3). These results confirm that loss of *unc-4* is necessary for activation of *ceh-12* expression by *egl-20*/Wnt and that *egl-20* functions through MIG-1/Frz upstream of *ceh-12* (Fig. 4.2E). This finding also establishes that the *unc-4* mutation effectively sensitizes VA motor neurons throughout the length of the VNC to an available EGL-20/Wnt cue.

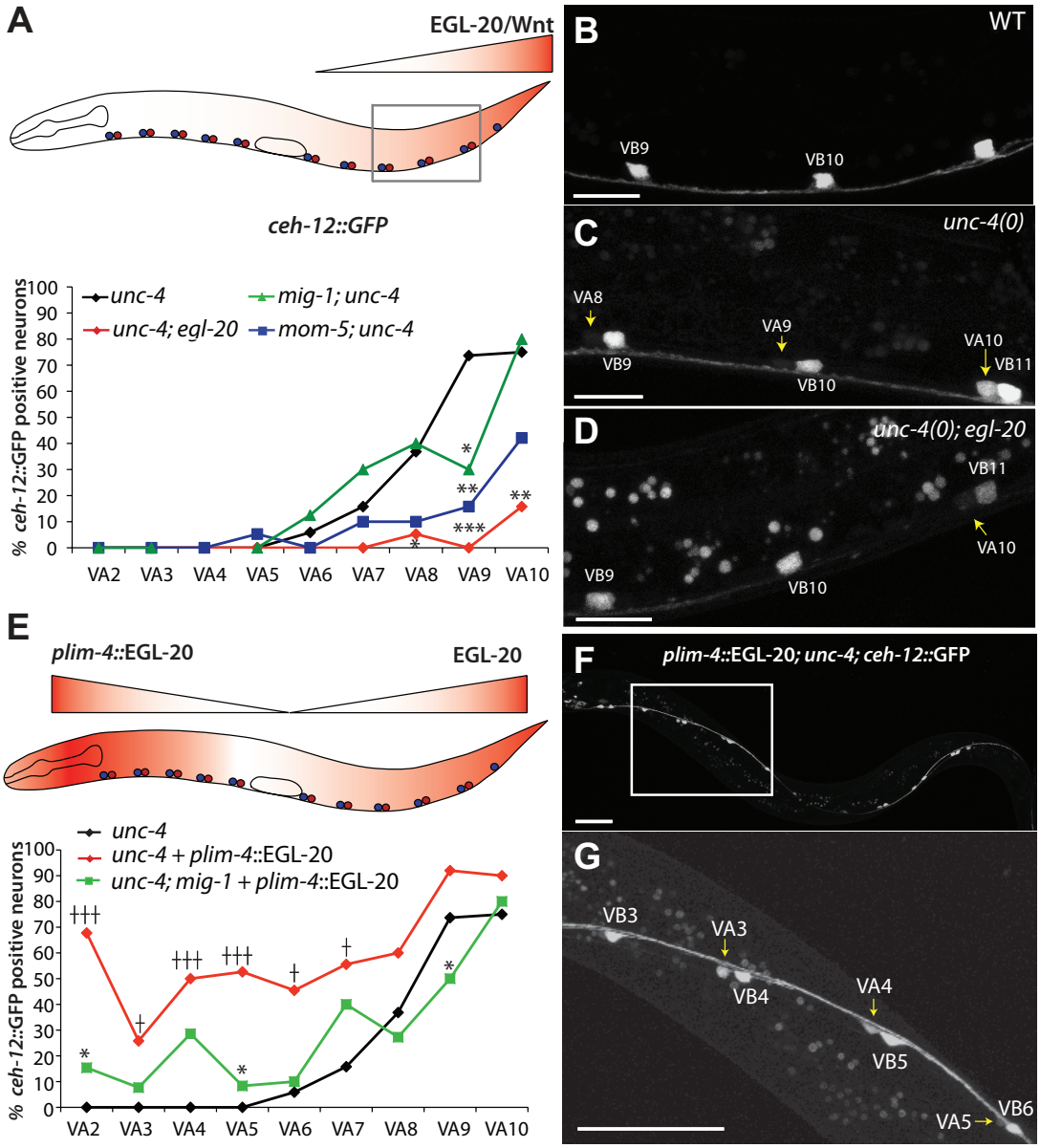

Figure 4.2. EGL-20/WNT is required for *ceh-12*/HB9 expression in *unc-4* mutant VA motor neurons. **A-D.** EGL-20/Wnt is secreted from cells in the tail. Boxed area denotes the region depicted in panels B-D. *ceh-12*::GFP is expressed in VB motor neurons in L2 stage wild-type (WT) animals (B) and in posterior VAs in *unc-4* mutants (A, C). Mutations in *egl-20*/Wnt (D), *mig-1*/Frz, or *mom-5*/Frz reduce ectopic *ceh-12*::GFP expression in posterior VAs, * p< 0.05, ** p< 0.01, *** p < 0.001 *vs. unc-4* (A). **E.** *ceh-12*::GFP is detected in anterior VAs when EGL-20 is expressed from the head neuron-specific transgene, *plim-4::*EGL-20, † p< 0.05, †† p< 0.01, †† p< 0.001 *vs. unc-4*. Ectopic *ceh-12*::GFP in anterior VAs is reduced in *mig-1*/Frz mutants, * p < 0.05 *vs. plim-4::*EGL-20*; unc-4*. **F-G.** *ceh-12*::GFP expression (boxed area in F enlarged in G) depicting anterior VA (arrows) and VB motor neurons. *unc-4(e120)* was used for all experiments. n ≥ 10 for each neuron. Scale bars= 10um (B-D); 15um (F-G).

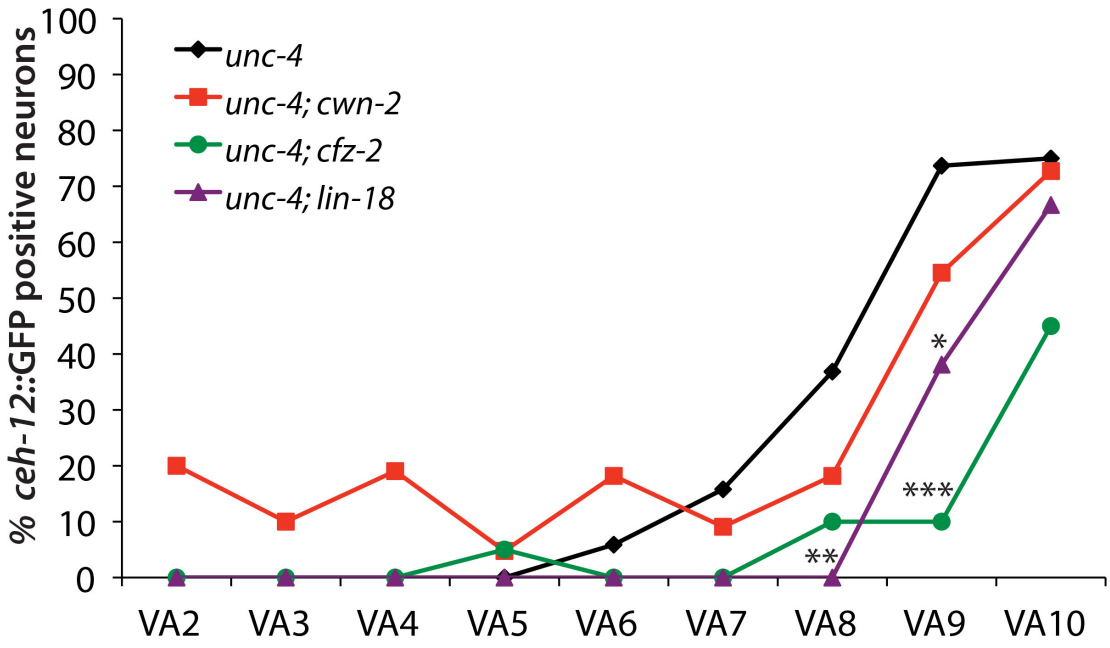

Figure 4.3. Wnt components differentially regulate ectopic *ceh-12*::GFP expression in *unc-4* mutant VA motor neurons. Apparent effects of *cwn-2*/Wnt (Red) on ectopic *ceh-12*::GFP expression are not statistically significant. *cfz-2*/Frz (Green) is required for ectopic *ceh-12*::GFP expression in VA9 and *lin-18*/Ryk (Purple) promotes ectopic *ceh-12*::GFP expression in VA8 and VA9. * $p < 0.05$, ** $p<0.01$, *** $p < 0.0001$ vs *unc-4*, Fisher's Exact Test. $n \geq 15$ for each neuron.

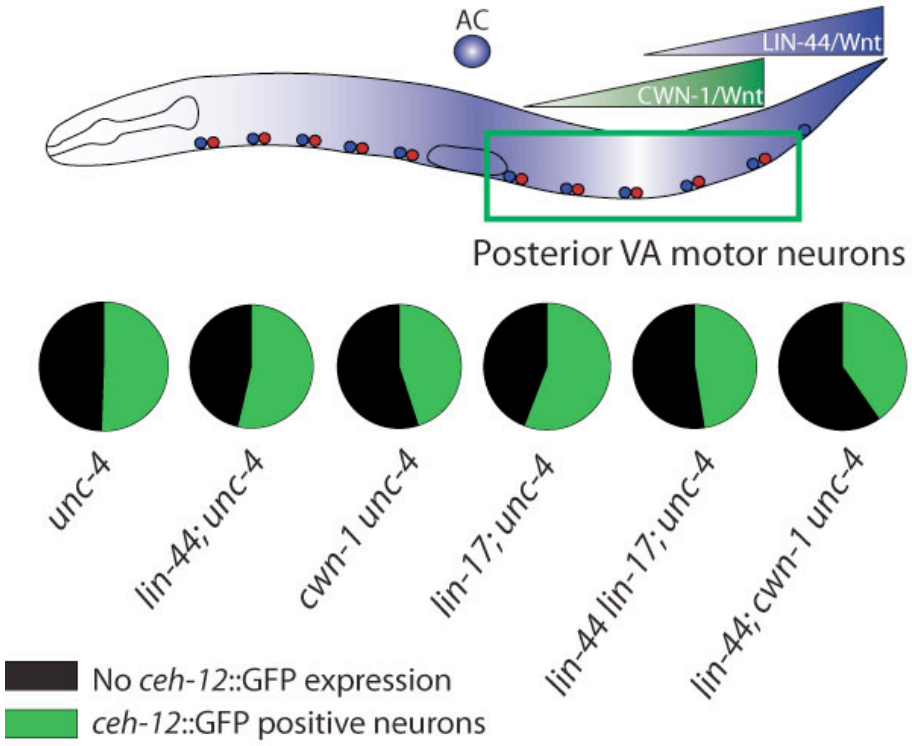

Figure 4.4. Components of the LIN-44-mediated pathway are not required for *ceh-12*::GFP expression in posterior VAs. Single and double mutants of *lin-44* and *cwn-1*/Wnt and *lin-17*/Frz do not significantly affect ectopic *ceh-12*::GFP expression in posterior VA motor neurons. Data from VA7-VA10 are pooled and the percentage of *ceh-12*::GFP positive and negative neurons is indicated. n ≥ 15 for each neuron.

EGL-20/Wnt signaling contributes to the Unc-4 movement defect.

We have previously shown that ectopic expression of *ceh-12*/HB9 contributes to the backward movement defect in *unc-4* mutants [42]. Because EGL-20/Wnt is necessary for *ceh-12*::GFP expression in posterior VAs, we reasoned that loss-of-function *egl-20* mutants should partially suppress the Unc-4 backward movement phenotype (Fig. 4.6). This trait can be detected in a "tapping assay" in which animals are touched on the head to stimulate backward locomotion (Fig. 4.6A-C) [42]. The missense mutants *unc-4(e2323)* and *unc-4(2322ts)* [35] were used to sensitize this assay because *ceh-12* mutations afford strong suppression of "weak" or hypomorphic *unc-4* alleles [42]. Our results show that the *egl-20* alleles *n585* and *mu39* and *egl-20* RNAi restore backward movement to *unc-4(e2323)* and *unc-4(e2322ts)* animals (Fig. 4.6D-E, Fig. 4.7, Table 4.6). *egl-20(n585)* also partially suppresses the backward Unc defect of a hypomorphic allele of the corepressor, *unc-37*/Groucho [40, 41] (Fig. 4.6D). The finding that *ceh-12* and *egl-20* mutations improve backward movement of an *unc-4* mutant (Fig. 4.6D, E) is predicted for a linear pathway in which *egl-20* functions upstream to activate *ceh-12/HB9* expression. To test this model, we used the *unc-4(e120)* and *unc-4(e2320)* null alleles, which are weakly suppressed by a mutation in *ceh-12*. *egl-20(n585)* does not enhance *ceh-12* suppression of *unc-4(e120)* and RNAi of *egl-20* does not improve backward locomotion in *ceh-12; unc-4(e2320)* (Fig. 4.6F, 4.7B). These observations favor a model in which *egl-20*/Wnt and *ceh-12*/HB9 function in a common pathway. We note that the *ceh-12* null allele does enhance *egl-20* suppression of *unc-4* and we attribute this effect to the hypomorphic *egl-20(n585)* allele used for this experiment (Fig. 4.6F). Experiments with the null allele *egl-20(hu120)* confirmed that EGL-20/Wnt is necessary for the miswiring of posterior VAs with gap junctions from AVB in *unc-4* but also suggest that a minimum level of EGL-20/Wnt activity may be required

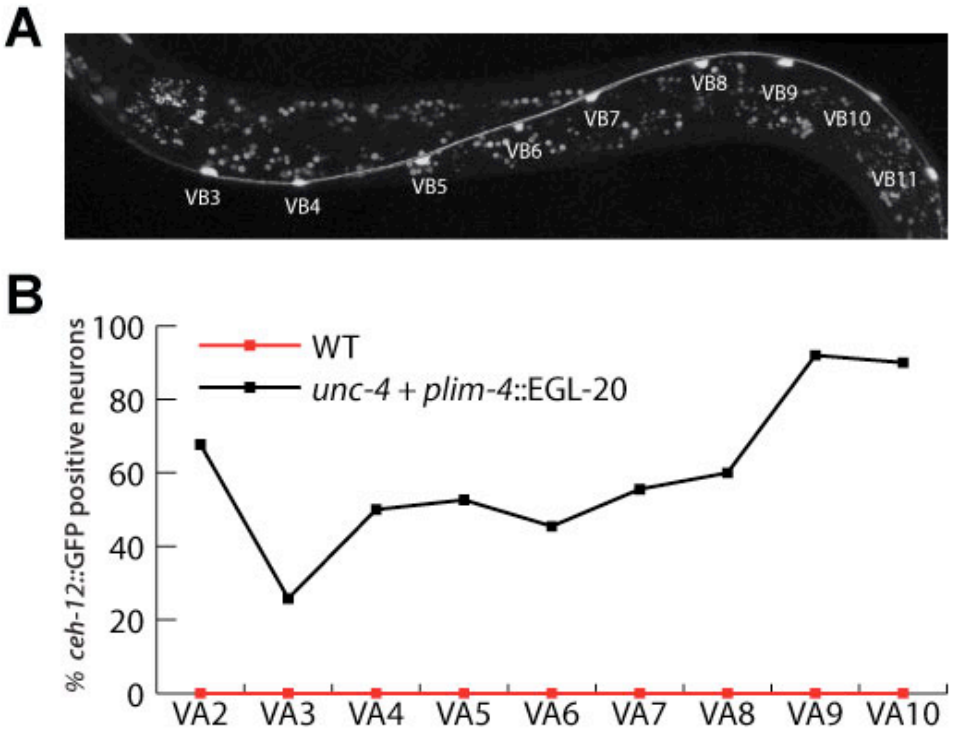

Figure 4.5. Ectopic expression of EGL-20/Wnt is not sufficient to induce *ceh-12* expression in wild-type (WT) VA motor neurons. **A**. Confocal image of a wild-type worm expressing *plim-4*::EGL-20 and *ceh-12*::GFP. **B.** Anterior ectopic EGL-20/Wnt expression (*plim-4*::EGL-20) does not result in ectopic *ceh-12*::GFP expression in a WT background (Red). Anteriorly expressed EGL-20/Wnt results in ecoptic *ceh-12*::GFP expression in *unc-4* mutant VAs throughout the length of the ventral nerve cord (Black). n ≥ 10 for each neuron.

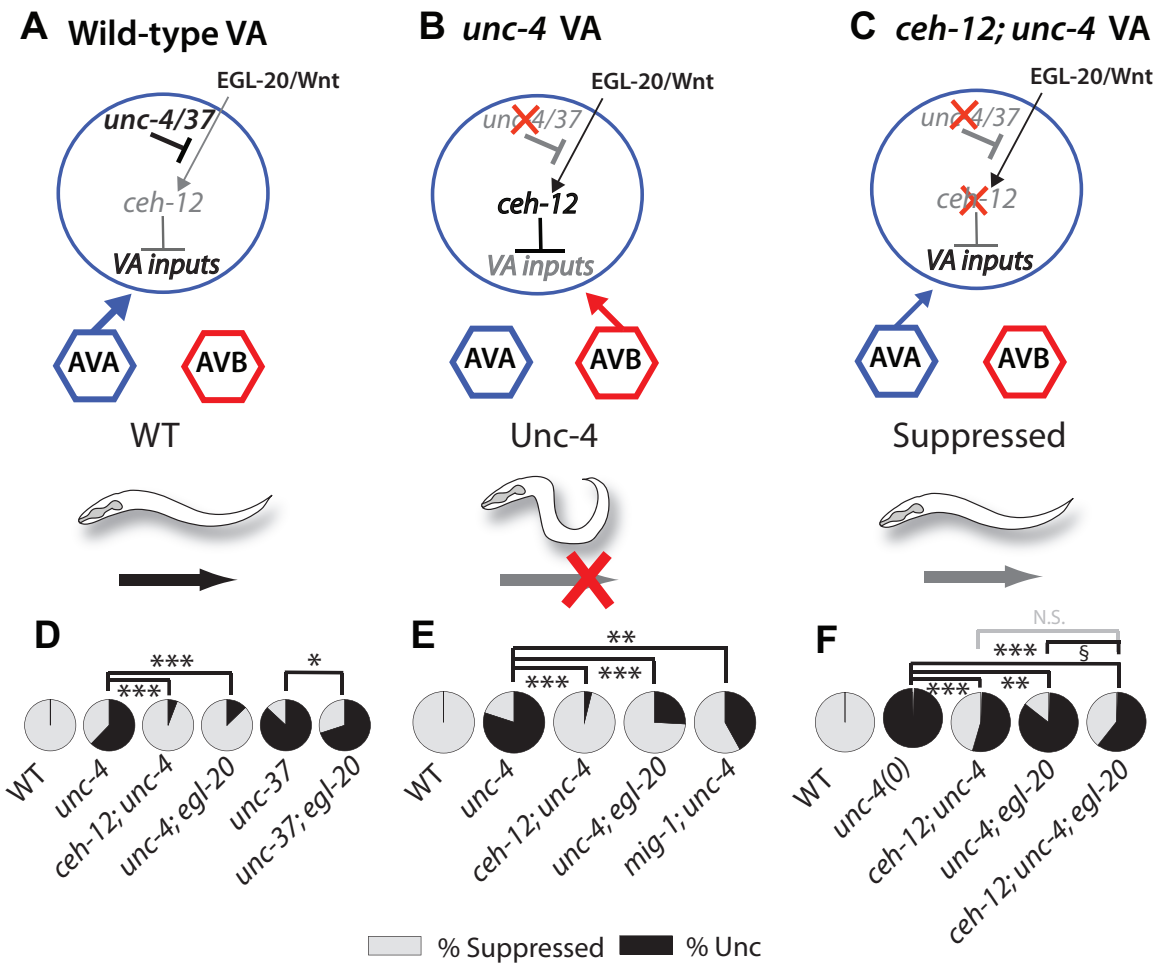

Figure 4.6. UNC-4 regulates connectivity in the motor neuron circuit. **A.** UNC-4 functions with co-repressor, UNC-37/Groucho to block expression of the VB gene, CEH-12/HB9 and to preserve VA-type inputs (Blue). **B.** De-repression of CEH-12/HB9 in posterior VAs in *unc-4* and *unc-37* mutants results in the miswiring of VAs with VB-type inputs (Red) and disrupted backward locomotion. EGL-20/Wnt promotes CEH-12 expression. **C.** Mutations in *ceh-12* eliminate ectopic connections with AVB and partially suppress the Unc-4 phenotype. **D-F**. Locomotion assays. "Unc" animals cannot crawl backward; "Suppressed" worms show detectable backward movement. *ceh-12(gk391)* and *egl-20(n585)* mutants strongly suppress the Unc-4 phenotype of hypomorphic alleles (D) *unc-4(e2323)* and *unc-37(e262)* and (E) *unc-4(e2322ts).* A *mig-1(e1787)* mutation partially suppresses Unc-4 movement. (F) *ceh-12* and *egl-20* mutants partially suppress the null allele, *unc-4(e120)*. * p< 0.05, ** p<0.01, *** p<0.0001. § p<0.05 *vs. unc-4; egl-20*. n ≥ 50.

Table 4.6. Compilation of Tapping Assay Data. Percentages of Unc versus Non-Unc animals in each genetic background tested are listed. n ≥ 50 for each genotype tested.

Strain	**% Unc**	**% Suppressed**
WT	0	100
unc-4(e2320)	98	2
ceh-12(gk391); unc-4(e2320)	58	42
unc-4(e120)	99	1
ceh-12(gk391); unc-4(e120)	54	46
unc-4(e120); egl-20(hu120)	92	8
ceh-12(gk391); unc-4(e120); egl-20(hu120)	75	25
unc-4(e120); egl-20(n585)	87	13
ceh-12(gk391); unc-4(e120); egl-20(n585)	65	35
unc-4(e2323)	63	38
ceh-12(gk391); unc-4(e2323)	6	94
unc-4(e2323); egl-20(n585)	13	87
unc-37(e262)	87	13
unc-37(e262); egl-20(n585)	70	30
unc-37(e262)	82	18
unc-37(e262); bar-1(mu63)	64	36
unc-4(e2323)	63	38
unc-4(e2323); bar-1(mu63)	54	46
unc-4(e120) Empty Vector RNAi	74	26
unc-4(e120) mom-5 RNAi	49	51
unc-4(e2322ts)	67	33
unc-4(e2322ts); lin-18 dpy-7	72	28
unc-4(e2322ts); cfz-2(ok1201)	67	33
unc-4(e2322ts); pop-1(hu9)	22	78
unc-4(e2322ts); dsh-1(ok1445)	29	71
WT	0	100
wdEx636	20	80
at 23C	**% Unc**	**% Suppressed**
WT	0	100

Table 4.6 cont.		
unc-4(e2322ts)	80	20
unc-4(e2322ts); egl-20(n585)	26	74
unc-4(e2322ts); mig-1(e1787)	42	58
unc-4(e2322ts); ceh-12(gk391)	4	96
WT	0	100
unc-4(e2322ts)	68	32
unc4(e2322ts) 1uM pyrvinium	52	48
unc4(e2322ts) 10uM pyrvinium	44	56
unc-4(e2322ts); egl-20(n585)	26	74
at 16C	**% Unc**	**% Suppressed**
WT	0	100
unc-4(e2322ts)	0	100
(WT) *dpy-20 wdEx639*	1	99
unc-4(e2322ts); dpy-20 wdEx639	38	62
ceh-12(gk391); dpy-20 wdEx639	1	99
ceh-12; unc-4; dpy-20 wdEx639	0	100
	% Unc	**% Suppressed**
unc-4(e2322ts)	0	100
lin-17(n671)	10	90
unc-4(e2322ts); lin-17(n671)	55	45
unc-4(e2322ts); cwn-1(ok546)	26	74
unc-4(e2322ts); lin-44(n1792)	24	76
unc-4(e2322ts)	0	100
pry-1(mu38)	0	100
unc-4(e1222ts);pry-1(mu38)	38	62
WT	0	100
ceh-12	1	99
WT + 10mM LiCl	77	23
ceh-12 + 10mM LiCl	62	38
ceh-12(gk391); unc-4(e2320) Empty Vector RNAi	91.5	8.5
ceh-12(gk391); unc-4(e2320) egl-20 RNAi	93.5	6.5

to promote the creation of normal backward locomotory inputs to VAs (Figure 4.7C,D).

To detect potential roles for Wnt receptors in VA input specificity, we tested mutant alleles of *mig-1, cfz-2* and *lin-18* for suppression of the Unc-4 backward movement defect. Mutations in *mig-1*/Frz but not *cfz-2*/Frz or *lin-18*/Ryk result in significant restoration of backward movement in *unc-4(e2322ts)* (Fig. 4.6E, 4.8). Although *cfz-2*/Frz *and lin-18*/Ryk are partially required for ectopic *ceh-12*::GFP expression (Fig. 4.3), this effect may be too weak to be detected in the tapping assay. RNAi of *mom-5/*Frz resulted in strong suppression of Unc-4 movement (Fig. 4.9). These results are consistent with a model in which MIG-1 and MOM-5/Frz are the principle receptors in an EGL-20/Wnt signaling pathway that contributes to synaptic miswiring in *unc-4* mutants.

UNC-4 limits expression of *mom-5* and *mig-1* in VA motor neurons.

Expression of *mig-1, mom-5* and *cfz-2*/Frz in VAs is supported by microarray results and by experiments with GFP reporters [43] (Table 4.7, Fig. 4.10). Microarray data also indicate that *mom-5* and *mig-1* transcripts are significantly upregulated in VA motor neurons when the *unc-4* pathway is disabled (Table 4.7, Fig. 4.10) [42]. Thus, *unc-4* may effectively quell the VA response to EGL-20/Wnt by preventing MOM-5 and MIG-1/Frz levels from exceeding a critical threshold. To test this idea, we used a quantitative method of *in situ* hybridization [167] to measure *mom-5* and *mig-1* transcripts in VAs (Fig. 4.11A). *mig-1* mRNA is significantly elevated in VA9 in *unc-37* and *unc-4* mutants (Fig. 4.11B). This result is consistent with the observed requirement for *mig-1* function for ectopic *ceh-12*::GFP expression in VA9 in *unc-4* (Fig. 4.2A). *mom-5* mRNA is increased in VA10 in *unc-4* and *unc-37* mutants but not in the adjacent VA9 motor neuron where MOM-5 promotes ectopic expression of *ceh-12*::GFP (Fig. 4.2A, 4.11C). This disparity could indicate that *unc-4* also antagonizes *mom-5* activity by an

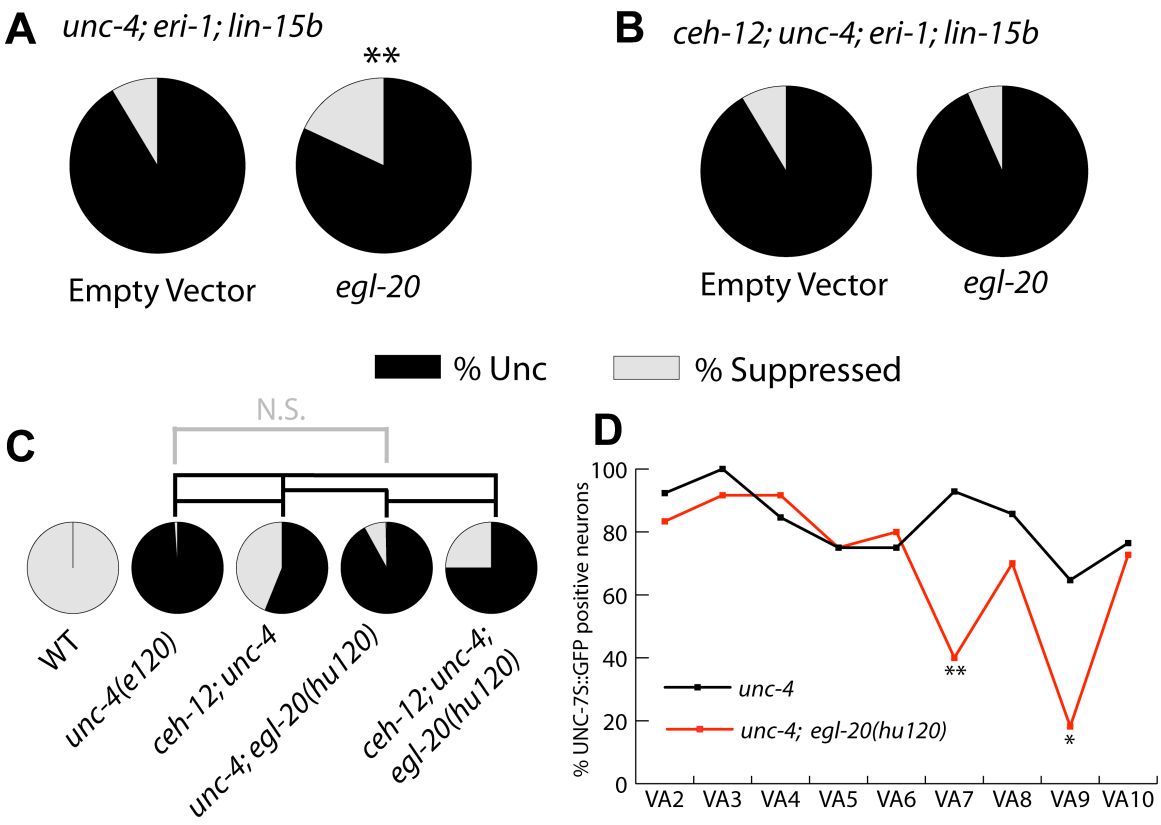

Figure 4.7. EGL-20/Wnt regulates the specificity of synaptic inputs to VA motor neurons. **A.** RNAi of *egl-20* in the hypormorphic *unc-4(e2323)* allele suppresses the Unc-4 backward movement defect. ** p<0.01 *vs unc-4*, Fisher's Exact Test, n=200. **B.** Movement of *ceh-12(gk391); unc-4(e2320); eri-1(mg366); lin-15b(n744)* worms is not significantly different when treated with *egl-20*/Wnt RNAi compared to treatment with the empty vector control, n=200 [170]. **C.** The deletion allele *ceh-12(gk391)* suppresses the Unc-4 backward movement defect of *unc-4(e120)* whereas the *egl-20(hu120)* null allele does not suppress *unc-4(e120)* and is partially epistatic to *ceh-12(gk391). egl-20(hu120)* alone does not show a backward movement defect (data not shown). Black brackets indicate significance of p<0.001 between connected pairs. N.S.= not significant. n≥ 50. **D.** Ectopic AVB gap junctions with VA7 and VA9 in *unc-4(e120)* are suppressed by *egl-20(hu120)*. *p<0.05, **p<0.01. Taken together, these results indicate that EGL-20 may have separate threshold-dependent functions with competing outcomes: High levels of EGL-20 function are required for the creation of AVB to VA gap junctions and a minimum level of EGL-20 activity is necessary for the restoration of functional backward locomotory inputs to VAs in an *unc-4* mutant. Hence, both hypomorphic and null alleles of *egl-20* suppress the creation of ectopic AVB to VA gap junctions in *unc-4* (see Fig. 4.17D) whereas Unc-4 suppression is conferred by hypomorphic *egl-20* mutations (Fig. 4.6D, E and Table 4.6) but not by the *egl-20(hu120)* null allele. n ≥ 10 for each neuron.

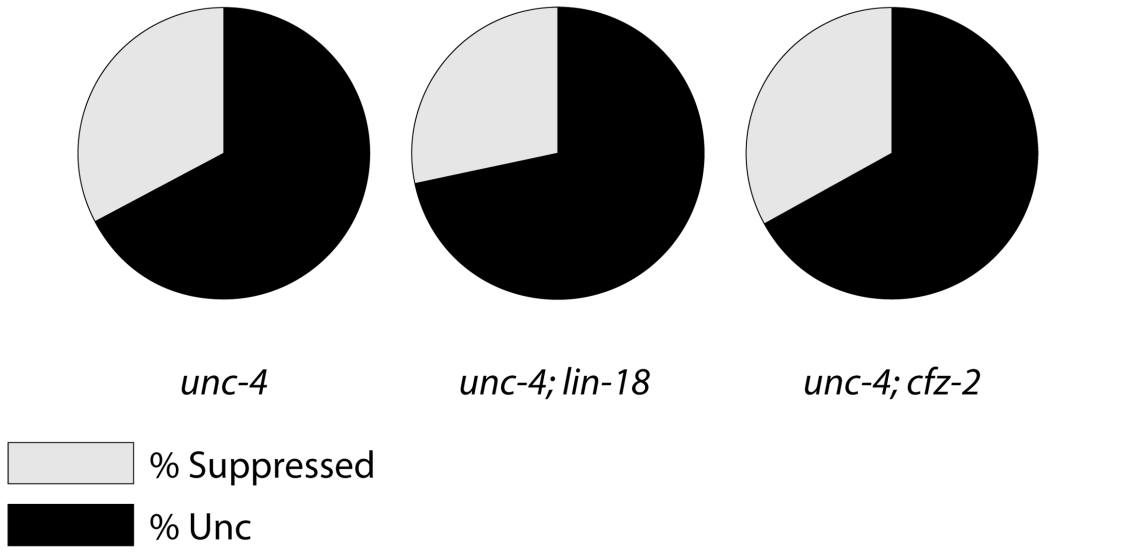

Figure 4.8. Mutations in Wnt receptors, *cfz-2*/Frizzled and *lin-18*/Ryk do not affect Unc-4 movement. Movement of *unc-4*; *lin-18* and *unc-4; cfz-2* double mutants is not significantly different ($p>0.05$) from *unc-4* single mutants. Fisher's Exact Test. $n \geq 50$.

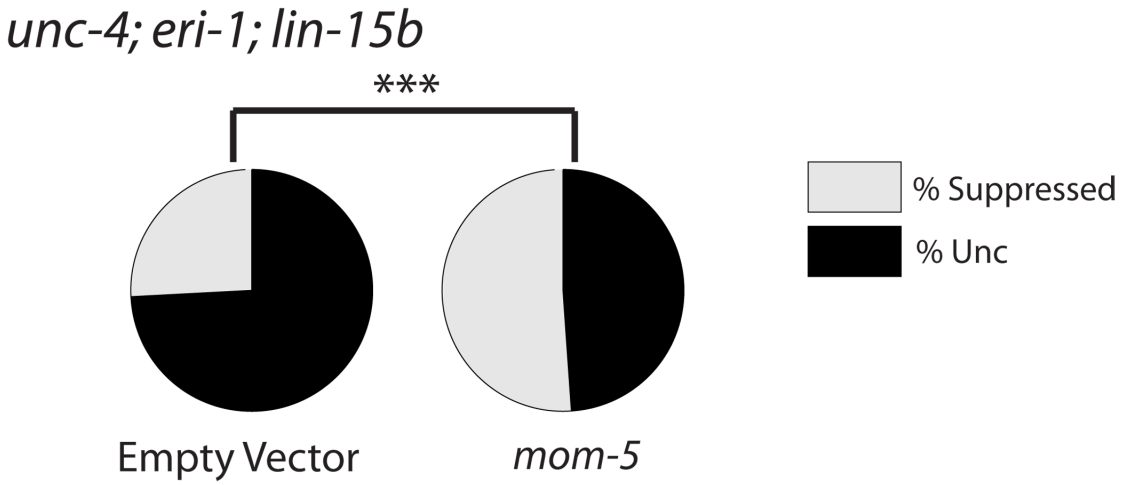

Figure 4.9. RNAi of *mom-5* in an *unc-4* RNAi-sensitive strain suppresses the Unc-4 movement defect. Movement of *unc-4(e2323); eri-1(mg366); lin-15b(n744)* worms is significantly suppressed when treated with *mom-5*/Frz RNAi compared to treatment with the empty vector control. *** $p < 0.0001$ Fisher's Exact Test. $n \geq 50$.

additional mechanism in VA9 that does not involve direct transcriptional repression (See Discussion). We observed statistically significant elevation of *mom-5* (VA6) and *mig-1* (VA2, VA6) in selected anterior VA motor neurons in *unc-4* and *unc-37* mutants, which might account for the sensitivity of these VA motor neurons to an anterior source of EGL-20/Wnt (Fig. 4.2E, 4.11B,C).

If UNC-4 antagonizes MIG-1 and MOM-5 to preserve VA-type inputs, then over-expression of these Frizzled receptors should be sufficient to induce an Unc-4-like phenotype. To test this model, we used the *unc-4* promoter to drive expression of MIG-1 in A-class motor neurons in the *unc-4(e2322ts)* mutant (Fig. 4.11D). At permissive temperature (16 °C), *unc-4(e2322ts)* animals display wild-type backward locomotion [35]. However, expression of *Punc-4::*MIG-1 in *unc-4(e2322ts)* resulted in strong Unc-4-like movement (Fig. 4.11D). Suppression of this effect by *ceh-12(0*) is predicted by the hypothesis that the Unc-4-like phenotype induced by *Punc-4::*MIG-1 depends on ectopic *ceh-12* expression and also rules out a model in which VA function is non-specifically disrupted by over-expression of MIG-1/Frz protein. These results are consistent with the proposal that UNC-4 limits the sensitivity of VA motor neurons to an available Wnt signal by inhibiting expression or function of the Frizzled receptors, *mig-1* and *mom-5*.

A separate Wnt signaling pathway opposes *ceh-12* expression in VA motor neurons.

We noted that a *lin-17/Frz* mutant enhanced the Unc-4 phenotype (Fig. 4.12A) in contrast to mutations in *mig-1*/Frz and *mom-5*/Frz which suppress the Unc-4 backward movement defect (Fig. 4.6E, 4.9). *unc-4(e2322ts)* animals normally display wild-type backward movement at 16 °C [35]. Backward locomotion is significantly impaired, however, in the *lin-17; unc-4(e2322ts)* double mutant compared to either *unc-4(ts)* or *lin-17/Frz* single mutants. In addition, mutation of *lin-17*/Frz alone shows a weak backward

	Microarray Data			GFP reporters	
Wnt Receptors	**[1,]WT DA**	**[2] WT VA**	**[3]*unc-37* VA**	**Transgenics**	**VA**
mom-5	EG	EG	1.8X	*mom-5::GFP*	Yes
mig-1	EG	1.6X	1.8X	*mig-1::GFP*	Yes
lin-17	1.7X	ND	ND	*lin-17::GFP*	Yes
cfz-2	ND	EG	ND	?	
lin-18	ND	ND	ND	?	
cam-1	EG	EG	ND	?	

[1] [44]
[2] [171]
[3] [172]

Table 4.7. Microarray results detect Wnt receptors that are expressed in A-class motor neurons and negatively regulated by the UNC-4 pathway.
Microarray experiments were performed with transcripts isolated from embryonic DA motor neurons and from larval VA motor neurons. Transcripts enriched in wildtype DA (*lin-17* = 1.7X) or VA motor neurons (*mig-1* = 1.6X) were identified by comparison to corresponding reference profiles of all cells. “EG” (Expressed Gene) denotes transcripts that are detected but not enriched [44, 171]. promoter::GFP reporter genes for *mom-5, mig-1* and *lin-17* were detected in VA motor neurons [44] but expression or GFP reporters for *cfz-2, lin-18* and *cam-1* has not been reported (?). *mom-5* and *mig-1* transcripts are also upregulated (1.8X) in microarray profiles of *unc-37* mutant VA motor neurons suggesting that the UNC-4 pathway negatively regulates *mom-5* and *mig-1* expression [171].

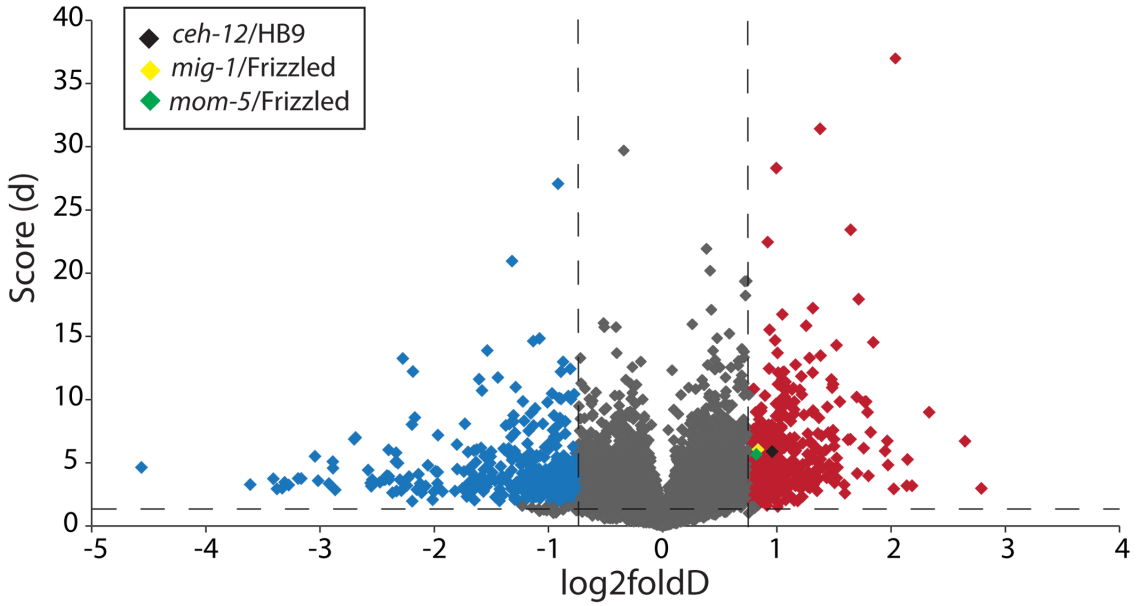

Figure 4.10. Microarray analysis detects transcripts regulated by the *unc-4* pathway in VA motor neurons. Microarray profiles of *unc-37* mutant vs. wild-type VA motor neurons were compared to detect differentially expressed transcripts [164]. Fold change (x-axis) is plotted on a log2 scale against a significance score (y-axis). Thresholds for identifying transcripts with significantly different levels in *unc-37* vs. wild-type VAs were ≤5% FDR (False Discovery Rate) (horizontal dashed line) and fold change ≥ ±1.7x (vertical dashed lines). Blue diamonds correspond to transcripts down-regulated in *unc-37* mutant VAs and red diamonds represent transcripts that are upregulated in *unc-37* vs. WT VA motor neurons. Gray diamonds represent transcripts with no significant fold change difference between *unc*-37 mutant and WT VAs. Enrichment in *unc-37* VA motor neurons for selected genes *ceh-12/HB9* (black diamond) (1.9x) and *mig-1* (yellow diamond) (1.8x) and *mom-5* (green diamond) (1.8x).

Unc defect. Mutations in *lin-44/Wnt* and *cwn-1/*Wnt also display a similar Unc-4 enhancer effect (Fig. 4.12A).

One explanation for these results is that LIN-44/Wnt, CWN-1/Wnt and LIN-17/Frz normally function to prevent expression of *ceh-12* in VA motor neurons. This model is consistent with experiments showing that over-expression of CEH-12 protein in VAs induces an Unc-4-like movement defect [42]. We note that ectopic expression of *ceh-12::*GFP is enhanced in anterior VA motor neurons (VA2-6) in *lin-44; unc-4(0)* and *cwn-1 unc-4(0)* mutants, whereas expression of *ceh-12*::GFP in posterior VAs (VA7-10) was unaffected (Fig. 4.4, 4.12B). *ceh-12*::GFP expression is detected in *lin-17; unc-4(0)* in anterior VAs, although not statistically significant from wild type (Fig. 4.12B). A linear pathway involving LIN-44/Wnt, CWN-1/Wnt and LIN-17/Frz that limits ectopic CEH-12 expression could explain these results. Our finding that *lin-44* fails to enhance ectopic *ceh-12*::GFP expression in *lin-17* mutants is consistent with this model (Fig. 4.12B). However, other genetic interactions are also suggestive of a more complex mechanism. For example, the *lin-44; cwn-1* double mutant does not result in further elevation of ectopic *ceh-12::*GFP expression in comparison to each single mutant as would be expected if LIN-44 and CWN-1 exercise similar roles upstream of LIN-17/Frz (Fig 4.12B). This effect may be attributed to a partially redundant function for CWN-2 (Fig 4.3). In addition, loss of *egl-20* function fails to suppress ectopic *ceh-12*::GFP in anterior VA motor neurons in a *lin-44; unc-4* mutant (Fig. 4.12B). This result suggests that *ceh-12* expression is not regulated by EGL-20/Wnt in most anterior VAs. In contrast, the *lin-44* mutation partially restores *ceh-12*::GFP expression to posterior VAs in an *egl-20; unc-4* background (Fig. 4.13). This result is consistent with the proposal that LIN-44

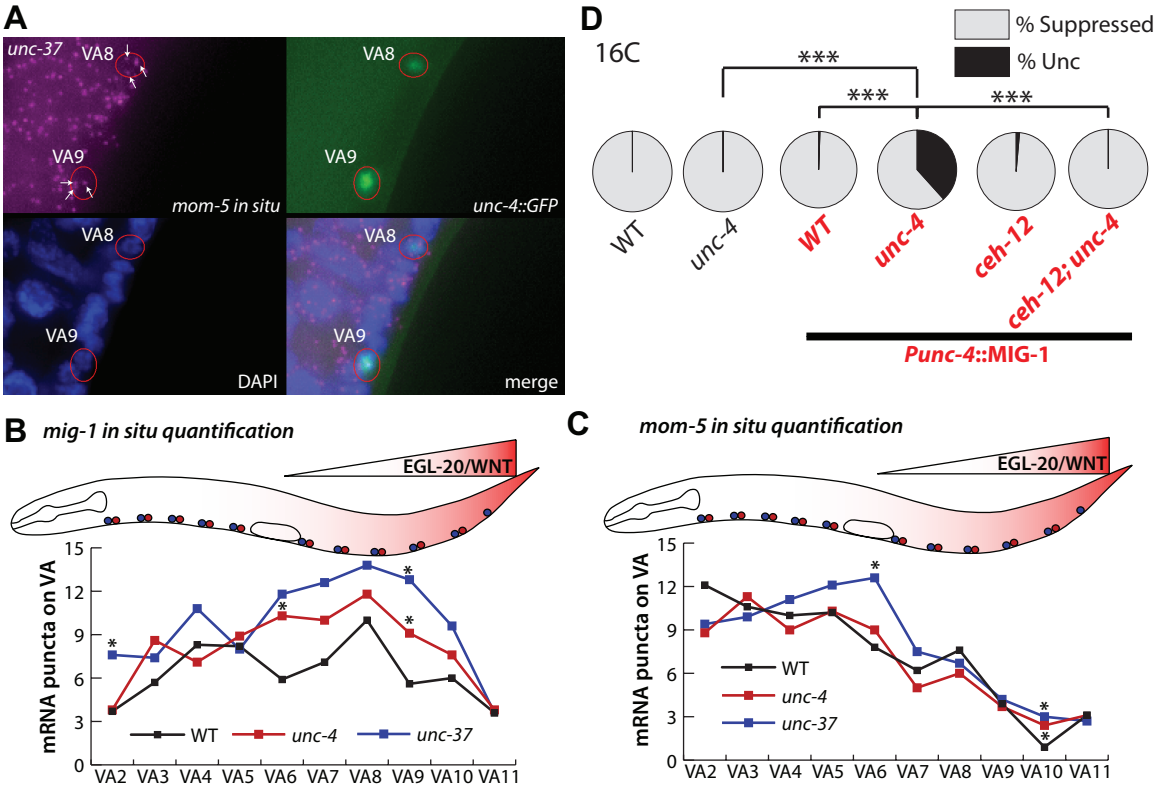

Figure 4.11. *mom-5* and *mig-1*Frz are negatively regulated by *unc-4/unc-37* in VA motor neurons. **A.** Fluorescence in situ hybridization detects *mom-5* transcripts as fluorescent puncta (purple, arrows) in VA motor neurons marked with *unc-4::*GFP (green) and DAPI (blue). Puncta overlapping each VA (red circles) were counted for wild type (WT), *unc-4(e120)* and *unc-37(e262).* **B**. *mig-1* mRNA is elevated in VA2 and VA9 in *unc-37* and in VA6 and VA9 in *unc-4,* * p< 0.05. n ≥ 5 for each neuron. **C.** *mom-5* mRNA is upregulated in VA10 in *unc-4* mutants and in VA6 and VA10 in *unc-37* mutants. * p< 0.05. n ≥ 5 for each neuron. **D.** Over-expression of MIG-1/Frz in VAs enhances Unc-4 movement. WT and *unc-4(e2322ts)* show normal backward movement at 16°C. MIG-1 expression in A-class motor neurons with *Punc-4::*MIG-1 (red text) enhances the backward movement defect of *unc-4(e2322ts)* but not WT. *ceh-12(gk391)* suppresses the MIG-1-induced backward movement phenotype. *** p<0.001 *vs. unc-4*. n ≥ 50.

antagonizes EGL-20-dependent expression of *ceh-12* in posterior VAs and likely reflects the posterior origins of LIN-44 Wnt signals (Fig. 4.12D) [167]. This observation also reveals a "ground" state in which *ceh-12*::GFP expression is activated by an additional pathway when *lin-44* and *egl-20* function are eliminated [86].

Opposing Wnt signaling pathways regulate the specificity of interneuron gap junctions with VA motor neurons.

The AVB interneuron normally forms gap junctions with DB and VB motor neurons [1] which can be detected with a GFP-tagged gap junction protein (innexin), UNC-7S::GFP, expressed in AVB. UNC-7S::GFP puncta are localized to motor neuron cell soma and therefore allow ready identification of AVB motor neuron partners in animals counter-stained with a DNA dye (DAPI) [114] (Fig. 4.14). We used this assay to confirm that *unc-4* mutant VAs display ectopic AVB to VA gap junctions (Fig. 4.14B) [38] and that *ceh-12*/HB9 is required for the creation of AVB gap junctions with posterior VAs [42]. Therefore, if EGL-20/Wnt is necessary for ectopic *ceh-12*/HB9 in posterior VAs (Fig. 4.2A, 4.12D), then these aberrant AVB gap junctions should be reduced in *egl-20*/Wnt mutants. The frequency of UNC-7S::GFP puncta associated with posterior VAs is substantially reduced in *unc-4; egl-20(n585)* and in *unc-4; egl-20(hu120)* mutants (Fig. 4.7D, Fig. 4.14D). MIG-1/Frz is also required for ectopic AVB gap junctions with posterior VAs (Fig. 4.14B,D). A synthetic lethal phenotype prevented us from performing this test with *mom-5* (data not shown). These results are consistent with the proposal that EGL-20/Wnt and MIG-1/Frz function together to promote *ceh-12*/HB9 expression, thereby leading to the creation of ectopic gap junctions between

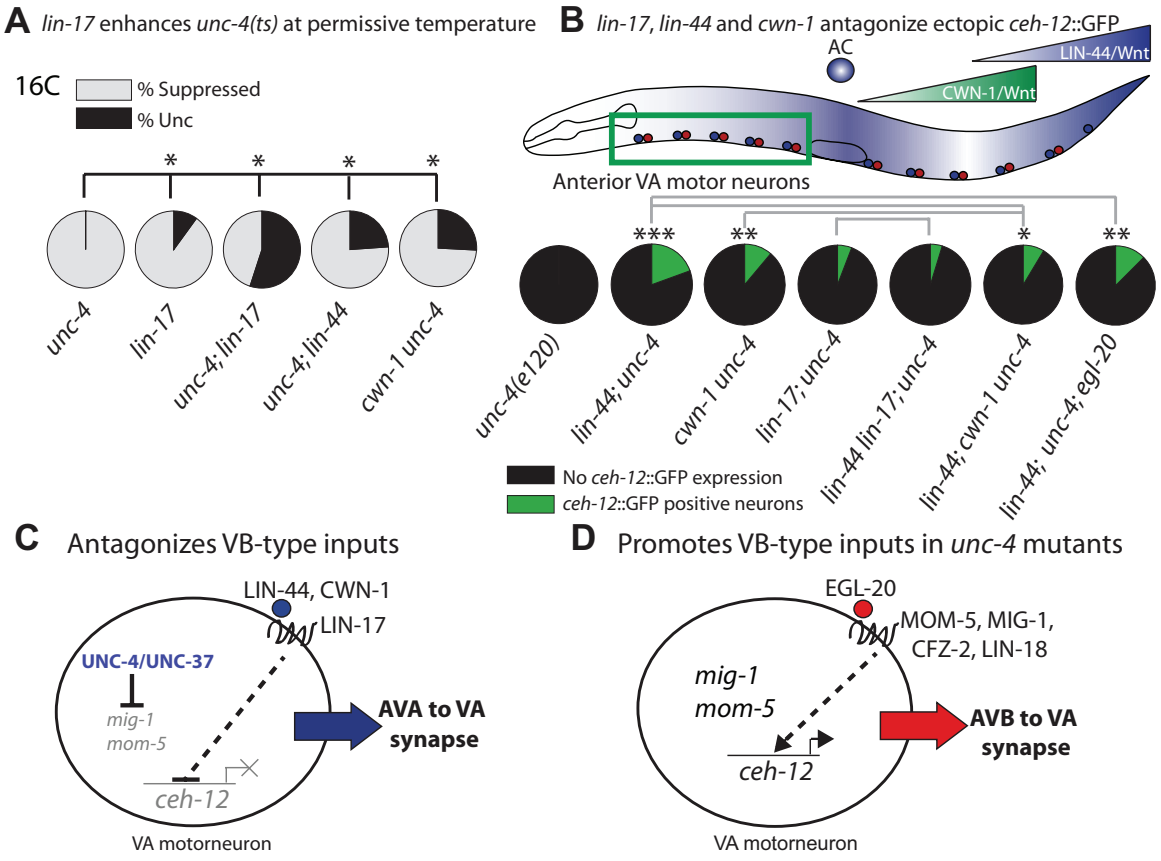

Figure 4.12. *lin-17/Frz* promotes VA-type inputs in opposition to *egl-20*/Wnt signaling. **A**. *unc-4(e2322ts)* shows wild-type backward locomotion at 16 °C. Mutations in *lin-17*/Frz, *lin-44*/Wnt and *cwn-1*/Wnt enhance Unc-4 backward movement. *lin-44* and *cwn-1* single mutants show wild-type movement (data not shown). **B.** LIN-44 is expressed in the tail and in the Anchor Cell (AC); CWN-1 is expressed in posterior cells. Mutations in *cwn-1*/Wnt and *lin-44*/Wnt enhance ectopic *ceh-12*::GFP expression in anterior VAs in *unc-4(e120)*, *** p<0.001, ** p<0.01,* p<0.05 *vs. unc-4*. n ≥ 16 for each neuron. Green box denotes group of anterior VA neurons scored in (B). Gray brackets denote no significant difference (p>0.05, Fisher's Exact Test) between compared strains. **C.** LIN-44/Wnt, CWN-1/Wnt and LIN-17/Frz inhibit *ceh-12* expression to preserve AVA inputs to anterior VAs. UNC-4 and UNC-37 antagonize *mig-1* and *mom-5* activity by transcriptional repression or by an indirect mechanism involving an intermediate target gene. **D.** EGL-20/Wnt signaling promotes the creation of AVB inputs to VAs. Elevated expression or function of MOM-5/Frz and MIG-1/Frz in *unc-4* and *unc-37* mutants confers sensitivity to a local EGL-20/Wnt cue that activates *ceh-12* expression and the creation of VB-type inputs. CFZ-2/Wnt and LIN-18/Frz may also function in this pathway (Fig. 4.3).

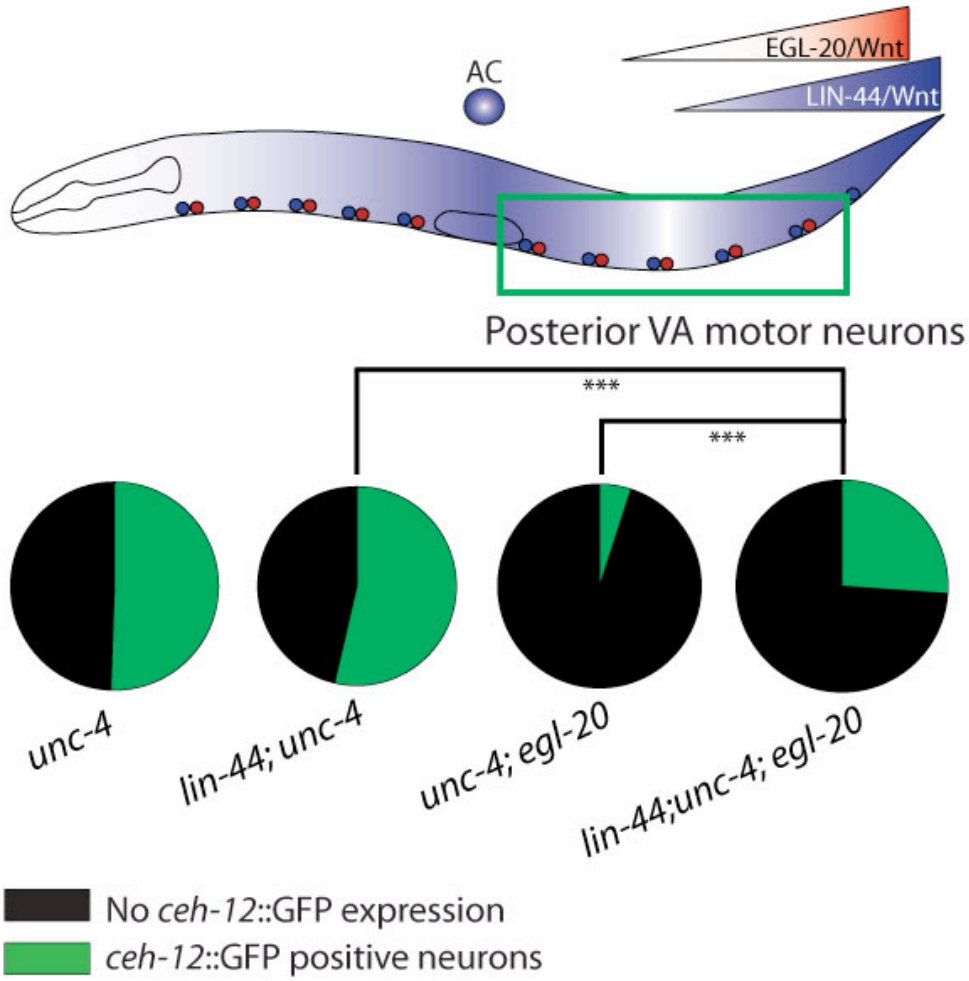

Figure 4.13. LIN-44/Wnt antagonizes EGL-20-dependent expression of *ceh-12*::GFP in *unc-4* mutant VA motor neurons. The double mutant *lin-44; unc-4* has a similar effect on posterior *ceh-12* expression as the *unc*-4 single mutant. EGL-20/Wnt is required for posterior *ceh*-12::GFP expression in *unc-4* mutants. Ectopic *ceh-12*::GFP expression is partially restored in *lin-44; unc-4; egl-20* triple mutants thereby demonstrating that *lin-44* antagonizes *ceh-12*::GFP expression in posterior VAs. The occurrence of significantly more posterior *ceh-12*::GFP expression in *lin-44; unc-4; egl-20* compared to *unc-4; egl-20* also indicates that another pathway is promoting *ceh-12* expression in these neurons in the absence of EGL-20/Wnt and LIN-44/Wnt activity. *** $p < 0.001$ Fisher's Exact Test. Posterior VA motor neurons are grouped VA7-10. $n \geq 15$ for each neuron.

AVB and VA motor neurons. We note that *egl-20, mig-1* and *ceh-12* also suppress the Unc-4 AVB gap junction defect for VA2 in the anterior ventral nerve cord [42]. This finding suggests that *ceh-12* expression is regulated by the EGL-20/Wnt pathway in this anterior VA motor neuron although we were unable to detect this effect with the *ceh-12*::GFP reporter as noted above.

To determine if *lin-17*/Frz normally antagonizes the formation of AVB to VA gap junctions, we investigated UNC-7S::GFP localization in a *lin-17* mutant; this test detected ectopic UNC-7S::GFP puncta for VA6 and VA10 (Figs. 4.14A, C). Although aberrant AVB gap junctions are limited to a subset of VAs in this experiment, these effects are statistically significant and are consistent with the mild backward movement defect of the *lin-17* mutant (Fig. 4.14A, 4.15, Table 4.6). Moreover, the strong *lin-17*-dependent enhancement of Unc-4 movement for the hypomorphic *unc-4(e2322ts)* allele (Fig. 4.12A) suggests that LIN-17/Frz might also act in additional VAs to oppose the creation of AVB to VA gap junctions. Similarly, a *cwn-1*/Wnt mutation results in ectopic AVB gap junctions with anterior VAs (Fig. 4.15A). Due to synthetic lethality, *lin-44* could not be tested (data not shown). Taken together, these data support the hypothesis that LIN-17/Frz and CWN-1/Wnt prevent the imposition of ectopic AVB inputs to VA motor neurons by opposing the activity of an EGL-20/Wnt signaling pathway that functions principally through *mom-5*/Frz and *mig-1*/Frz (Fig. 4.12C, D).

EGL-20/Wnt opposes the formation of AVA to VA chemical synaptic connections.

Mutations in *unc-4* alter the connectivity of VA motor neurons by replacing gap junctions and chemical synapses from AVA interneurons with gap junctions from AVB [38, 42]. We have established that a posterior EGL-20/Wnt signal, functioning via

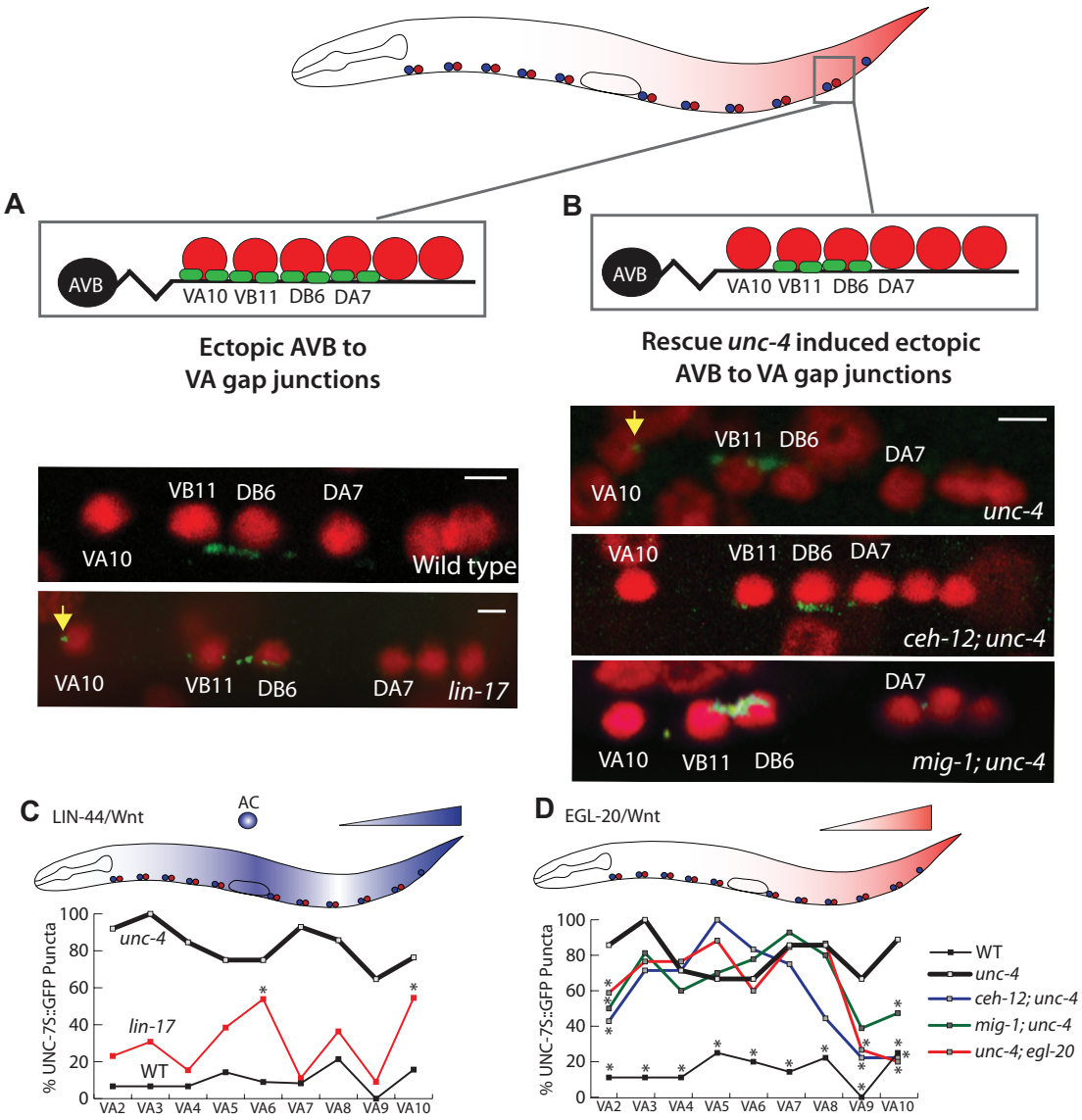

Figure 4.14. Opposing Wnt pathways regulate the specificity of gap junction inputs to VA motor neurons. **A.** AVB gap junctions (Green) with the cell soma of VB and DB motor neurons (Red). Mutants of *lin-17* (A) and *unc-4* (B) show ectopic AVB to VA gap junctions (yellow arrows). **B.** AVB gap junctions with posterior VAs depend on EGL-20/Wnt. Mutations in *ceh-12* and *mig-1*/Frz suppress ectopic AVB gap junctions with VA10 in *unc-4(e120)* mutants. **C.** *lin-17* mutants display ectopic gap junctions near known sources of LIN-44/Wnt in the anchor cell (AC) (VA6) and tail region (VA10). **D.** *ceh-12*/HB9, *mig-1*/Frz and *egl-20(n585)* mutants suppress ectopic AVB gap junctions with posterior VAs in *unc-4(e120)* mutants and with VA2. * p< 0.05 *vs.* WT (C) or *unc-4* (D). n ≥ 10 for each neuron.

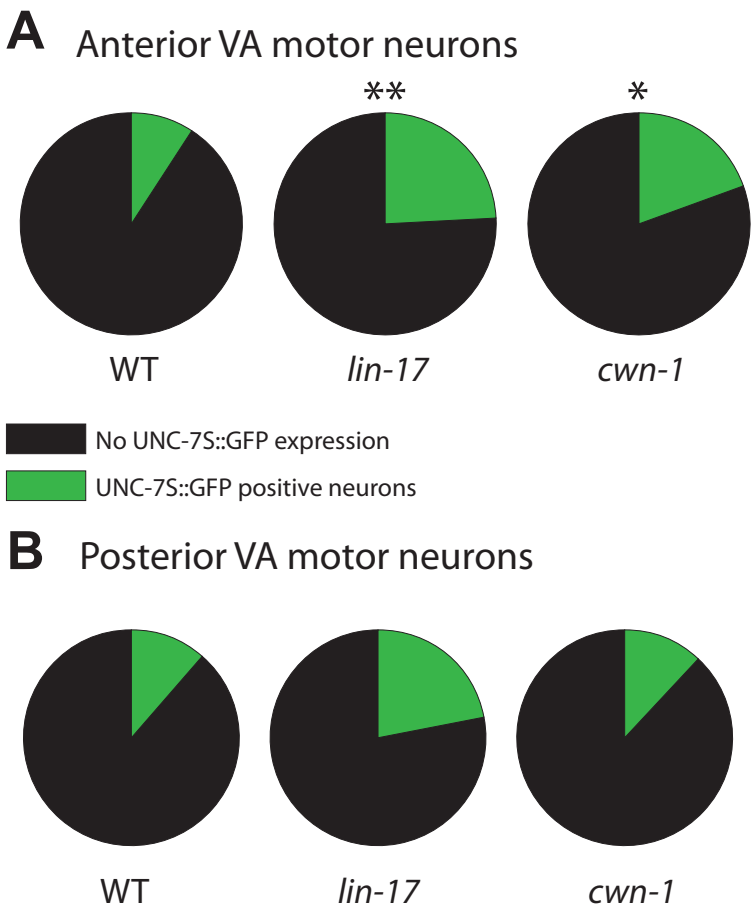

Figure 4.15. Components of the LIN-17/Frz pathway prevent the formation of VB-type inputs in VAs. **A.** "Anterior" VAs (VA2-6) show significantly more ectopic AVB to VA gap junctions in *lin-17* and *cwn-1* mutants vs. WT. **B.** No difference is detected in ectopic AVB to VA gap junctions in "Posterior" VAs (VA7-10). ** $p<0.01$, * $p<0.05$, Fisher's Exact Test vs. WT. $n \geq 10$ for each neuron.

ceh-12, directs the formation of ectopic gap junctions between posterior VAs and AVB in *unc-4* mutants (Figs. 4.14B, D) [42]. To determine if EGL-20/Wnt signaling is also necessary for eliminating normal VA inputs from AVA in *unc-4* animals, we utilized a GRASP (GFP Reconstitution Across Synaptic Partners) assay (Fig. 4.16A). GRASP uses split-GFP to label chemical synapses between specific pairs of neurons (Figs. 4.16A-C). These split-GFP puncta include AVA synapses with both DA and VA motor neurons which cannot be readily distinguished except within a region between VA10 and DA7 (Fig. 4.16B). We confirmed that the AVA to VA10 GRASP signal is significantly weaker in *unc-4* mutants (Figs. 4.16C-D) [103] and show that mutations in *ceh-12* or *egl-20* restore wild-type levels of split-GFP signal to AVA synapses with VA10 (Figs. 4.16C-D). These results indicate that EGL-20/Wnt signaling, acting through *ceh-12*/HB9, is responsible for eliminating AVA synapses with posterior VAs in addition to its role in establishing ectopic gap junctions with AVB.

UNC-4 antagonizes a canonical Wnt signaling pathway.

In *C. elegans*, canonical Wnt signaling involves the β-catenin protein, BAR-1, whereas non-canonical or atypical Wnt pathways utilize other members of the β-catenin family [173]. In the canonical pathway, Wnt interaction with a Frizzled receptor stabilizes BAR-1 by inhibiting the activity of a "destruction complex" that includes the proteins Axin, GSK3β, and Casein Kinase Iα. In the absence of Wnt, the destruction complex phosphorylates cytosolic BAR-1 leading to its degradation [158]. Thus, if BAR-1/β-catenin functions in a canonical Wnt pathway to promote VA miswiring, then a loss-of-function *bar-1* mutation should suppress this defect. We observe weak suppression of Unc-37 backward movement by the *bar-1(mu63)* allele but not *unc-4* (Fig. 4.17). One explanation for this ambiguous result is that *bar-1* mutant animals are Unc possibly due

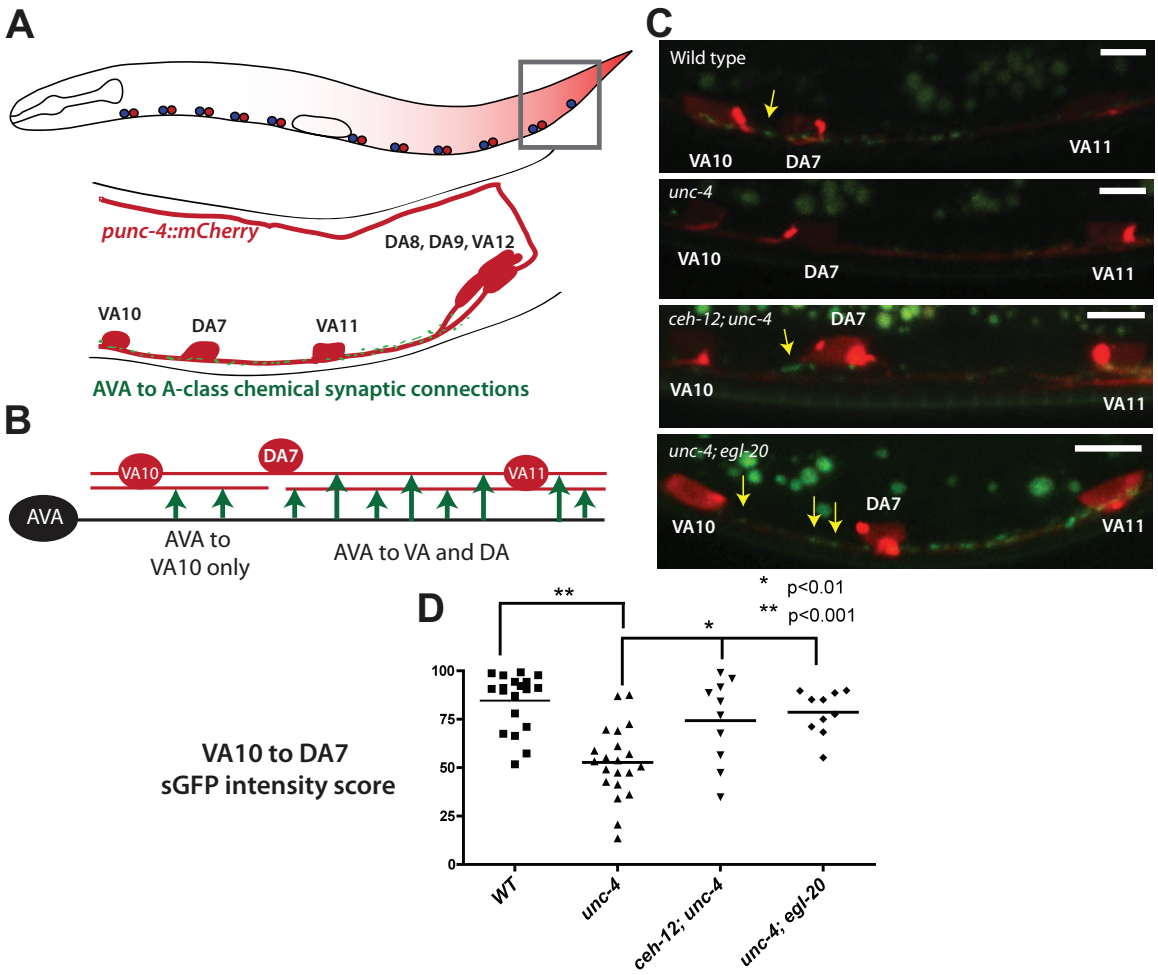

Figure 4.16. GRASP markers detect chemical synapses between AVA and A-motor neuron partners. **A.** AVA synapses with DA and VA motor neurons in wild type. Inset shows the posterior region between VA10 and DA7 (B) where AVA synapses specifically with VA10. **C.** GRASP-dependent GFP puncta (yellow arrows) with VA10 (red) are reduced in *unc-4(e120)* and restored by *ceh-12(gk391)* or *egl-20(n585).* **D.** Intensity values of GFP puncta were quantified from line scans of this region (see Methods). * p< 0.01, ** p<0.001, Analysis of Variance (ANOVA). n ≥ 10 for each neuron.

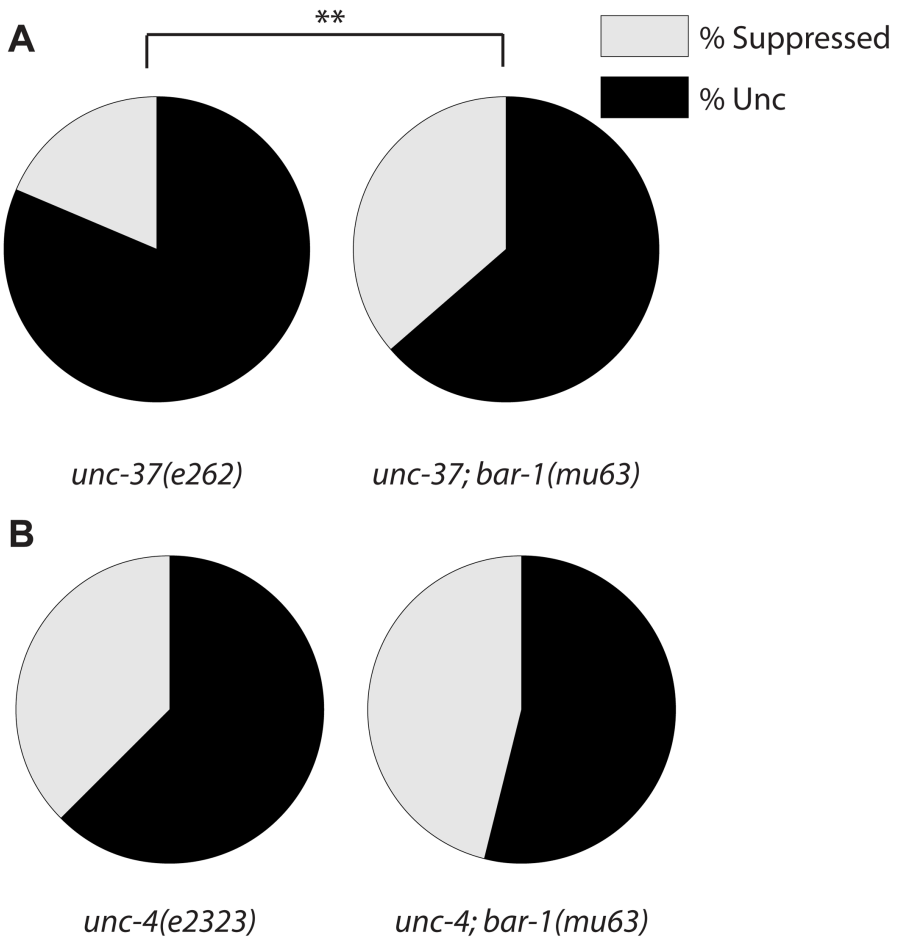

Figure 4.17. BAR-1/β-catenin differentially affects movement in *unc-37* and *unc-4* mutants. Mutation of *bar-1* suppresses the Unc-37 backward movement defect (A) but not Unc-4 ($p>0.05$) (B). Movement was assessed with the tapping assay. $n \geq 40$.
** $p < 0.01$, Fisher's Exact Test.

to a required function in another motor neuron class [174]. The stronger effect of the *bar-1* mutation on the Unc-37 phenotype could also result from dual roles of UNC-37/Groucho as a co-repressor with UNC-4 and with the TCF-LEF family member POP-1 [175] both of which probably function to block *ceh-12* expression.

To confirm that canonical Wnt signaling is involved upstream of *ceh-12*, we tested for potential roles of the Wnt pathway destruction complex in the Unc-4 phenotype. Genetic ablation of the Axin-like *pry-1* effectively activates canonical Wnt signaling by preventing degradation of BAR-1/β-catenin [158]. It follows that if PRY-1/Axin negatively regulates EGL-20/Wnt-dependent signaling in VA motor neurons, then a mutation in *pry-1* should constitutively activate this pathway. Backward locomotion is strongly impaired in the *pry-1; unc-4(e2322ts)* double mutant compared to the *unc-4(e2322ts)* and *pry-1* single mutants (Fig. 4.18A). This synthetic Unc-4 phenotype is consistent with a model in which both *unc-4* and *pry-1* normally function as negative regulators of a Wnt pathway that leads to VA miswiring (Fig. 4.18E).

Next, we treated animals with LiCl to inhibit GSK3β activity [176] and thus hyper-activate canonical Wnt signaling. Exposure of wild-type animals to 10mM LiCl induces a strong backward movement defect (Fig. 4.18B). Although lithium-dependent inhibition of other targets in *C. elegans* [177] could potentially impede locomotion, this LiCl-induced Unc-4 phenotype is attenuated in a *ceh-12* null mutant (Fig. 4.18B). This result is consistent with the model that VA miswiring depends on activation of *ceh-12* expression by canonical Wnt signaling (Fig. 4.18E).

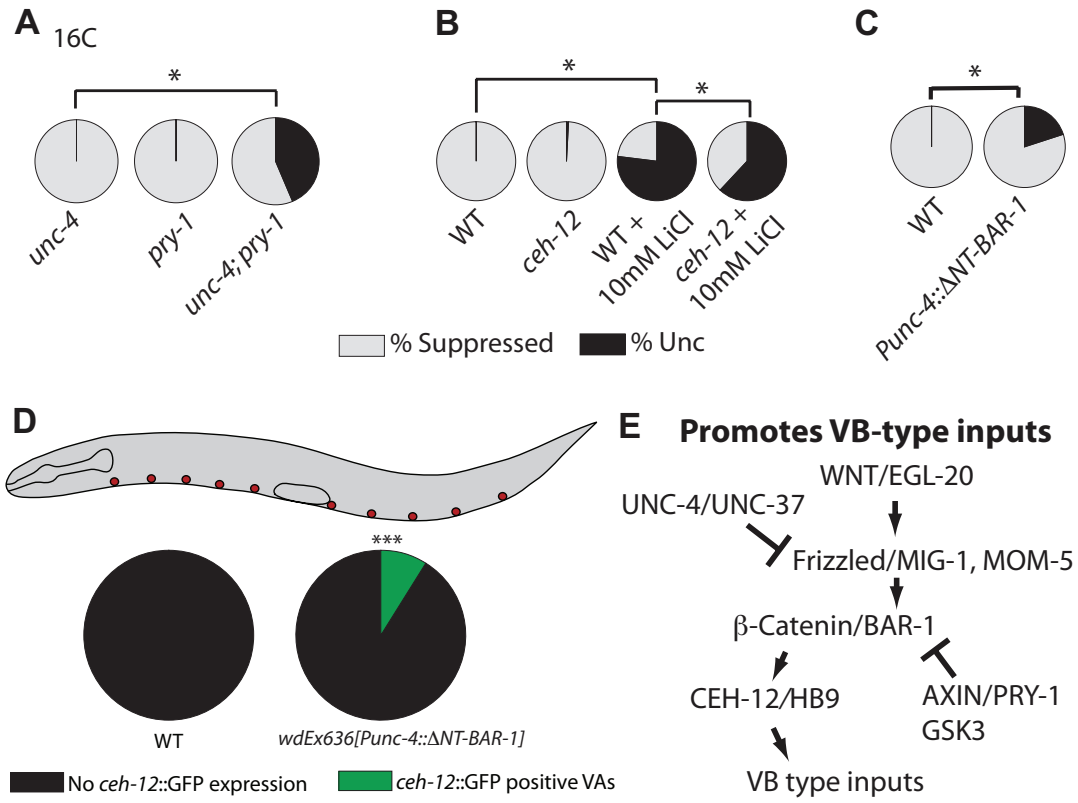

Figure 4.18. Canonical Wnt signaling functions upstream of *ceh-12* in *unc-4* mutant VA motor neurons. **A.** *pry-1(mu38)*/Axin enhances the Unc-4 backward movement phenotype of *unc-4(e2322ts)* at 16 °C. n ≥ 50. **B.** The GSK-3β inhibitor, LiCl, induces a backward movement defect in WT animals that is partially rescued by *ceh-12(gk391)*. n ≥ 150. **C.** Constitutive activation of BAR-1/β-catenin in WT A-class motor neurons with P*unc-4*::ΔNT-BAR-1 results in Unc-4-like movement, * p<0.05. n ≥ 50. **D.** *ceh-12*::GFP is ectopically expressed in VAs when BAR-1/β-catenin is constitutively activated in a wild-type background, *** p<0.001 *vs.* WT. n ≥ 20 for each neuron. **E.** UNC-4 antagonizes a canonical Wnt signaling pathway to preserve VA-type inputs.

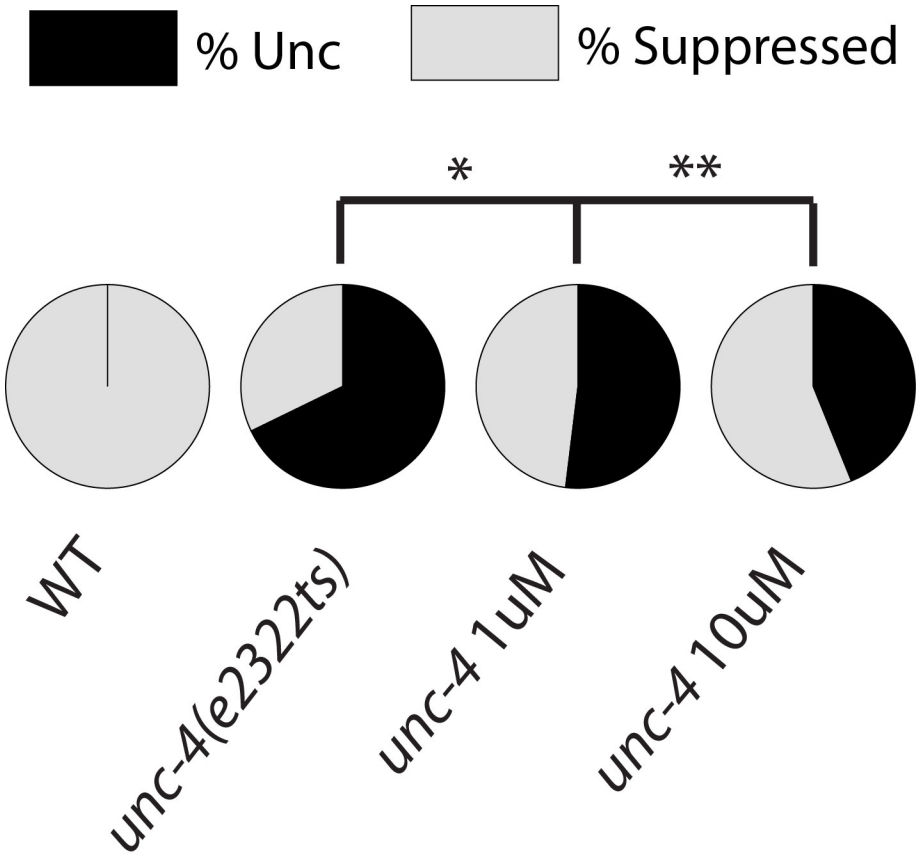

Figure 4.19. The Wnt inhibitor, Pyrvinium suppresses *unc-4(e2322ts)* movement defect at 23 °C. A tapping assay was performed to determine if the canonical Wnt inhibitor pyrvinium was capable of suppressing the backword movement defect in a weak allele of *unc-4*. Pyrvinium showed a dose dependent effect on suppression of Unc-4 movement.* $p<0.05$, ** $p\leq0.001$, *** $p<0.0001$ Fisher's Exact Test. $n\geq 100$.

If inhibition of the destruction complex by either the *pry-1*/Axin mutation or by LiCl prevents degradation of BAR-1/β-catenin, then a constitutively active BAR-1/β-catenin protein should produce a similar phenotypic effect. We tested this prediction with *ΔNT-BAR-1*, a truncated β-catenin protein lacking N-terminal phosphorylation sites that trigger Axin/GSK3-mediated degradation [158]. Expression of *Punc-4::ΔNT-BAR-1* in A-class motor neurons results in Unc-4-like movement resembling that produced by CEH-12/HB9 overexpression (Fig. 4.18C) [42]. Moreover, the *Punc-4::ΔNT-BAR-1* transgene induced ectopic *ceh-12*::GFP expression in VA motor neurons in which wild-type *unc-4* function is intact (Fig. 4.18D) thereby supporting the idea that canonical Wnt signaling is sufficient to activate *ceh-12* expression in VA motor neurons.

In a final experiment, we utilized the canonical Wnt-pathway inhibitor, pyrvinium, which interacts with Casein Kinase 1α to activate the destruction complex and downregulate β-catenin. Experiments in *C. elegans* have confirmed that pyrvinium disrupts canonical Wnt signaling [178]. Thus, if the Unc-4 movement defect arises from ectopic activation of canonical Wnt signaling then this effect should be ameliorated by treatment with pyrvinium. This prediction is substantiated by the finding that pyrvinium suppresses the Unc-4 movement phenotype of *unc-4(e2322ts)* (Fig. 4.19). Taken together, our results support the hypothesis that UNC-4 preserves VA type synaptic inputs by antagonizing an EGL-20/Wnt-dependent canonical signaling pathway.

DISCUSSION

Neural networks are defined by the creation of synapses between specific neurons. In *C. elegans*, the UNC-4 homeodomain protein functions in VA motor neurons

to prevent the formation of inputs normally reserved for VB motor neurons [35, 36, 38]. We have shown that this synaptic choice depends on UNC-4 inhibition of a canonical Wnt signaling pathway that promotes VB-type inputs. UNC-4 is required in posterior VAs to block the effects of an EGL-20/Wnt cue secreted from adjacent epithelial cells in the tail. The outcome of EGL-20/Wnt signaling is also opposed by a separate pathway involving the LIN-44/Wnt, CWN-1/Wnt and LIN-17/Frz. We propose that this mechanism could be generally employed by neuron-specific transcription factors to diversify local circuits during neural development in which graded Wnt signals are widely utilized to specify neurogenic fates.

Wnt signaling regulates synaptic choice

Wnt signaling can either promote or inhibit synaptic assembly. Wnt exercises a positive role at central synapses and at motor neuron inputs to muscle [154]. For example, in the cerebellum, Wnt7a is provided by granule cell target neurons to activate presynaptic assembly in migrating mossy fiber axons [83]. Wnt7a also promotes postsynaptic development of excitatory neurons in the hippocampus [179]. At the mammalian neuromuscular junction, Wnt activates postsynaptic clustering of acetylcholine receptors and can be provided by either the innervating motor neuron [180] or by nearby non-neuronal tissues [181]. In these instances, the Wnt signal is transduced by non-canonical pathways that act locally and apparently do not require transcription [81, 154, 182-184]. Wnt signals may also act as negative cues at neuromuscular synapses. In *C. elegans*, LIN-44/Wnt functions through LIN-17/Frz to exclude synapses from a nearby motor neuron axonal compartment [79]. In *Drosophila*, Wnt4 is selectively expressed in a specific embryonic muscle to prevent inappropriate motor neuron inputs [19]. Together, these results are indicative of multiple alternative pathways for Wnt signaling that either stimulate or limit synaptogenesis. However, with

the exception of the negative role of Wnt4 in blocking input from specific motor axons in the fly embryonic musculature, Wnt signaling has not been previously shown to drive the selection of particular pairs of synaptic partners. We describe a mechanism in which EGL-20/Wnt favors the creation of synapses between one set of neurons *versus* another. EGL-20/Wnt activates a canonical pathway that promotes expression of the homeodomain transcription factor CEH-12/HB9. In turn, CEH-12/HB9 exercises the dual function of favoring the creation of VB-type inputs (*e.g*., gap junction from AVB, Fig. 4.14) with VA motor neurons while simultaneously blocking the formation of endogenous VA-type connections (*e.g.,* synapses from AVA, Fig. 4.16) [42]. The identification of CEH-12/HB9-regulated genes should help elucidate the mechanism of these effects. The central roles of HB9 homologs of CEH-12 in *Drosophila* and vertebrate motor neuron differentiation [45-47] suggest that these targets could also function in more complex motor circuits [42]. The function of UNC-4 in VA-input specificity must involve additional downstream genes, however, as the Unc-4 miswiring defect in VA motor neurons in the anterior ventral nerve cord does not depend on *ceh-12*/HB9 [42]. The recent isolation of Unc-4 suppressor mutations that function in parallel to *ceh-12* is consistent with this model (J. Schneider, R. Skelton, D. Ruley, Z. Xu, I. Boothby, D. M. Miller, unpublished). The existence of alternative pathways for driving the creation of VB-type inputs could explain why VB motor neurons, which normally express CEH-12/HB9, are not miswired in either *ceh-12* or *egl-20* mutants [42].

Wnt signaling regulates the specificity of electrical synapses in the motor circuit.

In the *C. elegans* motor circuit, gap junctions are assembled between specific neuron pairs and in specific neuronal compartments. For example, the gap junction component, UNC-7, is expressed in AVB interneurons where it localizes adjacent to the cell soma of target B-class (DB and VB) motor neurons [1, 42, 114]. Our results show

that the UNC-4 pathway controls both the location and specificity of UNC-7 gap junctions. UNC-4 normally prevents the formation of AVB gap junctions with VA motor neurons, and ectopic CEH-12/HB9 expression in posterior, *unc-4* mutant VAs is required for this effect [42]. We have shown that EGL-20/Wnt signaling is also necessary for the creation of AVB to VA gap junctions, presumably through the activation of ectopic CEH-12/HB9 expression in *unc-4* mutant VAs. In these cases, gap junctions with AVB are placed on the VA cell soma whereas the usual wild-type gap junctions with AVA are located on VA neuron processes [1, 42] (Fig. 4.14). Thus, UNC-4 is likely to antagonize a cell biological mechanism that places AVB gap junctions on the VA cell soma whereas EGL-20/Wnt signaling acting through CEH-12/HB9 favors this choice. Gap junctions are widespread in the developing nervous system where they mediate synchronous activity that presages mature circuits of chemical synaptic connections [147]. Gap junctions are more limited in the mature vertebrate brain and spinal cord [185] but recent results indicate that these electrical synapses are important for function [150, 151]. The mechanisms that define the specificity and localization of gap junction components are largely unknown [146]. Thus, future studies of the downstream genes that are regulated by the antagonistic activities of UNC-4 *versus* EGL-20/Wnt and CEH-12/HB9 could provide a foundation for understanding the cell biology of neuron-selective gap junction assembly.

Multiple Wnt cues and receptors regulate synaptic specificity

The *C. elegans* genome encodes five Wnt ligands, CWN-1, CWN-2, EGL-20, LIN-44, MOM-2 and six Wnt receptors including the Frizzled homologs, CFZ-2, LIN-17, MIG-1, MOM-5, and LIN-18/Ryk and CAM-1/Ror [58, 90]. Studies in *C. elegans* have revealed roles for these components in cell migration, axon guidance, synaptogenesis, and cell fate determination [52, 56, 57, 79, 86, 162, 167, 186, 187]. Our results parallel

the finding that multiple Wnts and receptors may contribute to each of these features [188]. For example, we show that EGL-20/Wnt and the Frz receptors MIG-1 and MOM-5 activate expression of CEH-12/HB9 in VA motor neurons to promote the creation of VB-type inputs (*i.e.,* gap junctions with AVB) (Fig. 4.14) and to oppose VA-type inputs (*i.e.,* synapses from AVA) (Fig. 4.16). This observation is consistent with earlier studies that detected overlapping functions for MOM-5/Frz and MIG-1/Frz in other EGL-20/Wnt-dependent signaling pathways [56, 188]. Conversely, a LIN-17/Frz–dependent function opposes the outcome of the EGL-20/Wnt signal in a pathway that probably responds to LIN-44/Wnt and CWN-1/Wnt. Opposing roles for MIG-1 *vs.* LIN-17-dependent signaling have been previously noted but the downstream mechanisms that account for this effect are not known [56]. Our evidence indicates that the EGL-20/Wnt interaction with MIG-1 and MOM-5 functions through a canonical signaling pathway involving BAR-1/β-catenin to activate expression of CEH-12/HB9. The independent identification of *unc-4*-interacting (i.e., suppressor) mutations in the canonical signaling protein POP-1/TCF (J. Schneider, R Skelton, D. Miller, unpublished) is consistent with this model. We did not detect evidence of roles for these components in LIN-17-dependent regulation of VA input specificity, which therefore probably utilizes an atypical or non-canonical pathway. A recent report of opposing roles for canonical vs. noncanonical Wnt signaling in hippocampal neuron synaptogenesis [85] suggests that related antagonistic mechanisms for modulating Wnt signaling output may also be utilized during vertebrate neural development.

Transcriptional mechanisms preserve motor circuit fidelity by preventing selected neurons from responding to available Wnt cues.

Our results are consistent with the idea that UNC-4 functions in VA motor neurons via a transcriptional mechanism that limits expression of the MOM-5 and MIG-

1/Frizzled and thereby effectively quells the sensitivity of VA motor neurons to an available EGL-20/Wnt cue. The effect of UNC-4 on *mig-1* and *mom-5* transcript levels is modest, however. Thus, our results do not rule out the possibility that UNC-4-dependent inhibition of the EGL-20/Wnt signaling pathway could also require transcriptional repression of additional UNC-4 target genes. In any case, the function of UNC-4 reported here is important because it preserves VA inputs that are required for normal locomotion [38]. The extensive occurrence of graded Wnt signals in vertebrate nervous systems [75, 189] suggests that comparable mechanisms could be utilized to differentiate the Wnt sensitivity of local groups of neurons in order to diversify functional circuits. For example, a Wnt signal (Wnt4, Wnt5a, Wnt5b) originates from the floorplate on the ventral side of the spinal cord to promote differentiation of motor neurons in the Median Motor Column (MMC). These MMC neurons, which sit on the proximal edge of the developing spinal column, eventually innervate axial muscles that control body movement. However, progenitors in the P3 ventral domain that directly abut the floorplate and are therefore likely to experience a higher concentration of Wnt4/5 than more dorsal regions, do not adopt the MMC fate. The insensitivity of P3 precursors to Wnt4/5 is maintained by the transcription factor Nkx2.2 but the mechanism of this effect is unknown [80]. We note a striking parallel to the role of UNC-4 in the *C. elegans* ventral nerve cord, which prevents VA motor neurons from responding to an EGL-20/Wnt gradient originating from adjacent epithelial cells.

CHAPTER IV.A:

ADDITIONAL GENETIC EXPERIMENTS REVEAL COMPLEXITIES BETWEEN WNT SIGNALING PATHWAYS THAT REGULATE SYNAPTIC CHOICE

INTRODUCTION AND RATIONALE

To further characterize the Wnt signaling pathways that regulate synaptic choice, I tested additional Wnt mutants for roles in the *unc-4* pathway. Based on multiple genetic experiments, it is clear that a complex coordination of Wnt signaling is involved in the wiring of wild-type VA motor neurons as well as the regulation of the miswiring of *unc-4* mutant VAs. The experiments described below are preliminary findings that require additional testing in order to fully understand the mechanisms of how these Wnt pathways converge to regulate synaptic specificity.

RESULTS

Downstream Wnt components have complex roles in the *unc-4* pathway

In Chapter IV, we established that canonical Wnt signaling is activated in *unc-4* mutant VAs, and this pathway is required for ectopic *ceh-12* expression (Fig. 4.18). To identify potential downstream Wnt signaling components, we tested the effects of mutations in the TCF-LEF family member, *pop-1* and the Disheveled homolog, *dsh-1* on Unc-4 movement. The hypomorphic *pop-1(hu9)* allele suppressed the backward movement defect of *unc-4(2322ts)* animals (Fig. 4A.1A). Mutation in *dsh-1(ok1445)* also suppressed Unc-4 movement (Fig. 4A.1A); however, the movement of *dsh-1(ok1445) unc-4(e2322ts)* animals was unique in that the animals initiated backward movement,

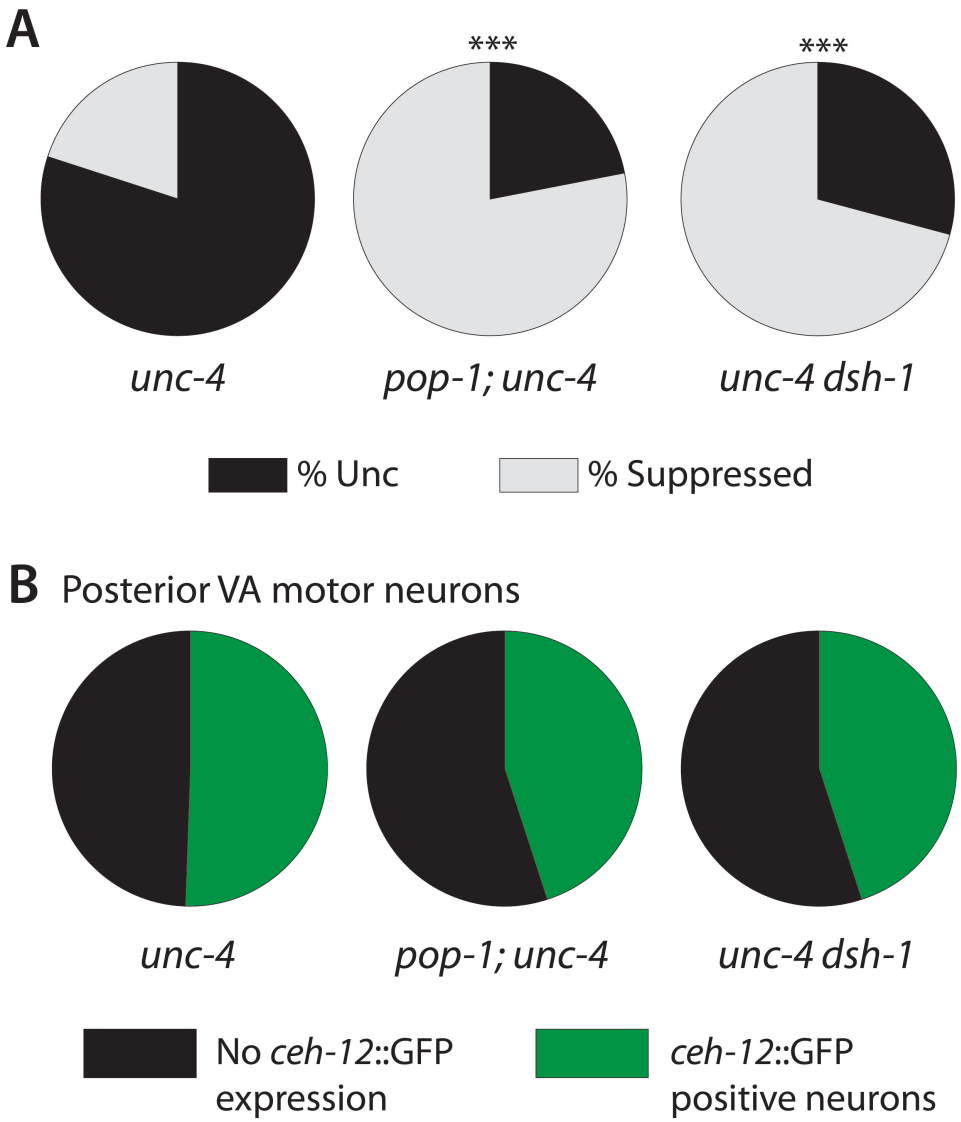

Figure 4A.1. Downstream Wnt components function in the *unc*-4 pathway. **A.** Tapping assay shows that mutation in *pop-1(hu9)* and *dsh-1(ok1445)* suppress the backward movement defect of *unc-4(e2322ts)*. *** $p < 0.001$, Fisher's Exact Test *vs. unc-4*. $n \geq 50$ animals. **B.** Mutations in *pop-1* and *dsh-1* do not affect ectopic *ceh-12*::GFP expression in *unc-4* mutant posterior VA motor neurons. $n \geq 10$ for each neuron.

paused, and then executed a backward body bend. This movement phenotype differs from other Unc-4 suppressor genes, including other Wnt signaling components, suggesting that *dsh-1* may be involved in additional Wnt pathways in VA motor neurons (see below).

Because mutants of *dsh-1* and *pop-1* suppressed Unc-4 backward locomotion and both genes encode Wnt signaling components, we predicted that these genes would be required for ectopic *ceh-12*::GFP expression in posterior VA motor neurons. However, mutations in either *pop-1* or *dsh-1* had no effect on ectopic *ceh-12*::GFP expression (Fig. 4A.1B). Although *pop-1*/TCF is a core component of canonical Wnt signaling, we see no regulation of *ceh-12*, suggesting that *pop-1* might be playing multiple roles downstream of *unc-4*. Similarly, in combination with the movement phenotype of *unc-4 dsh-1* animals, we propose that either *dsh-1* function is required only in select VA motor neurons, or *dsh-1* is functioning in multiple pathways to regulate synaptic choice (see below).

Compound mutant analysis reveals complex pathways that regulate *ceh-12*::GFP expression

To further characterize the Wnt signaling components that function to promote *versus* antagonize ectopic *ceh-12*::GFP expression in VA motor neurons, we tested several additional compound mutant lines. As described in Chapter IV, LIN-44 and CWN-1/Wnt and LIN-17/Frz antagonize *ceh-12*::GFP expression in anterior VA motor neurons. The *ceh-12*::GFP expression seen in *lin-44 lin-17; unc-4* mutants phenocopied the expression pattern observed in *lin-17; unc-4* mutants (Fig. 4.12B). *lin-44; cwn-1 unc-4* triple mutants do not have enhanced ectopic *ceh-12*::GFP expression in anterior VA motor neurons *vs. lin-44; unc-4* or *cwn-1 unc-4*, as would have been predicted if these Wnt ligands function redundantly to oppose *ceh-12* expression in VAs (Fig. 4.12B).

Additionally, mutation in *egl-20* does not suppress the ectopic *ceh-12*::GFP expression seen in *lin-44; unc-4* mutants, which indicates that EGL-20 is not the Wnt ligand required for ectopic *ceh-12*::GFP expression in anterior VAs (Fig. 4.12B).

We demonstrated that MIG-1/Frz is required for ectopic *ceh-12*::GFP expression in anterior VA motor neurons when EGL-20/Wnt was expressed from an anterior source (Fig. 4.2E). These results are in addition to the requirement for *mig-1*/Frz for ectopic *ceh-12*::GFP expression in VA9 (Fig. 4.2A). Thus, we reasoned that MIG-1/Frz may normally be expressed in anterior as well as and posterior VA motor neurons and may be responsive to multiple Wnt ligands in addition to EGL-20, that promote ectopic *ceh-12*::GFP expression in the absence of *lin-44* and *unc-4*. Therefore, ectopic *ceh-12*::GFP expression in anterior VAs in *lin-44; unc-4* double mutants should be lost with the addition of a mutation in *mig-1*. In fact, *mig-1 lin-44; unc-4* triple mutants show a complete suppression (or reduction) of ectopic *ceh-12*::GFP expression in anterior VA motor neurons (Fig. 4A.2A) and significantly less ectopic *ceh-12*::GFP expression in posterior VAs compared to *lin-44; unc-4* (Fig. 4A.3A). The *ceh-12*::GFP expression pattern in *mig-1 lin-44; unc-4* triple mutants is not significantly different *versus mig-1; unc-4.* These data establish a "ground" state in which MIG-1/Frz function is required for any ectopic *ceh-12*::GFP expression in anterior VAs in the absence of *unc-4* and *lin-44*/Wnt function (Fig. 4A.2B). In addition, MIG-1/Frz is partially required for ectopic *ceh-12*::GFP expression in posterior VAs in *lin-44 and unc-4* mutants (Fig. 4A.2B). These results also solidify the model that LIN-44/Wnt has an opposing role to MIG-1/Frz to control *ceh-12* expression in VA motor neurons.

Our data show that the Wnt receptors *mig-1*/Frz and *lin-18*/Ryk are required for ectopic *ceh-12*::GFP expression in VA9 and VA8 and VA9, respectively (Figs. 4.2, 4.3). If *mig-1* and *lin-18* have partially redundant functions to promote ectopic *ceh-12*::GFP

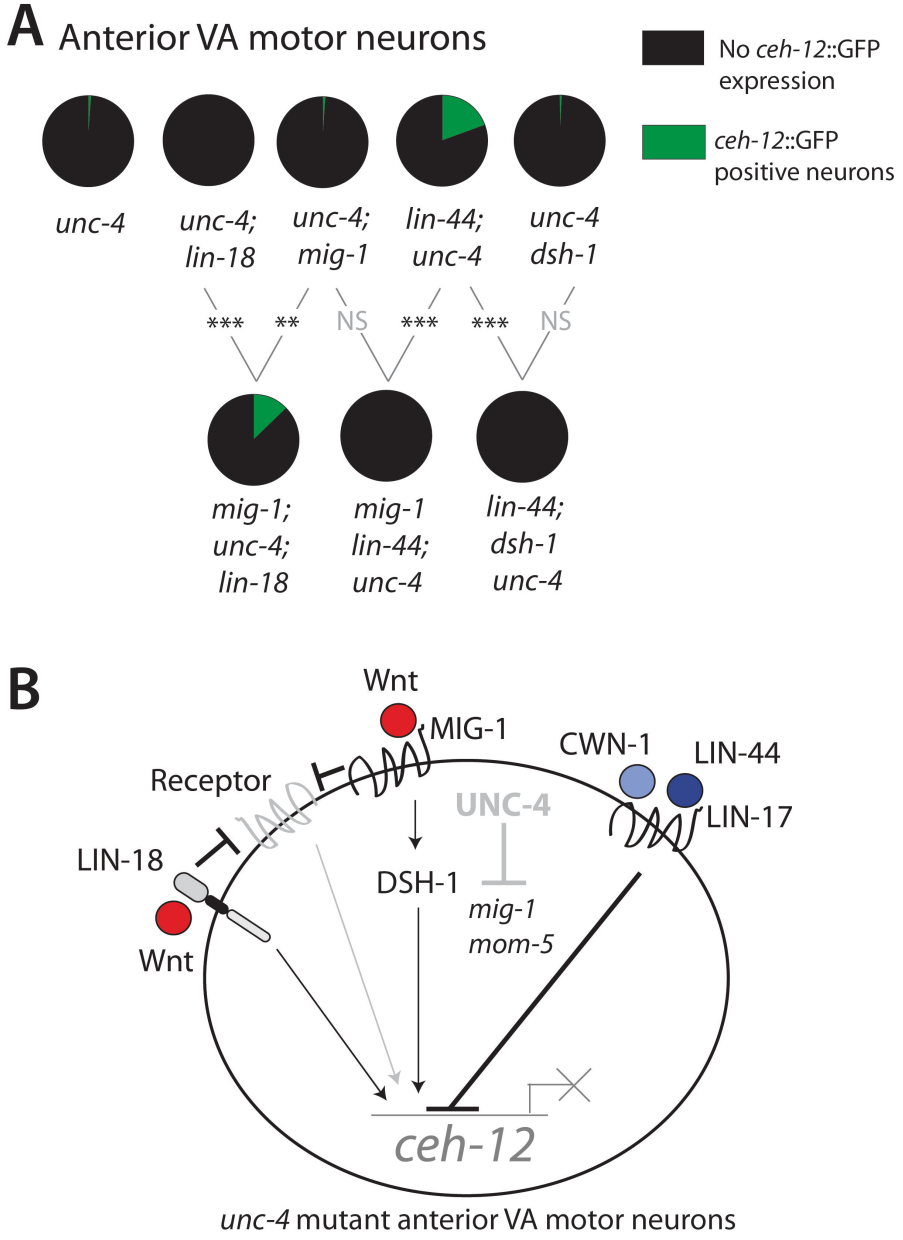

Figure 4A.2. Compound genetic analysis reveals complex interactions that regulate *ceh-12* expression in anterior VA motor neurons. **A.** *mig-1; unc-4; lin-18* triple mutants have significantly more ectopic *ceh-12*::GFP expression *vs.* the double mutants, suggesting that *mig-1* and *lin-18* normally repress the function of a third Wnt receptor upstream of *ceh-12* (B). *mig-1* and *dsh-1* are required for ectopic *ceh-12*::GFP in anterior VA motor neurons in the absence of both *lin-44* and *unc-4*. *** $p<0.001$, ** $p<0.01$, N.S.= Not significant, Fisher's Exact Test. $n\geq10$ for each neuron, anterior VAs are pooled (see Methods). **B.** Model for Wnt signaling pathways in *unc-4* mutant anterior VAs. LIN-18/Ryk and MIG-1/Frz, through DSH-1, normally respond to an unidentified Wnt ligand to promote *ceh-12* expression in the absence of the LIN-44-mediated pathway. LIN-18 and MIG-1 redundantly repress the function of a third Wnt receptor that becomes activated and competent to respond to a Wnt signal in the absence of *mig-1* and *lin-18*.

expression, then we would expect to see a decrease, or suppression of ectopic *ceh-12*::GFP expression in the *mig-1; lin-18* double mutant. Surprisingly, there is no significant difference in ectopic *ceh-12*::GFP expression in posterior VAs between the *mig-1; unc-4; lin-18* triple mutant and *lin-18; unc-4* or *mig-1; unc-4* double mutants (Fig. 4A.3A). Additionally, we observed an increase in ectopic anterior *ceh-12*::GFP expression in the *mig-1; unc-4; lin-18* triple mutant (Fig. 4A.2A), which is contradictory to our simple model. One explanation for the increase in anterior *ceh-12*::GFP expression in that another Wnt receptor, for example, *mom-5* or *cfz-2*, is normally unable to bind to the Wnt signal due to competition from *mig-1* and *lin-18*. Mutation in both *mig-1* and *lin-18* releases this competition and results in an increase in Wnt signaling through the alternative Wnt receptor and subsequent activation of ectopic *ceh-12*::GFP expression in anterior VAs (Fig 4A.2B).

As described above, we discovered conflicting results with *dsh-1*/Disheveled. Mutation in *dsh-1*/Disheveled suppressed the Unc-4 movement defect (Fig. 4A.1A); however, *ceh-12*::GFP expression in *dsh-1 unc-4* double mutants was unchanged *versus unc-4* single mutants (Fig. 4A.1B). Because the suppression of movement conferred in *dsh-1 unc-4* animals was slightly different than that seen with other Wnt mutations (see above), we considered the possibility that *dsh-1* might be functioning in multiple pathways upstream of *ceh-12*. Interestingly, *lin-44; dsh-1 unc-4* mutants showed complete suppression of the ectopic *ceh-12*::GFP expression in anterior VAs (Fig. 4A.2A) and significantly less *ceh-12*::GFP expression posterior neurons *vs. lin-44; unc-4* (Fig. 4A.3A). Thus, *dsh-1*/Dsh function is required for any ectopic *ceh-12* expression in anterior VAs (Fig. 4A.2B) and partially required in posterior VAs in the absence of *lin-44* and *unc-4* (Fig. 4A.2B). The residual *ceh-12*::GFP expression in posterior VAs might be due to DSH-1-independent EGL-20/Wnt signaling, possibly through a noncanonical signaling pathway.

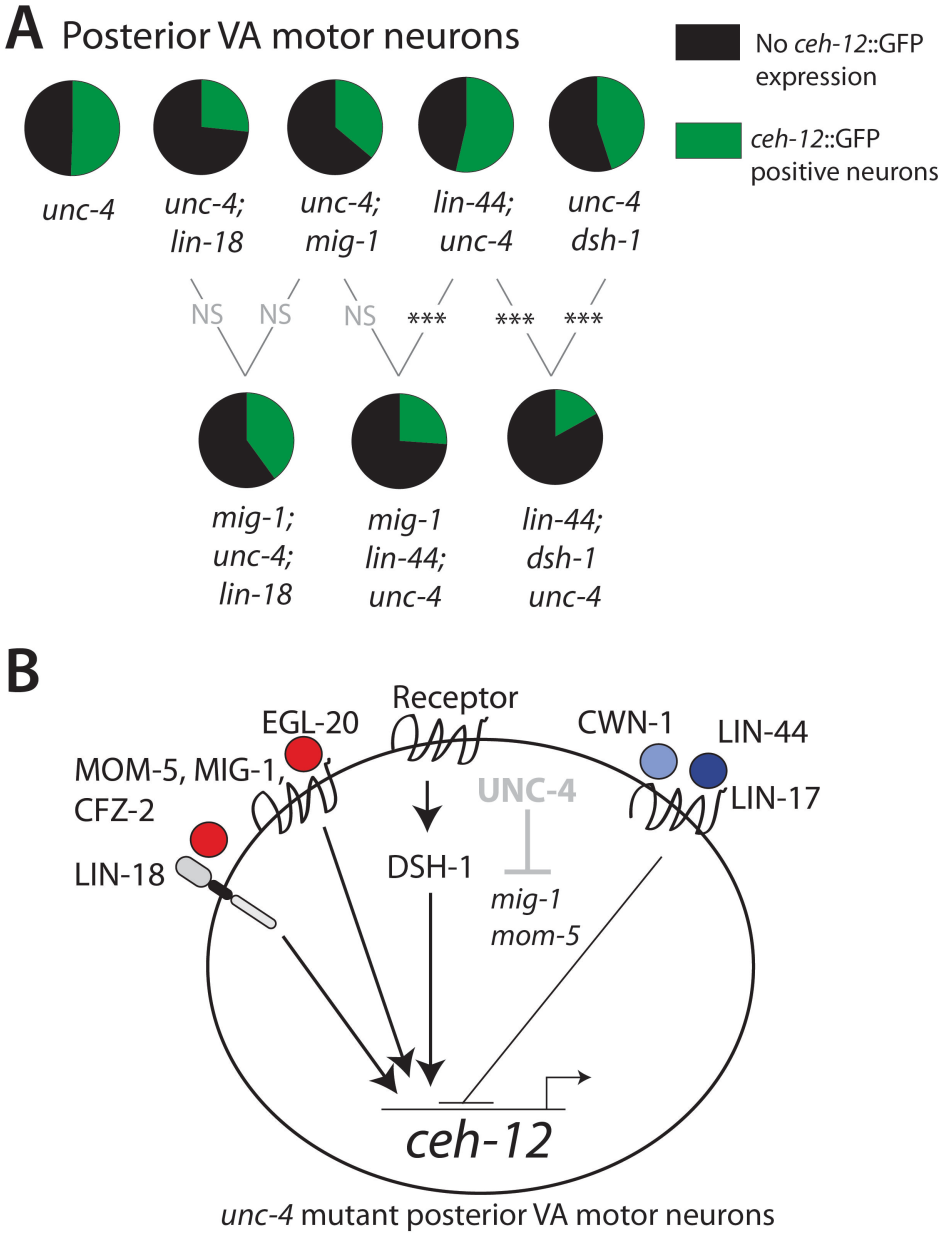

Figure 4A.3. Compound genetic analysis reveals complex interactions that regulate *ceh-12* expression in posterior VA motor neurons. **A.** *mig-1; unc-4; lin-18* triple mutants have no effect ectopic *ceh-12*::GFP expression *vs.* the double mutants, suggesting that a third Wnt receptor promote *ceh-12* expression in parallel (B). *mig-1* is required for ectopic *ceh-12*::GFP in anterior VA motor neurons in the absence of both *lin-44* and *unc-4*. *dsh-1* is required for *ceh-12* expression in the absence of both *lin-44* and *unc-4*, in parallel to *mig-1*. *** p<0.001, N.S.= Not significant, Fisher's Exact Test. n≥10 for each neuron, posterior VAs are pooled (see Methods). **B.** Model for Wnt signaling pathways in *unc-4* mutant posterior VAs. LIN-18/Ryk and MIG-1/Frz respond to a EGL-20/Wnt signal and promote *ceh-12* expression. A third pathway involving an unidentified Wnt receptor signals through DSH-1 to promote *ceh-12* expression in the absence of the LIN-44-mediated pathway.

DISCUSSION AND FUTURE DIRECTIONS

Compound genetic mutant analysis has revealed that a complex coordination of multiple Wnt signaling pathways function in VA motor neurons. For example, our experiments have established that at least one additional Wnt signaling pathway promotes *ceh-12* expression in the absence of *mig-1* and *lin-18* function in anterior VAs (Fig. 4A.2B) or *mig-1, dsh-1* and *lin-44* in posterior VAs (Fig. 4A.3B). Thus, additional genetic experiments might provide further insight into the complex interactions between Wnt components. Our evidence suggests that *mig-1* function is required for *ceh-12* expression in anterior VAs in the absence of LIN-44-mediated signaling; thus we would expect that *mig-1; unc-4 cwn-1* triple mutants would show similar suppression of ectopic *ceh-12*::GFP expression as *mig-1 lin-44; unc-4* animals. Additionally, we propose that MIG-1 and LIN-18 might repress the function of another Wnt receptor that also promotes *ceh-12*::GFP expression in the absence of *mig-1* and *lin-18* (Fig. 4A.2B). Thus, additional genetic tests, *i.e.* constructing mutants *mig-1 mom-5; lin-18* or *mig-1; cfz-2; lin-18* might reveal the identity of the Wnt receptor and provide information as to the nature of the competitive interactions between Wnt receptors.

We noticed that the effects of *dsh-1* on *ceh-12*::GFP expression were strikingly similar to the effects seen with *mig-1*/Frz (Figs. 4A.2, 4A.3). Based on these data, we predict that *mig-1*/Frz has multiple roles upstream of *ceh-12* and that *dsh-1* transduces the signal from MIG-1 in anterior VA motor neurons, while functioning in parallel to MIG-1 in posterior VAs. In the absence of *unc-4* function, *mig-1* is required for ectopic *ceh-12*::GFP expression in VA9 downstream of EGL-20 (Fig. 4.2). Because *dsh-1* does not affect *ceh-12*::GFP expression, we propose that DSH-1 functions in parallel to MIG-1 in posterior VAs (Fig. 4A.3B). In the absence of both *lin-44* and *unc-4*, *mig-1* and *dsh-1* are required for any ectopic *ceh-12*::GFP expression in anterior VAs (Fig. 4A.2) and are partially required for *ceh-12* expression in posterior VAs (Fig. 4A.3). Thus, we propose

that DSH-1 functions downstream of MIG-1 in anterior VAs to promote ectopic *ceh-12*::GFP expression (Fig 4A.2B). To test this, we could assay the *unc-4 dsh-1* mutant for suppression of the Unc-4 movement defect caused by expression of MIG-1 in VAs (Fig. 4.11D).

We showed that mutation in *pop-1*/TCF-LEF suppressed the Unc-4 movement defect, but did not affect ectopic *ceh-12*::GFP expression in posterior VA motor neurons. To test whether POP-1 is required for canonical Wnt signaling downstream of BAR-1/β-catenin, we could assay a *pop-1* mutant for suppression of the Unc-4 movement defect caused by expression of the constitutively active BAR-1 (ΔNT::BAR-1) in VA motor neurons (Fig. 4.18C). Additionally, we could test for a role for *pop-1* downstream of *mig-1* and *dsh-1* in ectopic expression of *ceh-12*::GFP in anterior VA motor neurons (Fig. 4A.2). Together, these experiments have demonstrated that there is a great deal of complexity in the Wnt signaling pathways that regulate synaptic choice in VA motor neurons.

CHAPTER V:

OPPOSING G-PROTEIN PATHWAYS REGULATE GAP JUNCTION SPECIFICITY IN THE MOTOR CIRCUIT

INTRODUCTION

A functional neural circuit is defined by connections between specific neuron partners. Neurons make two types of connections: chemical synapses, which utilize neurotransmitters to signal between presynaptic and postsynaptic neurons, and gap junctions, or electrical synapses, that regulate electrical coupling and small molecule transport between partner neurons [147, 190, 191]. Both the formation and activity of these synapses is highly regulated. However, much less is known about mechanisms that regulate the formation of gap junctions between partner neurons [190, 192] than pathways that trigger assembly of chemical synapses between specific neurons [145, 193].

Gap junctions are composed of four pass transmembrane domain proteins [192]. Two related classes of gap junction proteins, connexins and pannexins, are utilized in mammals [192]. Members of a second class of topologically similar proteins called innexins are assembled into invertebrate gap junctions. In all of these cases, multimeric assemblage of six subunits called connexons, or hemichannels, are initially generated within the trans-Golgi network [192]. These hemichannels are then transported to the plasma membrane where they are positioned in apposition to another hemichannel complex in the plasma membrane of an adjacent cell. The resultant gap junction plaques [194] create an intercellular pore for transport of small molecules (< 1kDa) and ions

[192]. The hemichannels can be assembled from a single type of subunit (homomeric) or from molecularly distinct components (heteromeric). In addition, the gap junction plaques may be composed of hemichannels of identical (homotypic) or different (heterotypic) subunit composition.

Gap junction function can be regulated by mechanisms that control assembly or gating of gap junction hemichannels. The opening and closing, or gating, of gap junction channels is responsive to intracellular and extracellular voltage changes, cytosolic pH levels, changes in intracellular calcium concentrations and chemical uncouplers [195]. For example, a transient increase in cytoplasmic calcium results in the closure of gap junction channels via interaction between the calcium binding protein, calmodulin, and connexin proteins [191]. G-protein signaling pathways have been implicated in gap junction regulation at multiple levels, including the localization [98] and assembly of gap junction components [95, 99]. Additionally, GPCR activation can inhibit gap junction function by regulating the gating of the channel, thus allowing for fine-tuned regulation of cell-cell communication [97].

The basic mechanism of G-protein dependent signaling involves the α, β and γ G-protein subunits (See Fig. 1.6). The GDP-bound form of the α subunit is stably integrated into a heterotrimeric complex with the β and γ subunits. Upon ligand binding to a 7-transmembrane G protein coupled receptor (GPCR), GTP displaces GDP and the Gα subunit dissociates from the βγ complex. Both the Gα subunit and the tightly associated Gβγ dimer can then interact with effectors (see below). Autocatalytic conversion of GTP-Gα to GDP-Gα inactivates Gα-dependent signaling in a process that can be stimulated by associated RGS (Regulator of G protein Signaling) proteins [93]. The GDP-Gα then reassociates with the Gβγ subunits to reconstitute the signaling inactive G-protein heterotrimer [94].

The *C. elegans* genome contains 21 genes that encode Gα proteins with at least one ortholog of each mammalian Gα family [95]. Additionally, two genes encode Gβ and Gγ proteins, *gpb-1, gpb-2* and *gpc-1, gpc-2*, respectively [95]. G proteins regulate multiple cellular processes in *C. elegans*, including viability, embryonic spindle pole positioning and hatching. Multiple G-protein pathways involving the opposing functions of GOA-1/Gαo, EGL-30/Gαq and GSA-1/Gαs converge to control egg laying and locomotion through the regulation of acetylcholine release [95].

G protein regulation of acetylcholine release at the *C. elegans* neuromuscular junction has been extensively studied [95], however, little is known of how G proteins regulate gap junction assembly in *C. elegans*. In the developing *C.elegans* oocyte, *goa-1*/Gαo and *gsa-1/*Gαs function antagonistically to control gap junction function, possibly through regulation of channel gating [96, 196]. In vertebrates, Gαq and Gαs pathways regulate the assembly and localization of multiple gap junction proteins including connexin43 (Cx43) [97, 98]. Additionally, the Gαs second messenger, cAMP, regulates the synthesis, trafficking to the plasma membrane, and gating of the gap junction channel via phosphorylation of Cx43 [100].

Downstream signaling pathways are well established for Gαq and Gαs pathways, whereas little is known of the specific effector molecules regulated by Gαo (Fig. 1.6) [92]. Activated Gαq stimulates phospholipase C beta (PLCβ) to hydrolyze Phosphatidylinositol 4,5-bisphosphate (PIP2) into inositol tri-phosphate (IP3) and diacylglycerol (DAG) (Fig. 1.6). IP3 signaling elevates intracellular calcium levels (see below) and DAG binds several downstream effectors, including protein kinase C (PKC), and UNC-13 [92, 95]. As mentioned above, cAMP can function as a second messenger in the Gαs pathway. cAMP levels are elevated by Gαs activation of adenylyl cyclase. In turn, cAMP activates downstream effector molecules including protein kinase A (PKA)

and effector protein of cAMP (Epac) [92]. In *C. elegans,* EAT-16/RGS and DGK-1/diacylglycerol kinase function as effectors of GOA-1/Gαo signaling. Genetic experiments have shown that these GOA-1 effectors antagonize the EGL-30/Gαq and GSA-1/Gαs pathways to prevent the release of acetylcholine at the neuromuscular junction [95].

Because the neuron specificity of gap junction assembly is altered in *unc-4* mutants, we wondered if G-protein signaling is required for this synaptic choice. As described earlier (Fig. 1.3), wild-type VA motor neurons establish gap junctions with AVA interneurons. In *unc-4* mutants, these AVA to VA connections are replaced by gap junctions with AVB interneurons. Here, we report the finding that opposing G-protein pathways regulate this switch in neuron specificity through gap junction assembly.

GOA-1/Gαo in concert with EAT-16/RGS is required for the creation of gap junctions between AVB and VA motor neurons in *unc-4* mutants. This outcome is opposed by the combined action of the Gα proteins, EGL-30/Gαq (which acts through EGL-8/PLCβ) and GSA-1/Gαs and its downstream effector, ACY-1/adenylyl cyclase. Thus, this work defines a mechanism whereby antagonistic G-protein signaling pathways regulate the synaptic specificity of gap junction connections.

MATERIALS AND METHODS

Nematode Strains and Genetics

Nematodes were cultured using standard methods [112]. Mutants were obtained from the *Caenorhabditis* Genetics Center (CGC) or by generous donations from other labs. Table 5.1 describes the alleles and sequencing primers used in this study.

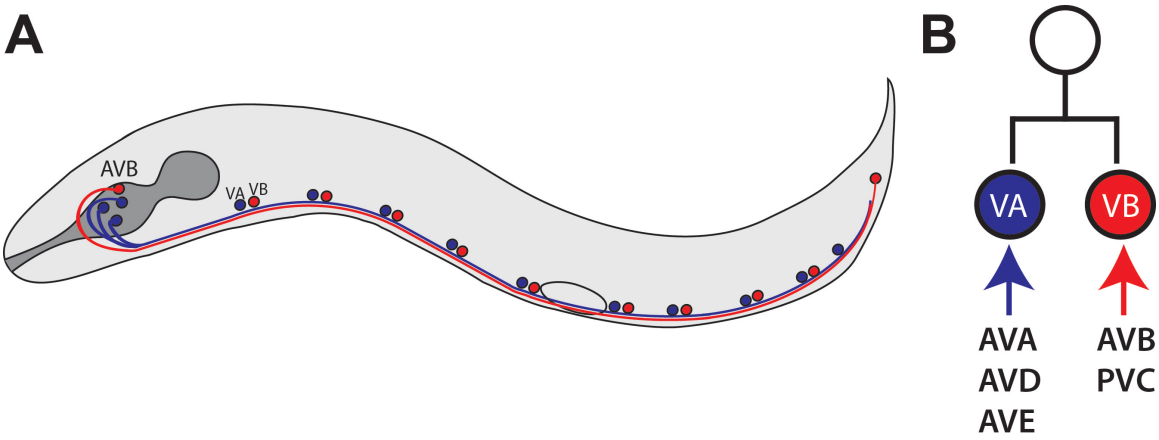

Figure 5.1. The *C. elegans* motor circuit. **A.** Command interneurons from the head and tail extend processes to synapse with motor neurons in the ventral nerve cord. **B.** VA and VB motor neurons are lineal sisters but adopt inputs from different sets of interneurons. VA motor neurons receive inputs from command interneurons that control backward locomotion (AVA, AVD, AVE) and VB motor neurons receive inputs from the forward circuit command interneurons (AVB, PVC).

Molecular Biology and Transgenic strains

Constitutively active GOA-1

To create a plasmid that expressed constitutively active GOA-1 in A-class motor neurons, GOA-1^{Q205L} was PCR amplified from pJM70C [197] with AscI (5') and PmeI (3') sites (See Table 5.2 for primer sequences). This fragment was cloned into the pCR8/GW/TOPO cloning vector (Invitrogen) to make pRLS13. To put GOA-1^{Q205L} under the *unc*-4 promoter, pRLS13 and pRLS9 (*Punc-4*::PTX+ *unc-119* minigene) were digested with AscI/PmeI and ligated to make pRLS8 (*Punc-4::* GOA-1^{Q205L} + *unc-119* minigene). Two separate strains were created that contained this transgene. Microparticle bombardment of *unc-119* mutant animals [134] was used to generate strains for tapping assays (Fig. 5.2B). The coselectable marker *Punc*-4::mcherry offered visualization of expression of the array. 15 ug each of pRLS8 and *Punc-4::mcherry* were digested with PacI and ligated for bombardment to create the *wdEx702* array (Fig. 5.2B). The *wdEx873* array was created by microinjection of pRLS8 (30 ng/ul) and pCW2.1 (*ceh-22*::GFP) (15 ng/ul) into *unc-4(e120); wdIs54* animals and was used in the Gap Junction Assay (Fig. 5.4).

Cell-specific expression of GOA-1

Site-directed mutagenesis (Stratagene QuikChange II XL) of pRLS8 was used to convert L205 to the wild-type Q205 to make pRLS56 (*Punc-4*::GOA-1) (see Table 5.2 for primer sequences). The nucleotide change was confirmed by sequencing. pRLS56 (30 ng/ul) was coinjected with pCW2.1 (*ceh-22*::GFP) (15 ng/ul) into *goa-1(n1134); unc-4(e120); blr-1(wd76); wdIs54* for expression of wild-type GOA-1 in A class motor neurons (Fig. 5.2G).

Table 5.1. Table of alleles used in this study and sequencing primers if applicable. Mutants without sequencing primers were identified based on phenotype.

Gene	Allele	Forward primer	Reverse primer
goa-1	*n1134*	GTCGCCTTGACGACGTGC	CCAAGTAGCAGCAGTTTGATATC
gsa-1	*ce81*	GACACTAATAGGATCATTC	GTGTATTGTCCTCCCAGAGTAC
egl-30	*n686*	TGGATTTCGAGTCGGTGAC	CGGAAAGCGCCACCAGGAAC
egl-10	*md176*	GATCCACTGTTAACGCCTCC	CATTGACCGGCGACGTTGCC
eat-16	*ep273*	GACGATGAGGCTGAAGCGAG	CACTTGCCGTCCTATAGGATC
dgk-1	*nu62*	GACATTGAGTGAGGTACTTTTG	CATCGGCAGCTCGGTTCGAG
egl-8	*md1971*	CTGACACTATTCGTAAGGAGC	CTGATCACCCCTAGCCGACC
rap-1	*pk2082*	CTCGGATCTGGAGGAGTAGG	CACGAGCAGCACTGCTTATTTG
rgef-1	*ok675*	GGAATTGCGAGCTATGGTGT	TGTCGGCTTCTCTGTTGTTG
unc-13	*e51*	N/A	N/A
unc-17	*e113*	N/A	N/A

Table 5.2 Table of transgenic arrays used in this study. For each array, primers for construction and concentration used in microinjection are listed.

Strain name	Array name	Array contents	Concentration (ng/ul)	Primers for plasmid construction	Primer Sequence
NC2588	*wdEx873*	pRLS8 (*Punc-4*::GOA-1 Q205L)	30 ng	goa-1_Q205L_PmeI	GGGGGTTTAAACTTAATACAAGCCGCATCCAC
		ceh-22::GFP	15 ng	goa-1_Q205L_AscI	GGGGGCGCGCCATGGGTTGTACCATGTCACAG
NC2595	*wdEx876*	pRLS57 (*Punc-4*::EGL-30)	30 ng	EGL-30_cDNA-AscI-F	GGGGCGCGCCATGGCCTGCTGTTTATCCG
		ceh-22::GFP	15 ng	EGL-30_cDNA-KpnI-R	CCGGTACCTTACACCAAGTTGTACTCC
		pBluescript	30 ng		
NC2609	*wdEx885*	pRLS56 (*Punc-4*::GOA-1)	20 ng	GOA-1 cDNA site dir-F	GTTCGATGTGGGAGGTCAAAGATCAGAAAGGAAG
		ceh-22::GFP	15 ng	GOA-1 cDNA site dir-R	CTTCCTTTCTGATCTTTGACCTCCCACATCGAAC
		pBluescript	25 ng		
NC2654	*wdEx898*	pRLS60 (*Punc-4*::GSA-1)	30 ng	GSA-1_cDNA-AscI-F	GGGGCGCGCCATGGGGTGCGTCGGCGCTGG
		ceh-22::GFP	15 ng	GSA-1_cDNA-KpnI-R	CCGGTACCTTATAGAAGCTCGTACTGTCG
		pBluescript	30 ng		
NC2716	*wdEx922*	pRLS62 (*Punc-4*::MYC::UNC-9)	5 ng	Punc-9_MYC_AscI	ggGGCGCGCCTCTAGAaatggcACCGGTCG
		ceh-22::GFP	15 ng	Punc-9_MYC_KpnI	ccGGTACCGAGCTCACACGTCGTGCA
		pBluescript	55 ng		

Construction of a goa-1 *RNAi clone*

PCR was used to amplify an 816 bp fragment of the *goa-1* cDNA sequence, flanked with PmeI using the primers goa-1_cDNA-F 5' GTTTAAACggcatgcaagcggcaaaag and goa-1_cDNA-R 5' GTTTAAACctgggaagcagatcgttaacg. The PCR product was inserted into pCR8/GW with TOPO TA cloning (Invitrogen) to make pRLS18. The *goa-1* RNAi fragment from pRLS18 was put into the L4440 RNAi feeding vector (Addgene plasmid #11344) by Gateway cloning (Invitrogen).

Expression of EGL-30 in A-class motor neurons

EGL-30 cDNA was PCR amplified to generate flanking AscI (5') and KpnI (3') restriction sites (see Table 5.2 for primer information). The PCR product and pRLS50 (*Ppag-3*::FLAG) were digested with AscI/KpnI and ligated to generate pRLS54 (*Ppag-3*::EGL-30). Next, the *pag-3* promoter was replaced with the *unc-4* promoter at SphI/AscI sites to make pRLS57 (*Punc-4*::EGL-30). pRLS57 (30 ng/ul) was coinjected with the coselectable marker pCW2.1 (*ceh-22*::GFP) (15 ng/ul) into *unc-4(e120);wdIs54*.

Expression of GSA-1 in A-class motor neurons

GSA-1 cDNA was PCR amplified to generate flanking AscI (5') and KpnI (3') restriction sites (see Table 5.2 for primer information). The PCR product and pRLS57 (*Punc-4*::EGL-30) were digested with AscI/KpnI and ligated to generate pRLS60 (*Punc-4*::GSA-1). pRLS60 (30 ng/ul) was coinjected with the coselectable marker pCW2.1 (*ceh-22*::GFP) (15 ng/ul) into *unc-4(e120);wdIs54*.

ceh-12::GFP expression

ceh-12 expression was assayed with *wdIs85* (*ceh-12*::GFP) [42, 104]. L2 larval VA and VB neurons were scored for the presence or absence of *ceh-12*::GFP expression (n > 10 for each neuron). Animals were anesthetized with either 0.25% tricaine/0.025% tetramisole or with 10mM levamisole on a thin 2% agarose pad. The experimenter was blinded to genotype to avoid bias. Fisher's Exact Test was used to determine statistical significance.

Tapping Assay

Tapping assays detected effects of specific mutants on Unc-4 backward locomotion [42]. For each genotype, L4-young adults (n $\geq$ 50) were tapped once on the head with a platinum wire. Backward movement was scored as either **Unc** (coiled instantly, no net backward movement), **Initiate** (attempted to execute backward locomotion or movement of tail) as **Suppressed** (detectable backward movement of posterior region or entire body in locomotory sinusoidal waves). The experimenter was blinded to genotype to avoid bias.

cha-1 movement assays

The temperature sensitive *cha-1(y226)* allele [198] was utilized to determine if acetylcholine is required during the UNC-4 temperature-sensitive period (TSP) [35]. All experiments were performed in parallel with the *unc-4(e2322ts)* allele [35]. Both alleles are wild type at the permissive temperature of 16 °C. Eggs were collected by hypochlorite treatment and directly plated onto pre-cooled (16 °C) nematode growth media (NGM) plates and grown at 16 °C for either 64.5 or 68.5 hours. Plates were then transferred to the nonpermissive temperature of 23 °C for either 13 or 9 hours, respectively. After the temperature shift, animals were allowed to develop at 16 °C until

L4/young adult stage. Movement was assessed with tapping assays (see Methods above) at 16 °C. The experimenter was blinded to genotype to avoid bias. n ≥ 50 animals.

Detecting AVB gap junctions (UNC-7S::GFP) with ventral cord motor neurons

The strain NC1694 *wdIs54 (Punc-7*::UNC-7S:GFP, *col-19*::GFP) *unc-7*(*e5*) X was integrated by gamma irradiation (4000 Rads) of EH578 [114] and 10X backcrossed into wild type. AVB gap junctions with ventral cord motor neurons were detected by anti-GFP immunostaining in synchronized L4 larvae as previously described [42]. VA neurons were identified based on the stereotypic position of their DAPI stained nuclei as previously described [42]. Animals carrying transgenic arrays were identified based on *ceh-22*::GFP expression in the pharynx. The experimenter was blinded to genotype to avoid bias. n ≥ 10 for each neuron. VA motor neurons were pooled for each genotype and are represented in pie charts. Table 5.3 includes all data used to generate pie charts.

Microscopy

*wdIs54 (Punc-7::*UNC-7S::GFP) and *wdIs85 (Pceh-12::GFP)* were scored with a 100x objective in a Zeiss Axioplan microscope equipped with a Hammamatsu Orca camera. Images of UNC-7S::GFP puncta and DAPI stained nuclei were obtained with an Olympus FV-1000 confocal microscope with a 60x/1.45 Plan-Apochromat lens. Pseudocolors and image overlays were generated using Image J.

Table 5.3 Summary of data represented in pie charts of UNC-7S::GFP expression. Sum of all VA motor neurons scored is also listed.

Gene(Allele)	% VAs with ectopic UNC-7S::GFP	% VAs with no UNC-7S::GFP	Σ VA Neurons Scored
unc-4	82	18	125
goa-1; unc-4	49	51	181
goa-1; unc-4 $^{unc\text{-}4::GOA\text{-}1}$	82	18	98
unc-4::GOA-1^{Q205L}	18	82	149
eat-16; unc-4	60	40	98
wdIs55	4	96	81
unc-4; wdIs55	95	5	93
unc-4; wdIs55; dgk-1 unc-7	96	4	90
wdIs54	10	90	133
unc-13	9	91	159
unc-17	6	94	128
unc-4; egl-20	64	36	140
goa-1; unc-4; egl-20	26	74	102
gsa-1; unc-4	51	49	97
acy-1; unc-4	63	37	137
unc-4 $^{unc\text{-}4::GSA\text{-}1}$	71	29	95
unc-4 $^{unc\text{-}4::EGL\text{-}30}$	56	44	98
unc-4; egl-8 $^{unc\text{-}4::EGL\text{-}30}$	75	25	88
epac-1	11	89	93
rgef-1	8	92	90
epac-1; rgef-1	11	89	102

RESULTS

GOA-1/Gαo is required in VA motor neurons for the Unc-4 backward movement defect

To determine if *goa-1*/Gαo is required for the Unc-4 backward movement defect, we assessed *goa-1; unc-4* double mutants with the tapping assay (Methods). The *goa-1(n1134)* loss of function allele strongly suppresses the backward movement defect of a hypomorphic, or weak, *unc-4(e2322ts)* mutation (Fig. 5.2A). In addition, two separate *goa-1* RNAi clones suppress the backward movement defect of the *unc-4(e2323)* hypomorphic allele (Fig. 5.3). These results show that GOA-1/Gαo is required for the Unc-4 backward movement phenotype and therefore suggests that GOA-1 promotes VB-type inputs with VA motor neurons.

To test the idea that GOA-1/Gαo functions in VA motor neurons to promote the Unc-4 miswiring defect, we expressed constitutively active GOA-1/Gαo [199] in VA motor neurons (*Punc-4*::GOA-1^{Q205L}) in *unc-4(e2322ts)*. At the permissive temperature of 16 °C, *unc-4(e2322ts)* animals show wild-type backward movement (Fig. 5.2B). Transgenic expression of *Punc-4*::GOA-1^{Q205L} in *unc-4(e2322ts)* significantly enhanced the Unc-4 backward movement defect in all lines tested in comparison to non-transgenic controls (Fig. 5.2B). In addition, in *goa-1; unc-4* double mutants, the *Punc-4*::GOA-1^{Q205L} transgene complements the *goa-1* loss of function allele to restore a strong Unc-4 backward movement defect to *goa-1(n1134); unc-4(e2322ts)* animals (Fig 5.2B). Thus, our results demonstrate that expression of activated GOA-1/Gαo in VA motor neurons is sufficient to induce an Unc-4 movement defect.

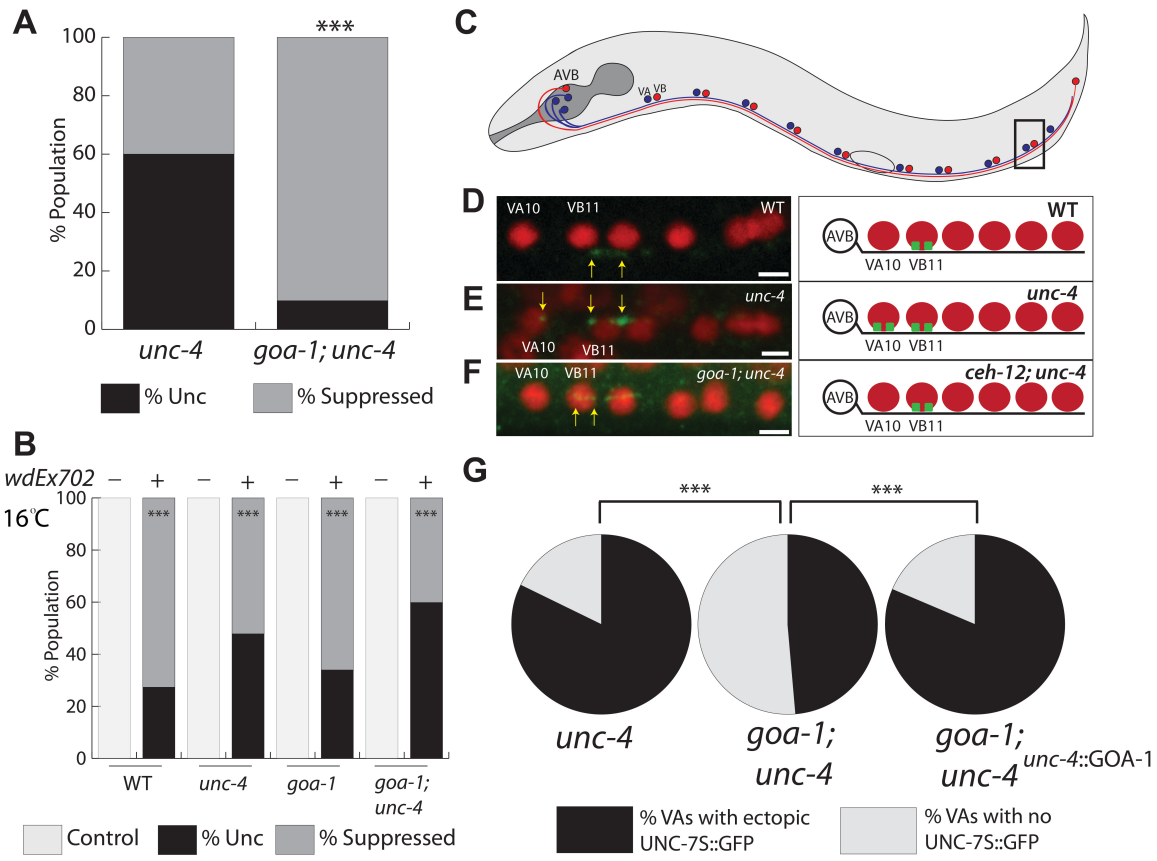

Figure 5.2. GOA-1/Gαo is required for VB-type inputs in *unc-4* mutants. **A.** Tapping assay for locomotion. A majority of *unc-4(e2322ts)* mutants are unable to crawl backward at 23 °C. *goa-1(n1134); unc-4(e2322ts)* double mutants show significantly improved backward locomotion. *** $p < 0.001$ *vs. unc-4*, Fisher's exact test. $n \geq 50$. **B.** VA expression of constitutively active GOA-1 (*wdEx702* (*Punc-4*::GOA-1^{Q205L}), +, dark bars) results in Unc-4-like backward locomotion *vs*. non-transgenic controls (-, light bars). *unc-4(e2322ts)* animals are wild-type at the permissive temperature of 16 °C but Unc-4 when expressing *wdEx702*. Expression of *wdEx702* rescues Unc-4 suppression in *goa-1(n1134); unc-4(e2322ts)* animals. *** $p < 0.001$, Fisher's exact test *vs.* corresponding non-transgenic controls. $n \geq 50$. **C.** Expression of UNC-7S::GFP marks AVB gap junctions with motor neuron cell soma. Inset denotes location of images (D-F). **D-F.** Confocal images of the posteriorly located VA10 and VB11. DAPI (red); UNC-7S::GFP anti-GFP antibody staining (green). **D.** The AVB command interneuron makes gap junctions with VB motor neurons in the wild type (WT). **E-G.** *unc-4(e120)* mutants show ectopic gap junctions with VA motor neurons. *goa-1(n1134); unc-4(e120)* double mutants show fewer ectopic AVB to VA gap junctions in select neurons. **G.** VA expression of *wdEx897* (*Punc-4*::GOA-1) restores the AVB to VA gap junction defect to *unc-4* levels. These findings indicate that GOA-1 functions cell autonomously in VA motor neurons to specify VB-type inputs. *** $p < 0.001$, Fisher's Exact test. $n \geq 98$ ($n \geq 10$ for each specific VA neuron).

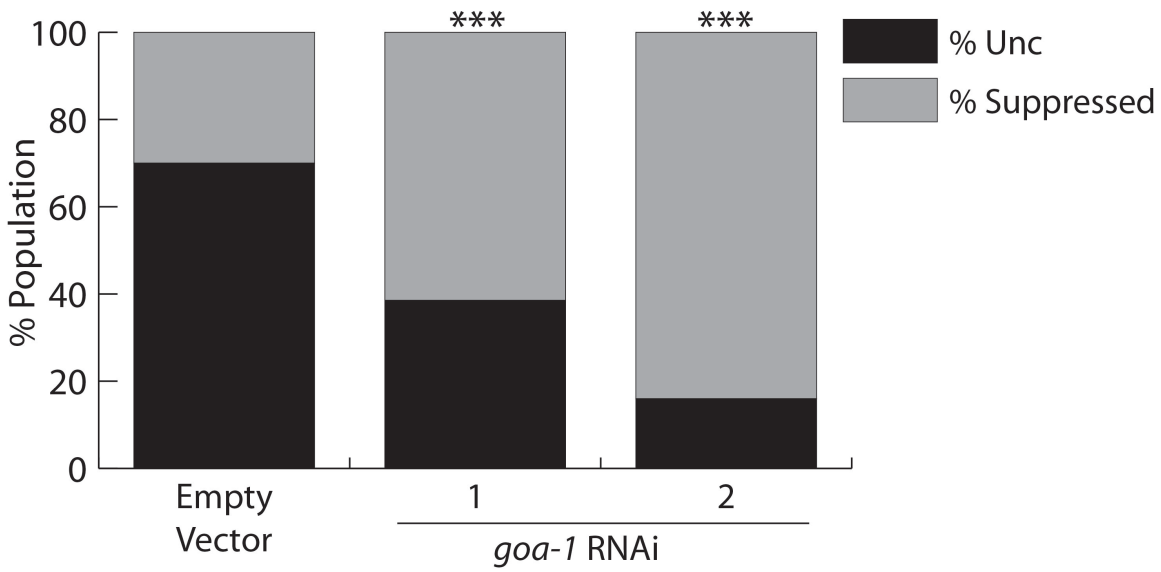

Figure 5.3. *goa-1* is partially required for the Unc-4 backward movement defect. *goa-1* RNAi knockdown in *unc-4(e2323); eri-1(mg366); lin-15b* animals with a clone from the Ahringer RNAi library (1) [200] or generated in the Miller lab (2) suppresses Unc-4 backward movement.

GOA-1/Gαo promotes VB-type inputs in *unc-4* mutant VA motor neurons

Our lab and others have previously demonstrated the use of a fluorescently tagged innexin protein, UNC-7S::GFP, to visualize gap junctions between the AVB command interneuron and its motor neuron partners in the ventral nerve cord [42, 114]. In the wild-type, AVB gap junctions are limited to B-class motor neurons (DB and VB) (Fig 5.2C, D) but are also established with A-class motor neurons (DA and VA) in *unc-4* mutants (Fig 5.2E, G) [42] [104]. Because either RNAi knockdown or genetic ablation of *goa-1* suppresses the Unc-4 movement defect (Fig. 5.2A, 5.3), we hypothesized that *goa-1* function was required for the creation of gap junctions between AVB and VA motor neurons. This idea was confirmed by the finding that the loss of function mutant, *goa-1(n1134)*, suppresses ectopic AVB gap junctions with *unc-4* mutant VAs (Fig 5.2F, G). Expression of wild-type GOA-1 specifically in A-class motor neurons restores the AVB to VA gap junction defect (Fig. 5.2G). Furthermore, expression of constitutively active GOA-1^{Q205L} in wild-type A-class motor increases the occurrence of ectopic AVB to VA gap junctions (Fig. 5.4). This result is consistent with the backward movement defect that is induced by VA by expression of this transgene (Fig. 5.2B). Together, these results indicate that GOA-1/Gαo functions cell autonomously in VA motor neurons to promote VB-type inputs.

Specific components of the GOA-1/Gαo signaling pathway are required for VB-type wiring

To determine if other of GOA-1/Gαo components signaling are required for the creation of VB-type inputs with *unc-4* mutant VAs, we assayed known effectors of GOA-1, *eat-16*/RGS and *dgk-1*/diacylglycerol kinase for roles in the VA-dependent backward

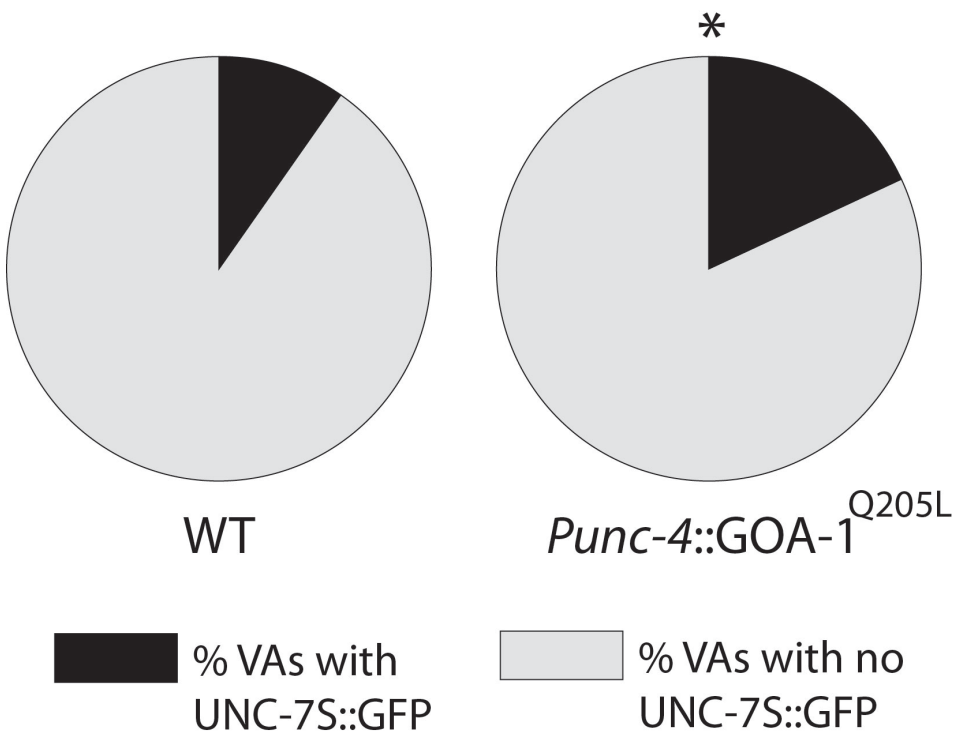

Figure 5.4. Constitutively active GOA-1 shows increased ectopic UNC-7S::GFP puncta on VA motor neuron cell soma. Wild-type VAs (WT) have a basal level of ectopic AVB to VA gap junctions, visualized with UNC-7S::GFP. Expression of constitutively active GOA-1^{Q205L} specifically in A-class motor neurons increases the frequency of ectopic AVB to VA gap junctions. p=0.05, Fisher's Exact Test. n=149 neurons (n ≥ 10 for specific VA motor neurons).

movement circuit [95]. A mutation in *eat-16*/RGS suppresses the Unc-4 backward movement defect to a level comparable to that of to *goa-1; unc-4* double mutants (Fig. 5.5A). In addition, *eat-16; unc-4* mutant animals show significantly fewer ectopic AVB to VA gap junctions. These results are consistent with a model in which EAT-16 functions downstream of *goa-1* to promote VB-type inputs (Fig. 5.5B). In contrast, a loss-of-function mutation in *dgk-1* had no effect on AVB to VA gap junctions (Fig. 5.5C). This result suggests that a diacylglycerol (DAG)-mediated pathway (Fig. 5.7) [201] does not regulate synaptic choice in VA motor neurons.

The regulator of G protein signaling protein, EGL-10/RGS has been shown to promote the GTPase function of GOA-1/Gαo and effectively inactivate GOA-1 downstream signaling [202]. In this role, EGL-10/RGS is predicted to regulate VA input since GOA-1/Gαo exercises this function. However, a loss of function *egl-10(md176)* mutation fails to enhance the Unc-4 backward movement defect of *unc-4(e2322ts)* as would be expected for a GOA-1 pathway gene that promotes the VA miswiring defect (Fig. 5.6). This result indicates that EGL-10/RGS does not function upstream of GOA-1/Gαo in this network. Alternatives include RGS-1 and RGS-2, which function redundantly to regulate GOA-1 signaling in egg laying [203].

Multiple G protein pathways regulate synaptic choice

Mutations in *gsa-1*/Gαs and *egl-30*/Gαq have been shown to affect different behavioral processes in *C. elegans*, including locomotion and egg laying [199, 201, 204-206]. Of particular note are previous findings that EGL-30 and GSA-1 function in opposition to GOA-1 to promote cholinergic motor neuron activity (Fig. 5.7). Thus, if

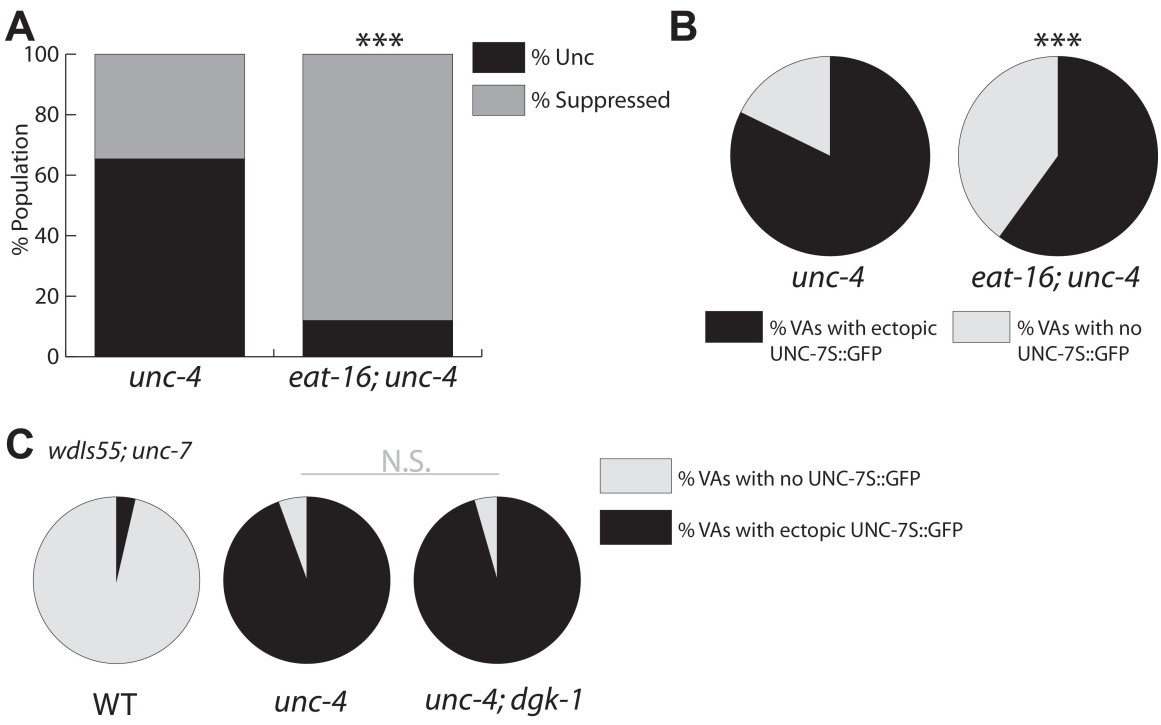

Figure 5.5. Downstream effectors of GOA-1/Gαo function in the *unc-4* pathway. **A.** Tapping assay for locomotion. The majority of *unc-4(e2322ts)* animals cannot crawl backward at 23 °C. *eat-16(md176); unc-4(e2322ts)* double mutants show significant suppression of the Unc-4 backward movement defect. *** p <0.001 *vs. unc-4*, Fisher's Exact Test. n ≥ 50. **B.** *eat-16(md176)* suppresses the ectopic AVB to VA gap junction defect of *unc-4(e120).* * p <0.01, Fisher's Exact Test. n ≥ 10 for each neuron. **C.** The *Punc-7*::UNC-7S::GFP marker, *wdIs55* shows negligible levels of ectopic AVB to VA gap junctions in *unc-4(+)* animals, but robust levels of VA-localized UNC-7S::GFP puncta in *unc-4(e120)* animals. *unc-4(e120); dgk-1(n62)* double mutants have no effect on AVB to VA gap junctions, indicating that *dgk-1* does not function downstream of *goa-1* in this pathway. N.S.= not significant, Fisher's Exact Test. n=81 (n ≥ 9 for each specific VA motor neuron).

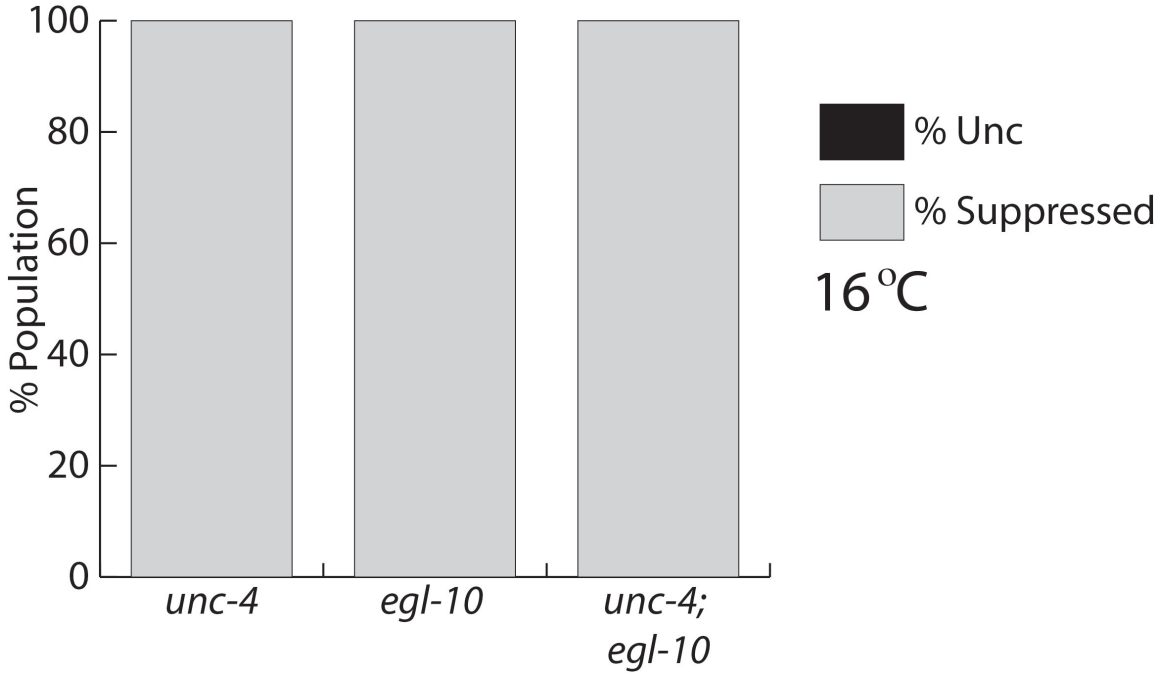

Figure 5.6. The loss of function mutation *egl-10(md176)* does not enhance the backward movement defect of *unc-4(e2322ts)*. Results are dervied from the tapping assay of animals grown at 16 °C. n ≥ 50.

egl-30/Gαq and *gsa*-1/Gαs also function in opposition to the *goa-1* pathway to regulate synaptic choice, then *egl-30* and *gsa-1* are predicted to promote the creation of wild-type inputs to VA motor neurons. This idea is consistent with our finding that the loss-of-function allele *egl-30(n686)* enhances the backward movement defect of *unc-4(e2322ts)* (Fig. 5.8A). We next tested whether EGL-30/Gαq had a role in regulating AVB to VA gap junctions. Expression of EGL-30 specifically in VA motor neurons *(unc-4*::EGL-30) reduced the frequency of ectopic AVB to VA gap junctions in *unc-4* mutant VAs (Fig. 5.8B). In addition, a mutation in one of the canonical downstream *egl-30* effectors, *egl-8*/PLCβ [207], reversed the effect (Fig. 5.8B). Together, these results indicate that a canonical EGL-30/Gαq pathway functions autonomously in VA motor neurons to oppose VB-type inputs.

Independent experiments were conducted to ask if *gsa-1*/Gαs exercises a similar role to *egl-30*/Gαq. The gain-of-function *gsa-1(ce81)* mutation locks the GSA-1 protein in an active, GTP-bound state [208]. As previously observed for overexpression of EGL-30/Gαq (Fig. 5.8B), activated GSA-1/Gαs reduced the occurrence of ectopic AVB to VA gap junctions in *unc-4(e120)* (Fig. 5.8C). Over-expression of wild-type GSA-1 in VA motor neurons showed a similar but weaker negative effect on AVB to VA gap junctions (Fig. 5.9). Finally, a gain-of-function mutation in the canonical *gsa-1* effector, *acy-1*/adenylyl cyclase, also suppressed the AVB to VA gap junction defect in *unc-4* mutant VAs (Fig. 5.8C), suggesting that *acy-1* functions downstream of *gsa-1*. Together, these results indicate that EGL-30 and GSA-1 pathways function in VA motor neurons to inhibit VB-type inputs. In contrast, GOA-1/Gαo functions to promote VB-type inputs in VA motor neurons (Fig. 5.8D).

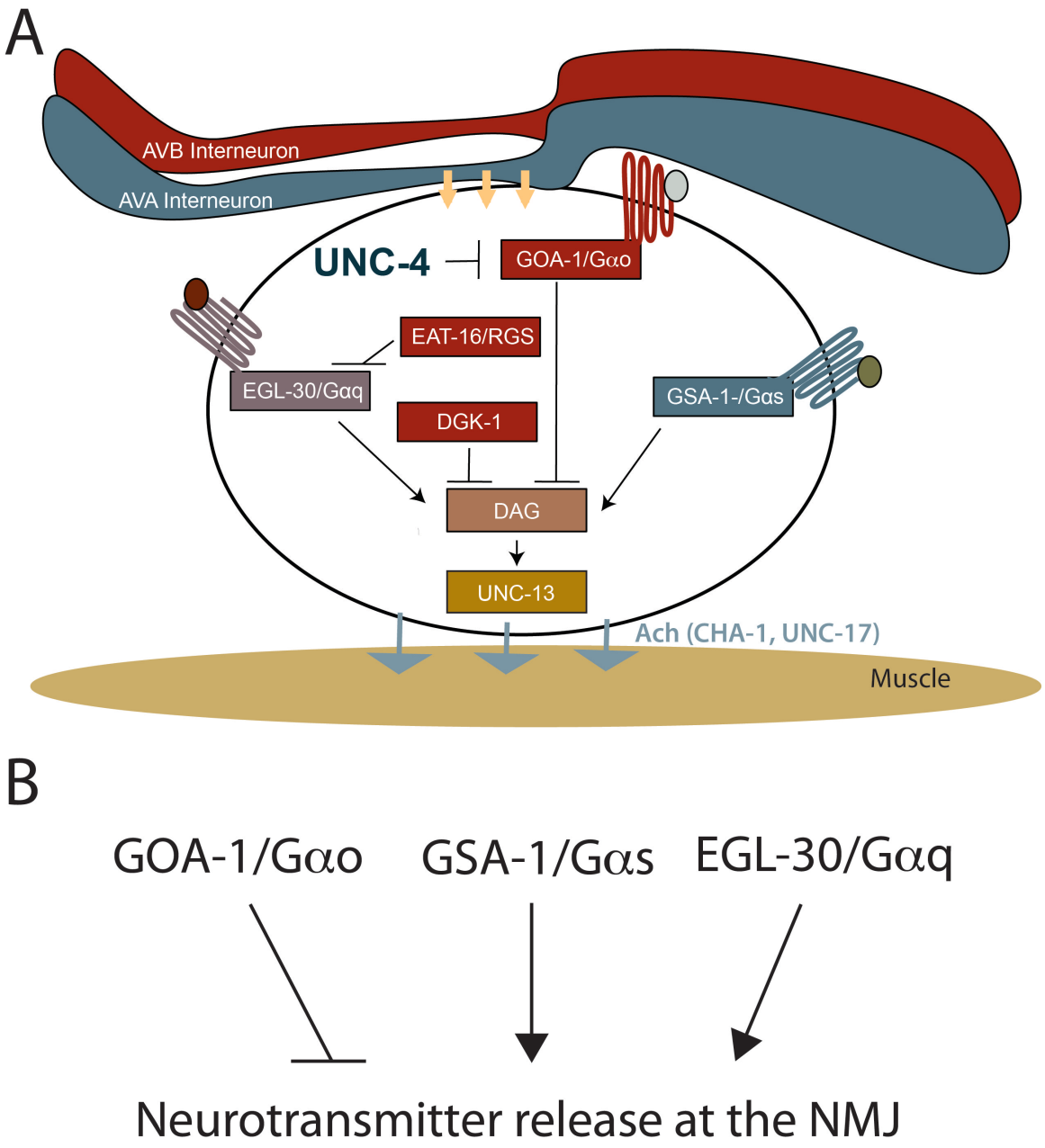

Figure 5.7. GOA-1, EGL-30 and GSA-1 regulate neurotransmitter release at the *C. elegans* neuromuscular junction (NMJ) [95]. **A.** GOA-1 functions through DGK-1/diacylglycerol kinase and EAT-16/RGS to inhibit DAG production and EGL-30 function, respectively. EGL-30 activates EGL-8/PLCβ, which produces DAG. GSA-1 functions through ACY-1/adenylyl cyclase and cAMP to promote DAG binding to UNC-13, which is required for synaptic vesicle fusion with syntaxin [95]. **B.** GOA-1 signaling inhibits acetylcholine (Ach) release in opposition to the EGL-30 and GSA-1 (see Fig. 1.6). Downstream effectors of EGL-30 and GSA-1 pathways not shown for simplicity.

RGEF-1 and EPAC-1 do not regulate synaptic choice in VA motor neurons

Both RGEF-1 and EPAC-1 are G-protein signaling effectors and have been implicated in gap junction regulation. Diacylglycerol (DAG) binds RGEF-1, a RasGRP protein that functions as a GEF for the small GTPases Ras and Rap1 [209, 210]. In mammalian cells, Rap1 regulates gap junction biogenesis [101]. Additionally, Epac, a cAMP effector protein, has been shown to bind Rap1 and may regulate Cx43 trafficking to the plasma membrane [101]. Epac functions cooperatively with PKA, which regulates gating of the hemichannel to enhance gap junction function [98, 101, 211]. In this model, *rgef-1* (functioning downstream of DAG and the EGL-30-mediated pathway) and *epac-1* (functioning downstream of cAMP and the GSA-1-mediated pathway) preserve normal AVA to VA gap junctions. This model predicts that ectopic AVB to VA gap junctions should be elevated in *rgef-1* and *epac-1* mutants. However, *rgef-1* or *epac-1* single mutants as well as the *rgef-1; epac-1* double mutant showed no significant increase in ectopic AVB to VA gap junctions (Fig. 5.10). In combination our previous finding that loss of *dgk-1* (which results in subsequent increase in DAG accumulation) does not regulate ectopic AVB to VA gap junctions (Fig. 5.5C), these results indicate that the diacylglycerol (DAG)-mediated pathway is not involved in synaptic choice in VA motor neurons. Additionally, we discovered that Epac is not required for synaptic choice, suggesting that other cAMP signaling pathways, such as calcium signaling, might function downstream of GSA-1 (see Discussion).

The Unc-4 miswiring defect is not regulated by VA motor neuron cholinergic activity

Genetic and drug-treatment studies suggest that acetylcholine (Ach) release is enhanced in *goa-1* mutants [206]. Thus, it is reasonable to consider the possibility that excess Ach release from VA motor neurons could be sufficient to account for the

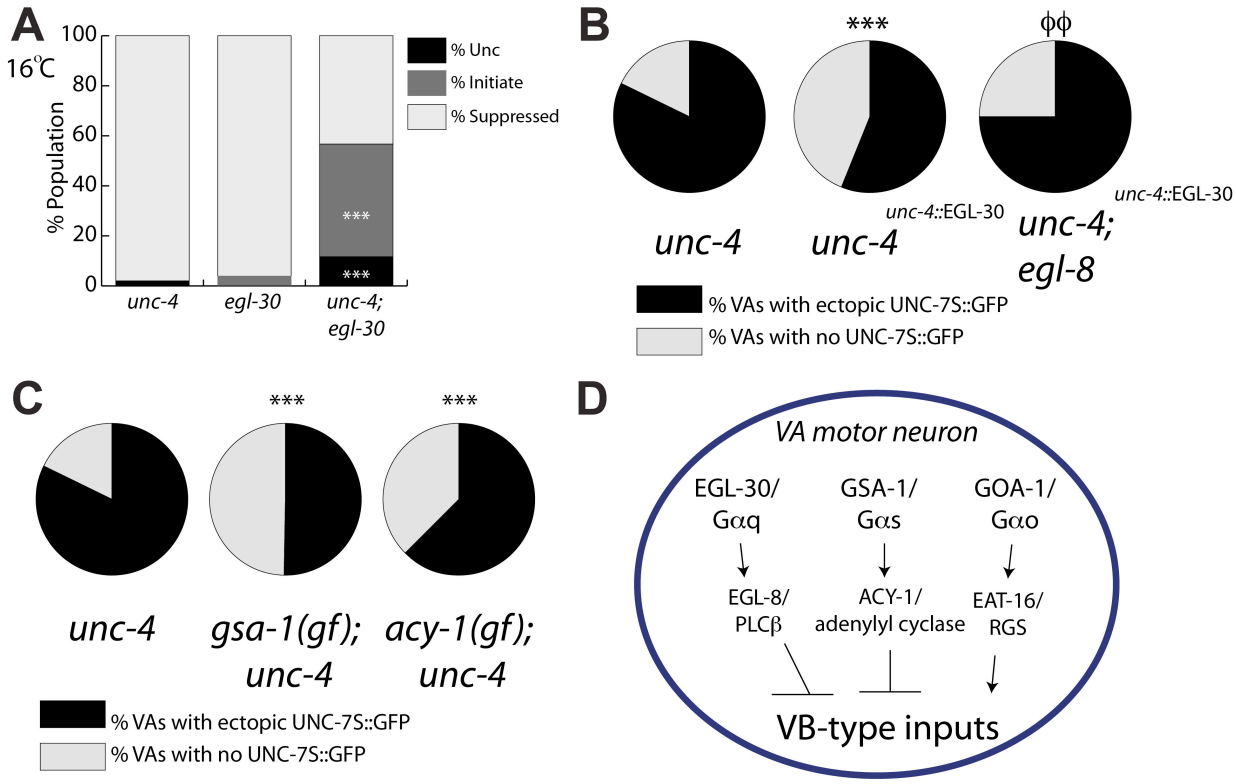

Figure 5.8. Gαq and Gαs favor the creation of wild-type VA inputs. **A.** *unc-4(e2322ts)*; *egl-30(n686)* animals have an enhanced backward movement defect *vs.* the single mutants at the permissive temperature of 16 °C. *** p< 0.001 Fisher's Exact Test. n ≥ 50. **B.** Expression of EGL-30/Gαq in *unc-4(e120)* mutant A-class motor neurons (*Punc-4*::EGL-30) reduces the % of VAs with ectopic AVB gap junctions. Mutation in *egl-8*/PLCβ rescues this suppression, indicating that EGL-30 functions through EGL-8. *** p < 0.001 *vs. unc-4,* ϕϕ p < 0.01 *vs. unc-4* $^{unc\text{-}4::\text{EGL-}30}$ Fisher's Exact Test. n ≥ 9 for each neuron. **C.** The constitutively active *gsa-1(ce81)* reduces the % of VAs with ectopic AVB gap junctions. The gain-of-function *acy-1(ce2)* allele suppresses AVB to VA gap junctions, suggesting that ACY-1 functions downstream of GSA-1. *** p < 0.001 Fisher's Exact Test *vs. unc-4*. n≥10 for each neuron. **D.** Model of G protein signaling in VA motor neurons. EGL-30/Gαq functions through EGL-8/PLCβ; GSA-1/Gαs functions through ACY-1/adenylyl cyclase to inhibit VB-type inputs to VA motor neurons. GOA-1/Gαo functions through EAT-16/RGS to promote VB-type inputs onto VA motor neurons.

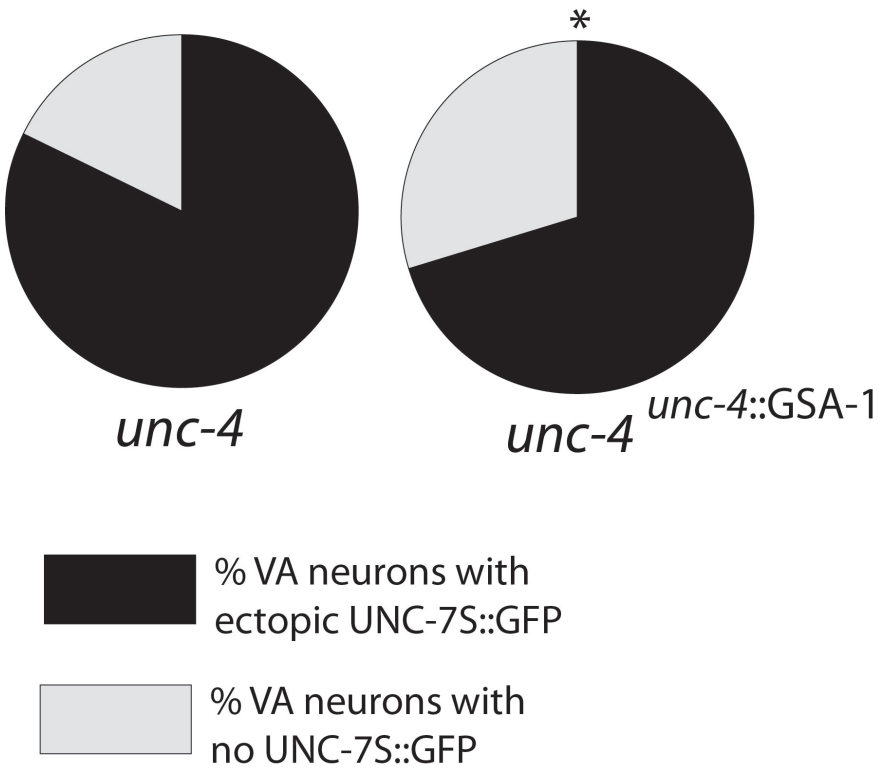

Figure 5.9. GSA-1 functions in VA motor neurons to prevent VB-type inputs. Expression of wild-type GSA-1 under the *unc-4* promoter suppressed AVB to VA gap junctions. * p= 0.05 *vs. unc-4*, Fisher's Exact test. n=95 (n ≥ 10 for each neuron).

improved backward movement of *unc-4* mutants that carry a *goa-1* loss-of-function mutation (Fig. 5.2A). This mechanism could also potentially compensate for previously observed depletion of synaptic vesicles at *unc-4* mutant A-class motor neuron synapses with body muscle [212]. This possibility is ruled out by our finding that a loss-of-function mutation in the GOA-1 effector, *dgk-1*, which results in accumulation of diacylglycerol (DAG) and increased neurotransmitter release (Fig. 5.7), does not affect the wiring of VA motor neurons (Fig. 5.5C).

A second explanation for the effects of these G protein pathways on synaptic choice is that the Unc-4 wiring defect is due to reduced neurotransmitter release, a possibility suggested by the finding that synaptic vesicles are depleted in *unc*-4 mutant A-class motor neurons [212]. This model is supported by findings that retrograde signals from active postsynaptic targets can influence biogenesis of the presynaptic apparatus [84]. This model predicts that mutations that block or impair Ach release in VA motor neurons should phenocopy Unc-4 and show comparable defects in backward locomotion and VA input specificity. We examined mutants of three key genes, *cha-1, unc-17* and *unc-13*, to test this idea. Ach signaling depends on the conserved roles of the biosynthetic protein, CHA-1 (choline acetyltransferase) and the vesicular Ach transporter, UNC-17 [213]. As noted earlier, UNC-13 mediates a key step in synaptic vesicle release by altering the confirmation of syntaxin, which is necessary for Ach signaling by VA motor neurons [214].

In the first experiment, we utilized temperature-sensitive alleles of *unc-4(e2322ts)* and *cha-1(y226ts)*. Grown at the permissive temperature (16 °C), both *unc-4* and *cha-1* sustain wild-type levels of backward locomotion (Fig. 5.11A, B). However, when transiently exposed to non-permissive temperature (25 °C) during the larval period in

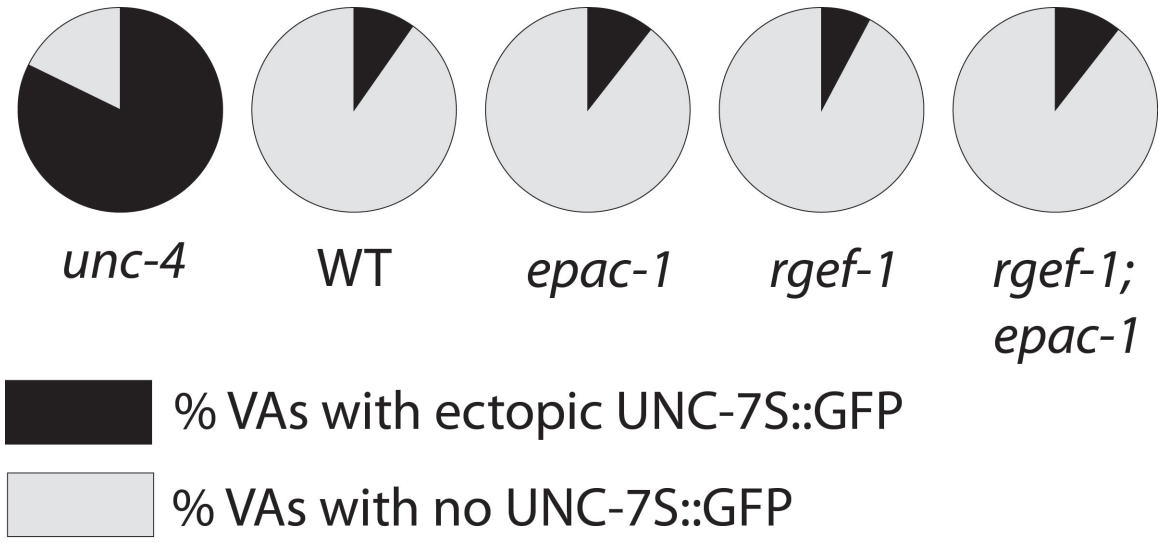

Figure 5.10. Mutations in potential downstream components of EGL-30/Gαq and GSA-1/Gαs signaling do not affect AVB to VA gap junctions. *epac-1, rgef-1* and *epac-1; rgef-1* are not signficiantly different *vs.* WT. Fisher's Exact Test. n ≥ 90 (n ≥ 10 for each specific VA motor neuron).

which UNC-4 function is required [35] *cha-1* mutants do not show impaired movement (Fig. 5.11A, B, Methods),. In contrast, similarly treated *unc-4(e2322ts)* control animals show a strong backward movement defect (Fig. 5.11B). This result indicates that impaired Ach release from VA motor neurons is not sufficient to induce an Unc-4-like miswiring defect.

As an additional test of this hypothesis, we exploited the hypomorphic allele *unc-17(e113)* in which *unc-17*/VAchT expression is selectively eliminated in A and B class motor neurons (includes VAs and VBs) (K. Lickteig, Dissertation). In this case, we determined that the *unc-17(e113)* mutant does not result in ectopic AVB to VA gap junctions (Fig. 5.11C). Thus, our results contradict the predictions of a model in which VA input specificity in *unc-4* mutants is regulated by Ach release from VA motor neurons.

To consider the possibility that release of an unknown neurotransmitter could regulate VA input specificity, we examined the *unc-13(e51)* mutant which is predicted to block all synaptic vesicle fusion [214, 215]. However, we determined that VA motor neurons in the *unc-13(e51)* mutant are not miswired with ectopic AVB gap junctions (Fig 5.11C). Thus, the combined results of experiments with mutants of *cha-1*, *unc-17* and *unc-13*, rule out models in which neurotransmitter release from VA motor neurons determines the specificity of VA inputs.

goa-1/Gαo functions in parallel to the EGL-20/Wnt signaling pathway to specify inputs to VA motor neurons

We have previously shown that a canonical Wnt signaling pathway functions upstream of the *ceh-12*/HB9 homeodomain transcription factor to promote miswiring of VA motor neurons in *unc-4* mutants (Chapter IV) [104]. In this mechanism, EGL-20/Wnt, which is expression in the tail region, functions through the Frizzled receptors, MOM-5

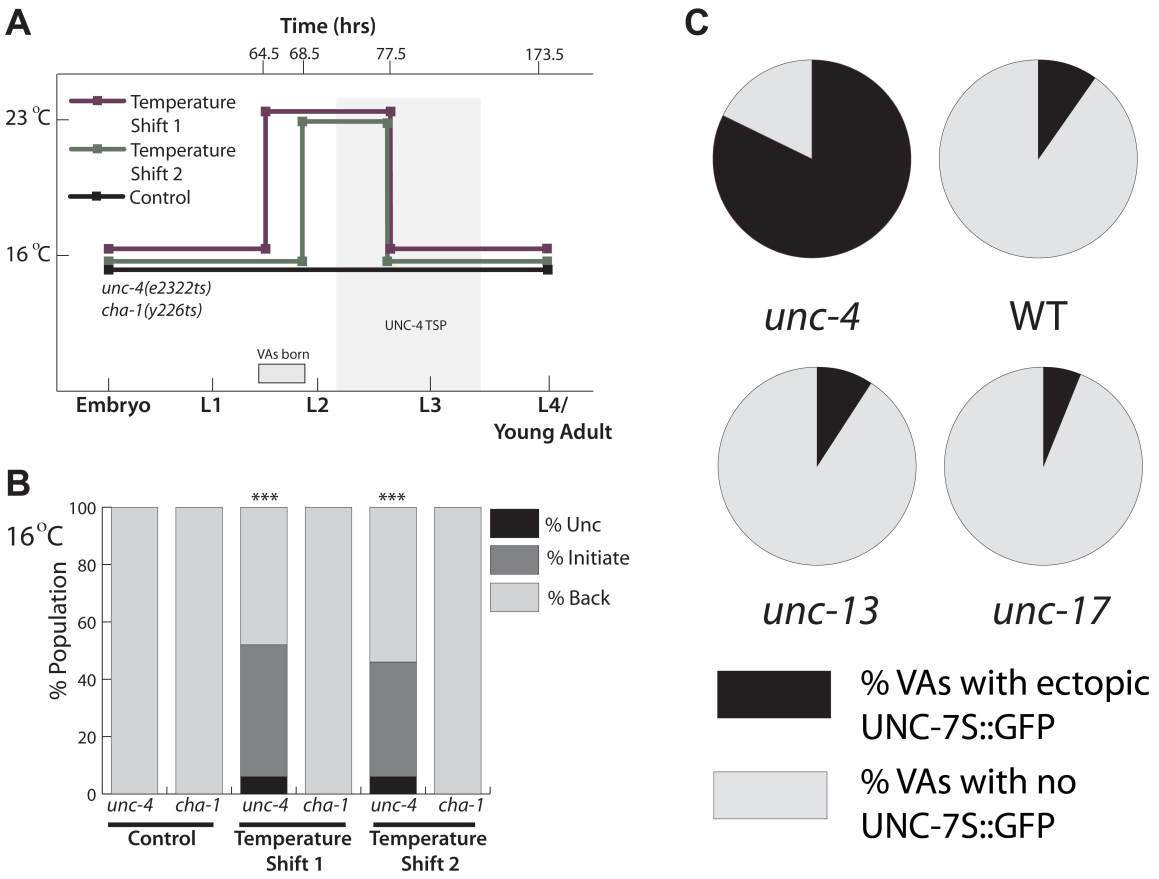

Figure 5.11. Normal VA connectivity is not dependent on acetylcholine release from VA motor neurons. **A.** Schematic of temperature shift experiments in **B.** The temperature sensitive alleles *cha-1(y226ts)* and *unc-4(e2322ts)* were grown at 16 °C for either 64.5 (Experiment 1) or 68.5 (Experiment 2) hours and shifted to the non-permissive temperature of 23 °C for either 13 (Experiment 1) or 9 hours (Experiment 2). Animals were then propagated at 16 °C until L4/young adult stage. The UNC-4 temperature sensitive period (TSP) corresponds to the developmental time period in which UNC-4 function is required [35]. **B.** Tapping assay of *cha-1(y226ts)* and *unc-4(e2322ts)*. Both alleles have wild-type locomotion at the permissive temperature of 16 °C (Control). When transferred to the non-permissive temperature of 23 °C, *unc-4* worms display backward movement defects while *cha-1* animals move wild-type. **C.** *unc-4(e120)* mutants have ectopic AVB to VA gap junctions *vs.* wild type (same data as Fig. 5.2). Mutation in *unc-13(e51),* which is required for VA presynaptic signaling onto muscle, does not induce ectopic AVB to VA gap junctions. A VA/VB-specific knockout of the vesicular acetylcholine transporter, *unc-17(e113),* results in loss of signaling from these neurons onto muscle. Mutation in *unc-17* does not induce ectopic AVB to VA gap junctions.

and MIG-1, to activate *ceh-12* expression and thereby promote ectopic AVB gap junctions with VA motor neurons in the posterior nerve cord. Because Frizzled receptors have been to regulate G-protein signaling [216-223], we considered the possibility that *goa-1*/Gαo could be activated by the EGL-20/Wnt pathway. This model predicts that *goa-1* should be required for ectopic *ceh-12*::GFP expression in posterior *unc-4* mutant VA motor neurons, since *egl-20* is necessary for this effect. However, our results show that the loss of function allele, *goa-1(n1134)* does not block ectopic *ceh-12*::GFP expression in posterior VAs (Fig. 5.12A). Thus, we conclude that *goa-1*/Gαo functions in parallel to EGL-20/*ceh-12* or possibly downstream of *ceh-12* (Fig. 5.12A).

We performed an additional genetic experiment to distinguish between these models. We have previously shown that the backward movement defect of *unc-4* null alleles (*e.g. e120*) is only partially suppressed by mutations in *ceh-12* [42] (Fig. 5.12B, EV). We attribute this weak effect to the finding that *ceh-12* is unequally required for miswiring of a small subset of VA motor neurons in the tail. The net effect is that the majority of VA motor neurons that are located anterior to this region are still miswired with VB-type inputs in *ceh-12; unc-4* double mutants and thus backward movement remains strongly impaired [41]. In this setting, a mutation that disables a pathway which functions in parallel to *ceh-12* would be expected to restore normal inputs to anterior VAs. This effect should be detected as enhanced suppression of the Unc-4 movement defect, whereas a mutation in a gene that functions downstream of *ceh-12* would result in impaired backward locomotion.

We determined that treatment of *ceh-12(0); unc-4(0)* with two independent *goa-1* RNAi clones enhanced backward movement (Fig. 5.12B). This result is consistent with a model in which *goa-1* functions in parallel to *ceh-12* and rules out the model in which *goa-1* functions downstream of *ceh-12* (Fig. 5.12E). This conclusion is substantiated by

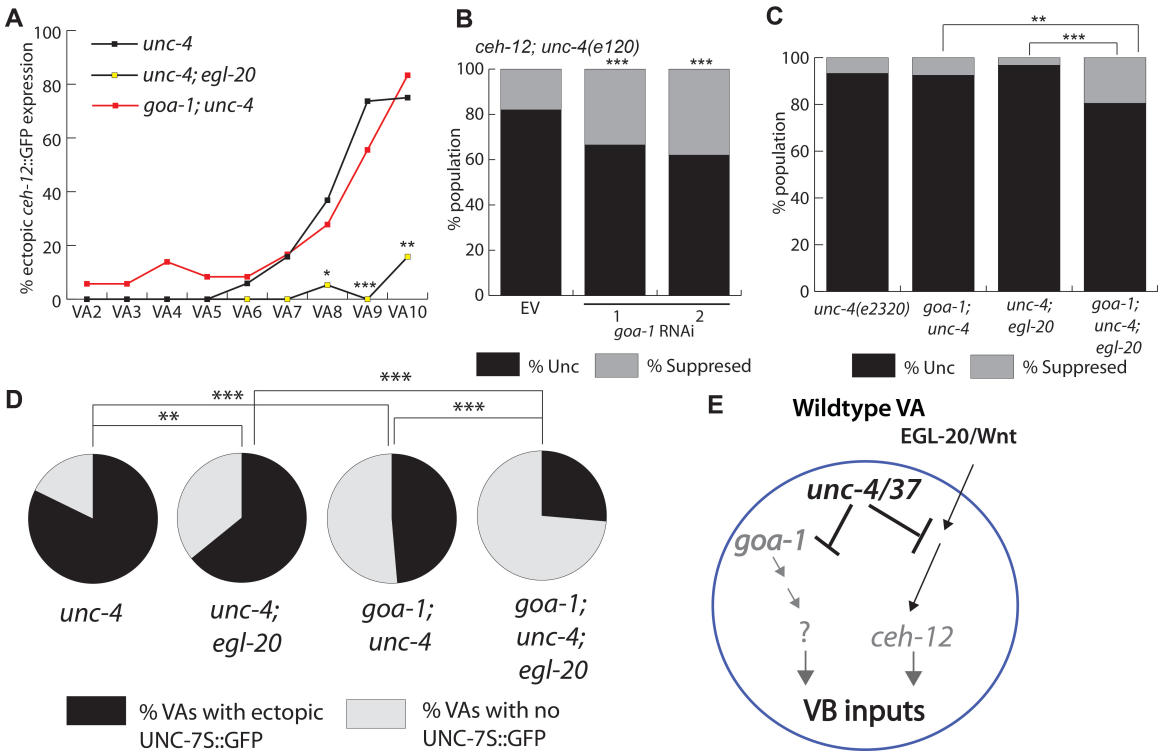

Figure 5.12. GOA-1/Gαo functions in parallel to the EGL-20/Wnt-CEH-12 pathway. **A.** Mutation in unc-4 results in ectopic *ceh-12*::GFP expression in posterior VA motor neurons. *egl-20*/Wnt is required for the ectopic ceh-12::GFP expression; *goa-1*/Gαo does not regulate ectopic *ceh-12*::GFP expression in an unc-4 mutant. * p<0.05, ** p<0.001, *** p<0.001, Fisher's Exact Test. n ≥ 15 for each neuron. **B.** Mutation in *ceh-12* partially suppresses the backward movement defect of *unc-4(e120).* RNAi using two different clones against *goa-1* enhances *ceh-12* suppression of Unc-4 movement. *** p≤0.001, Fisher's Exact Test. n ≥ 50. **C.** *unc-4(e2320)* worms are largely unable to execute backward locomotion. Mutations in *goa1(n1134)* or *egl-20(n585)* do not suppress Unc-4 backward movement. Enhanced suppression of the Unc-4 backward movement defect is seen in the triple *goa-1; unc-4; egl-20* mutant. **D.** Mutation in unc-4 results in ectopic AVB to VA gap junctions that are suppressed by mutation in goa-1 (data from Fig. 5.2A). Mutation in *egl-20* also suppresses ectopic AVB to VA gap junctions vs. *unc-4. goa-1; unc-4; egl-20* triple mutants show enhanced suppression of AVB to VA gap junctions vs. goa-1; unc-4. ** p < 0.01, *** p< 0.001, Fisher's Exact Test. n≥10 for each neuron. **E.** Model of wild type VA motor neurons. UNC-4 represses parallel G protein and Wnt/CEH-12 pathways that regulate synaptic choice.

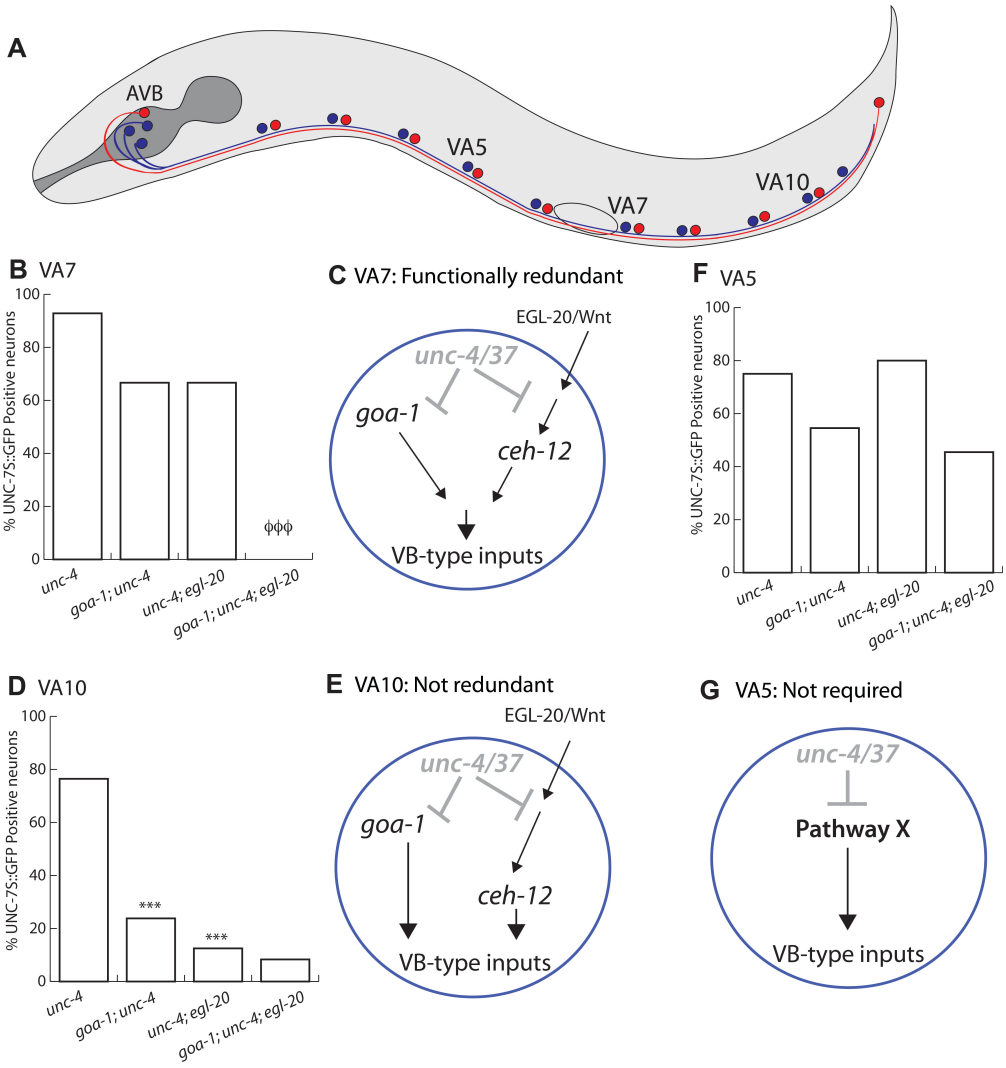

Figure 5.13. VB-type inputs to specific VA motor neurons are differentially affected by the GOA-1 and Wnt pathways. **A.** Schematic of *C.* elegans motor circuit. VA5, VA7 and VA10 are indicated. **B.** AVB to VA7 gap junctions are unaffected *vs*. *unc-4* in *goa-1* or *egl-20* single mutants. In contrast, *goa-1; unc-4; egl-20* triple mutants completely suppress AVB to VA7 gap junctions. This result indicates that GOA-1 and EGL-20 signaling are both required for ectopic AVB to VA7 gap junctions (**C**). ϕϕϕ $p < 0.001$ *vs. goa-1; unc-4; egl-20*, Fisher's exact test. **D-E.** *goa-1* and *egl-20* are required but do not function redundantly to regulate AVB to VA10 gap junctions. *** $p < 0.05$ *vs. unc-4*, Fisher's Exact Test. $n \geq 10$ for each neuron. **F.** AVB to VA5 gap junctions are unaffected *vs. unc-4* in *goa-1*, *egl-20* single mutants or in the *goa-1; unc-4; egl-20* triple mutant. **G.** This result indicates that *goa-1* or *egl-20*/Wnt signaling is not required for ectopic AVB to VA5 gap junctions (C).

the additional finding of enhanced suppression of the AVB to VA gap junction defect in *goa-1; unc-4; egl-20* mutants (Fig. 5.12D).

We observed varying requirements for *goa-1* and *egl-20* signaling in specific VA motor neurons. For example, in VA7, single mutations in either *goa-1* or *egl-20* have no effect on the frequency of AVB to VA gap junctions, whereas the *goa-1; egl-20* double mutant completely eliminates ectopic AVB gap junctions with *unc-4* mutant VA7 (Fig. 5.13B, C). In VA10, the AVB gap junction defect is more strongly suppressed by mutations in either *goa-1* or *egl-20* (5.13D), thus both pathways appear to be necessary for specification of VA inputs (Fig. 5.13E). Finally, ectopic AVB gap junctions with VA5 are unaffected by mutations in *goa-1* or *egl-20* (Fig. 5.13F). This result suggests that an unknown pathway promotes VB-type inputs to *unc-4* mutant VA motor neurons (Fig. 5.13G). Together, these data indicate that individual VA motor neurons respond differently to G protein and Wnt signals to regulate synaptic choice.

unc-4 regulates UNC-9/innexin localization in VA motor neurons

In the wild-type, AVA gap junctions with VAs are rarely observed on the VA cell soma and are more often located on VA processes in the ventral nerve cord fascicle (wormatlas.org). In contrast, in *unc-4* mutants, these AVA to VA gap junctions are replaced with AVB gap junctions that are exclusively localized to the VA cell soma [38]. AVB gap junctions are also selectively placed on the cell soma of B-class motor neurons [114]. The innexin proteins, UNC-7 (in the AVB interneuron) and UNC-9 (in motor neurons) are both required for the localization of AVB gap junctions to the B-class motor neuron soma [114]. We therefore hypothesized that the appearance of UNC-7S::GFP puncta on VA soma in *unc-4* mutants would be accompanied by the misplacement of UNC-9/Innexin to this location. To test this idea, we used the *acr-5* promoter to drive expression of GFP-labeled UNC-9 in B-class motor neurons [114]. In a wild-type

background, *acr-5* is selectively expressed in B-class motor neurons and strong UNC-9::GFP are detected on B motor neuron soma (Fig. 5.15A, C) [114]. In *unc-4* mutants, ectopic expression of *acr-5* in A-class motor neurons [41] is accompanied by a substantial increase in frequency of UNC-9::GFP puncta on VA cell soma (Fig. 5.14 B, C). These results show that both innexins, UNC-9 and UNC-7, are mislocalized to VA soma in *unc-4* mutants.

DISCUSSION

To execute coordinated locomotion, motor circuits must be organized such that the appropriate pre- and postsynaptic partners create functional synapses. Gap junctions, or electrical synapses, allow for electrical signals and small molecule transmission between partner neurons. In *unc-4* mutants, VA motor neurons are miswired with connections normally reserved for VB sister cells. We have shown that opposing G- protein pathways regulate synaptic choice in *unc*-4 mutant VA motor neurons. GOA-1/Gαo promotes VB-type inputs; EGL-30/Gαq and GSA-1/Gαs inhibit VB-type gap junctions with VAs. Interestingly, the mechanism by which these G protein pathways regulate synaptic choice is separate from the well-established signaling cascade through diacylglycerol (DAG) by which these pathways converge to control neurotransmitter release at the neuromuscular junction [95]. We propose that these G proteins regulate the localization of UNC-9/innexin to the cell soma of VA motor neurons, where it interacts heterotypically with UNC-7/innexin in the AVB interneuron. Evidence of G- protein signaling in the control of gap junction assembly and function in other organisms suggests that this mode of regulation may be generally employed in neurons to specify local inputs during neural development.

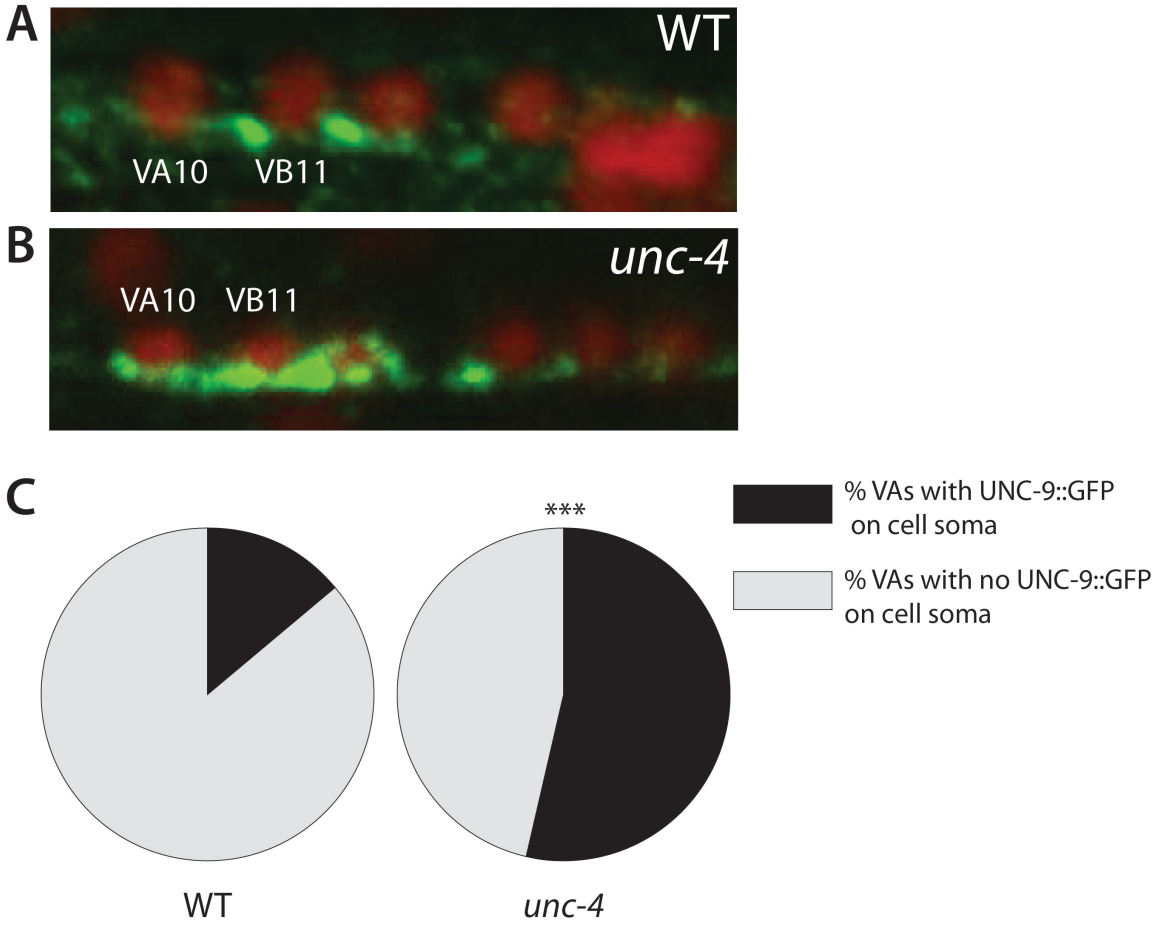

Figure 5.14. UNC-4 regulates the localization of UNC-9/Innexin in VA motor neurons. **A.** *Pacr*-5::UNC-9::GFP is localized to cell soma of VB motor neurons in wild type (WT). **B.** *unc-4(e120)* mutants have ectopic UNC-9/Innexin puncta on VA cell soma. **C.**Quantification of expression of UNC-9::GFP on VA cell soma in *unc-4* and wild type. *** $p<0.001$, Fisher's Exact Test. $n \geq 10$ for each neuron.

Mechanisms of opposing G-protein pathways

The canonical G-protein signaling pathways that regulate neurotransmitter release at the neuromuscular junction converge on diacylglycerol (DAG) (Fig. 5.7) [95]. The GOA-1/DGK-1/EAT-16 cascade inhibits DAG production either through direct phosphorylation of DAG by *dgk-1* or inhibition of EGL-30/Gαq signaling by EAT-16/RGS [206, 224]. Although the mechanism of how RGS proteins function in *C. elegans* is not fully understood, it is believed to include a feedback loop that involves the Gβ subunit, GPB-2. RGS proteins contain a *G g*amma–*l*ike (GGL) domain that in mammals, can bind to the Gβ5 subunit *in vivo* [225-228]. In *C. elegans,* all RGS proteins are members of the R7 family of proteins and contain a GGL domain that binds *gpb-2* [229]. At the neuromuscular junction, the GBP-2/EAT-16 heterodimer has been proposed to accelerate GTP hydrolysis and consequent deactivation of EGL-30/Gαq signaling [229]. This decrease in EGL-30 signaling is opposed by a negative feedback loop that indirectly inhibits the GOA-1 pathway. In this mechanism, GTP-bound EGL-30 binds GBP-2/EGL-10, which in turn accelerates the GTP hydrolysis of GOA-1. GDP-bound GOA-1 then reassociates with the GBP-2/EAT-16 heterodimer, thus sequestering EAT-16 and preventing it from deactivating EGL-30 [229]. These complex feedback mechanisms provide one possibility for how GOA-1 and EGL-30 signaling function in opposition. However, our results indicate that EGL-10/RGS does not have a role in synaptic choice in VA motor neurons (Fig. 5.6), thus, alternative members of the *C. elegans* RGS family might be involved in the antagonism between GOA-1 and EGL-30 in synaptic specificity.

Downstream of the GOA-1/EGL-30 negative feedback loop, GTP-bound EGL-30 activates EGL-8/PLCβ to increase DAG production [95]. We show that EGL-30 and GSA-1 oppose the creation of AVB to VA gap junctions (Fig. 5.8), whereas GOA-1 is required for these ectopic connections (Fig. 5.2). However, we have also shown that

dgk-1 (Fig. 5.5) and the DAG binding proteins, *rgef-1* (Fig. 5.10) and *unc-13* (Fig. 5.11) are not required for the formation of ectopic AVB gap junctions with VA motor neurons. Thus, we propose that DAG-dependent pathways are not involved in this mechanism and that these G-protein pathways might function via alternative signaling cascades to regulate gap junction connections with VA motor neurons.

Our evidence also indicates that GSA-1/Gαs inhibits AVB to VA gap junctions in opposition to GOA-1 (Fig. 5.8). We show that gain-of-function mutants in GSA-1/Gαs and ACY-1/adenylyl cyclase both oppose the formation of ectopic AVB to VA gap junctions (Fig. 5.8). These data are consistent with a model in which *gsa-1* functions through *acy-1* to inhibit the creation of AVB to VA gap junctions. We propose that the mechanism of antagonism between the GOA-1 and GSA-1 pathways might involve the direct inhibition of adenylate cyclase activity by GOA-1 or its associated βγ subunit [230, 231]. Because ACY-1 shares 40% sequence homology with mouse adenylyl cyclase type 9 [230], it seems likely that GOA-1/Gαo could also limit cAMP levels in *C. elegans* by direct inhibition of ACY-1/adenylyl cyclase activity. An additional experiment to support this model is to test a loss of function in *acy-1* with RNAi knockdown. The model predicts that loss of *acy-1* function would restore ectopic AVB to VA gap junctions in the presence of constitutively active GSA-1 (Fig. 5.8). Further genetic experiments could test if GOA-1 inhibits ACY-1 activity. For example, *goa-1; unc-4* double mutants show incomplete suppression of ectopic AVB to VA gap junctions; additional knockdown of *acy-1* would enhance these ectopic connections.

UNC-4 regulation of Gαo signaling

Our results do not directly address how UNC-4 regulates G protein signaling to specify synaptic choice. Microarray analysis suggests that *goa-1* mRNA levels are increased in VA motor neurons when the *unc*-4 pathway is inactive (Fig. 5.15). Thus,

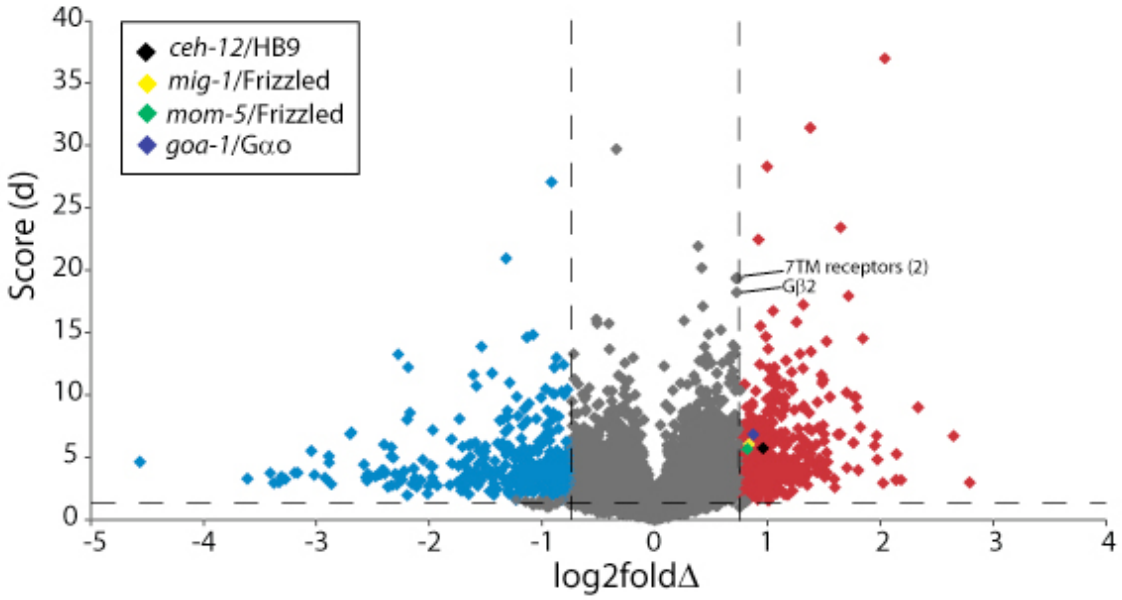

Figure 5.15. Microarray analysis detects *unc-4*-regulated transcripts in VA motor neurons. Microarray profiles of *unc-37* mutant vs. wild-type VA motor neurons were compared to detect differentially expressed transcripts [42]. Fold change (x-axis) is plotted on a log2 scale against a significance score (y-axis). A ≤5% FDR (False Discovery Rate) (horizontal dashed line) and fold change ≥ ±1.7x (vertical dashed lines) threshold were set to identify transcripts with significantly different levels in *unc-37* vs. wild-type VAs. Red diamonds represent transcripts that are upregulated; blue diamonds correspond to transcripts downregulated in *unc-37* mutant VAs and in *unc-37* vs. WT VA motor neurons. Gray diamonds represent transcripts with no significant fold change difference between *unc*-37 mutant and WT VAs. Enrichment in *unc-37* VA motor neurons for selected genes *ceh-12/HB9* (black diamond) (1.9x) and *goa-1* (blue diamond) (1.8x). The *unc-4* target genes, *mig-1* (yellow diamond) (1.8x) and *mom-5* (green diamond) (1.8x) are also upregulated [104].

UNC-4 might maintain GOA-1 expression at a particular threshold that is critical for maintaining VA-type inputs. However, Gαo is the most highly expressed G protein in the mammalian brain [232] and we observe strong constitutive expression of GOA-1::GFP in all classes of motor neurons, including VAs and VBs (data not shown). Therefore, it seems more likely that UNC-4 inhibits GOA-1 action through an alternative mechanism of blocking expression of a critical component of the GOA-1/Gαo signaling pathway.

G-protein pathways function in parallel to Wnt signaling to specify synaptic choice in VA motor neurons

We have previously shown that *unc-4* antagonizes a canonical Wnt signaling pathway. In this mechanism, EGL-20/Wnt activates ectopic *ceh-12* expression in *unc-4* mutant VA motor neurons (Chapter IV) [104]. G proteins have been shown to mediate signals that are transduced by Frizzled receptors [216-223]; thus, we tested whether GOA-1/Gαo and EGL-20/Wnt function in the same pathway to promote VB-type inputs to VA motor neurons. However, our data indicate that *goa-1* functions in parallel to *egl-20* and *ceh-12*. RNAi genetic knockdown of *goa-1* enhances *ceh-12* and *egl-20* suppression of the Unc-4 movement defect (Fig. 5.12B). Additionally, mutation in both *goa-1* and *egl-20* enhance suppression of ectopic AVB to VA gap junctions (Fig. 5.12D). Thus, parallel Wnt and G-protein signaling pathways are required for synaptic choice in VA motor neurons.

G proteins regulate trafficking of gap junction proteins to the plasma membrane

G-protein signaling has been shown to regulate gap junction assembly, function, and formation but the molecular mechanisms that drive these key processes are poorly defined. For example, Gαs and Gαq regulate localization and assembly of vertebrate

connexin43 channels [97]. In *C. elegans, goa-1*/Gαo and *gsa-1/*Gαs act antagonistically to control gap junction function between the developing oocyte and surrounding sheath cells [96, 196]. In this case, GSA-1, signaling through the adenylyl cyclase *acy-4*, inhibits innexin function, whereas GOA-1 exercises the opposite role of promoting gap junctions between oocytes and sheath cells [96, 196]. Despite implications in general gap junction function, virtually nothing is known about G-protein regulation of gap junctions between specific neuron partners.

Based on our preliminary evidence showing that UNC-9/Innexin is mislocalized to *unc-4* mutant VA cell soma (Fig. 5.14), we hypothesize that opposing G-protein pathways regulate the specificity of gap junction assembly by affecting the localization of UNC-9/Innexin in VA motor neurons. Thus, in *unc-4* mutants, UNC-9 is trafficked to the VA cell soma and interacts with UNC-7/Innexin in the AVB interneuron, forming an ectopic heterotypic gap junction in this location. In this model, *goa-1* promotes UNC-9 localization to the VA cell soma, whereas *egl-30* and *gsa-1* oppose this process (Fig. 5.8D).

One hypothesis to explain the mechanism by which G proteins regulate the UNC-9/UNC-7 channel formation is thorough the trafficking of UNC-9/Innexin to the plasma membrane. Much of what is known about the trafficking of gap junction components to the plasma membrane is derived from studies in mammalian cell culture. Connexins are synthesized by membrane-bound ribosomes and are presumed to reach the cell surface through the conventional secretory pathway via the ER and Golgi [194]. The formation of connexins into a connexon, or hemichannel, mainly occurs in the trans-Golgi network (TGN). Once the connexons are transported to the plasma membrane, they are assembled into gap junction plaques [194]. Multiple lines of evidence implicate G-protein pathways in the regulation of gap junction localization. For example, after treatment with the Gαo inhibitor pertussis toxin, less accumulation of connexin43 (Cx43) was observed

at the plasma membrane [98]. Additionally, phosphorylation of Cx43 occurs in response to elevated levels of the Gαq effector cAMP, leading to an increase in Cx43 trafficking to gap junction plaques at the plasma membrane [100, 233]. Furthermore, activation of PKA by cAMP has been shown to mediate increased movement of Cx43 to the plasma membrane, termed “enhanced assembly” [233]. PKA signals to the cAMP responsive element binding protein (CREB) in mammals, which is influenced by cytosolic calcium [234]. The *C. elegans* CREB homolog, *crh-1*, is broadly expressed in *C. elegans* (Wormviz) and thus could function in this pathway. Additionally, our hypothesis predicts that cAMP activity and subsequent activation of *kin-1*/PKA would inhibit the trafficking of AVB to VA gap junctions. Thus, GSA-1 signaling through activation of cAMP could inhibit UNC-9 localization to VA cell soma.

In addition to cAMP-mediated control of gap junction assembly, intracellular calcium, downstream of EGL-30/Gαq, might also regulate UNC-9/Innexin localization. EGL-30 activates EGL-8/PLCβ, which converts Phosphatidylinositol 4,5-bisphosphate (PIP2) into DAG and inositol tri-phosphate (IP3) (Fig. 1.6). IP3 can diffuse throughout the cytoplasm and bind to the ER-localized IP3 receptor homolog, ITR-1. Once bound by IP3, ITR-1 releases calcium from the ER, resulting in increased levels of cytosolic calcium [235]. Calcium has been shown to regulate gap junction assembly in mammalian cell culture systems. For example, increased intracellular calcium activates protein kinase C (PKC) [236], which inhibits the assembly of Cx43 by direct phosphorylation of the gap junction protein [98, 237]. Thus, we propose that EGL-30-mediated signaling might inhibit AVB to VA gap junctions by inhibiting the localization of UNC-9 and in turn assembly of the UNC-9/UNC-7 hemichannel. Based on these results, we propose that opposing G-protein pathways regulate the assembly of UNC-9/Innexin hemichannels by mediating trafficking of this gap junction component to the cell soma of VA motor neurons. To test this hypothesis, I have created the strain NC2716, which

expresses an N-terminal MYC tagged UNC-9 in addition to the UNC-7::GFP (see Table 5.2). A first attempt at visualizing colocalization of MYC::UNC-9 and UNC-7::GFP with the Finney-Ruvkun antibody staining protocol failed; thus, additional staining methods, including the Picric Acid protocol may be more successful at identifying UNC-9 and UNC-7 localization *in vivo*. Upon optimization of this staining protocol, we should be able to determine if UNC-9 colocalizes with UNC-7::GFP from the AVB interneuron on *unc-4* mutant VA cell soma. Additionally, this tool could be used to test G protein mutants for their roles in UNC-9/UNC-7 colocalization in VA motor neurons.

Understanding the mechanism by which these G-protein pathways regulate UNC-9 localization advances our knowledge of how synaptic specificity is regulated. A study in goldfish Mauthner neurons suggests that gap junction formation is induced by postsynaptic modifications of gap junction channels, which affect the rate that the connexin is inserted in the plasma membrane [238]. Insertion of the connexin protein in the postsynaptic membrane induces formation of a hemichannel with a connexin located in the presynaptic membrane [238]. Thus, localization of UNC-9 to the cell soma of *unc-4* mutant VAs, driven by GOA-1-mediated signaling, might induce hemichannel formation with UNC-7 in AVB. With additional experiments described above, our work might be the first to link the regulation of gap junction localization to the conserved process of G protein signaling, which subsequently directs synaptic partner selection.

Chapter VI

GENERAL DISCUSSION AND FUTURE DIRECTIONS

Many cellular components regulate synaptic specificity, including cell surface proteins, morphogenetic signals and transcription factors (see Chapter I). Results presented in this dissertation have expanded on our previous findings that the UNC-4 transcription factor specifies inputs to VA motor neurons. UNC-4, with the co-repressor, UNC-37/Groucho, maintains connections between VA motor neurons and subsequently the backward motor circuit by repressing the expression of VB-type genes that promote connections with the forward motor circuit [35, 42]. Thus, loss-of-function in *unc-4* results in ectopic VB-type inputs to VA motor neurons replacing normal VA-type connections. We utilized cell-specific microarray profiling and a genetic screen to identify VB-type genes that are potential UNC-4 targets. Here, I described our findings that Wnt signaling and G protein pathways regulate synaptic choice in the motor circuit (Fig. 6.1). These highly conserved pathways have previously been implicated in other aspects of neurodevelopment and function [7, 79, 95, 145, 239], but little evidence exists regarding their roles in synaptic choice. The in-depth genetic analysis described in the previous chapters has identified novel functions for these pathways in the regulation of synaptic specificity.

Transcription factors regulate synaptic choice

Transcription factors function to either activate or repress target genes, sometimes activating or repressing the expression of different target genes within the

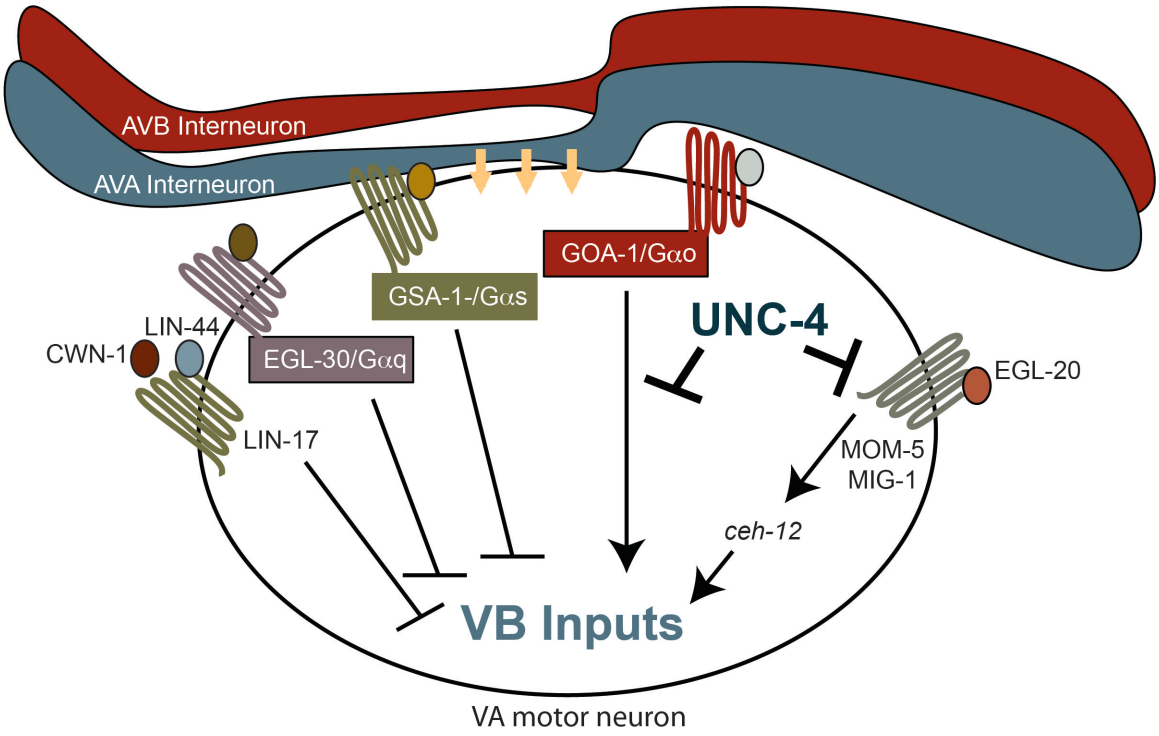

Figure 6.1. Multiple components regulate synaptic choice in VA motor neurons. Wild-type VA motor neurons receive *en passant* inputs from the AVA interneuron of the backward motor circuit (yellow arrows). *unc-4* mutant VA motor neurons receive inputs from the forward circuit AVB interneuron (not pictured). In VA motor neurons, UNC-4 antagonizes a canonical Wnt signaling pathway involving MOM-5, MIG-1/Frz and EGL-20/Wnt that activates *ceh-12* expression, which promotes VB-type inputs to VA motor neurons. Additionally, UNC-4 inhibits a pathway mediated by *goa-1*/Gαo that promotes VB-type inputs in VA motor neurons. Multiple distinct pathways inhibit VB-type motor neurons in VA motor neurons: LIN-44-mediated Wnt signaling, EGL-30/Gαq signaling and the GSA-1/Gαs pathway. Together, these signaling cascades regulate synaptic choice in VA motor neurons.

same cell. Different combinations of transcription factor expression (or transcription factor "codes") regulate synaptic choice at multiple levels. One mechanism for regulation involves repression of "default" synaptic programs that promote an alternative set of dysfunctional synaptic inputs. As described above, UNC-4 is expressed in VA motor neurons and represses the expression of "default" VB-type genes, allowing for VA-type inputs. A similar situation occurs in the *Drosophila* ommatidium. Synapses to the R7 *Drosophila* photoreceptor neuron are maintained by the NF-Y transcription factor, which represses expression of R8-type genes [17, 18]. Mutation of NF-Y results in ectopic activation of the R8-specific transcription factor, Senseless, and ectopic expression of a cell surface molecule, Capricious, in the R7 neuron. As a result, the R7 cell adopts R8-type synaptic connections, while maintaining other gene expression signatures normally present in R7 cells [28, 29]. Additionally, in the *Drosophila* M12 muscle cell, the transcription factor Tey represses expression of the transmembrane protein Toll. Toll is expressed in all ventral muscles except for M12, where Tey repression of Toll allows for selective innervation of the M12 muscle by the MN12 motor neuron [17, 18]. Thus, transcription factors can repress gene expression to specify synaptic inputs.

To identify downstream targets of UNC-4, we have utilized microarray profiles [35, 42] and a genetic screen approach. As described in Chapter II, we have identified 16 different mutations (*blr* mutants) that affect synaptic specificity in the *unc-4* pathway. After extensive phenotypic analysis, we have an understanding of both the regional roles for these mutants and whether they affect gap junction or chemical synapse function in VA motor neurons. With some additional analysis to refine the chromosomal location of the *blr* mutants, we should be able to utilize the whole genome sequencing data we have collected to find the genetic lesions that correspond to the Unc-4 suppressor phenotypes (Chapter II). Upon identification of the loci, our detailed phenotypic characterization of

the *blr* mutants should allow us proceed directly towards addressing the mechanism by which the gene regulates synaptic choice.

Additionally, Rebecca McWhirter, a research assistant in the Miller lab, has adapted a larval cell culture protocol [240], enabling us to isolate and profile gene expression in VB and mutant VA neurons. Prior to this, we were unable to generate a VB motor neuron or an *unc-4* mutant VA motor neuron profile due to technical limitations with the mRNA tagging strategy [42, 171]. Although we have obtained valuable information from the microarray datasets of *unc-37* mutant VA motor neurons (including identification of *egl-20*/Wnt [104] and *ceh-12* [42]), *unc-37*/Groucho is expressed ubiquitously and most likely has many functions that are separate from its role as an UNC-4 co-repressor. Thus, comparing upregulated genes in *unc-4* mutant VAs with normally expressed VB genes should identify key players that are required for promoting VB-type wiring. Lastly, throughout our studies, we have yet to perturb the wiring of VB motor neurons, indicating that multiple pathways act in parallel to promote VB-type inputs. The combination of these datasets should allow us to identify additional genes that are required for the "default" VB-type synapses and might be required for synaptic choice in other systems.

Synaptic specificity is regulated by opposing Wnt pathways

Wnt signaling regulates numerous developmental processes, including synaptogenesis [51], cardiovascular development [71] and the regulation of asymmetric cell divisions [72]. In Chapter IV we provide one of the first examples of Wnt signaling regulating synaptic choice. In VA motor neurons, UNC-4 prevents expression of the Frizzled receptors, *mom-5* and *mig-1*. Mutation in *unc-4* leads to increased MOM-5 and MIG-1 expression in VAs, which transduces a signal from the posteriorly expressed EGL-20/Wnt. Through a canonical signaling cascade this EGL-20 mediated pathway

activates expression of *ceh-12* (Fig. 6.1). The Miller lab has previously shown that ectopic expression of *ceh-12* is required for the miswiring of posterior VA motor neurons [42]. In this work, we have confirmed these effects on posterior VAs by showing similar requirements for components of the EGL-20/Wnt pathway.

Additionally, we uncovered a role for an opposing Wnt pathway that involves the Wnts LIN-44 and CWN-1 and the Frizzled receptor LIN-17 (Fig. 6.1). These genes do not signal via β-catenin and canonical Wnt signaling, however we have yet to identify the downstream mechanism. Future experiments include testing components of non-canonical Wnt signaling such as *vang-1*/Van Gogh, *prkl-1*/Prickle and *fmi-1*/Flamingo. Furthermore, the mechanism of antagonism between the LIN-44- and EGL-20-mediated Wnt pathways is unclear. Additional genetic experiments as well as biochemical assays might provide insight into how these two Wnt pathways antagonize one another to specify inputs to VA motor neurons. For example, Frizzled or Wnt-Frizzled chimeras have been used in mammalian systems to further elucidate the mechanisms of Wnt signaling [241].

Finally, through double mutant analysis, we have uncovered a third Wnt pathway that functions through DSH-1/Disheveled in posterior VAs and through an unidentified pathway in anterior VAs (Figs. 4A.1-3). Additional genetic experiments, including testing non-canonical Wnt signaling genes (see above) as well as further characterization of Wnt pathway mutants could identify additional Wnt components in this pathway.

Antagonistic G-protein pathways regulate synaptic choice

In addition to the role of Wnt signaling in synaptic choice, we describe the effects of G-protein signaling on this process. G-protein pathways have previously been implicated in gap junction regulation [98]. Here, we show that opposing G-protein pathways regulate gap junction formation between the AVB interneuron and VA motor

neurons (Chapter V). GOA-1/Gαo is partially required for ectopic AVB to VA gap junctions in *unc-4* mutants while expression of EGL-30/Gαq and GSA-1/Gαs in VAs inhibits the ectopic gap junctions (Fig. 6.1). These G-protein pathways interact through a separate pathway from the established mechanism of antagonism, which converges on diacylglycerol (DAG) to regulate neurotransmitter release at the neuromuscular junction (Fig. 5.7) [95]. Instead, the diacylglycerol kinase, *dgk-1*, does not have a role in the *unc-4* pathway, indicating that VA motor neurons utilize specific components from these G-protein signaling pathways to mediate the regulation of both pre- and postsynaptic connections.

We propose that in wild-type VA motor neurons, EGL-30 and GSA-1 pathways are active and use the second messengers calcium and cAMP to inhibit AVB gap junction assembly with VAs. Our evidence indicates that in *unc-4* mutants, GOA-1 antagonizes the EGL-30 pathway by activation of EAT-16/RGS. EAT-16 might deactivate EGL-30/Gαq signaling by hydrolyzing GTP-EGL-30 to GDP-EGL-30. Additionally, GOA-1 could oppose the GSA-1 pathway by direct inhibition of ACY-1/adenylyl cyclase. This model provides certain predictions that would be possible to test in the future. For example, an increase in cytosolic calcium in *unc-4* mutant VA motor neurons, through activation of the ER-localized IP3 receptor, *itr-1*, could suppress ectopic AVB to VA inputs, mimicking the effects of EGL-30-mediated signaling. Additionally, loss of function of the PKA regulatory subunit, *kin-2*, would be expected to increase PKA levels downstream of cAMP, and might result in ectopic AVB to VA inputs.

Finally, we propose that G-protein signaling might regulate the trafficking of UNC-9/Innexin, which is mislocalized to VA cell soma in *unc-4* mutants (Fig. 5.14). We show that mutations in the cAMP binding protein, *epac-1*, and the DAG target, *rgef-1*, do not regulate AVB to VA connections (Fig. 10). Thus, alternative downstream signaling mechanisms must have a role in synaptic choice. Predictions from this hypothesis

include that a loss-of-function mutation in *goa-1* or increased expression of *gsa-1* or *egl-30* would result in suppression of ectopic UNC-9 localization on the cell soma of *unc-4* mutant VAs. Using tagged versions of UNC-7 and UNC-9, we may be able to resolve whether increased UNC-9 expression on the cell soma of *unc-4* mutant VAs localizes with UNC-7 expression from the AVB interneuron. With this *in vivo* visualization strategy, future experiments include assessing whether G-protein signaling is required for the localization of these gap junction components.

in vivo microscopy allows visualization of synaptic choice dynamics

The power of *C. elegans* genetics (and its transparency) provide the ability to visualize the real-time dynamics of synaptic choice *in vivo*. For example, in Chapters III and IV, I described two visualization techniques allowing the examination of chemical synapses in various genetic backgrounds. The number of GFP::RAB-3 puncta, representing chemical synapses from the AVE interneuron of the backward circuit, was altered in *unc-4* mutants (Fig. 3.2). Additionally, using GFP Reconstitution Across Synaptic Partners (GRASP), I showed that chemical synapses from the AVA interneuron to VA10 motor neuron were lost in *unc-4* mutants (Fig. 3.3). The loss of AVA to VA connections is mediated by the EGL-20/Wnt pathway upstream of *ceh-12* (Fig. 4.16). Finally, I exploited the ability to visualize gap junction connections from the AVB interneuron using UNC-7S::GFP. We show that multiple *blr* mutants regulate the formation of ectopic AVB gap junctions with *unc-4* mutant VA motor neurons (Fig. 2.6). These *in vivo* microscopic techniques provide a toolkit to identify roles for genes that control specific aspects of synaptic choice. For example, as explained above, simultaneous visualization of both gap junction proteins UNC-7 and UNC-9 might allow us to assess the effects of G protein signaling on gap junction formation, assembly and localization.

To this end, great strides were recently made in mammalian systems to utilize GRASP assays to identify synaptic partners *in vivo*. Synaptic partners were previously only identified by the use of electron microscopy or inferred via electrophysiology [109]. As mentioned in Chapter III, alternative techniques including super-resolution microscopy and trans-synaptic tracing have provided some evidence of potential connections between partner neurons. However, GRASP technology allows for clear determination of synaptic interaction [109]. Two GRASP tools using neurexin and neuroligin, expressed in mouse by either viral [108] or transgenic methods [109], led to GRASP signal detection *in vivo* in hippocampal and thalamic regions [108], or between rod photoreceptors and the outer plexiform layer of the retina [109]. Thus, optimizing GRASP to study VA motor neuron partnerships is an important next step for this project.

With these recent advances in microscopy and transgenic techniques, genetic experiments can now be used to identify components that regulate connectivity *in vivo* in mammals. The roles for conserved Wnt and G protein pathways that I have discussed in this dissertation make these signaling cascades prime candidates to test for regulation of synaptic choice in mammalian systems.

REFERENCES

1. White JG, Southgate E, Thomson JN, Brenner S: **The structure of the nervous system of the nematode Caenorhabditis elegans.** *Philos Trans R Soc Lond B Biol Sci* 1986, **314:**1-340.
2. Hamos JE, Van Horn SC, Raczkowski D, Sherman SM: **Synaptic circuits involving an individual retinogeniculate axon in the cat.** *J Comp Neurol* 1987, **259:**165-192.
3. Dréau GL, Martí E: **Dorsal-Ventral Patterning of the Neural Tube: A tale of three signals** 2012**:**1-26.
4. Kolodkin AL, Tessier-Lavigne M: **Mechanisms and molecules of neuronal wiring: a primer.** *Cold Spring Harb Perspect Biol* 2011, **3**.
5. Tessier-Lavigne M, Goodman CS: **The molecular biology of axon guidance.** *Science* 1996, **274:**1123-1133.
6. Dickson BJ: **Molecular Mechanisms of Axon Guidance.** *Science* 2002, **298:**1959-1964.
7. Colon-Ramos DA: **Synapse formation in developing neural circuits.** *Curr Top Dev Biol* 2009, **87:**53-79.
8. Missler M: **Synaptic cell adhesion goes functional.** *Trends Neurosci* 2003, **26:**176-178.
9. Missler M, Sudhof TC, Biederer T: **Synaptic cell adhesion.** *Cold Spring Harb Perspect Biol* 2012, **4**.
10. Yamagata M, Sanes JR: **Dscam and Sidekick proteins direct lamina-specific synaptic connections in vertebrate retina.** *Nature* 2008, **451:**465-469.
11. Yamada M, Hashimoto T, Hayashi N, Higuchi M, Murakami A, Nakashima T, Maekawa S, Miyata S: **Synaptic adhesion molecule OBCAM; synaptogenesis and dynamic internalization.** *Brain Res* 2007, **1165:**5-14.
12. Suzuki SC, Takeichi M: **Cadherins in neuronal morphogenesis and function.** *Dev Growth Differ* 2008, **50 Suppl 1:**S119-130.
13. Schmucker D, Clemens JC, Shu H, Worby CA, Xiao J, Muda M, Dixon JE, Zipursky SL: **Drosophila Dscam is an axon guidance receptor exhibiting extraordinary molecular diversity.** *Cell* 2000, **101:**671-684.
14. Prakash S, Caldwell JC, Eberl DF, Clandinin TR: **Drosophila N-cadherin mediates an attractive interaction between photoreceptor axons and their targets.** *Nat Neurosci* 2005, **8:**443-450.
15. Yamagata M, Weiner JA, Sanes JR: **Sidekicks: synaptic adhesion molecules that promote lamina-specific connectivity in the retina.** *Cell* 2002, **110:**649-660.
16. Krueger DD, Tuffy LP, Papadopoulos T, Brose N: **The role of neurexins and neuroligins in the formation, maturation, and function of vertebrate synapses.** *Curr Opin Neurobiol* 2012.

17. Inaki M, Shinza-Kameda M, Ismat A, Frasch M, Nose A: **Drosophila Tey represses transcription of the repulsive cue Toll and generates neuromuscular target specificity.** *Development* 2010.
18. Rose D, Zhu X, Kose H, Hoang B, Cho J, Chiba A: **Toll, a muscle cell surface molecule, locally inhibits synaptic initiation of the RP3 motoneuron growth cone in Drosophila.** *Development* 1997, **124:**1561-1571.
19. Inaki M, Yoshikawa S, Thomas JB, Aburatani H, Nose A: **Wnt4 is a local repulsive cue that determines synaptic target specificity.** *Curr Biol* 2007, **17:**1574-1579.
20. Mast JD, Prakash S, Chen PL, Clandinin TR: **The mechanisms and molecules that connect photoreceptor axons to their targets in Drosophila.** *Semin Cell Dev Biol* 2006, **17:**42-49.
21. Lee RC, Clandinin TR, Lee CH, Chen PL, Meinertzhagen IA, Zipursky SL: **The protocadherin Flamingo is required for axon target selection in the Drosophila visual system.** *Nat Neurosci* 2003, **6:**557-563.
22. Shen K, Bargmann CI: **The immunoglobulin superfamily protein SYG-1 determines the location of specific synapses in C. elegans.** *Cell* 2003, **112:**619-630.
23. Colon-Ramos DA, Margeta MA, Shen K: **Glia Promote Local Synaptogenesis Through UNC-6 (Netrin) Signaling in C. elegans.** *Science* 2007, **318:**103-106.
24. Usui T, Shima Y, Shimada Y, Hirano S, Burgess RW, Schwarz TL, Takeichi M, Uemura T: **Flamingo, a seven-pass transmembrane cadherin, regulates planar cell polarity under the control of Frizzled.** *Cell* 1999, **98:**585-595.
25. Chen P-L, Clandinin TR: **The cadherin Flamingo mediates level-dependent interactions that guide photoreceptor target choice in Drosophila.** *Neuron* 2008, **58:**26-33.
26. Shen K, Fetter RD, Bargmann CI: **Synaptic specificity is generated by the synaptic guidepost protein SYG-2 and its receptor, SYG-1.** *Cell* 2004, **116:**869-881.
27. Ding M, Chao D, Wang G, Shen K: **Spatial Regulation of an E3 Ubiquitin Ligase Directs Selective Synapse Elimination.** *Science* 2007, **317:**947-951.
28. Shinza-Kameda M, Takasu E, Sakurai K, Hayashi S, Nose A: **Regulation of layer-specific targeting by reciprocal expression of a cell adhesion molecule, capricious.** *Neuron* 2006, **49:**205-213.
29. Morey M, Yee SK, Herman T, Nern A, Blanco E, Zipursky SL: **Coordinate control of synaptic-layer specificity and rhodopsins in photoreceptor neurons.** *Nature* 2008, **456:**795-799.
30. Dasen JS, Tice BC, Brenner-Morton S, Jessell TM: **A Hox regulatory network establishes motor neuron pool identity and target-muscle connectivity.** *Cell* 2005, **123:**477-491.
31. Dasen JS, Jessell TM: **Hox networks and the origins of motor neuron diversity.** *Curr Top Dev Biol* 2009, **88:**169-200.

32. Shah V, Drill E, Lance-Jones C: **Ectopic expression of Hoxd10 in thoracic spinal segments induces motoneurons with a lumbosacral molecular profile and axon projections to the limb.** *Dev Dyn* 2004, **231:**43-56.
33. Vrieseling E, Arber S: **Target-induced transcriptional control of dendritic patterning and connectivity in motor neurons by the ETS gene Pea3.** *Cell* 2006, **127:**1439-1452.
34. Pecho-Vrieseling E, Sigrist M, Yoshida Y, Jessell TM, Arber S: **Specificity of sensory-motor connections encoded by Sema3e-Plxnd1 recognition.** *Nature* 2009, **459:**842-846.
35. Miller DM, Shen MM, Shamu CE, Bürglin TR, Ruvkun G, Dubois ML, Ghee M, Wilson L: **C. elegans unc-4 gene encodes a homeodomain protein that determines the pattern of synaptic input to specific motor neurons.** *Nature* 1992, **355:**841-845.
36. Miller DM, Niemeyer CJ: **Expression of the unc-4 homeoprotein in Caenorhabditis elegans motor neurons specifies presynaptic input.** *Development* 1995, **121:**2877-2886.
37. Sulston JE, Horvitz HR: **Post-embryonic cell lineages of the nematode, Caenorhabditis elegans.** *Developmental Biology* 1977, **56:**110-156.
38. White JG, Southgate E, Thomson JN: **Mutations in the Caenorhabditis elegans unc-4 gene alter the synaptic input to ventral cord motor neurons.** *Nature* 1992, **355:**838-841.
39. Miller DM, Niemeyer CJ, Chitkara P: **Dominant unc-37 mutations suppress the movement defect of a homeodomain mutation in unc-4, a neural specificity gene in Caenorhabditis elegans.** *Genetics* 1993, **135:**741-753.
40. Pflugrad A, Meir JY, Barnes TM, Miller DM: **The Groucho-like transcription factor UNC-37 functions with the neural specificity gene unc-4 to govern motor neuron identity in C. elegans.** *Development* 1997, **124:**1699-1709.
41. Winnier AR, Meir JY-J, Ross JM, Tavernarakis N, Driscoll M, Ishihara T, Katsura I, Miller DM: **UNC-4/UNC-37-dependent repression of motor neuron-specific genes controls synaptic choice in Caenorhabditis elegans.** *Genes & Development* 1999, **13:**2774-2786.
42. Von Stetina SE, Fox RM, Watkins KL, Starich TA, Shaw JE, Miller DM: **UNC-4 represses CEH-12/HB9 to specify synaptic inputs to VA motor neurons in C. elegans.** *Genes & Development* 2007, **21:**332-346.
43. Von Stetina SE, Watson JD, Fox RM, Olszewski KL, Spencer WC, Roy PJ, Miller DM: **Cell-specific microarray profiling experiments reveal a comprehensive picture of gene expression in the C. elegans nervous system.** *Genome Biol* 2007, **8:**R135.
44. Fox RM, Von Stetina SE, Barlow SJ, Shaffer C, Olszewski KL, Moore JH, Dupuy D, Vidal M, Miller DM: **A gene expression fingerprint of C. elegans embryonic motor neurons.** *BMC Genomics* 2005, **6:**42.
45. Thaler J, Harrison K, Sharma K, Lettieri K, Kehrl J, Pfaff SL: **Active suppression of interneuron programs within developing motor**

neurons revealed by analysis of homeodomain factor HB9. *Neuron* 1999, **23:**675-687.
46. Arber S, Han B, Mendelsohn M, Smith M, Jessell TM, Sockanathan S: **Requirement for the homeobox gene Hb9 in the consolidation of motor neuron identity.** *Neuron* 1999, **23:**659-674.
47. Broihier HT, Skeath JB: **Drosophila homeodomain protein dHb9 directs neuronal fate via crossrepressive and cell-nonautonomous mechanisms.** *Neuron* 2002, **35:**39-50.
48. Odden JP, Holbrook S, Doe CQ: **Drosophila HB9 is expressed in a subset of motoneurons and interneurons, where it regulates gene expression and axon pathfinding.** *J Neurosci* 2002, **22:**9143-9149.
49. Gordon MD: **Wnt Signaling: Multiple Pathways, Multiple Receptors, and Multiple Transcription Factors.** *Journal of Biological Chemistry* 2006, **281:**22429-22433.
50. Korswagen HC: **Canonical and non-canonical Wnt signaling pathways inCaenorhabditis elegans: variations on a common signaling theme.** *Bioessays* 2002, **24:**801-810.
51. Sahores M, Salinas PC: **Activity-mediated synapse formation a role for Wnt-Fz signaling.** *Curr Top Dev Biol* 2011, **97:**119-136.
52. Goldstein B, Takeshita H, Mizumoto K, Sawa H: **Wnt signals can function as positional cues in establishing cell polarity.** *Dev Cell* 2006, **10:**391-396.
53. Yamaguchi TP: **Heads or tails: Wnts and anterior-posterior patterning.** *Curr Biol* 2001, **11:**R713-724.
54. Lyuksyutova AI: **Anterior-Posterior Guidance of Commissural Axons by Wnt-Frizzled Signaling.** *Science* 2003, **302:**1984-1988.
55. Coudreuse D, Korswagen HC: **The making of Wnt: new insights into Wnt maturation, sorting and secretion.** *Development* 2007, **134:**3-12.
56. Pan C-L, Howell JE, Clark SG, Hilliard M, Cordes S, Bargmann CI, Garriga G: **Multiple Wnts and frizzled receptors regulate anteriorly directed cell and growth cone migrations in Caenorhabditis elegans.** *Dev Cell* 2006, **10:**367-377.
57. Hilliard MA, Bargmann CI: **Wnt signals and frizzled activity orient anterior-posterior axon outgrowth in C. elegans.** *Dev Cell* 2006, **10:**379-390.
58. Eisenmann DM: **Wnt signaling.** *WormBook : the online review of C elegans biology* 2005**:**1-17.
59. Herman MA, Vassilieva LL, Horvitz HR, Shaw JE, Herman RK: **The C. elegans gene lin-44, which controls the polarity of certain asymmetric cell divisions, encodes a Wnt protein and acts cell nonautonomously.** *Cell* 1995, **83:**101-110.
60. Rocheleau CE, Downs WD, Lin R, Wittmann C, Bei Y, Cha YH, Ali M, Priess JR, Mello CC: **Wnt signaling and an APC-related gene specify endoderm in early C. elegans embryos.** *Cell* 1997, **90:**707-716.

61. Thorpe CJ, Schlesinger A, Carter JC, Bowerman B: **Wnt signaling polarizes an early C. elegans blastomere to distinguish endoderm from mesoderm.** *Cell* 1997, **90:**695-705.
62. Maloof JN, Whangbo J, Harris JM, Jongeward GD, Kenyon C: **A Wnt signaling pathway controls hox gene expression and neuroblast migration in C. elegans.** *Development* 1999, **126:**37-49.
63. Shackleford GM, Shivakumar S, Shiue L, Mason J, Kenyon C, Varmus HE: **Two wnt genes in Caenorhabditis elegans.** *Oncogene* 1993, **8:**1857-1864.
64. Whangbo J, Kenyon C: **A Wnt signaling system that specifies two patterns of cell migration in C. elegans.** *Molecular Cell* 1999, **4:**851-858.
65. Siegfried KR, Kidd AR, Chesney MA, Kimble J: **The sys-1 and sys-3 genes cooperate with Wnt signaling to establish the proximal-distal axis of the Caenorhabditis elegans gonad.** *Genetics* 2004, **166:**171-186.
66. Costa M, Raich W, Agbunag C, Leung B, Hardin J, Priess JR: **A putative catenin-cadherin system mediates morphogenesis of the Caenorhabditis elegans embryo.** *J Cell Biol* 1998, **141:**297-308.
67. Herman M: **C. elegans POP-1/TCF functions in a canonical Wnt pathway that controls cell migration and in a noncanonical Wnt pathway that controls cell polarity.** *Development* 2001, **128:**581-590.
68. Shetty P, Lo MC, Robertson SM, Lin R: **C. elegans TCF protein, POP-1, converts from repressor to activator as a result of Wnt-induced lowering of nuclear levels.** *Dev Biol* 2005, **285:**584-592.
69. Herman MA, Wu M: **Noncanonical Wnt signaling pathways in C. elegans converge on POP-1/TCF and control cell polarity.** *Front Biosci* 2004, **9:**1530-1539.
70. Buechling T, Bartscherer K, Ohkawara B, Chaudhary V, Spirohn K, Niehrs C, Boutros M: **Wnt/Frizzled signaling requires dPRR, the Drosophila homolog of the prorenin receptor.** *Curr Biol* 2010, **20:**1263-1268.
71. Rao TP, Kuhl M: **An updated overview on Wnt signaling pathways: a prelude for more.** *Circ Res* 2010, **106:**1798-1806.
72. Hardin J, King RS: **The long and the short of Wnt signaling in C. elegans.** *Curr Opin Genet Dev* 2008, **18:**362-367.
73. Sanchez-Alvarez L, Visanuvimol J, McEwan A, Su A, Imai JH, Colavita A: **VANG-1 and PRKL-1 cooperate to negatively regulate neurite formation in Caenorhabditis elegans.** *PLoS Genet* 2011, **7:**e1002257.
74. Speese SD, Budnik V: **Wnts: up-and-coming at the synapse.** *Trends Neurosci* 2007, **30:**268-275.
75. Ciani L, Salinas PC: **Signalling in neural development: WNTS in the vertebrate nervous system: from patterning to neuronal connectivity.** *Nat Rev Neurosci* 2005, **6:**351-362.
76. Ataman B, Ashley J, Gorczyca M, Ramachandran P, Fouquet W, Sigrist SJ, Budnik V: **Rapid activity-dependent modifications in synaptic**

structure and function require bidirectional Wnt signaling. *Neuron* 2008, **57:**705-718.
77. Dinamarca MC, Colombres M, Cerpa W, Bonansco C, Inestrosa NC: **Beta-amyloid oligomers affect the structure and function of the postsynaptic region: role of the Wnt signaling pathway.** *Neurodegener Dis* 2008, **5:**149-152.
78. Salinas PC, Zou Y: **Wnt signaling in neural circuit assembly.** *Annu Rev Neurosci* 2008, **31:**339-358.
79. Klassen MP, Shen K: **Wnt signaling positions neuromuscular connectivity by inhibiting synapse formation in C. elegans.** *Cell* 2007, **130:**704-716.
80. Agalliu D, Takada S, Agalliu I, Mcmahon AP, Jessell TM: **Motor neurons with axial muscle projections specified by Wnt4/5 signaling.** *Neuron* 2009, **61:**708-720.
81. Miech C, Pauer H-U, He X, Schwarz TL: **Presynaptic Local Signaling by a Canonical Wingless Pathway Regulates Development of the Drosophila Neuromuscular Junction.** *Journal of Neuroscience* 2008, **28:**10875-10884.
82. Cerpa W, Godoy JA, Alfaro I, Farias GG, Metcalfe MJ, Fuentealba R, Bonansco C, Inestrosa NC: **Wnt-7a Modulates the Synaptic Vesicle Cycle and Synaptic Transmission in Hippocampal Neurons.** *Journal of Biological Chemistry* 2007, **283:**5918-5927.
83. Ahmad-Annuar A: **Signaling across the synapse: a role for Wnt and Dishevelled in presynaptic assembly and neurotransmitter release.** *The Journal of Cell Biology* 2006, **174:**127-139.
84. Hall AC, Lucas FR, Salinas PC: **Axonal remodeling and synaptic differentiation in the cerebellum is regulated by WNT-7a signaling.** *Cell* 2000, **100:**525-535.
85. Davis EK, Zou Y, Ghosh A: **Wnts acting through canonical and noncanonical signaling pathways exert opposite effects on hippocampal synapse formation.** *Neural Dev* 2008, **3:**32.
86. Green JL, Inoue T, Sternberg PW: **Opposing Wnt pathways orient cell polarity during organogenesis.** *Cell* 2008, **134:**646-656.
87. Inoue T, Oz HS, Wiland D, Gharib S, Deshpande R, Hill RJ, Katz WS, Sternberg PW: **C. elegans LIN-18 is a Ryk ortholog and functions in parallel to LIN-17/Frizzled in Wnt signaling.** *Cell* 2004, **118:**795-806.
88. Liu Y, Shi J, Lu CC, Wang ZB, Lyuksyutova AI, Song XJ, Zou Y: **Ryk-mediated Wnt repulsion regulates posterior-directed growth of corticospinal tract.** *Nat Neurosci* 2005, **8:**1151-1159.
89. Miyashita-Lin EM, Hevner R, Wassarman KM, Martinez S, Rubenstein JL: **Early neocortical regionalization in the absence of thalamic innervation.** *Science* 1999, **285:**906-909.
90. Green JL, Inoue T, Sternberg PW: **The C. elegans ROR receptor tyrosine kinase, CAM-1, non-autonomously inhibits the Wnt pathway.** *Development* 2007, **134:**4053-4062.

91. Paganoni S, Bernstein J, Ferreira A: **Ror1-Ror2 complexes modulate synapse formation in hippocampal neurons.** *Neuroscience* 2010, **165:**1261-1274.
92. Neves SR, Ram PT, Iyengar R: **G protein pathways.** *Science* 2002, **296:**1636-1639.
93. Kach J, Sethakorn N, Dulin NO: **A finer tuning of G protein signaling through regulated control of RGS proteins.** *Am J Physiol Heart Circ Physiol* 2012.
94. Hepler JR, Gilman AG: **G proteins.** *Trends Biochem Sci* 1992, **17:**383-387.
95. Bastiani C, Mendel J: **Heterotrimeric G proteins in C. elegans.** *WormBook : the online review of C elegans biology* 2006**:**1-25.
96. Govindan JA, Cheng H, Harris JE, Greenstein D: **Gαo/i and Gαs Signaling Function in Parallel with the MSP/Eph Receptor to Control Meiotic Diapause in C. elegans.** *Current Biology* 2006, **16:**1257-1268.
97. van Zeijl L, Ponsioen B, Giepmans BNG, Ariaens A, Postma FR, Várnai P, Balla T, Divecha N, Jalink K, Moolenaar WH: **Regulation of connexin43 gap junctional communication by phosphatidylinositol 4,5-bisphosphate.** *The Journal of Cell Biology* 2007, **177:**881-891.
98. Lampe PD, Qiu Q, Meyer RA, TenBroek EM, Walseth TF, Starich TA, Grunenwald HL, Johnson RG: **Gap junction assembly: PTX-sensitive G proteins regulate the distribution of connexin43 within cells.** *Am J Physiol, Cell Physiol* 2001, **281:**C1211-1222.
99. Mendel J: **Go directly (or indirectly) to Gq.** *Neuron* 1999, **24:**287-288.
100. Schulz R, Heusch G: **Connexin 43 and ischemic preconditioning.** *Cardiovasc Res* 2004, **62:**335-344.
101. Somekawa S, Fukuhara S, Nakaoka Y, Fujita H, Saito Y, Mochizuki N: **Enhanced functional gap junction neoformation by protein kinase A-dependent and Epac-dependent signals downstream of cAMP in cardiac myocytes.** *Circ Res* 2005, **97:**655-662.
102. Dani A, Huang B, Bergan J, Dulac C, Zhuang X: **Superresolution imaging of chemical synapses in the brain.** *Neuron* 2010, **68:**843-856.
103. Feinberg EH, Vanhoven MK, Bendesky A, Wang G, Fetter RD, Shen K, Bargmann CI: **GFP Reconstitution Across Synaptic Partners (GRASP) defines cell contacts and synapses in living nervous systems.** *Neuron* 2008, **57:**353-363.
104. Schneider J, Skelton RL, Von Stetina SE, Middelkoop TC, van Oudenaarden A, Korswagen HC, Miller DM, 3rd: **UNC-4 antagonizes Wnt signaling to regulate synaptic choice in the C. elegans motor circuit.** *Development* 2012, **139:**2234-2245.
105. Park J, Knezevich PL, Wung W, O'hanlon SN, Goyal A, Benedetti KL, Barsi-Rhyne BJ, Raman M, Mock N, Bremer M, Vanhoven MK: **A conserved juxtacrine signal regulates synaptic partner recognition in Caenorhabditis elegans.** *Neural Dev* 2011, **6:**28.
106. Gordon MD, Scott K: **Motor control in a Drosophila taste circuit.** *Neuron* 2009, **61:**373-384.

107. Gong Z, Liu J, Guo C, Zhou Y, Teng Y, Liu L: **Two pairs of neurons in the central brain control Drosophila innate light preference.** *Science* 2010, **330:**499-502.
108. Kim J, Zhao T, Petralia RS, Yu Y, Peng H, Myers E, Magee JC: **mGRASP enables mapping mammalian synaptic connectivity with light microscopy.** *Nat Methods* 2012, **9:**96-102.
109. Yamagata M, Sanes JR: **Transgenic strategy for identifying synaptic connections in mice by fluorescence complementation (GRASP).** *Front Mol Neurosci* 2012, **5:**18.
110. Williams ME, de Wit J, Ghosh A: **Molecular mechanisms of synaptic specificity in developing neural circuits.** *Neuron* 2010, **68:**9-18.
111. Hakeda-Suzuki S, Berger-Muller S, Tomasi T, Usui T, Horiuchi SY, Uemura T, Suzuki T: **Golden Goal collaborates with Flamingo in conferring synaptic-layer specificity in the visual system.** *Nat Neurosci* 2011, **14:**314-323.
112. Brenner S: **The genetics of Caenorhabditis elegans.** *Genetics* 1974, **77:**71-94.
113. Warming S, Costantino N, Court DL, Jenkins NA, Copeland NG: **Simple and highly efficient BAC recombineering using galK selection.** *Nucleic Acids Res* 2005, **33:**e36.
114. Starich TA, Xu J, Skerrett IM, Nicholson BJ, Shaw JE: **Interactions between innexins UNC-7 and UNC-9 mediate electrical synapse specificity in the Caenorhabditis elegans locomotory nervous system.** *Neural Dev* 2009, **4:**16.
115. Davis MW, Hammarlund M, Harrach T, Hullett P, Olsen S, Jorgensen EM: **Rapid single nucleotide polymorphism mapping in C. elegans.** *BMC Genomics* 2005, **6:**118.
116. Bigelow H, Doitsidou M, Sarin S, Hobert O: **MAQGene: software to facilitate C. elegans mutant genome sequence analysis.** *Nat Methods* 2009, **6:**549.
117. Sarin S, Prabhu S, O'Meara MM, Pe'er I, Hobert O: **Caenorhabditis elegans mutant allele identification by whole-genome sequencing.** *Nat Methods* 2008, **5:**865-867.
118. Pickles LM, Roe SM, Hemingway EJ, Stifani S, Pearl LH: **Crystal structure of the C-terminal WD40 repeat domain of the human Groucho/TLE1 transcriptional corepressor.** *Structure* 2002, **10:**751-761.
119. Liu J, Ward A, Gao J, Dong Y, Nishio N, Inada H, Kang L, Yu Y, Ma D, Xu T, et al: **C. elegans phototransduction requires a G protein–dependent cGMP pathway and a taste receptor homolog.** *Nat Neurosci* 2010, **13:**715-722.
120. Yao J, Hiramatsu N, Zhu Y, Morioka T, Takeda M, Oite T, Kitamura M: **Nitric oxide-mediated regulation of connexin43 expression and gap junctional intercellular communication in mesangial cells.** *J Am Soc Nephrol* 2005, **16:**58-67.

121. Tran TS, Kolodkin AL, Bharadwaj R: **Semaphorin regulation of cellular morphology.** *Annu Rev Cell Dev Biol* 2007, **23:**263-292.
122. shen K SP: **Genetics and Cell Biology of Building Specific Synaptic Connectivity** 2010**:**1-35.
123. Patel MR, Shen K: **RSY-1 Is a Local Inhibitor of Presynaptic Assembly in C. elegans.** *Science* 2009, **323:**1500-1503.
124. Phelan P, Starich TA: **Innexins get into the gap.** *Bioessays* 2001, **23:**388-396.
125. Cardozo T, Pagano M: **The SCF ubiquitin ligase: insights into a molecular machine.** *Nat Rev Mol Cell Biol* 2004, **5:**739-751.
126. Yook K: **Complementation.** In *WormBook : the online review of C elegans biology*. pp. 1-17; 2005:1-17.
127. Hawley RS, and Walker, M.Y.: *Advanced genetic analysis: finding meaning in a genome* Malden, Massachusetts:: Oxford, Blackwell; 2003.
128. Hays TS, Deuring R, Robertson B, Prout M, Fuller MT: **Interacting proteins identified by genetic interactions: a missense mutation in alpha-tubulin fails to complement alleles of the testis-specific beta-tubulin gene of Drosophila melanogaster.** In *Mol Cell Biol*, vol. 9. pp. 875-884; 1989:875-884.
129. Zuryn S, Le Gras S, Jamet K, Jarriault S: **A strategy for direct mapping and identification of mutations by whole-genome sequencing.** *Genetics* 2010, **186:**427-430.
130. Roy PJ, Zheng H, Warren CE, Culotti JG: **mab-20 encodes Semaphorin-2a and is required to prevent ectopic cell contacts during epidermal morphogenesis in Caenorhabditis elegans.** *Development* 2000, **127:**755-767.
131. Taraska JW, Zagotta WN: **Fluorescence applications in molecular neurobiology.** *Neuron* 2010, **66:**170-189.
132. Varshney LR, Chen BL, Paniagua E, Hall DH, Chklovskii DB: **Structural Properties of the Caenorhabditis elegans Neuronal Network.** *PLoS Comput Biol* 2011, **7:**e1001066.
133. Chalfie M, Sulston JE, White JG, Southgate E, Thomson JN, Brenner S: **The neural circuit for touch sensitivity in Caenorhabditis elegans.** *J Neurosci* 1985, **5:**956-964.
134. Praitis V, Casey E, Collar D, Austin J: **Creation of low-copy integrated transgenic lines in Caenorhabditis elegans.** *Genetics* 2001, **157:**1217-1226.
135. Matteoli M, Takei K, Cameron R, Hurlbut P, Johnston PA, Sudhof TC, Jahn R, De Camilli P: **Association of Rab3A with synaptic vesicles at late stages of the secretory pathway.** *J Cell Biol* 1991, **115:**625-633.
136. Gracheva EO, Hadwiger G, Nonet ML, Richmond JE: **Direct interactions between C. elegans RAB-3 and Rim provide a mechanism to target vesicles to the presynaptic density.** *Neurosci Lett* 2008, **444:**137-142.
137. Nonet ML, Staunton JE, Kilgard MP, Fergestad T, Hartwieg E, Horvitz HR, Jorgensen EM, Meyer BJ: **Caenorhabditis elegans rab-3 mutant**

synapses exhibit impaired function and are partially depleted of vesicles. *J Neurosci* 1997, **17:**8061-8073.
138. Livet J: **[The brain in color: transgenic "Brainbow" mice for visualizing neuronal circuits].** *Med Sci (Paris)* 2007, **23:**1173-1176.
139. Micheva KD, Smith SJ: **Array tomography: a new tool for imaging the molecular architecture and ultrastructure of neural circuits.** *Neuron* 2007, **55:**25-36.
140. Wickersham IR, Lyon DC, Barnard RJ, Mori T, Finke S, Conzelmann KK, Young JA, Callaway EM: **Monosynaptic restriction of transsynaptic tracing from single, genetically targeted neurons.** *Neuron* 2007, **53:**639-647.
141. Todd KL, Kristan WB, Jr., French KA: **Gap junction expression is required for normal chemical synapse formation.** *J Neurosci* 2010, **30:**15277-15285.
142. Smith M, Pereda AE: **Chemical synaptic activity modulates nearby electrical synapses.** *Proc Natl Acad Sci U S A* 2003, **100:**4849-4854.
143. Li Q, Burrell BD: **CNQX and AMPA inhibit electrical synaptic transmission: a potential interaction between electrical and glutamatergic synapses.** *Brain Res* 2008, **1228:**43-57.
144. Shen K, Scheiffele P: **Genetics and cell biology of building specific synaptic connectivity.** *Annu Rev Neurosci* 2010, **33:**473-507.
145. Sanes JR, Yamagata M: **Many paths to synaptic specificity.** *Annu Rev Cell Dev Biol* 2009, **25:**161-195.
146. Hestrin S, Galarreta M: **Electrical synapses define networks of neocortical GABAergic neurons.** *Trends Neurosci* 2005, **28:**304-309.
147. Bennett MV, Zukin RS: **Electrical coupling and neuronal synchronization in the Mammalian brain.** *Neuron* 2004, **41:**495-511.
148. Westerfield M, Frank E: **Specificity of electrical coupling among neurons innervating forelimb muscles of the adult bullfrog.** *J Neurophysiol* 1982, **48:**904-913.
149. Charlton BT, Gray EG: **Comparative electron microscopy of synapses in the vertebrate spinal cord.** *J Cell Sci* 1966, **1:**67-80.
150. Li X-J, Zhang X, Johnson MA, Wang Z-B, Lavaute T, Zhang S-C: **Coordination of sonic hedgehog and Wnt signaling determines ventral and dorsal telencephalic neuron types from human embryonic stem cells.** *Development* 2009, **136:**4055-4063.
151. Van Der Giessen RS, Koekkoek SK, van Dorp S, De Gruijl JR, Cupido A, Khosrovani S, Dortland B, Wellershaus K, Degen J, Deuchars J, et al: **Role of olivary electrical coupling in cerebellar motor learning.** *Neuron* 2008, **58:**599-612.
152. Briscoe J, Pierani A, Jessell TM, Ericson J: **A homeodomain protein code specifies progenitor cell identity and neuronal fate in the ventral neural tube.** *Cell* 2000, **101:**435-445.
153. Shirasaki R, Pfaff SL: **Transcriptional codes and the control of neuronal identity.** *Annu Rev Neurosci* 2002, **25:**251-281.

154. Budnik V, Salinas PC: **Wnt signaling during synaptic development and plasticity.** *Curr Opin Neurobiol* 2011, **21:**151-159.
155. Packard M, Koo ES, Gorczyca M, Sharpe J, Cumberledge S, Budnik V: **The Drosophila Wnt, wingless, provides an essential signal for pre- and postsynaptic differentiation.** *Cell* 2002, **111:**319-330.
156. Haspel G, ODonovan MJ, Hart AC: **Motoneurons Dedicated to Either Forward or Backward**
Locomotion in the Nematode Caenorhabditis elegans. *The Journal of Neuroscience* 2010**:**1-6.
157. Ben Arous J, Tanizawa Y, Rabinowitch I, Chatenay D, Schafer WR: **Automated imaging of neuronal activity in freely behaving Caenorhabditis elegans.** *J Neurosci Methods* 2010, **187:**229-234.
158. Gleason JE: **Activation of Wnt signaling bypasses the requirement for RTK/Ras signaling during C. elegans vulval induction.** *Genes & Development* 2002, **16:**1281-1290.
159. Fire A, Albertson D, Harrison SW, Moerman DG: **Production of antisense RNA leads to effective and specific inhibition of gene expression in C. elegans muscle.** *Development* 1991, **113:**503-514.
160. Sawa H, Lobel L, Horvitz HR: **The Caenorhabditis elegans gene lin-17, which is required for certain asymmetric cell divisions, encodes a putative seven-transmembrane protein similar to the Drosophila frizzled protein.** *Genes & Development* 1996, **10:**2189-2197.
161. Korswagen HC: **The Axin-like protein PRY-1 is a negative regulator of a canonical Wnt pathway in C. elegans.** *Genes & Development* 2002, **16:**1291-1302.
162. Zinovyeva AY, Forrester WC: **The C. elegans Frizzled CFZ-2 is required for cell migration and interacts with multiple Wnt signaling pathways.** *Dev Biol* 2005, **285:**447-461.
163. Eisenmann DM, Maloof JN, Simske JS, Kenyon C, Kim SK: **The beta-catenin homolog BAR-1 and LET-60 Ras coordinately regulate the Hox gene lin-39 during Caenorhabditis elegans vulval development.** *Development* 1998, **125:**3667-3680.
164. Von Stetina S, Fox R, Watkins K, Starich T, Shaw J, Miller D: **UNC-4 represses CEH-12/HB9 to specify synaptic inputs to VA motor neurons in C. elegans.** *Genes Dev* 2007, **21:**332-346.
165. Esmaeili B, Ross JM, Neades C, Miller DM, Ahringer J: **The C. elegans even-skipped homologue, vab-7, specifies DB motoneurone identity and axon trajectory.** *Development* 2002, **129:**853-862.
166. Raj A, van den Bogaard P, Rifkin SA, van Oudenaarden A, Tyagi S: **Imaging individual mRNA molecules using multiple singly labeled probes.** *Nat Methods* 2008, **5:**877-879.
167. Harterink M, Kim DH, Middelkoop TC, Doan TD, van Oudenaarden A, Korswagen HC: **Neuroblast migration along the anteroposterior axis of C. elegans is controlled by opposing gradients of Wnts and a secreted Frizzled-related protein.** *Development* 2011, **138:**2915-2924.

168. R.A. F: *Statistical Methods for Research Workers.* Edinburgh: Oliver and Boyd; 1925.
169. Coudreuse DYM: **Wnt Gradient Formation Requires Retromer Function in Wnt-Producing Cells.** *Science* 2006, **312:**921-924.
170. Winnier AR, Meir JY, Ross JM, Tavernarakis N, Driscoll M, Ishihara T, Katsura I, Miller DM, 3rd: **UNC-4/UNC-37-dependent repression of motor neuron-specific genes controls synaptic choice in Caenorhabditis elegans.** *Genes Dev* 1999, **13:**2774-2786.
171. Von Stetina S, Watson J, Fox R, Olszewski K, Spencer W, Roy P, Miller D: **Cell-specific microarray profiling experiments reveal a comprehensive picture of gene expression in the C. elegans nervous system.** *Genome Biol* 2007, **8:**R135.
172. Von Stetina SE, Fox RM, Watkins KL, Starich TA, Shaw JE, Miller DM, 3rd: **UNC-4 represses CEH-12/HB9 to specify synaptic inputs to VA motor neurons in C. elegans.** *Genes Dev* 2007, **21:**332-346.
173. Korswagen HC, Herman MA, Clevers HC: **Distinct beta-catenins mediate adhesion and signalling functions in C. elegans.** *Nature* 2000, **406:**527-532.
174. Vashlishan AB, Madison JM, Dybbs M, Bai J, Sieburth D, Ch'ng Q, Tavazoie M, Kaplan JM: **An RNAi screen identifies genes that regulate GABA synapses.** *Neuron* 2008, **58:**346-361.
175. Calvo D, Victor M, Gay F, Sui G, Luke MP, Dufourcq P, Wen G, Maduro M, Rothman J, Shi Y: **A POP-1 repressor complex restricts inappropriate cell type-specific gene transcription during Caenorhabditis elegans embryogenesis.** *EMBO J* 2001, **20:**7197-7208.
176. McColl G, Killilea DW, Hubbard AE, Vantipalli MC, Melov S, Lithgow GJ: **Pharmacogenetic analysis of lithium-induced delayed aging in Caenorhabditis elegans.** *J Biol Chem* 2008, **283:**350-357.
177. Tanizawa Y, Kuhara A, Inada H, Kodama E, Mizuno T, Mori I: **Inositol monophosphatase regulates localization of synaptic components and behavior in the mature nervous system of C. elegans.** *Genes Dev* 2006, **20:**3296-3310.
178. Thorne CA, Hanson AJ, Schneider J, Tahinci E, Orton D, Cselenyi CS, Jernigan KK, Meyers KC, Hang BI, Waterson AG, et al: **Small-molecule inhibition of Wnt signaling through activation of casein kinase 1alpha.** *Nat Chem Biol* 2010, **6:**829-836.
179. Ciani L, Boyle KA, Dickins E, Sahores M, Anane D, Lopes DM, Gibb AJ, Salinas PC: **Wnt7a signaling promotes dendritic spine growth and synaptic strength through Ca(2)(+)/Calmodulin-dependent protein kinase II.** *Proc Natl Acad Sci U S A* 2011, **108:**10732-10737.
180. Henriquez JP, Webb A, Bence M, Bildsoe H, Sahores M, Hughes SM, Salinas PC: **Wnt signaling promotes AChR aggregation at the neuromuscular synapse in collaboration with agrin.** *Proc Natl Acad Sci U S A* 2008, **105:**18812-18817.

181. Jing L, Lefebvre JL, Gordon LR, Granato M: **Wnt signals organize synaptic prepattern and axon guidance through the zebrafish unplugged/MuSK receptor.** *Neuron* 2009, **61:**721-733.
182. Cerpa W, Godoy JA, Alfaro I, Farias GG, Metcalfe MJ, Fuentealba R, Bonansco C, Inestrosa NC: **Wnt-7a modulates the synaptic vesicle cycle and synaptic transmission in hippocampal neurons.** *J Biol Chem* 2008, **283:**5918-5927.
183. Purro SA, Ciani L, Hoyos-Flight M, Stamatakou E, Siomou E, Salinas PC: **Wnt regulates axon behavior through changes in microtubule growth directionality: a new role for adenomatous polyposis coli.** *J Neurosci* 2008, **28:**8644-8654.
184. Sahores M, Gibb A, Salinas P: **Frizzled-5, a receptor for the synaptic organizer Wnt7a,**
regulates activity-mediated synaptogenesis
. 2010**:**1-11.
185. Rash JE, Staines WA, Yasumura T, Patel D, Furman CS, Stelmack GL, Nagy JI: **Immunogold evidence that neuronal gap junctions in adult rat brain and spinal cord contain connexin-36 but not connexin-32 or connexin-43.** *Proc Natl Acad Sci U S A* 2000, **97:**7573-7578.
186. Song S, Zhang B, Sun H, Li X, Xiang Y, Liu Z, Huang X, Ding M: **A Wnt-Frz/Ror-Dsh pathway regulates neurite outgrowth in Caenorhabditis elegans.** *PLoS Genet* 2010, **6**.
187. Maro GS, Klassen MP, Shen K, Chédotal A: **A β-Catenin-Dependent Wnt Pathway Mediates Anteroposterior Axon Guidance in C. elegans Motor Neurons.** *PLoS ONE* 2009, **4:**e4690.
188. Zinovyeva AY, Yamamoto Y, Sawa H, Forrester WC: **Complex Network of Wnt Signaling Regulates Neuronal Migrations During Caenorhabditis elegans Development.** *Genetics* 2008, **179:**1357-1371.
189. Fradkin LG, Garriga G, Salinas PC, Thomas JB, Yu X, Zou Y: **Wnt signaling in neural circuit development.** *J Neurosci* 2005, **25:**10376-10378.
190. Meier C, Dermietzel R: **Electrical synapses--gap junctions in the brain.** *Results Probl Cell Differ* 2006, **43:**99-128.
191. Bloomfield SA, Volgyi B: **The diverse functional roles and regulation of neuronal gap junctions in the retina.** *Nat Rev Neurosci* 2009, **10:**495-506.
192. Sohl G, Maxeiner S, Willecke K: **Expression and functions of neuronal gap junctions.** *Nat Rev Neurosci* 2005, **6:**191-200.
193. Shen K, Scheiffele P: **Genetics and cell biology of building specific synaptic connectivity.** *Annu Rev Neurosci* 2010, **33:**473-507.
194. VanSlyke JK, Musil LS: **Analysis of connexin intracellular transport and assembly.** *Methods* 2000, **20:**156-164.
195. Bukauskas FF, Verselis VK: **Gap junction channel gating.** *Biochim Biophys Acta* 2004, **1662:**42-60.

196. Govindan JA, Nadarajan S, Kim S, Starich TA, Greenstein D: **Somatic cAMP signaling regulates MSP-dependent oocyte growth and meiotic maturation in C. elegans.** *Development* 2009, **136:**2211-2221.
197. Tanis JE, Moresco JJ, Lindquist RA, Koelle MR: **Regulation of serotonin biosynthesis by the G proteins Galphao and Galphaq controls serotonin signaling in Caenorhabditis elegans.** *Genetics* 2008, **178:**157-169.
198. Zhao H, Nonet ML: **A retrograde signal is involved in activity-dependent remodeling at a C. elegans neuromuscular junction.** *Development* 2000, **127:**1253-1266.
199. Mendel JE, Korswagen HC, Liu KS, Hajdu-Cronin YM, Simon MI, Plasterk RH, Sternberg PW: **Participation of the protein Go in multiple aspects of behavior in C. elegans.** *Science* 1995, **267:**1652-1655.
200. Kamath RS, Ahringer J: **Genome-wide RNAi screening in Caenorhabditis elegans.** *Methods* 2003, **30:**313-321.
201. Nurrish S, Ségalat L, Kaplan JM: **Serotonin inhibition of synaptic transmission: Galpha(0) decreases the abundance of UNC-13 at release sites.** *Neuron* 1999, **24:**231-242.
202. Patikoglou GA, Koelle MR: **An N-terminal region of Caenorhabditis elegans RGS proteins EGL-10 and EAT-16 directs inhibition of G(alpha)o versus G(alpha)q signaling.** *J Biol Chem* 2002, **277:**47004-47013.
203. Dong MQ, Chase D, Patikoglou GA, Koelle MR: **Multiple RGS proteins alter neural G protein signaling to allow C. elegans to rapidly change behavior when fed.** *Genes Dev* 2000, **14:**2003-2014.
204. Brundage L, Avery L, Katz A, Kim UJ, Mendel JE, Sternberg PW, Simon MI: **Mutations in a C. elegans Gqalpha gene disrupt movement, egg laying, and viability.** *Neuron* 1996, **16:**999-1009.
205. Ségalat L, Elkes DA, Kaplan JM: **Modulation of serotonin-controlled behaviors by Go in Caenorhabditis elegans.** *Science* 1995, **267:**1648-1651.
206. Miller KG, Emerson MD, Rand JB: **Goalpha and diacylglycerol kinase negatively regulate the Gqalpha pathway in C. elegans.** *Neuron* 1999, **24:**323-333.
207. Lackner MR, Nurrish SJ, Kaplan JM: **Facilitation of synaptic transmission by EGL-30 Gqalpha and EGL-8 PLCbeta: DAG binding to UNC-13 is required to stimulate acetylcholine release.** *Neuron* 1999, **24:**335-346.
208. Schade MA: **Mutations That Rescue the Paralysis of Caenorhabditis elegans ric-8 (Synembryn) Mutants Activate the G s Pathway and Define a Third Major Branch of the Synaptic Signaling Network.** *Genetics* 2005, **169:**631-649.
209. Kawasaki H, Springett GM, Mochizuki N, Toki S, Nakaya M, Matsuda M, Housman DE, Graybiel AM: **A family of cAMP-binding proteins that directly activate Rap1.** *Science* 1998, **282:**2275-2279.

210. Chen L, Fu Y, Ren M, Xiao B, Rubin CS: **A RasGRP, C. elegans RGEF-1b, couples external stimuli to behavior by activating LET-60 (Ras) in sensory neurons.** *Neuron* 2011, **70:**51-65.
211. de Rooij J, Zwartkruis FJ, Verheijen MH, Cool RH, Nijman SM, Wittinghofer A, Bos JL: **Epac is a Rap1 guanine-nucleotide-exchange factor directly activated by cyclic AMP.** *Nature* 1998, **396:**474-477.
212. Lickteig KM, Duerr JS, Frisby DL, Hall DH, Rand JB, Miller DM: **Regulation of neurotransmitter vesicles by the homeodomain protein UNC-4 and its transcriptional corepressor UNC-37/groucho in Caenorhabditis elegans cholinergic motor neurons.** *J Neurosci* 2001, **21:**2001-2014.
213. Rand JB: **Acetylcholine.** *WormBook* 2007**:**1-21.
214. Madison JM, Nurrish S, Kaplan JM: **UNC-13 interaction with syntaxin is required for synaptic transmission.** *Curr Biol* 2005, **15:**2236-2242.
215. Richmond JE, Davis WS, Jorgensen EM: **UNC-13 is required for synaptic vesicle fusion in C. elegans.** *Nat Neurosci* 1999, **2:**959-964.
216. Malbon CC: **Frizzleds: new members of the superfamily of G-protein-coupled receptors.** *Front Biosci* 2004, **9:**1048-1058.
217. Koval A, Purvanov V, Egger-Adam D, Katanaev VL: **Yellow submarine of the Wnt/Frizzled signaling: Submerging from the G protein harbor to the targets.** *Biochemical Pharmacology* 2011.
218. Jernigan KK, Cselenyi CS, Thorne CA, Hanson AJ, Tahinci E, Hajicek N, Oldham WM, Lee LA, Hamm HE, Hepler JR, et al: **G Activates GSK3 to Promote LRP6-Mediated -Catenin Transcriptional Activity.** *Science Signaling* 2010, **3:**ra37-ra37.
219. Katanaev VL, Ponzielli R, Sémériva M, Tomlinson A: **Trimeric G protein-dependent frizzled signaling in Drosophila.** *Cell* 2005, **120:**111-122.
220. Katanaev VL, Tomlinson A: **Dual roles for the trimeric G protein Go in asymmetric cell division in Drosophila.** *Proc Natl Acad Sci USA* 2006, **103:**6524-6529.
221. Egger-Adam D, Katanaev VL: **Trimeric G protein-dependent signaling by Frizzled receptors in animal development.** *Front Biosci* 2008, **13:**4740-4755.
222. Egger-Adam D, Katanaev V: **The trimeric G protein Go inflicts a double impact on axin in the Wnt/frizzled signaling pathway.** *Dev Dyn* 2009.
223. Bikkavilli RK, Feigin ME, Malbon CC: **G alpha o mediates WNT-JNK signaling through dishevelled 1 and 3, RhoA family members, and MEKK 1 and 4 in mammalian cells.** *J Cell Sci* 2008, **121:**234-245.
224. Hajdu-Cronin YM, Chen WJ, Patikoglou G, Koelle MR, Sternberg PW: **Antagonism between G(o)alpha and G(q)alpha in Caenorhabditis elegans: the RGS protein EAT-16 is necessary for G(o)alpha signaling and regulates G(q)alpha activity.** *Genes & Development* 1999, **13:**1780-1793.
225. Witherow DS, Wang Q, Levay K, Cabrera JL, Chen J, Willars GB, Slepak VZ: **Complexes of the G protein subunit gbeta 5 with the regulators**

of G protein signaling RGS7 and RGS9. Characterization in native tissues and in transfected cells. *J Biol Chem* 2000, **275:**24872-24880.
226. Cabrera JL, de Freitas F, Satpaev DK, Slepak VZ: **Identification of the Gbeta5-RGS7 protein complex in the retina.** *Biochem Biophys Res Commun* 1998, **249:**898-902.
227. Makino ER, Handy JW, Li T, Arshavsky VY: **The GTPase activating factor for transducin in rod photoreceptors is the complex between RGS9 and type 5 G protein beta subunit.** *Proc Natl Acad Sci U S A* 1999, **96:**1947-1952.
228. Zhang JH, Simonds WF: **Copurification of brain G-protein beta5 with RGS6 and RGS7.** *J Neurosci* 2000, **20:**RC59.
229. Chase DL, Patikoglou GA, Koelle MR: **Two RGS proteins that inhibit Galpha(o) and Galpha(q) signaling in C. elegans neurons require a Gbeta(5)-like subunit for function.** *Curr Biol* 2001, **11:**222-231.
230. Watts VJ, Neve KA: **Sensitization of adenylate cyclase by Galpha i/o-coupled receptors.** *Pharmacol Ther* 2005, **106:**405-421.
231. Dessauer CW, Chen-Goodspeed M, Chen J: **Mechanism of Galpha i-mediated inhibition of type V adenylyl cyclase.** *J Biol Chem* 2002, **277:**28823-28829.
232. Mao H, Zhao Q, Daigle M, Ghahremani MH, Chidiac P, Albert PR: **RGS17/RGSZ2, a novel regulator of Gi/o, Gz, and Gq signaling.** *J Biol Chem* 2004, **279:**26314-26322.
233. Solan JL, Lampe PD: **Connexin phosphorylation as a regulatory event linked to gap junction channel assembly.** *Biochim Biophys Acta* 2005, **1711:**154-163.
234. Ghosh-Roy A, Wu Z, Goncharov A, Jin Y, Chisholm AD: **Calcium and Cyclic AMP Promote Axonal Regeneration in Caenorhabditis elegans and Require DLK-1 Kinase.** *Journal of Neuroscience* 2010, **30:**3175-3183.
235. Baylis HA, Vazquez-Manrique RP: **Genetic analysis of IP(3) and calcium signalling pathways in C. elegans.** *Biochim Biophys Acta* 2011.
236. Zeng L, Webster SV, Newton PM: **The biology of protein kinase C.** *Adv Exp Med Biol* 2012, **740:**639-661.
237. King TJ, Lampe PD: **Temporal regulation of connexin phosphorylation in embryonic and adult tissues.** *Biochim Biophys Acta* 2005, **1719:**24-35.
238. Flores CE, Nannapaneni S, Davidson KGV, Yasumura T, Bennett MVL, Rash JE, Pereda AE: **Trafficking of gap junction channels at a vertebrate electrical synapse in vivo.** *Proc Natl Acad Sci USA* 2012.
239. Perez-Mansilla B, Nurrish S: **A network of G-protein signaling pathways control neuronal activity in C. elegans.** *Genetic Dissection of Neural Circuits and Behavior* 2009, **65:**145-192.
240. Zhang S, Banerjee D, Kuhn JR: **Isolation and culture of larval cells from C. elegans.** *PLoS ONE* 2011, **6:**e19505.

241. Bhat RA, Stauffer B, Della Pietra A, Bodine PV: **Wnt3-frizzled 1 chimera as a model to study canonical Wnt signaling.** *J Cell Biochem* 2010, **109:**876-884.